Design of a 3-D Rapidly Scanning Laser Doppler Velocimeter with Low SNR Signal Processing

by

Kevin A. Shinpaugh

Thesis submitted to the Faculty of the

Virginia Polytechnic Institute and State University

in partial fulfillment of the requirements for the degree of

Master of Science

in

Aerospace Engineering

APPROVED:

Roger L. Simpson, Chairman

Dana A. Walker

Alfred L. Wicks

July, 1989

Blacksburg, Virginia

Design of a 3-D Rapidly Scanning Laser Doppler Velocimeter with Low SNR Signal Processing

by

Kevin A. Shinpaugh

Roger L. Simpson, Chairman

Aerospace Engineering

(ABSTRACT)

A rapidly scanning directionally sensitive three-velocity-component laser Doppler velocimeter (RSLDV) has been designed. It permits scans through three-dimensional flows to obtain space-time velocity information and almost "instantaneous" velocity profiles vital to understanding such flows.

A flexible optical system allows for easy variation of the fringe spacing as well as the location and size of the measurement volume. Several optical techniques to maintain coincidence between the horizontal, U and W, and vertical, V, probe volumes were investigated. A lens, used like a prism, and two plane mirrors for the out of plane scanning laser beam maintains good coincidence between the probe volumes, while maintaining some flexibilty. Moving fringe patterns in the horizontal and vertical planes are produced by two solid state Bragg cells. The Doppler frequency is independent of the position of the receiving optics, and only one photomultiplier tube (PMT) is needed to receive the signals for all three velocity components.

A data acquisition, control and processing system has also been designed for use with the RSLDV. The PMT signal and location of the measurement

volume are recorded simultanoeusly by two transient recorders. The system provides storage for up to 1.25 gigabytes (6 secs.) of LDV data, with permanent storage onto optical disk. A 20 MFLOP array processor provides for fast computation of velocity information.

The Pisarenko harmonic decomposition (PHD) and fast Fourier transform (FFT) algorithms, with various interpolation techniques, were investigated for processing low signal-to-noise ratio signals for use with the RSLDV. The PHD algorithm was found to be unsuitable for use with processing RSLDV signals, however, the algorithm does provide superior frequency estimation for some frequency ratios at SNR levels above 30 dB, which are typical quality signals required for frequency counters. The FFT with zero-padding and log parabolic fit provides frequency estimates with RMS error below .1 % for signals with SNR above -5 dB. To obtain frequency estimates for signals with SNR below -5 dB, the FFT with zero-padding and parabolic fit must be used, signals with SNR down to -18 dB can be processed with this technique.

Acknowledgements

The author would like to express his deep appreciation to his advisor, Dr. Roger L. Simpson who gave invaluable guidance and assistance throughout this project. Without his encouragement, support and guidance, it would have been difficult to accomplish this work.

He also would like to thank Dr. Dana A. Walker and Dr. Alfred L. Wicks for serving on the Advisory Committee and for their helpful comments and suggestions on this project.

The author would also like to thank Dave Redding of IBM for his invaluable assistance with the IBM RT-PC, John McDonough of the LeCroy corporation for his assistance with the transient recorders.

He also wishes to thank his friends, in and outside of Blacksburg, for their time and support.

This project was supported under a grant from the Air Force Office of Scientific Research.

Table of Contents

List of Tables

List of Illustrations

List of Symbols

a .....reflection coefficient vector

A .....eigenfilter

AR .....autoregressive

d .....x location of prism apex

d_1 .....x location of mirror M13

d_2 .....x location of mirror M14

DFT.....discrete Fourier transform

f.....focal length of lens

f.....frequency

f_d.....Doppler frequency

F.....optimization parameter

FFT.....fast Fourier transform

I.....laser beam intensity

j .....imaginary constant, $\sqrt{-1}$

L.....location of measurement volume measured from final lens

L.....model order for PHD algorithm

L_p.....length of vertical probe volume

m.....magnification factor

n.....index of refraction

P.....sinusoid power

PHD.....Pisarenko harmonic decomposition

PMT.....photomultiplier tube

$r_{xx}(k)$.....autocorrelation sequence at lag k

RMS.....root mean square

R.....radius of curvature for concave mirror or lens surface

R.....autocorrelation matrix

s.....object distance from lens

s''.....image distance from lens

SNR.....signal to noise ratio

$S(f)$.....energy spectral density at frequency f

T.....temporal sampling interval

$\mathbf{T}_p$.....Hermitian Toeplitz matrix

U.....velocity component in the x direction

V.....velocity component in the y direction

V_s.....scan velocity of measurement volume

W.....velocity component in the z direction

x_p.....location of measurement volume measured from scanning mirror

$x(n)$.....digital time domain signal

$x(t)$ .....time domain signal

x_0.....path length difference between central beam and two side beams without mirrors M6 and M7

x_{M1}.....x location of beam C on mirror M13

x_{M2}.....x location of beam C on mirror M14

$X(f)$.....Fourier transform of signal $x(t)$

y .....scan height of measement volume

y_{M1} .....y location of beam C on mirror M13

y_{M2} .....y location of beam C on mirror M14

Z_R.....Rayleigh range of input beam, $\frac{\pi\omega_0^2}{\lambda}$

Z''_R .....Rayleigh range of output beam

Greek symbols

α .....angle of intersection between beams A and B or$D$

δ .....change in angle of beam C for concave mirror or prism

ε.....wedge angle for prism

η .....fringe visiblity

θ .....scan angle

θ_0.....angle between beams A and$C$ at scanning mirror

θ_1 .....angle of inclination of mirror M13

θ_2.....angle of inclination of mirror M14

θ_r .....angle of inclination of output beam C from last optics

λ .....wavelength of laser light

λ_{AB} .....fringe spacing for interfernce pattern between laser beams A and B

ξ .....angle of intersection between beams C and B or D

ϕ.....angle of intersection between beams $A$and$B$ forming the vertical probe volume

ω_0 .....input beam waist

ω''_0.....output beam waist

1.0 Introduction

The Laser Doppler Velocimeter (LDV) has been a valuable tool for experimental investigation in fluid mechanics. The obvious advantage of LDV is its high frequency response and its ability to measure direction and magnitude of the velocity accurately and non-intrusively under conditions where other instruments provide questionable results or cannot be used at all.

Although commercial pointwise LDV systems are available, further instrument development is needed. In order to obtain more detailed features in certain complicated flows, such as turbulent separated flows, "instantaneous" velocity profiles should be obtained. Therefore scanning LDV systems are needed because they yield nearly instantaneous velocity profiles and, concurrently, reduce the data acquisition time of velocity information in at least one direction. Furthermore, three-dimensional measurements should be made so that important space-time flow-structural information can be obtained.

One problem with scanning LDV systems is that the signal to noise ratio (SNR) of the resulting signals are typically lower than that from pointwise systems. Also a 3-D rapidly scanning LDV system has many fringe patterns with some very close together in frequency and near continuous processing is needed in order to get "instantaneous" velocity profiles. Although commercial LDV signal processors are available, these units tend to be single channel, have limited frequency response, low throughput and cannot handle the low SNR signals resulting from a scanning LDV system. Robust signal processing algorithms are needed for scanning LDV systems; they should be able to obtain fast accurate velocity estimation at low SNR with multiple Doppler signals on a large amount of data.

This work is concerned with the development of a three-component rapidly scanning laser Doppler velocimeter and the associated data acquisition and signal processing.

1.1 Background

Laser Doppler velocimetry (LDV) is an optical technique for measuring the local, instantaneous velocity of a flow. The basic principle of LDV is to split a laser beam into two equal intensity beams which are made to intersect at the measurement volume. The intersecting beams form stationary interference fringe patterns inside the measurement volume formed by the crossing beams.

The fringe pattern is made of light and dark regions and if the laser beams cross at their waists, parallel fringes will be formed with equal fringe spacing. The spacing of the fringes, λ_{AB}, is given by

$$\lambda_{AB} = \frac{\lambda}{2 \sin \varphi}$$

where φ is the half angle between the intersecting pair of beams and λ is the wavelength of the laser light.

In order to measure the velocity of the flow, tracer particles must be present in the fluid. These particles can be naturally occurring or artificially induced into the fluid but should be of appropriate size, density and shape so that the particles follow the flow. When a particle passes through the measuring volume it scatters light that can be detected by a photodetector. The Doppler frequency of the scattered light is directly proportional to the particle velocity which is given by

$$f_d = \frac{2|U|}{\lambda} \sin \varphi$$

where $|U|$ is the magnitude of the instantaneous velocity component perpendicular to the optical axis.

For more information on the principles and practices of LDV see Durst, Melling, and Whitelaw, 1981.

1.2 Previous Work: Scanning LDV

A brief description of a few scanning LDV systems developed and used so far, is given by Antoine (1985) and Simpson (1989). Bendick (1971) described an on-axis scanning LDV that used a translational oscillating mirror. This system was used for instantaneous velocity measurements in steady and pulsating water flow in a glass tube of 6 mm I. D. The operation of this design is limited to scan speeds of 0.4 m/s due to the inertia of the moving optics.

A two-color dual-beam backscatter LDV system accomplishing a scan by translating a lens in the direction of the optical axis was reported by Grant and Orloff (1973). Scan rates were limited to 1.5 m/s because of inertial considerations. More information concerning the application of this design is given by Orloff and Biggers (1974) and Orloff, *et al.* (1975).

A backscatter scanning system was reported by Rhodes (1976). It is able to scan a distance of 30 cm at a frequency of 30 Hz, and measure velocities at 16 discrete positions using a large rotating wheel containing 16 ports. For more information concerning this design, see Gartrell and Jordan (1977) and Meyers (1979).

An optical system capable of measuring true instantaneous velocity profiles was reported by Nakatani, *et al.* (1978). Instead of using a moving scanning device, it employed a cylindrical lens to form a vertical measurement volume along a straight line. The design is relatively impractical and expensive

because a series of optical fibers connected to photodetectors is needed to collect data over a large scan range with good resolution.

The design of Durst, Lehmann, and Tropea (1981) used a relatively large rotationally oscillating mirror in front of a conventional LDV optical system to scan the measurement volume perpendicular to the optical axis along an arc. Mean and RMS velocity profiles agreed well with pointwise measurements for low scan frequencies. The inertia of the oscillating mirror limited the scan frequency to about 15 Hz.

Owen (1984) developed a single velocity scanning LDV and made measurements in both water and air flows. A six-sided rotating polygon mirror was used and the scan rate was limited to 125 Hz due to restrictions on the data acquisition rates and the number of points required for one profile. Improvements were suggested for a second phase of the work which will enable two-component real-time scans through high speed air flows. The disadvantage of a rotating mirror polygon is that the reflected beams are in unwanted directions 90% of the time.

Chehroudi and Simpson (1983) developed a single-component rapidly scanning LDV that scanned up to 150 Hz over 40 cm. The proper operation and usefulness of this design was demonstrated in a separated flow studied in a boundary layer wind tunnel. "Instantaneous" velocity profiles could not be obtained due to the data acquisition system used.

Antoine and Simpson (1986) extended the design above to a three-component system. A Ronchi ruling was used to produces fringe patterns

in the horizontal plane to measure V. The fringe patterns produced by the Ronchi ruling were unsatisfactory.

Econonou extended the design of Chehroudi and Simpson (1983) to permit scans in the plane perpendicular to the mainstream flow velocity. This is a one component system and requires three scanners. For more information on this design see Econonou (1986).

1.3 Previous Work: LDV Signal Processing

Laser Doppler velocimetry is based on the formation of interference fringe patterns between two or more laser beams and the scattering of the modulated light by small particles, naturally occurring or artificially induced in the flow. This scattered light is received by a photomultiplier tube (PMT), where the frequency of the modulated signal is proportional to the fluid velocity. To extract this velocity information from the PMT signal, some form of signal processing system is needed. The required signal processing system depends on what properties are to be measured (U,U^2, $\overline{uv}$,etc), the required precision, and the signal-to-noise ratio (SNR) (Durst, Melling, and Whitelaw, 1981)

Swept spectrum analyzers were the initially applied instrument for LDV signal processing. They were readily available, had large dynamic range, and could handle low SNR signals. However, these units have a rather large dead time and low data rates. Frequency trackers and counter type processors are

alternatives to swept spectrum analyzers, providing improvements in reducing dead time and increasing data rates. Both instruments, however, are not well suited for use with the RSLDV system because of the multiple Doppler frequency, rapid change in velocities as the measurement volume is scanned, and ride range in SNR of the PMT signal.

Most of the current research in LDV signal processing is concentrated in the development of spectrum analyzers. Some of these advances include the Burst Spectrum Analyzer (BSA) made by Dantec, and the Laser Anemometry Research Processor (LARP) made by Macrodyne. The BSA is described by Lading (1987), Arik and Buchhave (1987) and the LARP by Baker, *et al.* (1988). Both units employ fast digitizers, burst detection circuits, and signal processing via hardwired FFT processors with a parabolic interpolation scheme to obtain Doppler frequency estimates. Unfortunately, both units are single channel and have limited memory. Kalb and Crosswy (1983), also describe a Fourier transform processor with parabolic interpolation.

Some recent work employing parametric frequency estimation has been done by Matovic,*et al.* (1987) and Swart, *et al.* (1981). Swart, Venter, and van der Merwe used a linear prediction filter using a fast Kalman algorithm to obtain Doppler frequency estimates. The Matovic, *et al.* method is based on a second order autoregressive (AR) model using the autocovariance function coefficients to obtain Doppler frequency estimates. They report that the frequency error remains under 1 % for SNR values above 0 dB, but the frequency error diverges rapidly at SNR values below 0 dB.

1.4 Objective of this Work

The motivation for developing a rapidly scanning LDV is to obtain space-time data for and a better understanding of separated turbulent boundary layers. The key to this understanding is in the instantaneous behavior of the large-scale structures which produce the large-scale diffusion of turbulence and momentum. A three component rapidly scanning LDV system would provide the necessary "instantaneous" velocity profile vital to understanding separating and separated turbulent boundary layers.

The behavior of these large-scale structures observed through the "instantaneous" velocity profiles would provide insight into a number of fundamental issues about separated turbulent flows. Among these issues are

1. the relationship between the large-scale structures and the on-set of instantaneous flow reversal.

2. the relationship between velocity and pressure fluctuations.

3. the relationship between large-scale structures and the lag and hysteresis of separated flows.

The almost instantaneous velocity profile provided by a three-component scanning LDV provides information to determine the inflows and outflows of turbulent kinetic energy and momentum and the many of the turbulent

contributions to the pressure fluctuations. Such separated flow data cannot be obtained by hot-wire arrays because flow reversal or by image-processing of particle tracking photographs because of the three dimensional nature of such flows.

The objectives of the present work are as follows:

1. Develop a three-component rapidly scanning laser Doppler velocimeter (RSLDV) capable of scanning at least 40 cm or longer at high frequencies.

2. Develop a data acquisition system for the system above.

3. Investigate and develop signal processing techniques for use with the RSLDV.

1.5 Outline of Thesis

Chapter 2 deals with the design of the RSLDV. The components of the transmitting optics are explained, as well as the problems with maintaining a coincident measuring volume over the scan length and techniques investigated to deal with this problem. The fringe patterns formed are also analyzed and discussed.

Chapter 3 describes the data acquisition and control hardware and logic.

Chapter 4 deals with the signal processing algorithms investigated. Theory of operation and implementation of each algorithm is discussed. Comparisons of the algorithms on simulated and experimental LDV signals are presented.

Chapter 5 gives the conclusion of this work and makes recommendations for future work and improvements.

2.0 Description of RSLDV Optical Configuration

"Instantaneous" three-component velocity profiles are needed in order to gain a better understanding of separated turbulent flows. These velocity profiles would provide insight into the behavior of the large-scale structures which are responsible for the large-scale diffusion of turbulence energy and momentum.

Laser Doppler velocimetry should be used since it provides low uncertainty measurements and does not disturb the flow field. An LDV system to provide the necessary "instantaneous" velocity profiles should be capable of scanning a 40 cm height at rates of up to 300 scans/sec. The LDV system should provide concurrent measurements of all three velocity components using an on-axis beam arrangement, an on-axis system requires no modifications to the facilities at VPI&SU. The LDV system should also allow for variations in scan height, scan rate, location of the measurement volume, and the fringe spacing to be made easily.

The LDV system described below should fulfill these requirements.

2.1 *General Description of Setup*

As shown in Figure 1, the incoming beam from an Argon ion laser (λ = 514.5 nm) passes through a pair of solid state Bragg cells (BC1,BC2), where it is split and frequency shifted. Bragg cell (BC1) operates at 30 MHz in the vertical plane and produces an unshifted beam and a shifted beam of +30MHz. Bragg cell (BC2) operates at 40 MHz in the horizontal plane and produces an unshifted beam and two shifted beams, +40 MHz and -40MHz, and some higher order modes. A total of six beams emerge from the bragg cell combination, but only four beams are used; +30MHz, +40MHz, -40MHz and the unshifted beam. Mirrors (M1,M2,M3) provide a longer path length to the beam expander optics for additional separation between the four beams. Lens combination (L1,L2) determines the size of the beam waists at the probe volume. One set of lenses is used for each beam so that each beam passes through the center of each lens pair, therefore minimizing spherical aberration. Focusing lenses (L3,L4) determine the position of the beam waists (the probe volume), and as above there is a set of lenses for each beam. The beams then reflect from mirrors (M4a,b,c,d) onto additional mirrors (M5a,b,c,d) which direct the beams at the proper angle onto the scanning mirror and also provide for path length equalization between the beams. The beams encounter additional optics necessary to produce the probe volume. Figure 2 shows the top and side view of the four beams intersecting to form the measurement volume. Figure 3 shows the on axis view of the four

beams forming the measurement volume. These optics and the fringe patterns formed are described in the following sections.

Using the same optical setup, the laser can be used in a multi-mode operation to allow a two color (λ = 514.5 nm and 488 nm) LDV system with the addition of some color filters. Beam *A* would consist of both wavelengths, beams *B* and *D* of wavelength λ = 514.5 nm, and beam *C* of wavelength λ = 488 nm. The on axis view of the four beams forming the measurement volume for this system is shown in Figure 4. The advantage of this arrangment is that there is more laser power in the measurement volume and only four fringe patterns are formed. With fewer fringe patterns the Doppler frequencies can vary more widely in frequency without overlapping.

2.1.1 Beam Expansion and Focusing Optics

The two lens combinations are used in order for the beams to cross at their waists, and to form an appropriate sized probe volume at the desired location in space.

The beam expanding lenses are positioned before the focusing lenses and consistes of a pair of plano-convex lenses (L1,L2). They determine the size of the beam waist focused at the back plane of the focusing optics. This determines the size of the probe volume, which influences fringe visibility and laser power density in the probe volume.

The focusing lenses determine the location of the beam waists and consist of a pair of plano-convex lenses. The input beam waist to this set of optics determines the size of the probe volume. The focal lengths and spacing between lenses are shown in Table 1.

The design of these two lens combinations depends upon several factors:

- The size of the probe volume necessary to maintain a coincident measuring volume (see 2.3 for more information).

- The minimum distance from the last lens set (L4) to the probe volume.

Since Guassian laser beams transform in a manner different form optical rays the normal thin lens equations (geometric optics) could not be used without large error (Yariv, 1985). Calculation of Guassian beam propagation through optical devices usually involves matrix transformations or 2-D Fourier transformations, which can be difficult to use. A more straight forward but less rigorous approach is given in Optics Guide 4 (1988).

In terms of input beam parameters:

$$\frac{1}{s+\frac{Z_R^2}{s-f}}+\frac{1}{s''}=\frac{1}{f} \qquad [2.1]$$

$$m=\frac{\omega''_0}{\omega_0}=\frac{1}{\sqrt{[1-\frac{s}{f}]^2+[\frac{Z_R}{f}]^2}} \qquad [2.2]$$

$$Z_R = \frac{\pi \omega_0^2}{\lambda} \qquad [2.3]$$

In terms of output beam parameters:

$$\frac{1}{s} + \frac{1}{s'' + \frac{Z''^2_R}{s'' - f}} = \frac{1}{f} \qquad [2.4]$$

where

s = object distance from lens

s'' = image distance from lens

f = focal length of lens

Z_R = Rayleigh range of input beam

Z''_R = Rayleigh range of output beam

m = magnification factor

ω_0 = input beam waist

ω''_0 = output beam waist

Lens combinations are handled by cascading the above equations; the image from the preceding lens is the object for the next lens in the optical system.

The design of the focusing lenses is considered first (see Figure 5). With the probe waist (ω''_{04}) and the location (d_{4p}) of the probe volume known and assuming reasonable values for f_3 and f_4, the following equations result

$$s''_3 = \frac{f_3}{1 + \frac{\lambda f_3}{\pi \omega_{03}^2}} \qquad [2.5]$$

$$\omega''_{03} = \frac{\frac{\lambda f_3}{\pi \omega_{03}}}{\sqrt{1 + \frac{\lambda f_3}{\pi \omega_{03}^2}}} \qquad [2.6]$$

$$\frac{1}{d_{34} - s'' + \frac{Z_{R_4}^2}{d_{34} - s''_3 - f_4}} + \frac{1}{d_{4p}} = \frac{1}{f_4} \qquad [2.7]$$

$$m = \frac{\omega''_{04}}{\omega''_{03}} = \frac{1}{\sqrt{[1 - \frac{d_{34} - s''_3}{f_4}]^2 + [\frac{Z_{R_4}}{f_4}]^2}} \qquad [2.8]$$

Equations [2.7] and [2.8] are iteratively solved for the spacing between the two lenses (d_{34}) and the beam input waist (ω_{03}).

The beam expander optics is based on a reversed Keplerian telescope (see Figure 5). The equations for this lens system reduces to:

$$\frac{\omega_{01}}{\omega''_{02}} = \frac{f_1}{f_2}, \quad d_{12} = f_1 + f_2, \quad d_{23} = f_2 \qquad [2.9]$$

Since $\omega''_{02} = \omega_{03}$ and ω_{01} is the beam waist from the laser, selecting f_1 determines the value of f_2. The beam profile through the optical system shown in Figure 5

is for the $1/e^2$ beam intensity location, which is a hyperbolic function in the traverse direction (Yariv, 1985).

This optical configuration of expanding optics and focusing optics has advantages in the flexibility of adjusting the size and location of the probe volume independently.

2.1.2 Scanner

The G325DT scanner from General Scanning Inc. is a moving iron galvanometer with a position transducer designed specifically for closed-loop operation. This transducer operates by detection of capacitance variation between the rotating armature and a set of stationary electrodes. The controller includes a heater control regulating the temperature of the scanner. The mirror is a front surface mirror with DuAg coating, and is flat to one tenth of a wavelength over the useable aperture. The shaft wobble is typically below 5 arc-seconds and the signal response time is 10 ns.

2.1.3 Receiving Optics

The receiving optics consist of two cylindrical lenses (CL1,CL2), a long front surface mirror (M13), and the PMT, all assembled inside a black box having a side door for any adjustments (Figure 6). The first cylindrical lens

(CL1) gathers light and enlarges the image of the measurement volume in the streamwise direction. The mirror deflects light onto the second cylindrical lens (CL2) which constructs the image of the measurement volume on the PMT aperture for any positions of scan. Both lenses and mirror can be moved independently from each other in the vertical and horizontal direction. For more information on the design of the receiving optics see Antoine (1985).

2.2 *Horizontal Plane Optics*

To measure the velocity components in the horizontal plane (U and W), three beams are used. The optical configuration follows the same concept used in the designs of Chehroudi and Simpson (1983) and Antoine (1985). Beams *A* (unshifted), *B* (-40 MHz) and *D* (+40 MHz) form the probe volume to measure U and W velocity components (see Figures 1,2,3 and 4).

Beam *A* is reflected from the scanner to mirrors (M6,M7,M8a) to the probe volume. Mirrors (M6,M7) serve to equalize optical path length from the scanner to the probe volume. This assures coherence between the three beams and that the beams scan the same position. Beam *B* is reflected from the scanner to mirrors (M8b,M9) and beam *D* to mirrors (M8d,M11,M12). The position and facing of mirrors (M9,M10,M11,M12) can be adjusted to allow changes in the horizontal fringe spacing and the position of the probe volume independently.

Mirrors (M6,M7) are adjusted so that the path length from the scanner to the probe volume is equal for all three beams.

This optical arrangement allows changes in fringe spacing and the probe volume position to be independently made. Also, since each beam has its own set of optics, system alignment can be made individually for each beam uncoupled from the other beams. The path scanned by the three beams forming the horizontal plane probe volume is a vertical line.

2.3 *Vertical Plane Optics*

The vertical plane optics, necessary to measure the V component of velocity, proved to be the most difficult aspect in designing a three component rapidly scanning LDV system. There were two major problems that needed to be solved:

- The angle of intersection between the two beams forming the vertical plane probe volume should have a fringe spacing on the order of a few microns.

- The probe volume tends to scan an arc; coincidence of the horizontal and vertical probe volumes is difficult to achieve.

The length of the vertical plane probe volume (L_p) measured as the projection along the central beam (A) can be found as follows

$$L_p = \frac{\omega_{0p}}{\sin \phi} + \frac{\omega_{0p}}{\tan \phi} \qquad [2.10]$$

where

ϕ = angle of intersection between beams A and C

ω_{0p} = the beam waist at the measurement volume

Coincidence of the probe volumes is maintained when the path of the vertical plane probe volume is located within this area. Outlined below are several methods investigated to solve the coincidence problem.

2.3.1 Plane Mirror Pair

The simplest technique (and the basis for some of the other techniques) to form the vertical plane probe volume is to use two plane mirrors arranged as shown in Figure 7. Beam C (+30 MHz) is reflected from the scanner at an angle of θ_0 to beam A to mirror (M13), located at a distance of d_1 from the scanner and angle θ_1 to the horizontal plane. Mirror (M14), located at d_2 from the scanner and an angle of θ_2 to the horizontal plane, reflects beam C to intersect beam A to form the probe volume. Deriving ray equations for beams A and C

For beam A:

$$y = (x + x_0) \tan \theta \qquad [2.11]$$

For beam C:

$$\alpha = \theta_0 + \theta \qquad [2.12]$$

$$x_{M1} = d_1 \frac{\tan\theta_0 - \tan\theta_1}{\tan\alpha - \tan\theta_1} \qquad [2.13]$$

$$y_{M1} = x_{M1} \tan\alpha \qquad [2.14]$$

$$\beta = 2\theta_1 - \theta_0 - \theta \qquad [2.15]$$

$$\gamma = 2\theta_1 - \theta_0 \qquad [2.16]$$

$$x_{M2} = \frac{x_{M1}\tan\beta + d_1\tan\theta_0 - (d_1 - d_2)\tan\gamma - d_2\tan\theta_2 - y_{M1}}{\tan\beta - \tan\theta_2} \qquad [2.17]$$

$$y_{M2} = (x_{M2} - x_{M1})\tan\beta + y_{M1} \qquad [2.18]$$

$$\theta_r = -(2\theta_1 - 2\theta_2 - \theta_0 - \theta) \qquad [2.19]$$

$$y = (x - x_{M2})\tan\theta_r + y_{M2} \qquad [2.20]$$

Equation [2.11] gives the location of beam A at any scan angle θ , where x_0 is the difference between the path length of beam A from the scanner to the probe volume and the probe volume distance from the scanner. Equations [2.13,2.14] give the location of beam C on mirror (M13) and [2.17,2.18] on mirror (M14). The location of the beam intersection can be found by setting equation [2.11] and [2.20] equal to each other and solving for x.

$$x = \frac{y_{M2} - x_{M2} \tan \theta_r - x_0 \tan \theta}{\tan \theta - \tan \theta_r} \qquad [2.21]$$

Equations [2.21] and [2.11] give the x,y position of the vertical probe volume as the beams are scanned. From these two equations a solution for the five variables $(\theta_0, \theta_1, \theta_2, d_1, d_2)$ needs to be found that maximizes the vertical and horizontal probe volume coincidence. Since the horizontal probe volume scans a vertical line, a solution can be found by considering the minimization of the following integral

$$F = \int_0^{\theta_{max}} (x_p - x)^2 \, d\theta \qquad [2.22]$$

which can be viewed as the difference squared between the areas swept by the two probe volumes. An optimization algorithm, Sequential Linear Least Squares Programming (SLLSQP) (Kraft, *et al.* 1981), was used to find the minimum of equation [2.22]. No global minimum was found using this approach, even when θ_0 was held constant at a suiTable value, due to the many peaks and valleys of many orders of magnitude across the domain space.

A brute force method was then used to find the minimum of eq. [2.22]; to reduce computer time and increase accuracy, the above equations were reformulated to reduce the number of free variables. To eliminate two of the variables, the beams were required to have an angle of intersection of ϕ and to cross at the required probe location x_p at a particular scan angle $\bar{\theta}$, in this case

$\frac{\theta_{max}}{2}$. This enables θ_2 and d_2 to be calculated in terms of the other variables as follows

$$\theta_2 = \frac{1}{2}(\phi - 2\theta_1 + \theta_0) \qquad [2.23]$$

$$d_2 = \frac{x_2 \tan\theta_2 - y_2 - x_1 \tan(2\theta_1 - \theta_0) + y_1}{\tan\theta_2 - \tan(2\theta_1 - \theta_0)} \qquad [2.24]$$

where

$$x_1 = d_1$$

$$y_1 = d_1 \tan\theta_0$$

$$x_2 = \frac{x_p \tan\theta_r(\bar{\theta}) - y_p - x_{M1}(\bar{\theta}) \tan\beta(\bar{\theta}) + y_{M1}(\bar{\theta})}{\tan\theta_r(\bar{\theta}) - \tan\beta(\bar{\theta})}$$

$$y_2 = (x_2 - x_p)\tan\theta_r(\bar{\theta}) + y_p$$

$$y_p = (x_p + x_0)\tan\bar{\theta}$$

The minimization algorithm increments d_1 across its domain while holding θ_1 and θ_0 constant; the computer program for this algorithm is in appendix A.1. The values of θ_2 and d_2 are calculated at each θ step via eqns. [2.23] and [2.24]. The value of F is calculated from eqns. [2.11 - 2.22]. The integral is approximated by using Simpson's rule. A minimum of F over the d_1 domain is obtained at each θ_1 step. The program can be run again with different θ_0 and ϕ values, some of the results are shown in Table 2.

The advantages of this optical arrangement are that it is simple and flexible: different probe volume locations and fringe spacing can be accommodated. The disadvantage is that coincidence is not maintained over a large scan length as can be seen from Figure 8.

2.3.2 Concave-Plane Mirror Pair

The path of the vertical probe volume formed by the two plane mirrors suggests that a concave mirror substituted for one of the plane mirrors would tend to converge the scan path closer to a vertical line. This optical arrangement can be seen in Figure 9. The development of the equations are similar to the above system

$$x_c = d_1 - R \sin \theta_1 \qquad [2.25]$$

$$y_c = d_1 \tan(\theta_0 + \theta_{max}) + R \cos \theta_1 \qquad [2.26]$$

$$x_{M1} = \frac{-b + \sqrt{b^2 - 4ac}}{2a} \qquad [2.27]$$

$$y_{M1} = x_{M1} \tan(\theta_0 + \theta) \qquad [2.28]$$

where

$$a = 1 + \tan^2(\theta_0 + \theta)$$

$$b = -2x_c - 2y_c \tan(\theta_0 + \theta)$$

$$c = x_c^2 + y_c^2 - R^2$$

$$\alpha = \theta_0 + \theta_{max} \qquad [2.29]$$

$$\delta = 2 \sin^{-1} \frac{\sqrt{(d_1 - x_{M1})^2 + (d_1 \tan \alpha - y_{M1})^2}}{2R} \qquad [2.30]$$

$$\beta = 2\theta_1 - \theta_0 - \theta_{max} \qquad [2.31]$$

$$\gamma = 2(\theta_1 - \delta) - \theta_0 - \theta \qquad [2.32]$$

$$x_{M2} = \frac{(d_2 - d_1)\tan\beta + d_1 \tan\alpha - d_2 \tan\theta_2 + x_{M1}\tan\gamma - Y_{M1}}{\tan\gamma - \tan\theta_2} \qquad [2.33]$$

$$y_{M2} = (x_{M2} - x_{M1})\tan\gamma + y_{M1} \qquad [2.34]$$

$$\theta_r = -[2(\theta_1 - \delta) - 2\theta_2 - \theta_0 - \theta] \qquad [2.35]$$

The location of the center of the radius of curvature for the concave mirror is given by eqns. [2.25] and [2.26]. Beam C's location on the concave mirror is given by eqns. [2.27] and [2.28]. Equation [2.30] describes the relative change in angle with respect to θ_1 of the mirrors surface for the beam as it scans. The beam's position on the plane mirror is given by eqns [2.33] and [2.34].

Variables d_2 and θ_2 are again eliminated by using the method outlined in sec. 2.3.1. This results in the following

$$\theta_2 = -\frac{1}{2}(\phi - 2\theta_1 + \theta_0) \qquad [2.36]$$

$$d_2 = \frac{y_p - x_p \tan\theta_r(\theta_{max}) - y_1 + x_1 \tan\gamma(\theta_{max})}{\tan\gamma - \tan\theta_r(\theta_{max})} \qquad [2.37]$$

where

$$x_1 = d_1$$

$$y_1 = d_1 \tan(\theta_0 + \theta_{max})$$

$$y_p = (x_p + x_0) \tan \theta_{max}$$

The beam intersection is found from eqn. [2.21] and the values above. The same type algorithm is employed to minimize F from eqn [2.22] except another loop is added to increment the radius of curvature for the concave mirror (see Appendix A.2). Some results are shown in Table 3 and Figure 10 shows the probe volume path for the minimum solution.

This technique results in better coincidence than that of the two plane mirrors, but changes in either the probe volume location or the fringe spacing may need a different concave mirror to obtain the best coincidence.

2.3.3 Prism

A prism, as shown in Figure 11, was another technique investigated to form the vertical plane probe volume. The following equations were derived considering the surface of the prism as a dielectric interface.

$$\alpha = \theta_0 + \theta \qquad [2.38]$$

$$\theta_1 = 90 - \theta_p + \frac{\varepsilon}{2} + \theta_0 + \theta \qquad [2.39]$$

$$\delta = \theta_1 + \sin^{-1}[\sqrt{(n^2 - \sin^2\theta_1)}\ \sin \varepsilon - \sin \theta_1 \cos \varepsilon] - \varepsilon \qquad [2.40]$$

$$\theta_2 = \sin^{-1}(\sin \frac{\theta_1}{n}) \qquad [2.41]$$

$$\beta = \theta_p - 90 - \frac{\varepsilon}{2} + \theta_2 \qquad [2.42]$$

$$\gamma = \theta_p - \frac{\varepsilon}{2} \qquad [2.43]$$

$$\psi = \theta_p + \frac{\varepsilon}{2} \qquad [2.44]$$

$$\theta_r = \theta + \theta_0 - \delta \qquad [2.45]$$

$$x_{s1} = \frac{D \tan(\theta_0 + \theta_{\max}) - D \tan \gamma}{\tan \alpha - \tan \gamma} \qquad [2.46]$$

$$y_{s1} = x_{s1} \tan \alpha \qquad [2.47]$$

$$x_{s2} = \frac{D \tan(\theta_0 + \theta_{\max}) - y_{s1} + x_{s1} \tan \beta - D \tan \psi}{\tan \beta - \tan \psi} \qquad [2.48]$$

$$y_{s2} = y_{s1} + (x_{s2} - x_{s1}) \tan \alpha \qquad [2.49]$$

$$x = \frac{y_{s2} - x_0 \tan \theta - x_{s2} \tan \theta_r}{\tan \theta - \tan \theta_r} \qquad [2.50]$$

The same type of algorithm is used to minimize F, see appendix A.3. Some results are shown in Table 4. This minimization technique did not work very well for this optical system, due to oversimplification in the optical system parameters.

2.3.4 Lens, Plane Mirror Pair

As shown in Figure 12, beam C passes through a plano-convex lens to the plane mirror system described in sec. 2.3.1. This method evolved from observation of the prism system above, a lens is used like a prism but provides a varying degree of deflection as the beam is scanned. The equations for this system are

$$x_L = \frac{d_L \tan(\theta_0 + \theta_{max}) - d_L \tan(90 + \theta_0 + \theta_{max})}{\tan(\theta_0 + \theta) - \tan(90 + \theta_0 + \theta_{max})} \qquad [2.51]$$

$$y_L = x_L \tan(\theta_0 + \theta) \qquad [2.52]$$

$$\varepsilon = \sin^{-1}\left[\frac{x_L - d_L}{R \sin(\theta_0 + \theta_{max})}\right] \qquad [2.53]$$

where

R = the radius of curvature of the lens $= f(n - 1)$

$$\delta = (\theta_{max} - \theta) + \sin^{-1}[\sqrt{n^2 - \sin^2(\theta_{max} - \theta)}\ \sin\varepsilon - \sin(\theta_{max} - \theta)\cos\varepsilon] - \varepsilon \qquad [2.54]$$

$$x_{M1} = \frac{x_L \tan(\theta_0 + \delta + \theta) - y_L + d_1(\tan\theta_0 - \tan\theta_1)}{\tan(\theta_0 + \delta + \theta) - \tan\theta_1} \qquad [2.55]$$

$$y_{M1} = x_{M1} \tan(\theta_0 + \delta + \theta) + y_L - x_L \tan(\theta_0 + \delta + \theta) \qquad [2.56]$$

$$\beta = 2\theta_1 - \theta_0 - \delta - \theta \qquad [2.57]$$

$$\gamma = 2\theta_1 - \theta_0$$

$$x_{M2} = \frac{(d_2 - d_1)\tan\gamma + x_{M1}\tan\beta + d_1\tan\theta_0 - d_2\tan\theta_2 - y_{M1}}{\tan\beta - \tan\theta_2} \qquad [2.58]$$

$$y_{M2} = (x_{M2} - x_{M1})\tan\beta + y_{M1} \qquad [2.59]$$

$$\theta_r = -(2\theta_1 - 2\theta_2 - \theta_0 - \delta - \theta) \qquad [2.60]$$

The variables d_2 and θ_2 are found from eqns [2.23] and [2.24], except they are evaluated at $\bar{\theta} = \theta_{max}$. The same algorithm is used to minimize F, eqn [2.22], with the focal length of the lens being changed for each run as necessary. Results are shown in Table 5 and Figure 13.

This technique maintains the best probe volume coincidence but requires more optical components, so set up is a little more complex. Changes in the probe volume location or fringe spacing can be made by changing the position and angles of the optics and may also require a different focal length lens for best results.

2.4 *Doppler Frequencies for the System*

The interference phenomena between the four laser beams produces six moving fringe patterns for the single color system, as shown in Figure 3, and four moving fringe patterns for the two color system (see Figure 4), that permit the measurement of the U, V, and W components of velocity. These moving fringe patterns produce Doppler frequencies around 30 MHz, two 40 MHz, and 80 MHz; the single color system as additional Doppler frequencies around 10 MHz and 70 MHz. The Doppler frequencies can be determined by taking the dot product of unit vector of the moving fringe pattern with the velocity vector, this results in the following equations (see Figure 2)

$$\lambda_{BD}\,(f - 80\text{MHz}) = -\,U \qquad [2.61]$$

$$\lambda_{AB}\,(f - 40\text{MHz}) = -\,U\cos\frac{\alpha}{2} - (V - V_s)\sin\frac{\alpha}{2}\sin\theta + W\sin\frac{\alpha}{2}\cos\theta \qquad [2.62]$$

$$\lambda_{AD}\,(f - 40\text{MHz}) = -\,U\cos\frac{\alpha}{2} + (V - V_s)\sin\frac{\alpha}{2}\sin\theta - W\sin\frac{\alpha}{2}\cos\theta \qquad [2.63]$$

$$\lambda_{AC}\,(f - 30\text{MHz}) = (V - V_s)\cos(\frac{\phi}{2} - \theta) - W\sin(\frac{\phi}{2} - \theta) \qquad [2.64]$$

$$\lambda_{BC}(f-70\text{MHz}) = -U\frac{\sin\alpha}{2\sin\xi/2} + (V-V_s)\frac{\sin(\phi-\theta)+\cos\alpha\sin\theta}{2\sin\xi/2} + W\frac{\cos(\phi-\theta)-\cos\alpha\cos\theta}{2\sin\xi/2} \quad [2.65]$$

$$\lambda_{CD}(f-10\text{MHz}) = -U\frac{\sin\alpha}{2\sin\xi/2} - (V-V_s)\frac{\sin(\phi-\theta)+\cos\alpha\sin\theta}{2\sin\xi/2} - W\frac{\cos(\phi-\theta)-\cos\alpha\cos\theta}{2\sin\xi/2} \quad [2.66]$$

where

$$\xi = \cos^{-1}(\cos\alpha\cos\phi)$$

$$\lambda_{BD} = \frac{\lambda}{2\sin\alpha}$$

$$\lambda_{AB} = \lambda_{AD} = \frac{\lambda}{2\sin\alpha/2}$$

$$\lambda_{AC} = \frac{\lambda}{2\sin\phi/2}$$

$$\lambda_{BC} = \lambda_{CD} = \frac{\lambda}{2\sin\xi/2}$$

The above equations can be solved for velocity components U, V, and W in two ways. If the frequency difference between equations 2.62 and 2.63 can be obtained the following system of equations result

$$\begin{bmatrix} U \\ V-V_s \\ W \end{bmatrix} = \begin{bmatrix} -1 & 0 & 0 \\ 0 & \frac{\sin(\phi/2-\theta)}{2\sin\alpha/2\cos\phi/2} & \frac{\cos\theta}{\cos\phi/2} \\ 0 & \frac{\cos(\phi/2-\theta)}{2\sin\alpha/2\cos\phi/2} & \frac{\sin\theta}{\cos\phi/2} \end{bmatrix} \begin{bmatrix} \lambda_{BD}(f-80MHz) \\ \lambda_{AB}(f_{AB}-f_{AD}) \\ \lambda_{AC}(f-30MHz) \end{bmatrix} \quad [2.67]$$

The frequency difference can be obtained by bandpass filtering around 40 MHz, then squaring the resulting signal and low pass filtering, this can be performed analogically before sampling or digitally during processing. If the frequency difference between the two 40 MHz signals can not be obtained, then the following system of equations can be solved for the velocity components

$$\begin{bmatrix} U \\ V - V_s \\ W \end{bmatrix} = \begin{bmatrix} -1 & 0 & 0 \\ \cos\frac{\alpha}{2} & \frac{\mp \sin(\phi/2 - \theta)}{\sin \alpha/2 \cos \phi/2} & \frac{\cos \theta}{\cos \phi/2} \\ 0 & \frac{\mp \cos(\phi/2 - \theta)}{\sin \alpha/2 \cos \phi/2} & \frac{\sin \theta}{\cos \phi/2} \end{bmatrix} \begin{bmatrix} \lambda_{BD}(f - 80MHz) \\ \lambda_{AB}(f - 40MHz) \\ \lambda_{AC}(f - 30MHz) \end{bmatrix} \quad [2.68]$$

In the equation above the minus sign (-) refers to the Doppler frequency from eqn [2.62] and the plus sign (+) to eqn [2.63]. For the single color system additional signals around 10 MHz and 70 MHz (eqns. 2.65,2.66) are present. With these two equations and the U velocity component calculated from one of the system of equations above, a second set of estimates for the V and W velocity components can be obtained. The two sets of estimates can then be averaged.

2.4.1 Uncertainty Analysis

An uncertainty analysis can be performed on the velocity estimates calculated from the equations above using a method given in Holman (1984).

We wish to estimate the uncertainty in the result R on the basis of the uncertainties in the primary measurements. The result R is a given function of independent variables $x_1, x_2, ..., x_n$. Thus,

$$R = R(x_1, x_2, ..., x_n) \qquad [2.69]$$

The uncertainty in R, w_R, given the uncertainty in the independent variables, $w_1, w_2, ..., w_n$, is given by

$$w_R = \left[\left(\frac{\partial R}{\partial x_1} w_1 \right)^2 + \left(\frac{\partial R}{\partial x_2} w_2 \right)^2 + ... + \left(\frac{\partial R}{\partial x_n} w_n \right)^2 \right]^{1/2} \qquad [2.70]$$

It should be noted that the uncertainty in the independent variables for this uncertainty analysis method are at the same given odds and that the variables are assumed to be normally distributed. The partial derivatives in the equation [2.70] above can be approximated by

$$\frac{\partial R}{\partial x_i} \simeq \frac{R(x_1, x_2, ..., x_i + \Delta x_i, ...x_n) - R(x_1, x_2, ..., x_i, ...x_n)}{\Delta x_i} \qquad [2.71]$$

This is useful when the data reduction is rather complicated and the analytical derivatives are difficult to derive.

The uncertainty analysis described above will be applied to the two color RSLDV setup with velocity estimates calculated from equation [2.67]. For illustrative purposes the following setup parameters will be used.

Beam intersection angles:

$\alpha = 6° \pm 0.5\ \%$

$$\phi = 10^\circ \pm 0.5\ \%$$

Fringe spacings:

$$\lambda_{BD} = 2.46\ \mu\text{m} \pm 0.1\ \%$$

$$\lambda_{AB} = \lambda_{AD} = 4.92\ \mu\text{m} \pm 0.1\ \%$$

$$\lambda_{AC} = 2.8\ \mu\text{m} \pm 0.1\ \%$$

Scan velocity

$$V_s = 60 \pm 0.05\ \text{m/s}$$

and the scan angle will be taken as:

$$\theta = 0^\circ \pm 0.01^\circ$$

We will consider a case where the signal-to-noise ratio (SNR) of the PMT signal is 20 dB and signal processing is performed via the fast Fourier trasnform (FFT) with zero-padding and log-parabolic interpolation algorithm (see chapter 4) with 1024 points in the data set. The uncertainty in the frequency estimates based on this algorithm and SNR is $\pm$10 KHz. The laser wavelengths and the Bragg cell frequencies are known with enough accuracy that they make negligible contribution to the overall velocity uncertainties.

For this analysis we consider the flowfield around a wing-body junction flow, from which we can determine a worst case and best case senario. The worst case will occur for the following velocity componets:

U = $\pm$30 m/s, V = -2 m/s, and W = 16 m/s

and the best case will be for:

U = 0 m/s, V = 2 m/s, and W = 0 m/s

The partial derivatives of the velocity estimates from eqn. [2.67] were calculated analytically with respect to the variables α, ϕ, θ, λ_{BD}, λ_{AB}, λ_{AC}, f, and V_s . Using the values given above for independent variables and their uncertainties in eqn. [2.70] we can calculate the worst and best case uncertainties in the velocity component estimates. For the worst case we obtain the following results:

U = 30 $\pm$0.04 m/s

V = -2 $\pm$0.1 m/s

W = 16 $\pm$0.47 m/s

and at best the uncertainties will be

U = 0 $\pm$0.02

V = 2 $\pm$0.1 m/s

W = 0 $\pm$0.47 m/s

However, through careful calibration it may be possible to reduce these uncertainties in the velocity estimates to some degree.

3.0 Data Acquisition and Control System

Ideally, in a scanning LDV system one needs to know the exact position of the measurement volume at the time when a "validated" velocity measurement is detected. Since the PMT signal contains six Doppler frequencies in high noise, this precludes the use of an online signal processing system. Therefore, the PMT signal needs to be digitized and stored, along with the position of the measurement volume, for later processing. Figure 14 shows the general layout for such a data acquisition and control system, each of the elements are described below.

3.1 IBM PC-RT Computer

The computer features a 32 bit RISC (Reduced Instruction Set Computer) technology CPU, 16 Megabytes of fast memory and AT compatible data bus and

card slots. The machine runs under AIX 2.2.1 which is a UNIX based operating system. Two 400 MB DASD (Direct Access Storage Device) drives and a 1.25 gigabyte optical disk drive are connected to the RT via a SCSI (Small Computer Systems Interface) adapter. The two DASD drives provide online storage of LDV data during data acquisition and the optical disk drive provides permanent storage of the LDV data. Sustained data write rates of up to 500 KB/sec are possible using the DASD drives and the SCSI interface.

A National Instruments PC III GPIB adapter provides an interface between the two transient recorders. Data transfer rates of up to 1 MB/sec are possible over this adapter.

3.2 Transient Recorders

Both transient recorders, from the LeCroy corporation, have the TR8828c digitizer. This digitizer samples at 200 mega-samples/sec with 8 bit resolution and 100 MHz bandwidth. The transient recorder used to record the PMT signal has 16 MB of memory, the other transient recorder has 32 KB of memory and is used to record the position output from the scanner control.

3.3 *Array Processor*

The array processor is a ZIP 3232-20 from Mercury Computer Systems. This system features 20 MFLOP performance, 2 MB of fast memory and a 40 MB/sec data way. Built in software routines are callable from fortran and new algorithms can be programmed via a software interface. A 1024 point real (non-complex data) FFT (fast Fourier transform) can be computed on this system in 1.3 msecs.

3.4 *Data Acquisition Procedure*

The whole data acquisition procedure is designed to minimize the amount of time required to gather a statistically significant record length, about 5 seconds or more of data. This is done so that variations in the tunnel properties can be minimized during the data acquisition procedure. A total of 80 transient recorder records are taken, this is about 1.25 gigabytes of data.

The RT computer controls the entire data acquisition and transfer process. Both transient recorders are triggered at the same time when the measurement volume is beginning a scan. Data is taken continuously until the transient recorder sampling the PMT signal has filled the 16 MB of memory, which sends a memory full signal to the RT over the GPIB interface. The RT then reads the

memory from the transient recorder and writes this data to a file on the DASD disks; this operation takes approximately one minute to complete. Once the entire 16 MB of memory has been transferred, the RT reads the memory of the other transient recorder containing the scan position and writes this data to a file. The whole process is repeated until the desired number of records has been obtained.

The files are stored with a sequential type file name, so the order of the files can be maintained. Also stored at the beginning of each file is the system time so that the exact time of each velocity realization can be easily determined. The data can be stored permanently to the optical disk once all the data has been collected; more data can be taken at another scan location or the data can be processed.

Using one of the signal processing algorithms, outlined in the next chapter, the data is read from disk and transferred to the array processor to determine the velocity of any Doppler bursts in the record. During processing, the computer keeps track of the time and location of each velocity measurement.

4.0 Low SNR Signal Processing Algorithms

The goal in designing the RSLDV system is to obtain near "instantaneous" velocity profiles. The nature of the signals produced by this system precluded the use of an online system. In order to obtain continuous velocity profiles and to maximize the use of the vast amounts of data stored, low signal-to-noise ratio signals need to be processed.

The SNR of the output signal from the photo detector is influenced by several factors. The size of the particle and its ratio to the fringe spacing greatly influences the signal level and quality seen by the photo detector (Durst, *et al.* 1981). Another primary factor affecting the SNR is the laser power density in the measurement volume and the fringe visibility, given by

$$\eta = \frac{I_{max} - I_{min}}{I_{max} - I_{min}}$$

If more than one particle is present in the measurement volume at a time, constructive and destructive interference of the scattered light will occur at the

photo detector surface leading to a degradation of the signal. Also, it is important to have the optics properly aligned and clean to avoid loss or reduction in signal quality. Figure 15 shows some simulated LDV bursts at various SNR levels.

Time domain processor, such as the frequency counter, operate reliably at high SNR usually well above 20 dB. Frequency counters operate by using a high speed clock to count the number of level crossing of the signal in a fixed gate time or the time for a set number of level crossings. The determination of level crossings are impacted by the presence of noise and can produce false counts (Durst, *et al.* 1981).

In order to obtain accurate frequency estimates, frequency domain (non-parametric) or parametric modeling in the time domain processing must be used. Processing in the frequency domain offers considerable appeal to the experimentalist from the standpoint of speed of computation and familiarity. The fast Fourier transform (FFT) algorithm has been effectively applied for the past 25 years and has become a fixture in the processing of LDV data. The FFT calculates a harmonically related set of sinusoidal components of an order equal to the number of data points in the data set. For example, a 128 point data set yields 64 equally spaced frequency components each having a single statistical degree of freedom. Thus, to improve the quality ensemble averaging is implied. This is typically not available or desirable.

In the time domain (parametric methods) *a priori* assumption of the deterministic content of the signal is made. The nature of the content is assessed

based on analysis or knowledge of the process producing the signals thereby increasing the available statistical degrees of freedom.

One problem with parametric methods is the need to specify the order of the model which most accurately describes the time series data. Inappropriate model order specification can result in spectral estimates neglecting signal content if specified too low or false or nonexistant spectral estimates if the model order is specified too high. This can lead to problems for subsequent analysis of the data based on poor model order specification. With frequency domain techniques model determination is not a problem since the order is implicitly implied by the number of data points in the data set.

The most commonly used non-parametric method is the Fourier transform usually computed by the fast Fourier transform (FFT). The FFT is employed in Doppler frequency estimation in conjunction with some interpolation scheme, the capabilities and limits of the FFT with several interpolation schemes are explored below. Parametric techniques make up two classes, autoregressive (AR) based methods and direct parameter estimation techniques. Autoregressive methods work best with wideband signals in noise and tend to produce better spectral shapes, but are not as good at locating spectral peaks as compared to direct parameter estimation methods (Marple, 1986). Direct parameter estimation methods work best with narrowband signals in noise, LDV signals fall into this class; the Pisarenko harmonic decomposition (PHD) falls into this class of spectral methods. The PHD has the ultimate resolution for sinusoids in noise.

4.1 Discussion of Techniques Studied

The fast Fourier transform (FFT) algorithm with various interpolation methods and the Pisarenko harmonic decomposition (PHD) algorithm are investigated for processing LDV signals. The FFT is studied here since it is becoming a widely used technique for processing LDV signals. We would like to know its limits and capabilities in more detail, and study the performance of the various interpolation schemes. Also, the FFT can be used as a standard to compare with other processing techniques.

The PHD is investigated since it is computationally faster than the FFT. Also, the PHD has the ultimate resolution for sinusoids in white noise (Kay and Marple, 1981), which can be viewed as an approximation to most LDV signals.

4.1.1 Fast Fourier Transform

The Fourier transform of a record $x(t)$ is given by

$$X(f) = \int_{-\infty}^{\infty} x(t)e^{(-j2\pi ft)}\,dt \qquad [4.1]$$

For a stationary random process, the transform $X(f)$ will not exist. However, by restricting the limits to a finite time interval, then the finite-range Fourier transform will exist, given by

$$X(f) = \int_0^T x(t)e^{(-j2\pi ft)}\,dt \qquad [4.2]$$

If the process is digitally sampled at some sample rate Δt, then the discrete version of eqn [4.2] is

$$X(f,T) = \Delta t \sum_{n=0}^{N-1} x_n \exp[-j2\pi fn\Delta t] \qquad [4.3]$$

This is known as the Discrete Fourier Transform or DFT (Bendat and Piersol, 1986).

The Fast Fourier transform (FFT) is a descriptive term for a number of computationally efficient algorithms for rapid computation of the discrete Fourier transform. The central concept of these algorithms is to divide an N-point DFT into two or more DFTs, which are individually computed and then linearly recombined to obtain the original DFT of the N-point set. These DFTs can also be divided into smaller DFTs of correspondingly smaller subsequences. In general this results in substantial savings in operations over a DFT from N^2 operations to $N \log_2 N$ operations (Marple, 1987).

4.1.1.1 Zero Padding

Zero-padding is a technique to interpolate values between spectral lines of an FFT (or DFT) by extending the data set by adding a set of zeros before transformation is done. If a data set containing N points is extended by adding a set of N zeros, N frequency components are calculated; N/2 of theses components are the interpolated values halfway between the normally obtained N/2 spectral lines. A common misconception is that zero-padding improves the resolution of the transform since the record is longer; the frequency resolution of the zero-padded transform is still $\Delta f = \frac{1}{T} = \frac{1}{N\Delta t}$. This interpolation technique, though, can help resolve ambiguities due to narrowband signals that lie between spectral lines and enhances the accuracy of estimating the frequency of spectral peaks (Kay and Marple, 1981).

4.1.1.2 Parabolic Fit

A common technique to improve the estimate for the Doppler frequency of an LDV burst is to fit a parabola through the spectral peak and several adjacent spectral lines (Kalb and Crosswy, 1983). The motivation for using a parabola is that it is a symmetric function and simple to evaluate, but it can also be shown to be the logical function to be used. The Fourier transform of a Gaussian function or window is also a Gaussian function or window. Thus, the Fourier transform of a Gaussian LDV burst results in a Gaussian function

centered at the Doppler frequency. Taking the natural logarithm of the spectrum results in a parabola centered at the Doppler frequency.

The estimate for the Doppler frequency is found from the zero-slope intercept of a parabolic regression applied to the largest and the two adjacent spectral lines. Taking $S(f_i)$ as the peak spectral line and $S(f_{i-1})$ and $S(f_{i+1})$ as the preceding and succeeding spectral lines respectively, the estimate for the Doppler frequency $\hat{f}_d$ is found from

$$\hat{f}_d = f_i + \left[\frac{S(f_{i-1}) - S(f_{i+1})}{2\{S(f_{i-1}) + S(f_{i+1}) - 2(f_i)\}} \right] \Delta f \qquad [4.4]$$

where Δf is the resulting frequency resolution with or without zero-padding. The parabolic fit can be applied to either the spectrum or natural log spectrum. The parabolic fit applied to an LDV burst is illustrated in Figure 16 and the log parabolic fit is shown in Figure 17.

4.1.1.3 Algorithm

The LDV signal processing algorithm based on the Fast Fourier transform reads in N data points for processing. The number of data points to be processed can be found by using a burst detection scheme based on energy or the self-correlation coefficients (Appel 1987). However, if the particle density is high enough, near continuous burst can be obtained and a burst detection scheme would not be necessary; this would also improve the resolution along a scan and

maximize the use of the data stored. The size of N can also be based on the mean residence time of a particle in the measurement volume.

The data can then be windowed if necessary to reduce leakage due to side lobes, but this also reduces the resulting resolution (Harris, 1978) so should be done only if two or more of the Doppler frequencies are very close together. The data can then be zero padded by adding a N length vector of zeros. The FFT is then applied to the data to obtain the power spectrum and a spectral peak is found within the specified frequency range. A parabolic fit is applied to this peak via eqn. [4.4], with the option of using the power or natural log power, to estimate the Doppler frequency. The computer program of this algorithm is in appendix A.5.

4.1.2 Pisarenko Harmonic Decomposition

The Pisarenko Harmonic Decomposition (PHD) is a parametric estimation method that assumes that the process consists of sinusoids in additive white noise (Pisarenko, 1973). The sinusoidal frequencies and white noise power is obtained from an eigenvalue analysis of the autocorrelation matrix. The noise power is equal to the minimum eigenvalue of the autocorrelation matrix of appropriate order and the sinusoidal frequencies are computed from the roots of characteristic (eigenfilter) polynomial associated with the minimum eigenvalue (Hayes and Clements, 1986).

To begin the formulation of the Pisarenko Harmonic Decompostion consider a random process of M sinusoids in white noise (Marple, 1987)

$$x(n) = \sum_{i=1}^{M} A_i \exp[j(2\pi f_i nT + \phi_i)] + w(n) \qquad [4.5]$$

where A_i is the amplitude of the sinusoid, ϕ_i is the phase, and $w(n)$ is a zero mean white noise with variance ρ_w. The autocorrelation sequence (ACS) of $x(n)$ is

$$r_{xx}(k) = \sum_{i=1}^{M} P_i \exp(j2\pi f_i kT) + \rho_w \delta(k) \qquad [4.6]$$

The autocorrelation sequence contains information concerning the power and frequency of each sinusoid; note that the white noise only affects the zeroth lag. The autocorrelation matrix $\mathbf{R}_{M+1}$ formed from the ACS will have the form

$$\mathbf{R}_{M+1} = \begin{bmatrix} r_{xx}(0) & \cdots & r_{xx}(M) \\ \vdots & \vdots & \vdots \\ r_{xx}(M) & \cdots & r_{xx}(0) \end{bmatrix}$$

The minimum eigenvalue of $\mathbf{R}_{M+1}$ and associated eigenvector $\mathbf{a}_{M+1}$ correspond to the white noise variance and the reflection coefficients, respectively. This can be expressed as

$$\mathbf{R}_{M+1}\mathbf{a}_{M+1} = \rho_w \mathbf{a}_{M+1} \qquad [4.7]$$

The eigenvector $\mathbf{a}_{M+1}$ associated with the minimum eigenvalue forms the characteristic equation

$$A(z) = \sum_{k=0}^{M} \mathbf{a}_{M+1}(k+1)z^{-k} \qquad [4.8]$$

where $A(z)$ is also known as the eigenfilter of $w(n)$. The roots of the eigenfilter will lie on the unit circle at angles $2\pi f_i T$ for $1 \leq i \leq M$, and hence determine the sinusoidal frequencies.

Once the frequencies have been determined, the sinusoidal powers can be found from

$$\mathbf{FP} = \mathbf{r} \qquad [4.9]$$

where

$$\mathbf{F} = \begin{bmatrix} \cos(2\pi f_1 \Delta t) & \cdots & \cos(2\pi f_M \Delta t) \\ \vdots & & \vdots \\ \cos(2\pi f_1 M \Delta t) & \cdots & \cos(2\pi f_M M \Delta t) \end{bmatrix}$$

$$\mathbf{P} = \begin{bmatrix} P_1 \\ \vdots \\ P_M \end{bmatrix} \quad \text{and} \quad \mathbf{r} = \begin{bmatrix} r_{xx}(1) \\ \vdots \\ r_{xx}(M) \end{bmatrix}$$

and solving the simultaneous set of equations given in [4.9] for the vector $\mathbf{P}$ (Kay and Marple, 1981).

For M real sinusoids in white noise, the ACS must be known for lags of 0 to 2M, 2M roots will be obtained from the eigenfilter.

4.1.2.1 Algorithm

The computer program for the LDV signal processing algorithm employing the Pisarenko Harmonic Decomposition is shown in appendix A.6. A set of N data points are read into memory, these points can be based on the results of a burst detection scheme, but as pointed out above, it is best to process the data in a continuous manner. The data is then bandpass filtered to contain the Doppler frequency of intrest, this can be done in either the time or frequency domain. The bandpass filter is used so that the time domain signal only contains one Doppler signal, this is done to avoid spectral line splitting and to obtain the highest possible resolution.

The model order (L) has to be specified, this is how many sinusoids the algorithm is to find. The autocorrelation sequence for $p = 2L$ lags are computed by

$$r_{xx}(p) = \frac{1}{N} \sum_{i=0}^{N-p-1} x(i+p)x(i)$$

which is a biased autocorrelation estimate. The biased autocorrelation estimate is used since it tends to have less mean-square error than the unbiased estimate

and also guarantees a positive-definite Toeplitz autocorrelation matrix (Kay and Marple, 1981).

The next step is to find the minimum eigenvalue and associated eigenvector of the autocorrelation matrix corresponding to the noise variance and reflection coefficients respectively. A Levinson algorithm is used to solve the following equation for the eigenvalue and eigenvector

$$\mathbf{T}_p \begin{bmatrix} 1 \\ \mathbf{a}_p \end{bmatrix} = \begin{bmatrix} \rho_p \\ \mathbf{0}_p \end{bmatrix}$$

where $\mathbf{T}_p$ is a Hermitian Toeplitz matrix which is the form of the autocorrelation matrix. The eigenvector or reflection coefficients are used in eqn [4.8] to form the characteristic equation or eigenfilter. A rooting program or the quadratic formula, if the model order is of order one, is used to find the roots of the eigenfilter. If necessary the sinusoidal powers can be calculated by solving equation [4.9], this would be needed if the model order used is greater than the number of Doppler frequencies contained in the filtered data, then the largest powered sinusoid would be the Doppler frequency estimate.

4.2 *Comparison of Algorithms Applied to Synthesized LDV Data*

The performance and capabilities of each algorithm will be evaluated with respect to frequency, sampling density, and signal-to-noise ratio. In order to accomplish this, simulated LDV signals with accurately known frequency, duration, and SNR need were used. The signal-to-noise ratio (SNR) is defined here as

$$SNR = 10 \log\left[\frac{\text{mean square of the signal}}{\text{variance of the noise}} \right]$$

The frequencies used in this study are normalized by the sampling frequency as given by

$$f = \frac{f_d}{f_s}$$

The mean error or bias error is given by

$$\varepsilon_b[\hat{f}] = \frac{1}{N} \sum_{i=1}^{N} \frac{\hat{f} - f}{f_s}$$

The root-mean-square error or random error is given by

$$\varepsilon[\hat{f}] = \left[\frac{1}{N-1} \sum_{i=1}^{N} \frac{\hat{f} - f}{f_s} \right]^{1/2}$$

The simulated LDV signals, a sinwave with Gaussian envelope and added white noise, are generated by a FORTRAN subroutine called SIGNAL as shown in appendix A.7. The subroutine generates a sinewave with a given frequency and number of data points, then a Guassian envelope is applied. The mean-square of this signal is found by AVEVAR, from this the mean-square value of the noise necessary to obtain the required SNR is calculated. The noise data is generated by subroutines RAN3 and GASDEV, the data returned is Gaussian distributed in amplitude with the required mean-square white noise. The two signals are superimposed and returned to the calling program. Some signal generated by this program are shown in Figure 15.

4.2.1 Results for FFT

The results for the fast Fourier transform with the various interpolation schemes applied to simulated LDV signals are shown in Figures 18-61.

Figures 18-21 show the RMS frequency error as a function of SNR and the number of sample points, N, at normalized frequency of $f = 0.225$ for the four interpolation schemes. The results for the FFT with parabolic interpolation is

shown in Figure 18, as expected, the RMS error decreases by a factor of about 2 as the number of samples in the data set doubles. The RMS error is also relatively constant with SNR down to 0 to -5 dB, depending on the number of samples, where the RMS error gradually increases. There is an SNR level at which the RMS error rapidly increases for each of the data record lengths, this is due to the signal in the frequency domain disappearring in the noise floor; for N=4096 this SNR value is -16 dB. This point will be considered as the SNR limit for that particular value of N. The results for the FFT with log parabolic interpolation is shown in Figure 19, the RMS error exhibts some of the same trends as the FFT with parabolic fit. However, this method reaches the SNR limit at higher values of SNR, above -10 dB. For SNR levels above the SNR limit this method has lower RMS error than the FFT with parabolic fit by a factor of approximately 3. Figure 20 shows the results for the FFT with zero-padding and parabolic interpolation, the RMS error is an order of magnitude smaller than the error obtained for the FFT with parabolic fit at SNR = 50 dB. However, the random error increases as the SNR decreases converging towards the same level at the SNR limit as compared to the FFT with parabolic fit. The results for the FFT with zero-padding and log parabolic interpoaltion is shown in Figure 21, again, the RMS error is about an order of magnitude smaller at SNR = 50 dB compared to the log parabolic interpolation method and increases to about the same level as the SNR limit is approached.

The bias error for the four schemes as a function of SNR and number of sample points is shown in Figures 22-25. The frequency estimate is biased

toward the nearest spectral line to the Doppler frequency for the methods using a parabolic fit and biased toward the next closest line for methods using the log parabolic fit. The bias error is reduced by factor between two and three by using a log parabolic fit and by an order of magnitude by zero-padding. When the SNR limit is reached for that particular scheme the bias error rapidly diverges.

The computation time for the four interpolation methods are shown in Figures 26-29 as a function of SNR and number of sample points. The results are for the IBM RT-PC with advanced floating point accelerator with DMA (direct memory access) transfere with the normal floating point accelerator. The computation time for all four methods is constant with SNR, the scatter in the data is the result of system overhead. The parabolic and log parabolic methods show no difference in computation time and zero-padding increase the computation time to the value for the next higher N, approximately doubling the time.

Figures 30-37 show the RMS frequency error for the parabolic fit as a function of Doppler frequency normalized by the sampling frequency and number of sample points for selected SNR ratios. Refering to Figure 30, the RMS error is fairly uniform with frequency except where the Doppler frequency corresponds to a FFT bin, resulting in a spike of improved resolution. In the real world, the Doppler frequency will hardly ever lie exactly on a FFT bin or spectral line so this level of resolution will not be realized. As can be seen from Figures 31-37, the random error remains fairly constant with frequency until the SNR ratio is -10 dB or lower. The large scale fluctuations of the RMS error for the

N = 512 at SNR = -10 dB (Figure 36) is due to the signal in the frequency domain being almost equal to the noise floor, thus any variations can raise or suppress the signal in this noise floor. The other curves probably exhibit this behavior but at some other SNR level which does not appear in the cases that have been presented.

Figures 38-45 show the bias error for the parabolic interpolation method as a function of normalized frequency and the number of data points at selected SNR ratios. Refering to Figure 38, the Doppler estimates are biased toward the nearest spectral line and the error is approximately equal to the amount of random error in the frequency estimate. From Figures 39-45, it can be seen that the bias error is nearly constant as the SNR decreases until the SNR limit is reached, then the bias error becomes very large. Also, the bias error shows asymmetry with respect to the half nyquist frequency, $f = 0.5$.

Figures 46-53 show the RMS frequency error for the log parabolic interpolation method as a function of normalized frequency and number of sample points. These results follow the same general trends as those for the parabolic interpolation method. The RMS error is fairly constant with frequency until the SNR limit is reached and spikes of improved resolution occur where the frequency coincides with a FFT bin. Again, the RMS error exhibts large fluctuations for SNR = -10 dB and N = 512 (Figure 52).

The bias error for the log parabolic interpolation method is shown in Figures 54-61 as a function of normalized frequency and number of samples. Again, the same general trends are followed as those observed for the parabolic

fit except that the frequency estimates are biased toward the next closest spectral line.

The bias error observed for the FFT with the various interpolation methods is due to a combination of effects. Probably the two primary factors are the effects of leakage when the signal is not harmonic within the time window and that the parabolic interpolations are using two spectral line on one side of the true frequency and one spectral line from the other side leading a sort of imbalance.

4.2.2 Results for PHD

The results for the Pisarenko harmonic decomposition applied to simulated LDV signals are shown in Figures 62-80. Figure 62 shows the RMS frequency error as a function of SNR and number of sample points. The RMS error is extremely low for high SNR, but increase almost linearly at an order of magnitude per decade. The bias error is approximately zero for SNR above 5 dB, and increases as the SNR falls below this point, as shown in Figure 63. Also the number of sample points does not appear to be a major factor in the bias error. Figure 64 shows the computation time of the PHD algorithm as a function of SNR and number of sample points, and there is a definite dependence on SNR.

Figures 65-72 show the RMS frequency error as a function of normalized frequency and number of sample points for the PHD algorithm. The RMS error is lowest for frequency near half the nyquist and increases for frequencies near

zero and the nyquist, similar results were obtained by Aktar, *et al* (1985) by theoretical analysis and simulation with sinusoids in white noise. The RMS error also shows a somewhat symmetric aspect around half the nyquist frequency. The apparent scatter at higher SNR is due to the affects of the implied Gaussian window, which gets buried in the noise as the SNR decreases.

The bias error as a function of normalized frequency and number of samples for the PHD algorithm is shown in Figures 73-80. The bias error is nearly zero across the frequency range, except for low N at frequencies near zero and the nyquist. Also, the bias error is antisymmetric about the half nyquist frequency. This pattern is followed down to a SNR of 10 dB, below this the bias error increases rapidly, but still exhibits the asymmetry.

4.2.3 Comparison of FFT and PHD

The zero-padding proceedure for the FFT with either the parabolic or log parabolic interpolation scheme, reduces the RMS or random error from a few percent at low SNR to an order of magnitude at high SNR compared to the same interpolation scheme without zero-padding. Also, zero-padding reduces the bias error by the same amount. However, zero-padding increases the computation time by a factor of two.

The log parabolic interpolation method for the FFT provides a factor of 3 improvement in the RMS and bias error at SNR levels above 0 dB compared to the FFT with the parabolic fit. Signals below about -5 dB cannot be processed

with this interpolation method because the signals are not as removed from the noise floor with a log power spectrum.

The PHD algorithm is typically an order of magnitude faster computationally compared to the FFT algorithms. The bias error for the PHD at higher SNR levels is smaller than the bias errors obtained for the FFT algorithms without zero-padding for frequencies away from zero and the nyquist. Only at high SNR levels, above 30 dB, and only at certain frequencies does the PHD algorithm out perform the FFT algorithms with respect to the level of random error. This can be seen in Figure 81, which shows the domain or region at which each algorithm is the most effective. As an example, if the SNR levels from the PMT were at 20 dB then the FFT with zero-padding and log parabolic interpolation would provide the most accurate frequency estimates. As can be seen from Figure 81, the switch points between the two FFT algorithms occurs at the same SNR level regardless of the frequency. However, the dividing line between when to use the PHD algorithm and the FFT with zero-padding and log parabolic interpolation algorithm is dependent on the frequency and the number of sample in the data record. From this map it is possible to tell which algorithm to use if an approximate SNR and frequency is known for the signal to be processed.

5.0 Conclusions and Recommendations for Future Work

5.1 Conclusions

A rapidly scanning three-velocity-component laser Doppler velocimeter has been designed, to obtain near instantaneous velocity profiles in complicated three dimensional flows.

The optical configuration allows the size and location of the measurement volume, as well as all the fringe spacings to be varied freely. The four beams have independent lens and mirror sets to avoid coupling, making system alignment easier, changes made for one beam do not affect another. Path equalization is maintained. Techniques to maintain coincidence between the vertical and horizontal probe volumes were investigated. The lens, plane-mirror pair maintained the highest level of coincidence between the two probe volumes, and

an appropriate lens has been manufactured by a local optician for use with the RSLDV.

Six moving fringe patterns at 10, 30, (2x) 40, 70, and 80 MHz are produced by two Bragg cells for the single color system. For the two color system, moving fringe patterns at 30, (2x) 40, and 80 MHz are produced by the two Bragg cells. The signal around 80 MHz is a direct measurement of the U velocity, and the signal around 30 MHz and the frequency difference between the two 40 MHz signals are used to calculate the V and W velocity components. An uncertainty analysis applied to the system of equations used to calculate the velocity components with a worst case senario, the uncertainties in U, V, and W velocity estimates are ± 0.04 m/s, $\pm$ 0.1 m/s, and ± 0.47 m/s respectively.

A data acquisition, control and processing system has also been designed for use with the RSLDV. The PMT signal is sampled at 200 MB/sec by a transient recorder and the position of the scanner is also recorded by a transient recorder. The data from the transient recorders is transferred over a GPIB interface to a mini-computer for storage, the data transfer rate is at 300 KB/sec. Online storage is provided for up to 1.25 gigabytes of data, this translates into 6 seconds worth of LDV data. Permanent storage is provided by an optical disk drive.

Two algorithms were investigated for processing low signal-to-noise ratio signals for use with the RSLDV. The Pisarenko harmonic decompostion has excellent frequency resolution for high SNR signals, above 30 dB, for frequencies near half the nyquist. The FFT with zero-padding and log parabolic

interpolation is the recommended technique if the SNR for the signal does not fall below -5 dB. For signal with SNR below -5 dB, the FFT with zero-padding and parabolic interpolation gives good performance.

5.2 *Recommendations for Future Work*

Now that an appropriate design has been made for a rapidly scanning three-velocity-component laser Doppler velocimeter, additional optics can be acquired and the system setup. The final setup may require some changes in a few of the configuration parameters, but these adjustments should be minor. The quality of the fringe patterns can then be observed and the system can be calibrated by using a rotating disk. The RSLDV will then be used to investigate some well documented turbulent flows in the Virginia Tech Boundary Layer Wind Tunnel, including some steady and unsteady separated flows and a wing-body junction flow.

Improvements to the optical system should be made on increasing the coincidence between the horizontal and vertical probe volumes. This could be accomplished by using a glass wedge of the proper shape, instead of the current lens, an elliptical or parabolic mirror or by using another scanner to scan the upper beam with a feedback control from the original scanner. By improving the coincidence between the two probe volumes, the size of the measurement volume

can be decreased, leading to improved resolution and higher SNR for the signal from the PMT.

The current seeding technique used in the wind tunnel is atomized DOP, this results in several orders of magnitude number of submicron particles compared to the micron sized particles. This results in more noise and a wider band Doppler signal. Monodispersed polystyrene particles can be produced by a method outlined by Nichols (1987). Using these monodispersed particles would increase the resulting SNR of the LDV signals in the wind tunnel.

The investigation into low SNR signal processing techniques should be continued. Marple (1986) gives an eigenfrequency spectral method known as MUSIC, MUlti SIgnal Classification, that works best for narrowband signals in noise. There are also some new algorithms designed to estimate the frequency of sinusoids in high amount noise (Kay and Marple, 1981).

In an extension to the current design of the RSLDV, a pockel cell can be placed just after the Bragg cells. This permits two parallel scan lines that are separated by a small distance, ΔX (about 6 mm), in the freestream direction. The pockel cell is switched on and off, synchronized with the up-and-down scanning of the measurement volume. The measurement volume is scanned up at one x_1 location while scanning down at an other x_2 location. This permits information on the streamwise changes in the flow to be obtained. Two separate PMTs would be needed in this arrangement.

References

Aktar, M., Sankur, B., and Istefanopulos, Y., "Properties of the Maximum Likelihood and Pisarenko Spectral Estimiates", *Signal Processing, vol. 8*, 1985.

Antoine, M., "A Rapidly Scanning Three-Velocity-Component Laser Doppler Anemometer", *MS Thesis, Dept. of Aerospace and Ocean Eng., VPI & SU*, Blacksburg, VA, 1985.

Antoine, M. and Simpson, R.L. , "A Rapidly Scanning Three-Velocity-Component Laser Doppler Anemometer", *J. Physics E: Sci. Inst., 19*, pp. 853-858, 1986.

Appel, J., "Structure of Data Processing System for Laser Anemometry" , *The Use of Computers in Laser Velocimetry, Inst. St. Louis Report R/05/87*, H.J. Pfeifer and B. Jaeggy, editors, 1987.

Arik, E. and Buchhave, P., "LDA Burst Spectrum Analyzer", *12th International Congress on Instrumentation in Aerospace Simulation Facilities*, Williamsburg, VA, 1987.

Baker, G.D., Murphy, R.J., and Meyers, J.F., "Development of an Adaptive LDV Signal Processor", *AIAA/NASA/AFWAL Conference on Sensors and Measurement Techniques for Aeronautical Applications*, Atlanta, GA, 1988.

Bendat, J.S., and Piersol, A.G., *Random Data Analysis and Measurement Procedures, 2nd ed.*, John Wiley and Sons, New York, 1986.

Bendick, P.J., "A Laser Doppler Velocimeter to Measure Instantaneous Velocity Profiles", *Proc. Flow Symposium*, Pittsburgh, PA, 1971.

Chehroudi, B. and Simpson, R.L., "A Rapidly Scanning Laser Doppler Anemometer", *Report WT-7, Dept. Civil/Mechanical Engr.*, Southern Methodist Univ., Dallas, Tx 75275: DTIS Report, 1983.

Durst, F., Lehmann, B., and Tropea, C., "Laser Doppler Systems for Rapid Scanning of Flow Fields", *Rev. Sci Instr., vol 52*, pp 1076-1681, 1981.

Durst, F., Melling, A., and Whitelaw, J.H., *Principles and Practices of Laser Doppler Anemometry*, 2nd ed., Academic Press, New york, 1981.

Econonou, M., "Design and Performance of a Scanning Laser Doppler Velocimeter", *MS Thesis, Mech. Eng., Ill. Inst Tech.*, Chicago, 1986.

Gartell, L.R., and Jordan, F.J., "Demonstration of a Rapid-Scan Two-Dimensional Laser Velocimetry in the Langley Vortex Research Facility for Research in Aerial Applications", *NASA TM-74081*, 1977.

Grant, G.R., and Orloff, K.L., "Two-Color Dual-Beam Backscatter Laser Doppler Velocimeter", *J. of Applied Optics, vol 12*, pp. 2913-2916, 1973.

Harris, F.J., "On the Use of Windows for Harmonic Analysis with the Discrete Fourier Transform", *Proc. IEEE, vol. 66, no. 1*, 1978.

Hayes, M.H., and Clements, M.A., "An Efficient Algorithm for Computing Pisarenko's Harmonic Decomposition Using Levinson's Recursion", *IEEE Trans. ASSP, vol ASSP-34, no 3*, 1986.

Holman, J.P., *Experimnetal Methods for Engineers*, McGraw-Hill, New York, 1984.

Kalb, H.T., and Crosswy, F.L., "Discrete Fourier Transform Signal Processor for Laser-Doppler Anemometry", *AEDC-TR-83-46*, Arnold Engineering Development Center AAFS, Tennessee, 1983.

Kay, S.M., and Marple, S.L., "Spectrum Analysis - A Modern Perspective", *Proc. IEE, vol 69*, pp 1380-1419, 1981.

Kraft, D., Oberpfaffenhofen, D., Schittkowski, K., "Sequentail Linear Least Squares Programming", Univ. Wuerzburg, 1981.

Lading, L., "Spectrum Analysis of LDA Signals", *The Use of Computers in Laser Velocimetry, Inst. St. Louis Report R/05/87*, H.J. Pfeifer and B. Jaeggy, editors, 1987.

Marple, S.L., Jr., *Digital Spectral Analysis with Applications*, Prentice Hall, New Jersey, 1987.

Matovic, D., Tropea, I.C., and Martinuzzi, R., "Frequency Estimation of LDA Signals by Model Parametric Estimation", *The Use of Computers in Laser Velocimetry, Inst. St. Louis Report R/05/87*, H.J. Pfeifer and B. Jaeggy, editors, 1987.

Optics Guide 4, Melles Griot, 1988.

Meyers, J.F., "Application of Laser Velovimetry to Large Scale and Specialized Aerodynamic Tests", *TST Quart., vol 5, iss 4*, pp 5-12, 1979.

Nakatani, N., Yorisue, R., and Yamada, T., "Simultaneous Measurements of Flow Velocities in Multipoint by the Laser Doppler Velocimeter", *Proc. Dynamic Flow Conf.*, pp 583-590, Marseille-Baltimore, 1978.

Nichols, C.E., Jr., "Preparation of Polystyrene Microspheres for Laser Velocimetry in Wind Tunnels", , *NASA TM 89163*, 1987.

Orloff, K.L., and Biggers, J.C., "Laser Velocimeter Measurements of Developing and Periodic Flows", *Proc. 2nd Int. Workshop on LDV, 2*, pp 143-168, Purdue University, 1974.

Orloff, K.L., Corsiglia, V.R., Biggers, J.C., and Ekstedt, T.W., "The Accuracy of Flow Measurements by Laser Doppler Methods", *Proc. LDA Symp.*, pp 624-643, Copenhagen, 1975.

Owen, F.K., "A Scanning Laser Velocimeter for Turbulence Research", *NASA Contractor Report 172493*, 1984.

Pisarenko, V.F., "The Retrieval of Harmonics from a Covariance Function", *Geophys. J. Roy. Astron. Soc.*, pp 347-366, 1973.

Press, W.H., Flannery, B.P., Teukolsky, S.A., and Vetterling, W.T., *Numerical Recipes The Art of Scientific Computing*, Cambridge University Press, New York, 1986.

Rhodes, D.B., "Optical Scanning Systems for Laser Velocimeter", *SPIE, vol 84*, pp 78-84, 1976.

Simpson, R.L., "Scanning Laser Anemometry and Other Measurement Techniques for Separated Flows", *Advances in Fluid Mechanics Measurements Lecture Notes in Engineering*, Vol. 45, pp. 357-400, ed. M. Gad-el-Hak, Springer-Verlag, New York, 1989.

Swart, P.L., Venter, C-V., and Vander Merwe, D.F., "Parametric Spectral Estimation Applied to Laser Anemometry", *3rd Int. Symp. on Appl. of Laser Anemometry to Fluid Mech.*, Lisbon, Portugal, 1986.

Yariv, A., *Optical Electronics*, Holt, Rinehart and Winston, Inc., New York, 1985.

Tables

Table 1. Characteristic Dimension of the RSLDV Optics

Components	Parameter	Value
Mirrors M1, M2	size	35 mm x 35 mm
Mirrors M3 - M5	size	22 mm x 22 mm
Scanner Mirror SM	size	24 mm x 21 mm
Mirrors M6 - M14	size	25 mm x 254 mm
Lenses L1	focal length	100 mm
d_{12}	distance between L1 and L2	900 mm
Lenses L2	focal length	800 mm
d_{23}	distance between L2 and L3	800 mm
Lenses L3	focal length	100 mm
d_{34}	distance between L3 and L4	181 mm
Lenses L4	focal length	80 mm
d_{4p}	distance from L4 to probe volume	4.960 m

Table 2. Optimization Results for Plane Mirror Pair

$\phi = 10.0$
$\theta_0 = 0.0$

F	θ_1 (deg)	θ_2 (deg)	d_1 (m)	d_2 (m)
$.1114 \times 10^{-03}$	55.000	50.000	2.250	2.155
$.1302 \times 10^{-03}$	56.000	51.000	2.250	2.144
$.1516 \times 10^{-03}$	57.000	52.000	2.250	2.133
$.1762 \times 10^{-03}$	58.000	53.000	2.250	2.121
$.2043 \times 10^{-03}$	59.000	54.000	2.250	2.109
$.2366 \times 10^{-03}$	60.000	55.000	2.250	2.096
$.2737 \times 10^{-03}$	61.000	56.000	2.250	2.083
$.3165 \times 10^{-03}$	62.000	57.000	2.250	2.069
$.3660 \times 10^{-03}$	63.000	58.000	2.250	2.054
$.4233 \times 10^{-03}$	64.000	59.000	2.250	2.038
$.4901 \times 10^{-03}$	65.000	60.000	2.250	2.021
$.5682 \times 10^{-03}$	66.000	61.000	2.250	2.003
$.6600 \times 10^{-03}$	67.000	62.000	2.250	1.983
$.7684 \times 10^{-03}$	68.000	63.000	2.250	1.962
$.8975 \times 10^{-03}$	69.000	64.000	2.250	1.939
$.1052 \times 10^{-02}$	70.000	65.000	2.250	1.914
$.1239 \times 10^{-02}$	71.000	66.000	2.250	1.886
$.1466 \times 10^{-02}$	72.000	67.000	2.250	1.855
$.1746 \times 10^{-02}$	73.000	68.000	2.250	1.821
$.2096 \times 10^{-02}$	74.000	69.000	2.250	1.782
$.2538 \times 10^{-02}$	75.000	70.000	2.250	1.737
$.3105 \times 10^{-02}$	76.000	71.000	2.250	1.686
$.3849 \times 10^{-02}$	77.000	72.000	2.250	1.625
$.4845 \times 10^{-02}$	78.000	73.000	2.250	1.553
$.6218 \times 10^{-02}$	79.000	74.000	2.250	1.466
$.8174 \times 10^{-02}$	80.000	75.000	2.250	1.358
$.1108 \times 10^{-01}$	81.000	76.000	2.250	1.219
$.1566 \times 10^{-01}$	82.000	77.000	2.250	1.034
$.2340 \times 10^{-01}$	83.000	78.000	2.250	.776
$.3801 \times 10^{-01}$	84.000	79.000	2.250	.388
$.7050 \times 10^{-01}$	85.000	80.000	2.250	-.262
$.1672 \times 10^{+00}$	86.000	81.000	2.250	-1.582
$.7384 \times 10^{+00}$	87.000	82.000	2.250	-5.721
$.1522 \times 10^{+03}$	88.000	83.000	2.250	115.484
$.5997 \times 10^{+00}$	89.000	84.000	2.250	9.281

$\phi = 15.0$
$\theta_0 = 0.0$

F	θ_1 (deg)	θ_2 (deg)	d_1 (m)	d_2 (m)
$.2830 \times 10^{-03}$	55.000	47.500	2.250	2.104
$.3168 \times 10^{-03}$	56.000	48.500	2.250	2.087
$.3548 \times 10^{-03}$	57.000	49.500	2.250	2.069
$.3978 \times 10^{-03}$	58.000	50.500	2.250	2.050
$.4465 \times 10^{-03}$	59.000	51.500	2.250	2.030
$.5018 \times 10^{-03}$	60.000	52.500	2.250	2.009
$.5651 \times 10^{-03}$	61.000	53.500	2.250	1.986
$.6376 \times 10^{-03}$	62.000	54.500	2.250	1.963
$.7212 \times 10^{-03}$	63.000	55.500	2.250	1.937
$.8180 \times 10^{-03}$	64.000	56.500	2.250	1.910
$.9308 \times 10^{-03}$	65.000	57.500	2.250	1.880
$.1063 \times 10^{-02}$	66.000	58.500	2.250	1.848
$.1219 \times 10^{-02}$	67.000	59.500	2.250	1.813
$.1406 \times 10^{-02}$	68.000	60.500	2.250	1.775
$.1629 \times 10^{-02}$	69.000	61.500	2.250	1.733
$.1901 \times 10^{-02}$	70.000	62.500	2.250	1.685
$.2235 \times 10^{-02}$	71.000	63.500	2.250	1.632
$.2650 \times 10^{-02}$	72.000	64.500	2.250	1.572
$.3176 \times 10^{-02}$	73.000	65.500	2.250	1.502
$.3852 \times 10^{-02}$	74.000	66.500	2.250	1.422
$.4740 \times 10^{-02}$	75.000	67.500	2.250	1.326
$.5938 \times 10^{-02}$	76.000	68.500	2.250	1.212
$.7604 \times 10^{-02}$	77.000	69.500	2.250	1.071
$.1001 \times 10^{-01}$	78.000	70.500	2.250	.894
$.1366 \times 10^{-01}$	79.000	71.500	2.250	.663
$.1955 \times 10^{-01}$	80.000	72.500	2.250	.348
$.2997 \times 10^{-01}$	81.000	73.500	2.250	-.107
$.5097 \times 10^{-01}$	82.000	74.500	2.250	-.823
$.1034 \times 10^{+00}$	83.000	75.500	2.250	-2.125
$.3036 \times 10^{+00}$	84.000	76.500	2.250	-5.238
$.3374 \times 10^{+01}$	85.000	77.500	2.250	-22.671
$.2019 \times 10^{+01}$	86.000	78.500	2.250	21.483
$.2683 \times 10^{+00}$	87.000	79.500	2.250	9.240
$.1016 \times 10^{+00}$	88.000	80.500	2.250	6.537
$.5343 \times 10^{-01}$	89.000	81.500	2.250	5.347

$\phi = 20.0$
$\theta_0 = 0.0$

F	θ_1 (deg)	θ_2 (deg)	d_1 (m)	d_2 (m)
$.4769 \times 10^{-03}$	55.000	45.000	2.250	2.048
$.5278 \times 10^{-03}$	56.000	46.000	2.250	2.023
$.5851 \times 10^{-03}$	57.000	47.000	2.250	1.997
$.6501 \times 10^{-03}$	58.000	48.000	2.250	1.969
$.7239 \times 10^{-03}$	59.000	49.000	2.250	1.939
$.8083 \times 10^{-03}$	60.000	50.000	2.250	1.908
$.9052 \times 10^{-03}$	61.000	51.000	2.250	1.874
$.1017 \times 10^{-02}$	62.000	52.000	2.250	1.838
$.1147 \times 10^{-02}$	63.000	53.000	2.250	1.798
$.1300 \times 10^{-02}$	64.000	54.000	2.250	1.756
$.1480 \times 10^{-02}$	65.000	55.000	2.250	1.709
$.1694 \times 10^{-02}$	66.000	56.000	2.250	1.657
$.1951 \times 10^{-02}$	67.000	57.000	2.250	1.599
$.2264 \times 10^{-02}$	68.000	58.000	2.250	1.535
$.2649 \times 10^{-02}$	69.000	59.000	2.250	1.462
$.3130 \times 10^{-02}$	70.000	60.000	2.250	1.379
$.3740 \times 10^{-02}$	71.000	61.000	2.250	1.283
$.4530 \times 10^{-02}$	72.000	62.000	2.250	1.171
$.5577 \times 10^{-02}$	73.000	63.000	2.250	1.037
$.7003 \times 10^{-02}$	74.000	64.000	2.250	.874
$.9014 \times 10^{-02}$	75.000	65.000	2.250	.672
$.1197 \times 10^{-01}$	76.000	66.000	2.250	.413
$.1658 \times 10^{-01}$	77.000	67.000	2.250	.069
$.2430 \times 10^{-01}$	78.000	68.000	2.250	-.413
$.3873 \times 10^{-01}$	79.000	69.000	2.250	-1.136
$.7050 \times 10^{-01}$	80.000	70.000	2.250	-2.349
$.1642 \times 10^{+00}$	81.000	71.000	2.250	-4.811
$.7122 \times 10^{+00}$	82.000	72.000	2.250	-12.533
$.1442 \times 10^{+03}$	83.000	73.000	2.250	213.565
$.5587 \times 10^{+00}$	84.000	74.000	2.250	15.454
$.1502 \times 10^{+00}$	85.000	75.000	2.250	9.120
$.6889 \times 10^{-01}$	86.000	76.000	2.250	6.914
$.3953 \times 10^{-01}$	87.000	77.000	2.250	5.790
$.2569 \times 10^{-01}$	88.000	78.000	2.250	5.108
$.1807 \times 10^{-01}$	89.000	79.000	2.250	4.649

$\phi = 10.0$
$\theta_0 = 5.0$

F	θ_1 (deg)	θ_2 (deg)	d_1 (m)	d_2 (m)
$.2142 \times 10^{-05}$	55.000	47.500	2.000	1.965
$.2150 \times 10^{-05}$	56.000	48.500	2.025	1.987
$.2191 \times 10^{-05}$	57.000	49.500	2.050	2.010
$.2166 \times 10^{-05}$	58.000	50.500	2.050	2.005
$.2142 \times 10^{-05}$	59.000	51.500	2.075	2.028
$.2172 \times 10^{-05}$	60.000	52.500	2.100	2.051
$.2192 \times 10^{-05}$	61.000	53.500	2.100	2.046
$.2142 \times 10^{-05}$	62.000	54.500	2.125	2.070
$.2187 \times 10^{-05}$	63.000	55.500	2.150	2.094
$.2187 \times 10^{-05}$	64.000	56.500	2.150	2.089
$.2145 \times 10^{-05}$	65.000	57.500	2.175	2.114
$.2266 \times 10^{-05}$	66.000	58.500	2.200	2.139
$.2152 \times 10^{-05}$	67.000	59.500	2.200	2.134
$.2200 \times 10^{-05}$	68.000	60.500	2.225	2.159
$.2203 \times 10^{-05}$	69.000	61.500	2.225	2.154
$.2162 \times 10^{-05}$	70.000	62.500	2.250	2.181
$.2295 \times 10^{-05}$	71.000	63.500	2.250	2.175
$.3104 \times 10^{-05}$	72.000	64.500	2.250	2.169
$.4817 \times 10^{-05}$	73.000	65.500	2.250	2.162
$.7745 \times 10^{-05}$	74.000	66.500	2.250	2.155
$.1232 \times 10^{-04}$	75.000	67.500	2.250	2.147
$.1916 \times 10^{-04}$	76.000	68.500	2.250	2.138
$.2914 \times 10^{-04}$	77.000	69.500	2.250	2.127
$.4356 \times 10^{-04}$	78.000	70.500	2.250	2.115
$.6436 \times 10^{-04}$	79.000	71.500	2.250	2.101
$.9459 \times 10^{-04}$	80.000	72.500	2.250	2.085
$.1391 \times 10^{-03}$	81.000	73.500	2.250	2.065
$.2061 \times 10^{-03}$	82.000	74.500	2.250	2.041
$.3101 \times 10^{-03}$	83.000	75.500	2.250	2.010
$.4785 \times 10^{-03}$	84.000	76.500	2.250	1.971
$.7677 \times 10^{-03}$	85.000	77.500	2.250	1.916
$.1308 \times 10^{-02}$	86.000	78.500	2.250	1.838
$.2455 \times 10^{-02}$	87.000	79.500	2.250	1.714
$.5464 \times 10^{-02}$	88.000	80.500	2.250	1.490
$.1749 \times 10^{-01}$	89.000	81.500	2.250	.953

$\phi = 15.0$
$\theta_0 = 5.0$

F	θ_1 (deg)	θ_2 (deg)	d_1 (m)	d_2 (m)
$.3236 \times 10^{-04}$	55.000	45.000	2.250	2.198
$.3716 \times 10^{-04}$	56.000	46.000	2.250	2.190
$.4262 \times 10^{-04}$	57.000	47.000	2.250	2.182
$.4884 \times 10^{-04}$	58.000	48.000	2.250	2.173
$.5594 \times 10^{-04}$	59.000	49.000	2.250	2.165
$.6406 \times 10^{-04}$	60.000	50.000	2.250	2.155
$.7336 \times 10^{-04}$	61.000	51.000	2.250	2.146
$.8403 \times 10^{-04}$	62.000	52.000	2.250	2.136
$.9634 \times 10^{-04}$	63.000	53.000	2.250	2.125
$.1106 \times 10^{-03}$	64.000	54.000	2.250	2.113
$.1271 \times 10^{-03}$	65.000	55.000	2.250	2.101
$.1464 \times 10^{-03}$	66.000	56.000	2.250	2.088
$.1690 \times 10^{-03}$	67.000	57.000	2.250	2.074
$.1956 \times 10^{-03}$	68.000	58.000	2.250	2.059
$.2272 \times 10^{-03}$	69.000	59.000	2.250	2.042
$.2650 \times 10^{-03}$	70.000	60.000	2.250	2.024
$.3106 \times 10^{-03}$	71.000	61.000	2.250	2.004
$.3660 \times 10^{-03}$	72.000	62.000	2.250	1.982
$.4341 \times 10^{-03}$	73.000	63.000	2.250	1.957
$.5190 \times 10^{-03}$	74.000	64.000	2.250	1.929
$.6261 \times 10^{-03}$	75.000	65.000	2.250	1.897
$.7634 \times 10^{-03}$	76.000	66.000	2.250	1.860
$.9432 \times 10^{-03}$	77.000	67.000	2.250	1.816
$.1184 \times 10^{-02}$	78.000	68.000	2.250	1.765
$.1514 \times 10^{-02}$	79.000	69.000	2.250	1.702
$.1985 \times 10^{-02}$	80.000	70.000	2.250	1.624
$.2684 \times 10^{-02}$	81.000	71.000	2.250	1.524
$.3782 \times 10^{-02}$	82.000	72.000	2.250	1.391
$.5640 \times 10^{-02}$	83.000	73.000	2.250	1.205
$.9139 \times 10^{-02}$	84.000	74.000	2.250	.925
$.1691 \times 10^{-01}$	85.000	75.000	2.250	.457
$.4003 \times 10^{-01}$	86.000	76.000	2.250	-.494
$.1764 \times 10^{+00}$	87.000	77.000	2.250	-3.476
$.3627 \times 10^{+02}$	88.000	78.000	2.250	83.842
$.1427 \times 10^{+00}$	89.000	79.000	2.250	7.332

$\phi = 20.0$
$\theta_0 = 5.0$

F	θ_1 (deg)	θ_2 (deg)	d_1 (m)	d_2 (m)
$.1514 \times 10^{-03}$	55.000	42.500	2.250	2.160
$.1666 \times 10^{-03}$	56.000	43.500	2.250	2.146
$.1835 \times 10^{-03}$	57.000	44.500	2.250	2.132
$.2024 \times 10^{-03}$	58.000	45.500	2.250	2.116
$.2237 \times 10^{-03}$	59.000	46.500	2.250	2.100
$.2478 \times 10^{-03}$	60.000	47.500	2.250	2.084
$.2750 \times 10^{-03}$	61.000	48.500	2.250	2.066
$.3061 \times 10^{-03}$	62.000	49.500	2.250	2.047
$.3417 \times 10^{-03}$	63.000	50.500	2.250	2.026
$.3826 \times 10^{-03}$	64.000	51.500	2.250	2.004
$.4300 \times 10^{-03}$	65.000	52.500	2.250	1.981
$.4853 \times 10^{-03}$	66.000	53.500	2.250	1.955
$.5502 \times 10^{-03}$	67.000	54.500	2.250	1.927
$.6271 \times 10^{-03}$	68.000	55.500	2.250	1.897
$.7190 \times 10^{-03}$	69.000	56.500	2.250	1.863
$.8300 \times 10^{-03}$	70.000	57.500	2.250	1.825
$.9657 \times 10^{-03}$	71.000	58.500	2.250	1.782
$.1134 \times 10^{-02}$	72.000	59.500	2.250	1.734
$.1345 \times 10^{-02}$	73.000	60.500	2.250	1.678
$.1616 \times 10^{-02}$	74.000	61.500	2.250	1.614
$.1970 \times 10^{-02}$	75.000	62.500	2.250	1.537
$.2446 \times 10^{-02}$	76.000	63.500	2.250	1.446
$.3104 \times 10^{-02}$	77.000	64.500	2.250	1.333
$.4050 \times 10^{-02}$	78.000	65.500	2.250	1.191
$.5479 \times 10^{-02}$	79.000	66.500	2.250	1.006
$.7779 \times 10^{-02}$	80.000	67.500	2.250	.754
$.1183 \times 10^{-01}$	81.000	68.500	2.250	.389
$.1995 \times 10^{-01}$	82.000	69.500	2.250	-.185
$.4016 \times 10^{-01}$	83.000	70.500	2.250	-1.228
$.1170 \times 10^{+00}$	84.000	71.500	2.250	-3.722
$.1290 \times 10^{+01}$	85.000	72.500	2.250	-17.690
$.7661 \times 10^{+00}$	86.000	73.500	2.250	17.687
$.1010 \times 10^{+00}$	87.000	74.500	2.250	7.879
$.3797 \times 10^{-01}$	88.000	75.500	2.250	5.712
$.1983 \times 10^{-01}$	89.000	76.500	2.250	4.759

$\phi = 10.0$
$\theta_0 = 10.0$

F	θ_1 (deg)	θ_2 (deg)	d_1 (m)	d_2 (m)
$.2202 \times 10^{-05}$	55.000	45.000	1.500	1.478
$.2142 \times 10^{-05}$	56.000	46.000	1.525	1.500
$.2218 \times 10^{-05}$	57.000	47.000	1.550	1.523
$.2143 \times 10^{-05}$	58.000	48.000	1.550	1.519
$.2222 \times 10^{-05}$	59.000	49.000	1.575	1.542
$.2143 \times 10^{-05}$	60.000	50.000	1.575	1.538
$.2253 \times 10^{-05}$	61.000	51.000	1.600	1.562
$.2142 \times 10^{-05}$	62.000	52.000	1.600	1.558
$.2255 \times 10^{-05}$	63.000	53.000	1.600	1.554
$.2152 \times 10^{-05}$	64.000	54.000	1.625	1.579
$.2206 \times 10^{-05}$	65.000	55.000	1.625	1.575
$.2202 \times 10^{-05}$	66.000	56.000	1.650	1.602
$.2155 \times 10^{-05}$	67.000	57.000	1.650	1.597
$.2352 \times 10^{-05}$	68.000	58.000	1.675	1.625
$.2149 \times 10^{-05}$	69.000	59.000	1.675	1.621
$.2240 \times 10^{-05}$	70.000	60.000	1.675	1.616
$.2280 \times 10^{-05}$	71.000	61.000	1.700	1.645
$.2144 \times 10^{-05}$	72.000	62.000	1.700	1.641
$.2386 \times 10^{-05}$	73.000	63.000	1.700	1.636
$.2254 \times 10^{-05}$	74.000	64.000	1.725	1.666
$.2160 \times 10^{-05}$	75.000	65.000	1.725	1.661
$.2573 \times 10^{-05}$	76.000	66.000	1.725	1.656
$.2275 \times 10^{-05}$	77.000	67.000	1.750	1.689
$.2174 \times 10^{-05}$	78.000	68.000	1.750	1.683
$.2784 \times 10^{-05}$	79.000	69.000	1.750	1.677
$.2387 \times 10^{-05}$	80.000	70.000	1.775	1.712
$.2167 \times 10^{-05}$	81.000	71.000	1.775	1.706
$.3007 \times 10^{-05}$	82.000	72.000	1.775	1.699
$.2785 \times 10^{-05}$	83.000	73.000	1.800	1.738
$.2142 \times 10^{-05}$	84.000	74.000	1.800	1.731
$.3227 \times 10^{-05}$	85.000	75.000	1.800	1.721
$.4370 \times 10^{-05}$	86.000	76.000	1.825	1.768
$.2301 \times 10^{-05}$	87.000	77.000	1.825	1.758
$.3434 \times 10^{-05}$	88.000	78.000	1.825	1.744
$.1375 \times 10^{-04}$	89.000	79.000	1.850	1.810

$\phi = 15.0$
$\theta_0 = 10.0$

F	θ_1 (deg)	θ_2 (deg)	d_1 (m)	d_2 (m)
$.2162 \times 10^{-05}$	55.000	42.500	2.100	2.090
$.2143 \times 10^{-05}$	56.000	43.500	2.100	2.087
$.2150 \times 10^{-05}$	57.000	44.500	2.100	2.085
$.2188 \times 10^{-05}$	58.000	45.500	2.100	2.083
$.2195 \times 10^{-05}$	59.000	46.500	2.125	2.109
$.2156 \times 10^{-05}$	60.000	47.500	2.125	2.107
$.2142 \times 10^{-05}$	61.000	48.500	2.125	2.105
$.2160 \times 10^{-05}$	62.000	49.500	2.125	2.103
$.2215 \times 10^{-05}$	63.000	50.500	2.125	2.100
$.2238 \times 10^{-05}$	64.000	51.500	2.150	2.129
$.2177 \times 10^{-05}$	65.000	52.500	2.150	2.127
$.2145 \times 10^{-05}$	66.000	53.500	2.150	2.125
$.2149 \times 10^{-05}$	67.000	54.500	2.150	2.123
$.2198 \times 10^{-05}$	68.000	55.500	2.150	2.120
$.2305 \times 10^{-05}$	69.000	56.500	2.150	2.117
$.2308 \times 10^{-05}$	70.000	57.500	2.175	2.150
$.2213 \times 10^{-05}$	71.000	58.500	2.175	2.148
$.2154 \times 10^{-05}$	72.000	59.500	2.175	2.146
$.2146 \times 10^{-05}$	73.000	60.500	2.175	2.143
$.2208 \times 10^{-05}$	74.000	61.500	2.175	2.140
$.2367 \times 10^{-05}$	75.000	62.500	2.175	2.137
$.2662 \times 10^{-05}$	76.000	63.500	2.175	2.133
$.2482 \times 10^{-05}$	77.000	64.500	2.200	2.174
$.2297 \times 10^{-05}$	78.000	65.500	2.200	2.171
$.2171 \times 10^{-05}$	79.000	66.500	2.200	2.168
$.2151 \times 10^{-05}$	80.000	67.500	2.200	2.164
$.2313 \times 10^{-05}$	81.000	68.500	2.200	2.160
$.2795 \times 10^{-05}$	82.000	69.500	2.200	2.154
$.3855 \times 10^{-05}$	83.000	70.500	2.200	2.147
$.4314 \times 10^{-05}$	84.000	71.500	2.225	2.208
$.3652 \times 10^{-05}$	85.000	72.500	2.225	2.205
$.2905 \times 10^{-05}$	86.000	73.500	2.225	2.200
$.2239 \times 10^{-05}$	87.000	74.500	2.225	2.192
$.2646 \times 10^{-05}$	88.000	75.500	2.225	2.178
$.1211 \times 10^{-04}$	89.000	76.500	2.225	2.145

$\phi = 20.0$
$\theta_0 = 10.0$

F	θ_1 (deg)	θ_2 (deg)	d_1 (m)	d_2 (m)
$.2707 \times 10^{-04}$	55.000	40.000	2.250	2.228
$.2912 \times 10^{-04}$	56.000	41.000	2.250	2.223
$.3138 \times 10^{-04}$	57.000	42.000	2.250	2.218
$.3386 \times 10^{-04}$	58.000	43.000	2.250	2.213
$.3662 \times 10^{-04}$	59.000	44.000	2.250	2.207
$.3968 \times 10^{-04}$	60.000	45.000	2.250	2.202
$.4309 \times 10^{-04}$	61.000	46.000	2.250	2.196
$.4691 \times 10^{-04}$	62.000	47.000	2.250	2.189
$.5120 \times 10^{-04}$	63.000	48.000	2.250	2.183
$.5605 \times 10^{-04}$	64.000	49.000	2.250	2.176
$.6156 \times 10^{-04}$	65.000	50.000	2.250	2.168
$.6783 \times 10^{-04}$	66.000	51.000	2.250	2.160
$.7504 \times 10^{-04}$	67.000	52.000	2.250	2.151
$.8337 \times 10^{-04}$	68.000	53.000	2.250	2.142
$.9306 \times 10^{-04}$	69.000	54.000	2.250	2.132
$.1044 \times 10^{-03}$	70.000	55.000	2.250	2.120
$.1179 \times 10^{-03}$	71.000	56.000	2.250	2.108
$.1340 \times 10^{-03}$	72.000	57.000	2.250	2.094
$.1534 \times 10^{-03}$	73.000	58.000	2.250	2.079
$.1772 \times 10^{-03}$	74.000	59.000	2.250	2.061
$.2067 \times 10^{-03}$	75.000	60.000	2.250	2.041
$.2440 \times 10^{-03}$	76.000	61.000	2.250	2.018
$.2920 \times 10^{-03}$	77.000	62.000	2.250	1.992
$.3552 \times 10^{-03}$	78.000	63.000	2.250	1.959
$.4410 \times 10^{-03}$	79.000	64.000	2.250	1.921
$.5612 \times 10^{-03}$	80.000	65.000	2.250	1.872
$.7373 \times 10^{-03}$	81.000	66.000	2.250	1.810
$.1010 \times 10^{-02}$	82.000	67.000	2.250	1.728
$.1465 \times 10^{-02}$	83.000	68.000	2.250	1.612
$.2310 \times 10^{-02}$	84.000	69.000	2.250	1.439
$.4163 \times 10^{-02}$	85.000	70.000	2.250	1.148
$.9599 \times 10^{-02}$	86.000	71.000	2.250	.559
$.4123 \times 10^{-01}$	87.000	72.000	2.250	-1.291
$.8268 \times 10^{+01}$	88.000	73.000	2.250	52.863
$.3173 \times 10^{-01}$	89.000	74.000	2.250	5.413

Table 3. Optimization Results for Concave-Plane Mirror Pair

$\phi = 10.0$
$\theta_0 = 0.0$

F	θ_1 (deg)	θ_2 (deg)	R (m)	d_1 (m)	d_2 (m)
$.6373 \times 10^{+01}$	74.000	69.000	0.250	1.750	1.238
$.7018 \times 10^{+01}$	60.000	55.000	0.500	2.000	1.853
$.3639 \times 10^{+01}$	79.000	74.000	0.750	0.500	-.770
$.5200 \times 10^{+00}$	88.000	83.000	1.000	0.500	-5.200
$.7538 \times 10^{-03}$	89.000	84.000	1.250	0.525	-8.200
$.2784 \times 10^{-04}$	89.000	84.000	1.500	0.625	-7.834
$.3796 \times 10^{-04}$	84.000	79.000	1.750	0.500	-1.818
$.1262 \times 10^{-04}$	82.000	77.000	2.000	0.500	-1.262
$.7716 \times 10^{-05}$	81.000	76.000	2.250	0.525	-1.029
$.6635 \times 10^{-05}$	80.000	75.000	2.500	0.550	-.834
$.1061 \times 10^{-04}$	83.000	78.000	2.750	0.725	-1.144
$.6193 \times 10^{-05}$	75.000	70.000	3.000	0.500	-.391
$.6457 \times 10^{-05}$	79.000	74.000	3.250	0.675	-.528
$.5870 \times 10^{-05}$	79.000	74.000	3.500	0.725	-.459
$.5823 \times 10^{-05}$	79.000	74.000	3.750	0.775	-.390
$.5703 \times 10^{-05}$	80.000	75.000	4.000	0.875	-.371
$.5302 \times 10^{-05}$	82.000	77.000	4.250	1.050	-.419
$.5727 \times 10^{-05}$	69.000	64.000	4.500	0.550	-.003
$.5096 \times 10^{-05}$	81.000	76.000	4.750	1.100	-.182
$.5436 \times 10^{-05}$	87.000	82.000	5.000	1.750	-.868
$.4862 \times 10^{-05}$	83.000	78.000	5.250	1.375	-.101
$.4379 \times 10^{-05}$	85.000	80.000	5.500	1.650	-.135
$.3996 \times 10^{-05}$	85.000	80.000	5.750	1.725	.002
$.3934 \times 10^{-05}$	84.000	79.000	6.000	1.675	.179
$.4794 \times 10^{-05}$	79.000	74.000	6.250	1.275	.302
$.4458 \times 10^{-05}$	79.000	74.000	6.500	1.325	.371
$.3594 \times 10^{-05}$	84.000	79.000	6.750	1.875	.519
$.3966 \times 10^{-05}$	79.000	74.000	7.000	1.425	.510
$.3861 \times 10^{-05}$	79.000	74.000	7.250	1.475	.579
$.3591 \times 10^{-05}$	82.000	77.000	7.500	1.825	.768
$.3053 \times 10^{-05}$	83.000	78.000	7.750	2.000	.903
$.3687 \times 10^{-05}$	81.000	76.000	8.000	1.825	.885
$.3101 \times 10^{-05}$	81.000	76.000	8.250	1.875	.959
$.2946 \times 10^{-05}$	81.000	76.000	8.500	1.925	1.033
$.2998 \times 10^{-05}$	81.000	76.000	8.750	1.975	1.106
$.3751 \times 10^{-05}$	79.000	74.000	9.000	1.800	1.028
$.3118 \times 10^{-05}$	79.000	74.000	9.250	1.850	1.098
$.2920 \times 10^{-05}$	79.000	74.000	9.500	1.900	1.167
$.3156 \times 10^{-05}$	79.000	74.000	9.750	1.950	1.236
$.3388 \times 10^{-05}$	78.000	73.000	10.000	1.875	1.200

$\phi = 15.0$
$\theta_0 = 0.0$

F	θ_1 (deg)	θ_2 (deg)	R (m)	d_1 (m)	d_2 (m)
$.2013 \times 10^{+02}$	72.000	64.500	0.250	1.675	.923
$.6921 \times 10^{+01}$	74.000	66.500	0.500	0.500	-.899
$.5090 \times 10^{+00}$	90.000	82.500	0.750	0.500	15.386
$.3299 \times 10^{-02}$	90.000	82.500	1.000	0.550	15.209
$.9663 \times 10^{-05}$	90.000	82.500	1.250	0.700	14.677
$.1505 \times 10^{-04}$	85.000	77.500	1.500	0.600	-6.174
$.1315 \times 10^{-04}$	83.000	75.500	1.750	0.625	-3.512
$.6509 \times 10^{-05}$	76.000	68.500	2.000	0.500	-1.191
$.6517 \times 10^{-05}$	79.000	71.500	2.250	0.650	-1.588
$.6034 \times 10^{-05}$	76.000	68.500	2.500	0.625	-1.001
$.5974 \times 10^{-05}$	70.000	62.500	2.750	0.525	-.459
$.5759 \times 10^{-05}$	72.000	64.500	3.000	0.625	-.504
$.5439 \times 10^{-05}$	77.000	69.500	3.250	0.850	-.822
$.5840 \times 10^{-05}$	72.000	64.500	3.500	0.725	-.368
$.5453 \times 10^{-05}$	74.000	66.500	3.750	0.850	-.400
$.4869 \times 10^{-05}$	79.000	71.500	4.000	1.150	-.730
$.5202 \times 10^{-05}$	82.000	74.500	4.250	1.425	-1.149
$.4740 \times 10^{-05}$	77.000	69.500	4.500	1.175	-.311
$.4425 \times 10^{-05}$	78.000	70.500	4.750	1.300	-.277
$.3902 \times 10^{-05}$	82.000	74.500	5.000	1.675	-.625
$.4152 \times 10^{-05}$	76.000	68.500	5.250	1.300	.022
$.3584 \times 10^{-05}$	79.000	71.500	5.500	1.575	.000
$.3648 \times 10^{-05}$	81.000	73.500	5.750	1.825	.001
$.3051 \times 10^{-05}$	81.000	73.500	6.000	1.900	.146
$.2809 \times 10^{-05}$	81.000	73.500	6.250	1.975	.291
$.2780 \times 10^{-05}$	80.000	72.500	6.500	1.950	.466
$.2903 \times 10^{-05}$	79.000	71.500	6.750	1.925	.600
$.3083 \times 10^{-05}$	76.000	68.500	7.000	1.725	.667
$.3041 \times 10^{-05}$	75.000	67.500	7.250	1.700	.728
$.2808 \times 10^{-05}$	77.000	69.500	7.500	1.925	.867
$.2631 \times 10^{-05}$	76.000	68.500	7.750	1.900	.932
$.2963 \times 10^{-05}$	75.000	67.500	8.000	1.875	.985
$.2556 \times 10^{-05}$	75.000	67.500	8.250	1.925	1.058
$.2586 \times 10^{-05}$	75.000	67.500	8.500	1.975	1.131
$.2721 \times 10^{-05}$	74.000	66.500	8.750	1.950	1.170
$.2488 \times 10^{-05}$	74.000	66.500	9.000	2.000	1.242
$.4496 \times 10^{-05}$	58.000	50.500	9.250	1.025	.743
$.3721 \times 10^{+00}$	90.000	82.500	9.500	0.850	14.145
$.4868 \times 10^{+00}$	90.000	82.500	9.750	1.100	13.259

$\phi = 20.0$
$\theta_0 = 0.0$

F	θ_1 (deg)	θ_2 (deg)	R (m)	d_1 (m)	d_2 (m)
$.4741 \times 10^{+02}$	70.000	60.000	0.250	1.600	.619
$.9151 \times 10^{+00}$	90.000	80.000	0.500	0.500	8.247
$.5432 \times 10^{-02}$	90.000	80.000	0.750	0.500	8.247
$.6440 \times 10^{-04}$	90.000	80.000	1.000	0.625	8.074
$.1499 \times 10^{-03}$	88.000	78.000	1.250	0.700	14.621
$.4230 \times 10^{-04}$	90.000	80.000	1.500	0.950	7.626
$.3885 \times 10^{-05}$	90.000	80.000	1.750	1.100	7.419
$.6739 \times 10^{-05}$	75.000	65.000	2.000	0.600	-1.774
$.6111 \times 10^{-05}$	71.000	61.000	2.250	0.575	-1.014
$.1057 \times 10^{-05}$	90.000	80.000	2.500	1.575	6.764
$.3382 \times 10^{-05}$	89.000	79.000	2.750	1.625	8.276
$.1789 \times 10^{-05}$	89.000	79.000	3.000	1.775	7.957
$.1991 \times 10^{-05}$	89.000	79.000	3.250	1.925	7.639
$.4184 \times 10^{-05}$	88.000	78.000	3.500	1.950	10.176
$.4867 \times 10^{-05}$	75.000	65.000	3.750	1.125	-.854
$.4594 \times 10^{-05}$	74.000	64.000	4.000	1.150	-.607
$.4474 \times 10^{-05}$	75.000	65.000	4.250	1.275	-.591
$.4301 \times 10^{-05}$	75.000	65.000	4.500	1.350	-.460
$.4144 \times 10^{-05}$	75.000	65.000	4.750	1.425	-.328
$.3693 \times 10^{-05}$	79.000	69.000	5.000	1.775	-.760
$.3732 \times 10^{-05}$	73.000	63.000	5.250	1.450	.049
$.3092 \times 10^{-05}$	79.000	69.000	5.500	1.950	-.361
$.2874 \times 10^{-05}$	78.000	68.000	5.750	1.950	-.035
$.2696 \times 10^{-05}$	77.000	67.000	6.000	1.950	.219
$.2794 \times 10^{-05}$	76.000	66.000	6.250	1.950	.424
$.3028 \times 10^{-05}$	71.000	61.000	6.500	1.650	.598
$.3003 \times 10^{-05}$	73.000	63.000	6.750	1.850	.692
$.2443 \times 10^{-05}$	74.000	64.000	7.000	2.000	.816
$.2775 \times 10^{-05}$	73.000	63.000	7.250	2.000	.933
$.2383 \times 10^{-05}$	72.000	62.000	7.500	1.975	.995
$.2932 \times 10^{-05}$	68.000	58.000	7.750	1.750	.989
$.2406 \times 10^{-05}$	70.000	60.000	8.000	1.950	1.128
$.2402 \times 10^{-05}$	70.000	60.000	8.250	2.000	1.201
$.2740 \times 10^{-05}$	69.000	59.000	8.500	1.975	1.235
$.2675 \times 10^{-05}$	68.000	58.000	8.750	1.975	1.299
$.2555 \times 10^{-05}$	67.000	57.000	9.000	1.950	1.324
$.2340 \times 10^{-05}$	67.000	57.000	9.250	2.000	1.391
$.2411 \times 10^{-05}$	66.000	56.000	9.500	1.975	1.410
$.2523 \times 10^{-05}$	65.000	55.000	9.750	1.950	1.427
$.2480 \times 10^{-05}$	65.000	55.000	10.000	2.000	1.491

$\phi = 10.0$
$\theta_0 = 5.0$

F	θ_1 (deg)	θ_2 (deg)	R (m)	d_1 (m)	d_2 (m)
$.5176 \times 10^{+01}$	79.000	71.500	0.250	1.725	1.357
$.5483 \times 10^{+01}$	59.000	51.500	0.500	1.975	1.929
$.4299 \times 10^{+01}$	83.000	75.500	0.750	0.500	-.868
$.5972 \times 10^{+00}$	88.000	80.500	1.000	0.500	-2.269
$.4305 \times 10^{-01}$	90.000	82.500	1.250	0.500	-3.969
$.1077 \times 10^{-03}$	90.000	82.500	1.500	0.525	-3.889
$.1470 \times 10^{-04}$	88.000	80.500	1.750	0.525	-2.210
$.3167 \times 10^{-04}$	87.000	79.500	2.000	0.550	-1.710
$.1870 \times 10^{-04}$	86.000	78.500	2.250	0.575	-1.337
$.7735 \times 10^{-05}$	82.000	74.500	2.500	0.500	-.732
$.1200 \times 10^{-04}$	83.000	75.500	2.750	0.575	-.742
$.7648 \times 10^{-05}$	79.000	71.500	3.000	0.500	-.433
$.6761 \times 10^{-05}$	83.000	75.500	3.250	0.675	-.575
$.6538 \times 10^{-05}$	78.000	70.500	3.500	0.550	-.286
$.6212 \times 10^{-05}$	82.000	74.500	3.750	0.725	-.370
$.6298 \times 10^{-05}$	86.000	78.500	4.000	0.975	-.545
$.6267 \times 10^{-05}$	80.000	72.500	4.250	0.725	-.180
$.5604 \times 10^{-05}$	83.000	75.500	4.500	0.900	-.198
$.5529 \times 10^{-05}$	84.000	76.500	4.750	1.000	-.153
$.5204 \times 10^{-05}$	86.000	78.500	5.000	1.175	-.149
$.4873 \times 10^{-05}$	85.000	77.500	5.250	1.150	-.026
$.4362 \times 10^{-05}$	89.000	81.500	5.500	1.550	-.100
$.4294 \times 10^{-05}$	90.000	82.500	5.750	1.725	-.041
$.4431 \times 10^{-05}$	85.000	77.500	6.000	1.275	.206
$.4985 \times 10^{-05}$	83.000	75.500	6.250	1.175	.263
$.4563 \times 10^{-05}$	82.000	74.500	6.500	1.150	.313
$.4272 \times 10^{-05}$	83.000	75.500	6.750	1.250	.389
$.3775 \times 10^{-05}$	85.000	77.500	7.000	1.425	.484
$.4025 \times 10^{-05}$	82.000	74.500	7.250	1.250	.474
$.3330 \times 10^{-05}$	86.000	78.500	7.500	1.575	.643
$.2780 \times 10^{-05}$	89.000	81.500	7.750	1.900	.842
$.2891 \times 10^{-05}$	88.000	80.500	8.000	1.825	.867
$.2802 \times 10^{-05}$	88.000	80.500	8.250	1.850	.927
$.3023 \times 10^{-05}$	88.000	80.500	8.500	1.875	.986
$.2765 \times 10^{-05}$	89.000	81.500	8.750	2.000	1.111
$.2438 \times 10^{-05}$	88.000	80.500	9.000	1.925	1.104
$.2926 \times 10^{-05}$	88.000	80.500	9.250	1.950	1.163
$.3049 \times 10^{-05}$	87.000	79.500	9.500	1.875	1.131
$.2458 \times 10^{-05}$	87.000	79.500	9.750	1.900	1.185
$.3756 \times 10^{-05}$	81.000	73.500	10.000	1.475	.896

$\phi = 15.0$
$\theta_0 = 5.0$

F	θ_1 (deg)	θ_2 (deg)	R (m)	d_1 (m)	d_2 (m)
$.1880 \times 10^{+02}$	78.000	68.000	0.250	1.675	.921
$.8647 \times 10^{+01}$	78.000	68.000	0.500	0.500	-1.027
$.6866 \times 10^{+00}$	76.000	66.000	0.750	0.500	-.768
$.1650 \times 10^{+00}$	85.000	75.000	1.000	0.500	-3.212
$.3403 \times 10^{-04}$	88.000	78.000	1.250	0.500	-7.314
$.1585 \times 10^{-04}$	85.000	75.000	1.500	0.500	-3.212
$.1266 \times 10^{-04}$	83.000	73.000	1.750	0.525	-2.149
$.1781 \times 10^{-04}$	84.000	74.000	2.000	0.625	-2.341
$.8022 \times 10^{-05}$	80.000	70.000	2.250	0.575	-1.237
$.6977 \times 10^{-05}$	77.000	67.000	2.500	0.550	-.809
$.6795 \times 10^{-05}$	75.000	65.000	2.750	0.550	-.587
$.6319 \times 10^{-05}$	72.000	62.000	3.000	0.525	-.368
$.6179 \times 10^{-05}$	76.000	66.000	3.250	0.675	-.498
$.5857 \times 10^{-05}$	76.000	66.000	3.500	0.725	-.420
$.5785 \times 10^{-05}$	81.000	71.000	3.750	0.975	-.691
$.5544 \times 10^{-05}$	78.000	68.000	4.000	0.900	-.364
$.5074 \times 10^{-05}$	82.000	72.000	4.250	1.150	-.553
$.4983 \times 10^{-05}$	78.000	68.000	4.500	1.000	-.198
$.4743 \times 10^{-05}$	79.000	69.000	4.750	1.100	-.150
$.4253 \times 10^{-05}$	85.000	75.000	5.000	1.550	-.482
$.4333 \times 10^{-05}$	79.000	69.000	5.250	1.200	.023
$.3702 \times 10^{-05}$	85.000	75.000	5.500	1.675	-.157
$.4032 \times 10^{-05}$	84.000	74.000	5.750	1.650	.069
$.3420 \times 10^{-05}$	84.000	74.000	6.000	1.700	.186
$.2879 \times 10^{-05}$	86.000	76.000	6.250	1.950	.254
$.2712 \times 10^{-05}$	86.000	76.000	6.500	2.000	.402
$.2560 \times 10^{-05}$	85.000	75.000	6.750	1.950	.558
$.2750 \times 10^{-05}$	84.000	74.000	7.000	1.900	.657
$.2606 \times 10^{-05}$	84.000	74.000	7.250	1.950	.774
$.2624 \times 10^{-05}$	83.000	73.000	7.500	1.900	.828
$.3171 \times 10^{-05}$	78.000	68.000	7.750	1.575	.756
$.2385 \times 10^{-05}$	82.000	72.000	8.000	1.900	.962
$.2895 \times 10^{-05}$	78.000	68.000	8.250	1.650	.880
$.2247 \times 10^{-05}$	82.000	72.000	8.500	1.975	1.113
$.2794 \times 10^{-05}$	81.000	71.000	8.750	1.925	1.117
$.2648 \times 10^{-05}$	79.000	69.000	9.000	1.825	1.102
$.2319 \times 10^{-05}$	80.000	70.000	9.250	1.925	1.202
$.2334 \times 10^{-05}$	80.000	70.000	9.500	1.950	1.248
$.2503 \times 10^{-05}$	78.000	68.000	9.750	1.850	1.212
$.2352 \times 10^{-05}$	78.000	68.000	10.000	1.875	1.253

$\phi = 20.0$
$\theta_0 = 5.0$

F	θ_1 (deg)	θ_2 (deg)	R (m)	d_1 (m)	d_2 (m)
$.4778 \times 10^{+02}$	75.000	62.500	0.250	1.575	.544
$.2015 \times 10^{+01}$	72.000	59.500	0.500	0.500	-.860
$.3173 \times 10^{+00}$	72.000	59.500	0.750	0.500	-.860
$.1945 \times 10^{-02}$	90.000	77.500	1.000	0.525	18.900
$.4005 \times 10^{-03}$	85.000	72.500	1.250	0.500	-8.072
$.2189 \times 10^{-04}$	82.000	69.500	1.500	0.525	-3.786
$.1598 \times 10^{-04}$	84.000	71.500	1.750	0.675	-5.396
$.8552 \times 10^{-05}$	74.000	61.500	2.000	0.500	-1.140
$.9399 \times 10^{-05}$	81.000	68.500	2.250	0.750	-2.584
$.6746 \times 10^{-05}$	71.000	58.500	2.500	0.550	-.667
$.6639 \times 10^{-05}$	72.000	59.500	2.750	0.625	-.667
$.6435 \times 10^{-05}$	76.000	63.500	3.000	0.800	-.962
$.6205 \times 10^{-05}$	74.000	61.500	3.250	0.800	-.644
$.5826 \times 10^{-05}$	68.000	55.500	3.500	0.675	-.208
$.5476 \times 10^{-05}$	79.000	66.500	3.750	1.125	-.986
$.5169 \times 10^{-05}$	77.000	64.500	4.000	1.100	-.593
$.5122 \times 10^{-05}$	72.000	59.500	4.250	0.950	-.166
$.4617 \times 10^{-05}$	77.000	64.500	4.500	1.225	-.357
$.4253 \times 10^{-05}$	79.000	66.500	4.750	1.400	-.401
$.3943 \times 10^{-05}$	81.000	68.500	5.000	1.600	-.475
$.3697 \times 10^{-05}$	80.000	67.500	5.250	1.600	-.197
$.3603 \times 10^{-05}$	84.000	71.500	5.500	2.000	-.612
$.3013 \times 10^{-05}$	83.000	70.500	5.750	1.975	-.175
$.3191 \times 10^{-05}$	82.000	69.500	6.000	1.950	.121
$.3089 \times 10^{-05}$	80.000	67.500	6.250	1.850	.374
$.2911 \times 10^{-05}$	77.000	64.500	6.500	1.700	.541
$.2571 \times 10^{-05}$	80.000	67.500	6.750	1.975	.659
$.2334 \times 10^{-05}$	79.000	66.500	7.000	1.950	.768
$.2202 \times 10^{-05}$	79.000	66.500	7.250	2.000	.874
$.2240 \times 10^{-05}$	78.000	65.500	7.500	1.975	.952
$.2331 \times 10^{-05}$	77.000	64.500	7.750	1.950	1.014
$.2093 \times 10^{-05}$	77.000	64.500	8.000	2.000	1.109
$.2130 \times 10^{-05}$	76.000	63.500	8.250	1.975	1.154
$.2172 \times 10^{-05}$	75.000	62.500	8.500	1.950	1.190
$.2221 \times 10^{-05}$	74.000	61.500	8.750	1.925	1.219
$.2277 \times 10^{-05}$	73.000	60.500	9.000	1.900	1.243
$.2159 \times 10^{-05}$	74.000	61.500	9.250	2.000	1.344
$.2138 \times 10^{-05}$	73.000	60.500	9.500	1.975	1.363
$.2167 \times 10^{-05}$	72.000	59.500	9.750	1.950	1.378
$.2229 \times 10^{-05}$	71.000	58.500	10.000	1.925	1.391

$\phi = 10.0$
$\theta_0 = 10.0$

F	θ_1 (deg)	θ_2 (deg)	R (m)	d_1 (m)	d_2 (m)
$.3397 \times 10^{+01}$	89.000	79.000	0.250	1.775	1.637
$.3197 \times 10^{+01}$	65.000	55.000	0.500	2.000	2.021
$.5287 \times 10^{+01}$	55.000	45.000	0.750	1.975	1.978
$.7164 \times 10^{+00}$	90.000	80.000	1.000	0.500	-1.807
$.1538 \times 10^{+00}$	90.000	80.000	1.250	0.500	-1.807
$.2921 \times 10^{-01}$	90.000	80.000	1.500	0.500	-1.807
$.1510 \times 10^{-02}$	90.000	80.000	1.750	0.500	-1.807
$.1126 \times 10^{-04}$	89.000	79.000	2.000	0.500	-1.455
$.2438 \times 10^{-04}$	90.000	80.000	2.250	0.600	-1.538
$.1925 \times 10^{-04}$	88.000	78.000	2.500	0.575	-1.024
$.8644 \times 10^{-05}$	86.000	76.000	2.750	0.550	-.723
$.7494 \times 10^{-05}$	83.000	73.000	3.000	0.500	-.474
$.8367 \times 10^{-05}$	85.000	75.000	3.250	0.600	-.499
$.7706 \times 10^{-05}$	86.000	76.000	3.500	0.675	-.477
$.6700 \times 10^{-05}$	82.000	72.000	3.750	0.575	-.266
$.6455 \times 10^{-05}$	86.000	76.000	4.000	0.750	-.330
$.6339 \times 10^{-05}$	90.000	80.000	4.250	1.000	-.466
$.6265 \times 10^{-05}$	78.000	68.000	4.500	0.550	-.068
$.6133 \times 10^{-05}$	78.000	68.000	4.750	0.575	-.031
$.5333 \times 10^{-05}$	89.000	79.000	5.000	1.050	-.121
$.4996 \times 10^{-05}$	90.000	80.000	5.250	1.150	-.064
$.5055 \times 10^{-05}$	87.000	77.000	5.500	1.000	.056
$.5555 \times 10^{-05}$	86.000	76.000	5.750	0.975	.111
$.4686 \times 10^{-05}$	89.000	79.000	6.000	1.175	.182
$.4274 \times 10^{-05}$	89.000	79.000	6.250	1.200	.243
$.4203 \times 10^{-05}$	89.000	79.000	6.500	1.225	.303
$.3922 \times 10^{-05}$	89.000	79.000	6.750	1.250	.364
$.4443 \times 10^{-05}$	89.000	79.000	7.000	1.275	.424
$.4200 \times 10^{-05}$	86.000	76.000	7.250	1.125	.406
$.3848 \times 10^{-05}$	87.000	77.000	7.500	1.200	.472
$.3602 \times 10^{-05}$	88.000	78.000	7.750	1.275	.539
$.3552 \times 10^{-05}$	89.000	79.000	8.000	1.350	.606
$.4248 \times 10^{-05}$	82.000	72.000	8.250	1.025	.476
$.3497 \times 10^{-05}$	87.000	77.000	8.500	1.275	.629
$.3145 \times 10^{-05}$	89.000	79.000	8.750	1.400	.728
$.4010 \times 10^{-05}$	82.000	72.000	9.000	1.075	.558
$.3301 \times 10^{-05}$	88.000	78.000	9.250	1.375	.762
$.3709 \times 10^{-05}$	83.000	73.000	9.500	1.150	.637
$.3028 \times 10^{-05}$	88.000	78.000	9.750	1.400	.818
$.3514 \times 10^{-05}$	84.000	74.000	10.000	1.225	.720

$\phi = 15.0$
$\theta_0 = 10.0$

F	θ_1 (deg)	θ_2 (deg)	R (m)	d_1 (m)	d_2 (m)
$.1568 \times 10^{+02}$	82.000	69.500	0.250	1.625	1.036
$.9105 \times 10^{+01}$	67.000	54.500	0.500	2.000	1.939
$.8042 \times 10^{+00}$	80.000	67.500	0.750	0.500	-.873
$.1980 \times 10^{+00}$	86.000	73.500	1.000	0.500	-2.241
$.8326 \times 10^{-02}$	90.000	77.500	1.250	0.500	-5.753
$.2636 \times 10^{-04}$	89.000	76.500	1.500	0.525	-4.184
$.3533 \times 10^{-04}$	88.000	75.500	1.750	0.575	-3.108
$.1044 \times 10^{-04}$	85.000	72.500	2.000	0.550	-1.764
$.1004 \times 10^{-04}$	82.000	69.500	2.250	0.525	-1.126
$.8828 \times 10^{-05}$	85.000	72.500	2.500	0.675	-1.467
$.7785 \times 10^{-05}$	79.000	66.500	2.750	0.550	-.666
$.6927 \times 10^{-05}$	75.000	62.500	3.000	0.500	-.388
$.6945 \times 10^{-05}$	83.000	70.500	3.250	0.775	-.796
$.6634 \times 10^{-05}$	75.000	62.500	3.500	0.575	-.274
$.6331 \times 10^{-05}$	81.000	68.500	3.750	0.800	-.451
$.6071 \times 10^{-05}$	86.000	73.500	4.000	1.075	-.758
$.5547 \times 10^{-05}$	83.000	70.500	4.250	0.975	-.381
$.5302 \times 10^{-05}$	85.000	72.500	4.500	1.125	-.399
$.5150 \times 10^{-05}$	81.000	68.500	4.750	0.975	-.124
$.5107 \times 10^{-05}$	90.000	77.500	5.000	1.600	-.689
$.4326 \times 10^{-05}$	86.000	73.500	5.250	1.325	-.113
$.4535 \times 10^{-05}$	84.000	71.500	5.500	1.250	.058
$.4461 \times 10^{-05}$	85.000	72.500	5.750	1.350	.134
$.3603 \times 10^{-05}$	86.000	73.500	6.000	1.450	.209
$.3769 \times 10^{-05}$	85.000	72.500	6.250	1.425	.312
$.3648 \times 10^{-05}$	86.000	73.500	6.500	1.525	.403
$.2725 \times 10^{-05}$	89.000	76.500	6.750	1.775	.507
$.2726 \times 10^{-05}$	88.000	75.500	7.000	1.725	.593
$.3106 \times 10^{-05}$	88.000	75.500	7.250	1.750	.673
$.2397 \times 10^{-05}$	89.000	76.500	7.500	1.850	.789
$.2406 \times 10^{-05}$	88.000	75.500	7.750	1.800	.834
$.2667 \times 10^{-05}$	88.000	75.500	8.000	1.825	.915
$.2732 \times 10^{-05}$	84.000	71.500	8.250	1.600	.832
$.1989 \times 10^{-05}$	89.000	76.500	8.500	1.925	1.070
$.2400 \times 10^{-05}$	88.000	75.500	8.750	1.875	1.076
$.2382 \times 10^{-05}$	86.000	73.500	9.000	1.775	1.048
$.2103 \times 10^{-05}$	87.000	74.500	9.250	1.850	1.137
$.2508 \times 10^{-05}$	89.000	76.500	9.500	1.975	1.258
$.2232 \times 10^{-05}$	86.000	73.500	9.750	1.825	1.177
$.1924 \times 10^{-05}$	89.000	76.500	10.000	2.000	1.352

$\phi = 20.0$
$\theta_0 = 10.0$

F	θ_1 (deg)	θ_2 (deg)	R (m)	d_1 (m)	d_2 (m)
$.5119 \times 10^{+02}$	76.000	61.000	0.250	1.375	.537
$.2484 \times 10^{+01}$	75.000	60.000	0.500	0.500	-.865
$.3706 \times 10^{+00}$	75.000	60.000	0.750	0.500	-.865
$.1011 \times 10^{+00}$	82.000	67.000	1.000	0.500	-2.375
$.8670 \times 10^{-04}$	88.000	73.000	1.250	0.500	-9.205
$.4503 \times 10^{-04}$	88.000	73.000	1.500	0.600	-8.616
$.1077 \times 10^{-04}$	81.000	66.000	1.750	0.500	-2.036
$.9338 \times 10^{-05}$	78.000	63.000	2.000	0.500	-1.323
$.1027 \times 10^{-04}$	75.000	60.000	2.250	0.500	-.865
$.7491 \times 10^{-05}$	75.000	60.000	2.500	0.550	-.781
$.7244 \times 10^{-05}$	75.000	60.000	2.750	0.600	-.696
$.7140 \times 10^{-05}$	74.000	59.000	3.000	0.625	-.542
$.6563 \times 10^{-05}$	73.000	58.000	3.250	0.650	-.402
$.6248 \times 10^{-05}$	78.000	63.000	3.500	0.850	-.651
$.6171 \times 10^{-05}$	81.000	66.000	3.750	1.025	-.840
$.5606 \times 10^{-05}$	79.000	64.000	4.000	1.000	-.513
$.5328 \times 10^{-05}$	80.000	65.000	4.250	1.100	-.474
$.5190 \times 10^{-05}$	77.000	62.000	4.500	1.025	-.189
$.5008 \times 10^{-05}$	77.000	62.000	4.750	1.075	-.097
$.4870 \times 10^{-05}$	87.000	72.000	5.000	1.725	-.995
$.4019 \times 10^{-05}$	82.000	67.000	5.250	1.425	-.110
$.3963 \times 10^{-05}$	82.000	67.000	5.500	1.475	.013
$.3199 \times 10^{-05}$	87.000	72.000	5.750	1.900	-.193
$.2875 \times 10^{-05}$	87.000	72.000	6.000	1.950	.036
$.3204 \times 10^{-05}$	85.000	70.000	6.250	1.825	.309
$.2402 \times 10^{-05}$	86.000	71.000	6.500	1.950	.449
$.2686 \times 10^{-05}$	83.000	68.000	6.750	1.775	.596
$.2178 \times 10^{-05}$	85.000	70.000	7.000	1.950	.722
$.2314 \times 10^{-05}$	83.000	68.000	7.250	1.850	.796
$.2071 \times 10^{-05}$	84.000	69.000	7.500	1.950	.916
$.2534 \times 10^{-05}$	81.000	66.000	7.750	1.800	.926
$.2106 \times 10^{-05}$	83.000	68.000	8.000	1.950	1.062
$.1928 \times 10^{-05}$	83.000	68.000	8.250	1.975	1.129
$.1951 \times 10^{-05}$	83.000	68.000	8.500	2.000	1.195
$.2084 \times 10^{-05}$	82.000	67.000	8.750	1.975	1.237
$.2068 \times 10^{-05}$	82.000	67.000	9.000	2.000	1.298
$.2768 \times 10^{-05}$	81.000	66.000	9.250	1.975	1.324
$.3026 \times 10^{-05}$	72.000	57.000	9.500	1.550	1.060
$.2863 \times 10^{-05}$	73.000	58.000	9.750	1.625	1.132
$.2567 \times 10^{-05}$	80.000	65.000	10.000	1.975	1.396

Table 4. Optimization Results for Prism

$\phi = 10.0$
$\theta_0 = 5.0$

F	ε (deg)	θ_p (deg)	d (m)
$.9752 \times 10^{-01}$	10.000	5.560	1.945
$.6863 \times 10^{-01}$	10.500	3.301	1.945
$.7192 \times 10^{-01}$	11.000	3.335	1.945
$.7587 \times 10^{-01}$	11.500	3.336	1.945
$.7888 \times 10^{-01}$	12.000	3.424	1.945
$.8385 \times 10^{-01}$	12.500	3.370	1.945
$.8478 \times 10^{-01}$	13.000	3.619	1.945
$.9374 \times 10^{-01}$	13.500	3.279	1.945
$.8521 \times 10^{-01}$	14.000	4.216	1.945
$.1101 \times 10^{+00}$	14.500	2.667	1.945
$.6654 \times 10^{-01}$	15.000	6.213	1.945
$.1105 \times 10^{+00}$	15.500	3.278	1.945
$.8688 \times 10^{-01}$	16.000	5.329	1.945
$.1265 \times 10^{+00}$	16.500	2.573	1.945
$.6400 \times 10^{-01}$	17.000	7.600	1.945
$.1118 \times 10^{+00}$	17.500	4.445	1.945
$.1245 \times 10^{+00}$	18.000	3.717	1.945
$.9912 \times 10^{-01}$	18.500	5.994	1.945
$.1403 \times 10^{+00}$	19.000	2.892	1.945
$.6839 \times 10^{-01}$	19.500	8.660	1.945
$.1209 \times 10^{+00}$	20.000	5.268	1.945
$.1424 \times 10^{+00}$	20.500	3.638	1.945
$.8726 \times 10^{-01}$	21.000	8.264	1.945
$.1380 \times 10^{+00}$	21.500	4.701	1.945
$.1220 \times 10^{+00}$	22.000	6.404	1.945
$.1567 \times 10^{+00}$	22.500	3.376	1.945
$.7171 \times 10^{-01}$	23.000	10.391	1.945
$.1292 \times 10^{+00}$	23.500	6.724	1.945
$.1620 \times 10^{+00}$	24.000	3.694	1.945
$.7481 \times 10^{-01}$	24.500	11.024	1.945
$.1337 \times 10^{+00}$	25.000	7.245	1.945
$.1675 \times 10^{+00}$	25.500	3.966	1.945
$.7595 \times 10^{-01}$	26.000	11.782	1.945
$.1364 \times 10^{+00}$	26.500	7.903	1.945
$.1723 \times 10^{+00}$	27.000	4.274	1.945
$.7746 \times 10^{-01}$	27.500	12.514	1.945
$.1393 \times 10^{+00}$	28.000	8.541	1.945
$.1764 \times 10^{+00}$	28.500	4.661	1.945
$.8062 \times 10^{-01}$	29.000	13.149	1.945
$.1432 \times 10^{+00}$	29.500	9.078	1.945
$.1802 \times 10^{+00}$	30.000	5.048	1.945
$.8330 \times 10^{-01}$	30.500	13.813	1.945

$\phi = 15.0$
$\theta_0 = 5.0$

F	ε (deg)	θ_p (deg)	d (m)
$.4685 \times 10^{-01}$	10.000	3.041	2.525
$.5908 \times 10^{-01}$	10.500	3.777	2.525
$.2839 \times 10^{-01}$	11.000	2.688	2.525
$.7082 \times 10^{-01}$	11.500	4.704	2.525
$.2093 \times 10^{-01}$	12.000	2.474	2.525
$.7944 \times 10^{-01}$	12.500	5.490	2.525
$.1951 \times 10^{-01}$	13.000	2.900	2.525
$.3683 \times 10^{-01}$	13.500	4.905	2.525
$.1726 \times 10^{-01}$	14.000	2.440	2.525
$.6626 \times 10^{-01}$	14.500	6.443	2.525
$.1728 \times 10^{-01}$	15.000	3.560	2.525
$.1803 \times 10^{-01}$	15.500	4.299	2.525
$.1741 \times 10^{-01}$	16.000	3.000	2.525
$.2912 \times 10^{-01}$	16.500	6.350	2.525
$.1795 \times 10^{-01}$	17.000	3.253	2.525
$.2260 \times 10^{-01}$	17.500	6.428	2.525
$.1945 \times 10^{-01}$	18.000	3.236	2.525
$.2422 \times 10^{-01}$	18.500	7.205	2.525
$.1930 \times 10^{-01}$	19.000	3.879	2.525
$.1631 \times 10^{-01}$	19.500	6.392	2.525
$.2386 \times 10^{-01}$	20.000	3.114	2.525
$.3330 \times 10^{-01}$	20.500	8.962	2.525
$.1806 \times 10^{-01}$	21.000	5.477	2.525
$.2437 \times 10^{-01}$	21.500	3.896	2.525
$.1783 \times 10^{-01}$	22.000	8.530	2.525
$.2296 \times 10^{-01}$	22.500	4.876	2.525
$.1723 \times 10^{-01}$	23.000	6.917	2.525
$.3049 \times 10^{-01}$	23.500	3.550	2.525
$.3163 \times 10^{-01}$	24.000	10.875	2.525
$.1910 \times 10^{-01}$	24.500	7.136	2.525
$.3297 \times 10^{-01}$	25.000	3.853	2.525
$.2859 \times 10^{-01}$	25.500	11.565	2.525
$.2006 \times 10^{-01}$	26.000	7.721	2.525
$.3543 \times 10^{-01}$	26.500	4.161	2.525
$.2651 \times 10^{-01}$	27.000	12.284	2.525
$.2095 \times 10^{-01}$	27.500	8.343	2.525
$.3763 \times 10^{-01}$	28.000	4.530	2.525
$.2371 \times 10^{-01}$	28.500	12.937	2.525
$.2217 \times 10^{-01}$	29.000	8.898	2.525
$.3973 \times 10^{-01}$	29.500	4.917	2.525
$.2141 \times 10^{-01}$	30.000	13.592	2.525
$.2342 \times 10^{-01}$	30.500	9.459	2.525
$.4172 \times 10^{-01}$	31.000	5.326	2.525
$.1945 \times 10^{-01}$	31.500	14.238	2.525

$\phi = 20.0$
$\theta_0 = 5.0$

F	ε (deg)	θ_p (deg)	d (m)
$.8933 \times 10^{-02}$	19.000	2.814	2.820
$.1546 \times 10^{-01}$	20.000	5.422	2.820
$.8197 \times 10^{-02}$	20.500	3.401	2.820
$.5898 \times 10^{-01}$	21.000	8.774	2.820
$.1027 \times 10^{-01}$	21.500	5.228	2.820
$.8665 \times 10^{-02}$	22.000	4.874	2.820
$.1210 \times 10^{-01}$	22.500	6.402	2.820
$.7415 \times 10^{-02}$	23.000	3.526	2.820
$.7137 \times 10^{-01}$	23.500	10.520	2.820
$.9998 \times 10^{-02}$	24.000	6.809	2.820
$.7580 \times 10^{-02}$	24.500	3.825	2.820
$.6456 \times 10^{-01}$	25.000	11.202	2.820
$.8879 \times 10^{-02}$	25.500	7.383	2.820
$.8034 \times 10^{-02}$	26.000	4.076	2.820
$.6345 \times 10^{-01}$	26.500	12.011	2.820
$.8279 \times 10^{-02}$	27.000	8.099	2.820
$.8612 \times 10^{-02}$	27.500	4.393	2.820
$.5941 \times 10^{-01}$	28.000	12.739	2.820
$.7638 \times 10^{-02}$	28.500	8.734	2.820
$.9210 \times 10^{-02}$	29.000	4.793	2.820
$.5199 \times 10^{-01}$	29.500	13.361	2.820
$.7014 \times 10^{-02}$	30.000	9.259	2.820
$.9906 \times 10^{-02}$	30.500	5.181	2.820
$.4709 \times 10^{-01}$	31.000	14.034	2.820
$.6630 \times 10^{-02}$	31.500	9.841	2.820
$.1060 \times 10^{-01}$	32.000	5.612	2.820
$.4145 \times 10^{-01}$	32.500	14.662	2.820
$.6368 \times 10^{-02}$	33.000	10.380	2.820
$.1136 \times 10^{-01}$	33.500	6.030	2.820
$.3757 \times 10^{-01}$	34.000	15.333	2.820
$.6241 \times 10^{-02}$	34.500	10.967	2.820
$.1209 \times 10^{-01}$	35.000	6.489	2.820
$.3305 \times 10^{-01}$	35.500	15.958	2.820
$.6226 \times 10^{-02}$	36.000	11.507	2.820
$.1288 \times 10^{-01}$	36.500	6.925	2.820
$.3025 \times 10^{-01}$	37.000	16.642	2.820
$.6271 \times 10^{-02}$	37.500	12.114	2.820

$\phi = 20.0$
$\theta_0 = 10.0$

F	ε (deg)	θ_p (deg)	d (m)
$.3532 \times 10^{+01}$	10.000	9.473	1.872
$.1661 \times 10^{+00}$	10.500	7.538	1.872
$.2979 \times 10^{+01}$	11.000	9.923	1.872
$.1088 \times 10^{+00}$	11.500	7.640	1.872
$.1129 \times 10^{+01}$	12.000	9.950	1.872
$.6496 \times 10^{-01}$	12.500	7.554	1.872
$.1183 \times 10^{+01}$	13.000	10.502	1.872
$.5439 \times 10^{-01}$	13.500	7.855	1.872
$.3910 \times 10^{+00}$	14.000	10.248	1.872
$.3827 \times 10^{-01}$	14.500	7.582	1.872
$.9348 \times 10^{+00}$	15.000	11.402	1.872
$.4157 \times 10^{-01}$	15.500	8.461	1.872
$.8418 \times 10^{-01}$	16.000	9.856	1.872
$.3751 \times 10^{-01}$	16.500	7.595	1.872
$.1146 \times 10^{+01}$	17.000	12.558	1.872
$.3865 \times 10^{-01}$	17.500	9.401	1.872
$.3555 \times 10^{-01}$	18.000	8.814	1.872
$.5678 \times 10^{-01}$	18.500	10.730	1.872
$.4773 \times 10^{-01}$	19.000	7.814	1.872
$.1071 \times 10^{+01}$	19.500	13.806	1.872
$.3532 \times 10^{-01}$	20.000	10.422	1.872
$.5052 \times 10^{-01}$	20.500	8.401	1.872
$.3204 \times 10^{+00}$	21.000	13.774	1.872
$.3752 \times 10^{-01}$	21.500	10.228	1.872
$.4314 \times 10^{-01}$	22.000	9.874	1.872
$.3437 \times 10^{-01}$	22.500	11.402	1.872
$.6662 \times 10^{-01}$	23.000	8.526	1.872
$.6079 \times 10^{+00}$	23.500	15.520	1.872
$.3571 \times 10^{-01}$	24.000	11.809	1.872
$.7373 \times 10^{-01}$	24.500	8.825	1.872
$.5315 \times 10^{+00}$	25.000	16.202	1.872
$.3715 \times 10^{-01}$	25.500	12.383	1.872
$.8148 \times 10^{-01}$	26.000	9.076	1.872
$.5654 \times 10^{+00}$	26.500	17.011	1.872
$.3775 \times 10^{-01}$	27.000	13.099	1.872
$.8826 \times 10^{-01}$	27.500	9.393	1.872
$.5322 \times 10^{+00}$	28.000	17.739	1.872
$.3917 \times 10^{-01}$	28.500	13.734	1.872
$.9387 \times 10^{-01}$	29.000	9.793	1.872
$.4269 \times 10^{+00}$	29.500	18.361	1.872
$.4197 \times 10^{-01}$	30.000	14.259	1.872
$.9953 \times 10^{-01}$	30.500	10.181	1.872
$.3717 \times 10^{+00}$	31.000	19.034	1.872
$.4442 \times 10^{-01}$	31.500	14.841	1.872

$\phi = 15.0$
$\theta_0 = 15.0$

F	ε (deg)	θ_p (deg)	d (m)
$.1843 \times 10^{+01}$	10.000	13.041	.071
$.2272 \times 10^{+01}$	10.500	13.777	.071
$.1171 \times 10^{+01}$	11.000	12.688	.071
$.1781 \times 10^{+01}$	11.500	14.704	.071
$.1238 \times 10^{+01}$	12.000	12.474	.071
$.2577 \times 10^{+01}$	12.500	15.490	.071
$.1243 \times 10^{+01}$	13.000	12.900	.071
$.1826 \times 10^{+01}$	13.500	14.905	.071
$.1274 \times 10^{+01}$	14.000	12.440	.071
$.1696 \times 10^{+01}$	14.500	16.443	.071
$.1259 \times 10^{+01}$	15.000	13.560	.071
$.1238 \times 10^{+01}$	15.500	14.299	.071
$.1284 \times 10^{+01}$	16.000	13.000	.071
$.8509 \times 10^{+01}$	16.500	16.350	.071
$.1288 \times 10^{+01}$	17.000	13.253	.071
$.1780 \times 10^{+01}$	17.500	16.428	.071
$.1295 \times 10^{+01}$	18.000	13.236	.071
$.3444 \times 10^{+01}$	18.500	17.205	.071
$.1294 \times 10^{+01}$	19.000	13.879	.071
$.1234 \times 10^{+01}$	19.500	16.392	.071
$.1306 \times 10^{+01}$	20.000	13.114	.071
$.1831 \times 10^{+01}$	20.500	18.962	.071
$.1287 \times 10^{+01}$	21.000	15.477	.071
$.1306 \times 10^{+01}$	21.500	13.896	.071
$.1590 \times 10^{+01}$	22.000	18.530	.071
$.1303 \times 10^{+01}$	22.500	14.876	.071
$.1281 \times 10^{+01}$	23.000	16.917	.071
$.1314 \times 10^{+01}$	23.500	13.550	.071
$.1731 \times 10^{+01}$	24.000	20.875	.071
$.1290 \times 10^{+01}$	24.500	17.136	.071
$.1316 \times 10^{+01}$	25.000	13.853	.071
$.3010 \times 10^{+01}$	25.500	21.565	.071
$.1293 \times 10^{+01}$	26.000	17.721	.071
$.1318 \times 10^{+01}$	26.500	14.161	.071
$.1416 \times 10^{+02}$	27.000	22.284	.071
$.1295 \times 10^{+01}$	27.500	18.343	.071
$.1320 \times 10^{+01}$	28.000	14.530	.071
$.3599 \times 10^{+01}$	28.500	22.937	.071
$.1298 \times 10^{+01}$	29.000	18.898	.071
$.1321 \times 10^{+01}$	29.500	14.917	.071
$.2227 \times 10^{+01}$	30.000	23.592	.071
$.1300 \times 10^{+01}$	30.500	19.459	.071
$.1322 \times 10^{+01}$	31.000	15.326	.071

Table 5. Optimization Results for Lens, Plane Mirror Pair

$\phi = 10.0$
$\theta_0 = 0.0$

F	θ_1 (deg)	θ_2 (deg)	d_L (m)	d_1 (m)	d_2 (m)
$.1464 \times 10^{-05}$	55.000	50.000	0.570	0.625	.437
$.1443 \times 10^{-05}$	56.000	51.000	0.600	0.625	.416
$.1423 \times 10^{-05}$	57.000	52.000	0.610	0.700	.475
$.1396 \times 10^{-05}$	58.000	53.000	0.650	0.675	.427
$.1385 \times 10^{-05}$	59.000	54.000	0.670	0.725	.458
$.1360 \times 10^{-05}$	60.000	55.000	0.690	0.775	.490
$.1347 \times 10^{-05}$	61.000	56.000	0.720	0.800	.494
$.1310 \times 10^{-05}$	62.000	57.000	0.750	0.825	.497
$.1296 \times 10^{-05}$	63.000	58.000	0.790	0.825	.471
$.1273 \times 10^{-05}$	64.000	59.000	0.800	0.925	.557
$.1276 \times 10^{-05}$	65.000	60.000	0.800	1.050	.672
$.1309 \times 10^{-05}$	66.000	61.000	0.780	1.225	.845
$.1189 \times 10^{-05}$	67.000	62.000	0.940	0.950	.499
$.1196 \times 10^{-05}$	68.000	63.000	0.920	1.125	.671
$.1149 \times 10^{-05}$	69.000	64.000	0.990	1.100	.608
$.1127 \times 10^{-05}$	70.000	65.000	1.020	1.175	.662
$.1087 \times 10^{-05}$	71.000	66.000	1.100	1.150	.594
$.1060 \times 10^{-05}$	72.000	67.000	1.150	1.200	.614
$.1012 \times 10^{-05}$	73.000	68.000	1.220	1.225	.601
$.1002 \times 10^{-05}$	74.000	69.000	1.270	1.300	.647
$.9571 \times 10^{-06}$	75.000	70.000	1.320	1.375	.690
$.9187 \times 10^{-06}$	76.000	71.000	1.380	1.450	.731
$.8985 \times 10^{-06}$	77.000	72.000	1.430	1.550	.801
$.9833 \times 10^{-06}$	78.000	73.000	1.500	1.625	.835
$.8792 \times 10^{-06}$	79.000	74.000	1.460	1.850	1.072
$.6008 \times 10^{-04}$	80.000	75.000	1.500	1.875	1.028
$.5108 \times 10^{-03}$	81.000	76.000	1.500	1.875	.933
$.1665 \times 10^{-02}$	82.000	77.000	1.500	1.875	.817
$.4044 \times 10^{-02}$	83.000	78.000	1.500	1.875	.674
$.8645 \times 10^{-02}$	84.000	79.000	1.500	1.875	.489
$.1751 \times 10^{-01}$	85.000	80.000	1.500	1.875	.243
$.3526 \times 10^{-01}$	86.000	81.000	1.500	1.875	-.102
$.7387 \times 10^{-01}$	87.000	82.000	1.500	1.875	-.624
$.1717 \times 10^{+00}$	88.000	83.000	1.500	1.875	-1.506
$.5030 \times 10^{+00}$	89.000	84.000	1.500	1.875	-3.331

$\phi = 15.0$
$\theta_0 = 0.0$

F	θ_1 (deg)	θ_2 (deg)	d_L (m)	d_1 (m)	d_2 (m)
$.1209 \times 10^{-05}$	55.000	47.500	0.940	0.950	.693
$.1220 \times 10^{-05}$	56.000	48.500	0.930	1.075	.801
$.1163 \times 10^{-05}$	57.000	49.500	1.000	1.025	.716
$.1142 \times 10^{-05}$	58.000	50.500	1.040	1.050	.713
$.1140 \times 10^{-05}$	59.000	51.500	1.070	1.100	.737
$.1090 \times 10^{-05}$	60.000	52.500	1.110	1.125	.733
$.1079 \times 10^{-05}$	61.000	53.500	1.140	1.175	.757
$.1039 \times 10^{-05}$	62.000	54.500	1.190	1.200	.750
$.1030 \times 10^{-05}$	63.000	55.500	1.210	1.275	.802
$.1001 \times 10^{-05}$	64.000	56.500	1.250	1.325	.824
$.9689 \times 10^{-06}$	65.000	57.500	1.320	1.325	.784
$.9400 \times 10^{-06}$	66.000	58.500	1.350	1.400	.834
$.9119 \times 10^{-06}$	67.000	59.500	1.400	1.450	.853
$.8670 \times 10^{-06}$	68.000	60.500	1.470	1.475	.838
$.8634 \times 10^{-06}$	69.000	61.500	1.490	1.575	.917
$.8911 \times 10^{-06}$	70.000	62.500	1.490	1.700	1.030
$.8723 \times 10^{-06}$	71.000	63.500	1.480	1.825	1.144
$.6015 \times 10^{-05}$	72.000	64.500	1.500	1.875	1.155
$.6725 \times 10^{-04}$	73.000	65.500	1.500	1.875	1.093
$.2205 \times 10^{-03}$	74.000	66.500	1.500	1.875	1.023
$.5058 \times 10^{-03}$	75.000	67.500	1.500	1.875	.944
$.9826 \times 10^{-03}$	76.000	68.500	1.500	1.875	.853
$.1742 \times 10^{-02}$	77.000	69.500	1.500	1.875	.746
$.2927 \times 10^{-02}$	78.000	70.500	1.500	1.875	.620
$.4773 \times 10^{-02}$	79.000	71.500	1.500	1.875	.469
$.7675 \times 10^{-02}$	80.000	72.500	1.500	1.875	.282
$.1235 \times 10^{-01}$	81.000	73.500	1.500	1.875	.047
$.2016 \times 10^{-01}$	82.000	74.500	1.500	1.875	-.261
$.3395 \times 10^{-01}$	83.000	75.500	1.500	1.875	-.681
$.6045 \times 10^{-01}$	84.000	76.500	1.500	1.875	-1.291
$.1183 \times 10^{+00}$	85.000	77.500	1.500	1.875	-2.260
$.2753 \times 10^{+00}$	86.000	78.500	1.500	1.875	-4.042
$.9401 \times 10^{+00}$	87.000	79.500	1.500	1.875	-8.422
$.1468 \times 10^{+02}$	88.000	80.500	1.500	1.875	-36.577
$.5583 \times 10^{+01}$	89.000	81.500	1.500	1.875	24.347

$\phi = 20.0$
$\theta_0 = 0.0$

F	θ_1 (deg)	θ_2 (deg)	d_L (m)	d_1 (m)	d_2 (m)
$.9821 \times 10^{-06}$	55.000	45.000	1.290	1.325	1.019
$.9501 \times 10^{-06}$	56.000	46.000	1.340	1.350	1.011
$.9342 \times 10^{-06}$	57.000	47.000	1.370	1.400	1.031
$.9162 \times 10^{-06}$	58.000	48.000	1.410	1.450	1.051
$.8781 \times 10^{-06}$	59.000	49.000	1.460	1.475	1.041
$.8514 \times 10^{-06}$	60.000	50.000	1.500	1.525	1.060
$.8528 \times 10^{-06}$	61.000	51.000	1.500	1.625	1.140
$.8496 \times 10^{-06}$	62.000	52.000	1.500	1.725	1.221
$.8554 \times 10^{-06}$	63.000	53.000	1.500	1.825	1.304
$.2605 \times 10^{-05}$	64.000	54.000	1.500	1.875	1.323
$.2092 \times 10^{-04}$	65.000	55.000	1.500	1.875	1.276
$.6387 \times 10^{-04}$	66.000	56.000	1.500	1.875	1.224
$.1389 \times 10^{-03}$	67.000	57.000	1.500	1.875	1.168
$.2558 \times 10^{-03}$	68.000	58.000	1.500	1.875	1.106
$.4281 \times 10^{-03}$	69.000	59.000	1.500	1.875	1.038
$.6741 \times 10^{-03}$	70.000	60.000	1.500	1.875	.962
$.1019 \times 10^{-02}$	71.000	61.000	1.500	1.875	.877
$.1500 \times 10^{-02}$	72.000	62.000	1.500	1.875	.781
$.2169 \times 10^{-02}$	73.000	63.000	1.500	1.875	.672
$.3104 \times 10^{-02}$	74.000	64.000	1.500	1.875	.545
$.4423 \times 10^{-02}$	75.000	65.000	1.500	1.875	.395
$.6315 \times 10^{-02}$	76.000	66.000	1.500	1.875	.218
$.9084 \times 10^{-02}$	77.000	67.000	1.500	1.875	.002
$.1326 \times 10^{-01}$	78.000	68.000	1.500	1.875	-.268
$.1980 \times 10^{-01}$	79.000	69.000	1.500	1.875	-.613
$.3061 \times 10^{-01}$	80.000	70.000	1.500	1.875	-1.074
$.4983 \times 10^{-01}$	81.000	71.000	1.500	1.875	-1.722
$.8783 \times 10^{-01}$	82.000	72.000	1.500	1.875	-2.700
$.1767 \times 10^{+00}$	83.000	73.000	1.500	1.875	-4.356
$.4584 \times 10^{+00}$	84.000	74.000	1.500	1.875	-7.777
$.2325 \times 10^{+01}$	85.000	75.000	1.500	1.875	-19.065
$.1096 \times 10^{+03}$	86.000	76.000	1.500	1.875	140.562
$.1619 \times 10^{+01}$	87.000	77.000	1.500	1.875	18.150
$.4940 \times 10^{+00}$	88.000	78.000	1.500	1.875	10.564
$.2469 \times 10^{+00}$	89.000	79.000	1.500	1.875	7.818

$\phi = 10.0$
$\theta_0 = 5.0$

F	θ_1 (deg)	θ_2 (deg)	d_L (m)	d_1 (m)	d_2 (m)
$.1580 \times 10^{-05}$	55.000	47.500	0.470	0.500	.368
$.1536 \times 10^{-05}$	56.000	48.500	0.480	0.550	.403
$.1544 \times 10^{-05}$	57.000	49.500	0.480	0.625	.465
$.1035 \times 10^{+00}$	58.000	50.500	1.500	1.875	1.813
$.1046 \times 10^{+00}$	59.000	51.500	1.500	1.875	1.806
$.1058 \times 10^{+00}$	60.000	52.500	1.500	1.875	1.799
$.1071 \times 10^{+00}$	61.000	53.500	1.500	1.875	1.792
$.1085 \times 10^{+00}$	62.000	54.500	1.500	1.875	1.785
$.1099 \times 10^{+00}$	63.000	55.500	1.500	1.875	1.777
$.1114 \times 10^{+00}$	64.000	56.500	1.500	1.875	1.769
$.1131 \times 10^{+00}$	65.000	57.500	1.500	1.875	1.761
$.1149 \times 10^{+00}$	66.000	58.500	1.500	1.875	1.752
$.1168 \times 10^{+00}$	67.000	59.500	1.500	1.875	1.743
$.1188 \times 10^{+00}$	68.000	60.500	1.500	1.875	1.733
$.1211 \times 10^{+00}$	69.000	61.500	1.500	1.875	1.723
$.1236 \times 10^{+00}$	70.000	62.500	1.500	1.875	1.712
$.1262 \times 10^{+00}$	71.000	63.500	1.500	1.875	1.700
$.1292 \times 10^{+00}$	72.000	64.500	1.500	1.875	1.688
$.1325 \times 10^{+00}$	73.000	65.500	1.500	1.875	1.674
$.1361 \times 10^{+00}$	74.000	66.500	1.500	1.875	1.659
$.1402 \times 10^{+00}$	75.000	67.500	1.500	1.875	1.643
$.1448 \times 10^{+00}$	76.000	68.500	1.500	1.875	1.625
$.1501 \times 10^{+00}$	77.000	69.500	1.500	1.875	1.605
$.1561 \times 10^{+00}$	78.000	70.500	1.500	1.875	1.583
$.1631 \times 10^{+00}$	79.000	71.500	1.500	1.875	1.558
$.1713 \times 10^{+00}$	80.000	72.500	1.500	1.875	1.530
$.1811 \times 10^{+00}$	81.000	73.500	1.500	1.875	1.498
$.1928 \times 10^{+00}$	82.000	74.500	1.500	1.875	1.460
$.2074 \times 10^{+00}$	83.000	75.500	1.500	1.875	1.415
$.2257 \times 10^{+00}$	84.000	76.500	1.500	1.875	1.362
$.2494 \times 10^{+00}$	85.000	77.500	1.500	1.875	1.296
$.2811 \times 10^{+00}$	86.000	78.500	1.490	1.875	1.212
$.3256 \times 10^{+00}$	87.000	79.500	1.490	1.875	1.103
$.3921 \times 10^{+00}$	88.000	80.500	1.490	1.875	.954
$.4998 \times 10^{+00}$	89.000	81.500	1.490	1.875	.738

$\phi = 15.0$
$\theta_0 = 5.0$

F	θ_1 (deg)	θ_2 (deg)	d_L (m)	d_1 (m)	d_2 (m)
$.1325 \times 10^{-05}$	55.000	45.000	0.770	0.850	.675
$.1285 \times 10^{-05}$	56.000	46.000	0.820	0.825	.622
$.1288 \times 10^{-05}$	57.000	47.000	0.820	0.900	.679
$.1257 \times 10^{-05}$	58.000	48.000	0.860	0.900	.652
$.2232 \times 10^{-03}$	59.000	49.000	0.740	0.750	.453
$.1448 \times 10^{+00}$	60.000	50.000	1.500	1.875	1.725
$.1478 \times 10^{+00}$	61.000	51.000	1.500	1.875	1.710
$.1510 \times 10^{+00}$	62.000	52.000	1.500	1.875	1.695
$.1544 \times 10^{+00}$	63.000	53.000	1.500	1.875	1.679
$.1582 \times 10^{+00}$	64.000	54.000	1.500	1.875	1.662
$.1622 \times 10^{+00}$	65.000	55.000	1.500	1.875	1.644
$.1667 \times 10^{+00}$	66.000	56.000	1.500	1.875	1.625
$.1715 \times 10^{+00}$	67.000	57.000	1.500	1.875	1.605
$.1768 \times 10^{+00}$	68.000	58.000	1.500	1.875	1.584
$.1826 \times 10^{+00}$	69.000	59.000	1.500	1.875	1.561
$.1891 \times 10^{+00}$	70.000	60.000	1.500	1.875	1.536
$.1964 \times 10^{+00}$	71.000	61.000	1.500	1.875	1.509
$.2046 \times 10^{+00}$	72.000	62.000	1.500	1.875	1.480
$.2138 \times 10^{+00}$	73.000	63.000	1.500	1.875	1.448
$.2243 \times 10^{+00}$	74.000	64.000	1.500	1.875	1.412
$.2364 \times 10^{+00}$	75.000	65.000	1.500	1.875	1.373
$.2505 \times 10^{+00}$	76.000	66.000	1.500	1.875	1.329
$.2670 \times 10^{+00}$	77.000	67.000	1.500	1.875	1.279
$.2868 \times 10^{+00}$	78.000	68.000	1.500	1.875	1.222
$.3106 \times 10^{+00}$	79.000	69.000	1.500	1.875	1.156
$.3401 \times 10^{+00}$	80.000	70.000	1.500	1.875	1.078
$.3772 \times 10^{+00}$	81.000	71.000	1.500	1.875	.986
$.4252 \times 10^{+00}$	82.000	72.000	1.500	1.875	.874
$.4894 \times 10^{+00}$	83.000	73.000	1.500	1.875	.734
$.5787 \times 10^{+00}$	84.000	74.000	1.500	1.875	.555
$.7100 \times 10^{+00}$	85.000	75.000	1.490	1.875	.315
$.9177 \times 10^{+00}$	86.000	76.000	1.490	1.875	-.021
$.1283 \times 10^{+01}$	87.000	77.000	1.490	1.875	-.529
$.2043 \times 10^{+01}$	88.000	78.000	1.490	1.875	-1.388
$.4175 \times 10^{+01}$	89.000	79.000	1.490	1.875	-3.164

$\phi = 20.0$
$\theta_0 = 5.0$

F	θ_1 (deg)	θ_2 (deg)	d_L (m)	d_1 (m)	d_2 (m)
$.1098 \times 10^{-05}$	55.000	42.500	1.100	1.150	.939
$.1062 \times 10^{-05}$	56.000	43.500	1.150	1.150	.907
$.1052 \times 10^{-05}$	57.000	44.500	1.170	1.200	.932
$.1046 \times 10^{-05}$	58.000	45.500	1.210	1.225	.928
$.1037 \times 10^{-05}$	59.000	46.500	1.240	1.250	.923
$.1006 \times 10^{-05}$	60.000	47.500	1.270	1.300	.949
$.9590 \times 10^{-06}$	61.000	48.500	1.310	1.325	.943
$.9456 \times 10^{-06}$	62.000	49.500	1.330	1.375	.968
$.9147 \times 10^{-06}$	63.000	50.500	1.380	1.400	.962
$.9142 \times 10^{-06}$	64.000	51.500	1.380	1.475	1.019
$.8741 \times 10^{-06}$	65.000	52.500	1.460	1.475	.979
$.8636 \times 10^{-06}$	66.000	53.500	1.490	1.525	1.003
$.8569 \times 10^{-06}$	67.000	54.500	1.490	1.600	1.062
$.8643 \times 10^{-06}$	68.000	55.500	1.490	1.675	1.122
$.8592 \times 10^{-06}$	69.000	56.500	1.480	1.750	1.183
$.8534 \times 10^{-06}$	70.000	57.500	1.480	1.825	1.246
$.9167 \times 10^{-06}$	71.000	58.500	1.500	1.875	1.272
$.1679 \times 10^{-04}$	72.000	59.500	1.500	1.875	1.219
$.6768 \times 10^{-04}$	73.000	60.500	1.500	1.875	1.159
$.1679 \times 10^{-03}$	74.000	61.500	1.500	1.875	1.091
$.3382 \times 10^{-03}$	75.000	62.500	1.500	1.875	1.014
$.6096 \times 10^{-03}$	76.000	63.500	1.500	1.875	.925
$.1029 \times 10^{-02}$	77.000	64.500	1.500	1.875	.822
$.1672 \times 10^{-02}$	78.000	65.500	1.500	1.875	.700
$.2657 \times 10^{-02}$	79.000	66.500	1.500	1.875	.553
$.4189 \times 10^{-02}$	80.000	67.500	1.500	1.875	.373
$.6635 \times 10^{-02}$	81.000	68.500	1.500	1.875	.145
$.1069 \times 10^{-01}$	82.000	69.500	1.500	1.875	-.153
$.1782 \times 10^{-01}$	83.000	70.500	1.500	1.875	-.561
$.3145 \times 10^{-01}$	84.000	71.500	1.500	1.875	-1.152
$.6107 \times 10^{-01}$	85.000	72.500	1.500	1.875	-2.091
$.1412 \times 10^{+00}$	86.000	73.500	1.500	1.875	-3.819
$.4794 \times 10^{+00}$	87.000	74.500	1.500	1.875	-8.064
$.7448 \times 10^{+01}$	88.000	75.500	1.500	1.875	-35.354
$.2819 \times 10^{+01}$	89.000	76.500	1.500	1.875	23.700

$\phi = 10.0$
$\theta_0 = 10.0$

F	θ_1 (deg)	θ_2 (deg)	d_L (m)	d_1 (m)	d_2 (m)
$.1761 \times 10^{-05}$	55.000	45.000	0.360	0.500	.421
$.1744 \times 10^{-05}$	56.000	46.000	0.380	0.500	.404
$.1797 \times 10^{-05}$	57.000	47.000	0.390	0.525	.414
$.1707 \times 10^{-05}$	58.000	48.000	0.320	0.750	.644
$.1567 \times 10^{-05}$	59.000	49.000	0.450	0.500	.353
$.1557 \times 10^{-05}$	60.000	50.000	0.450	0.550	.391
$.1564 \times 10^{-05}$	61.000	51.000	0.450	0.600	.430
$.1506 \times 10^{-05}$	62.000	52.000	0.500	0.550	.355
$.1526 \times 10^{-05}$	63.000	53.000	0.500	0.600	.394
$.1493 \times 10^{-05}$	64.000	54.000	0.530	0.600	.375
$.1469 \times 10^{-05}$	65.000	55.000	0.570	0.575	.326
$.1445 \times 10^{-05}$	66.000	56.000	0.590	0.600	.335
$.1430 \times 10^{-05}$	67.000	57.000	0.590	0.650	.375
$.1428 \times 10^{-05}$	68.000	58.000	0.610	0.675	.385
$.1407 \times 10^{-05}$	69.000	59.000	0.610	0.725	.425
$.1396 \times 10^{-05}$	70.000	60.000	0.630	0.750	.435
$.1385 \times 10^{-05}$	71.000	61.000	0.650	0.775	.444
$.1352 \times 10^{-05}$	72.000	62.000	0.690	0.775	.420
$.1350 \times 10^{-05}$	73.000	63.000	0.730	0.775	.395
$.1315 \times 10^{-05}$	74.000	64.000	0.760	0.800	.401
$.1318 \times 10^{-05}$	75.000	65.000	0.740	0.875	.477
$.1281 \times 10^{-05}$	76.000	66.000	0.770	0.900	.483
$.1220 \times 10^{-05}$	77.000	67.000	0.850	0.875	.416
$.1217 \times 10^{-05}$	78.000	68.000	0.860	0.925	.455
$.1211 \times 10^{-05}$	79.000	69.000	0.870	0.975	.495
$.1156 \times 10^{-05}$	80.000	70.000	0.940	0.975	.456
$.1162 \times 10^{-05}$	81.000	71.000	0.990	1.000	.453
$.1167 \times 10^{-05}$	82.000	72.000	0.970	1.075	.531
$.1124 \times 10^{-05}$	83.000	73.000	0.990	1.125	.567
$.1114 \times 10^{-05}$	84.000	74.000	1.010	1.175	.603
$.1070 \times 10^{-05}$	85.000	75.000	1.080	1.200	.591
$.1036 \times 10^{-05}$	86.000	76.000	1.160	1.225	.572
$.1029 \times 10^{-05}$	87.000	77.000	1.150	1.300	.650
$.9617 \times 10^{-06}$	88.000	78.000	1.260	1.325	.618
$.9351 \times 10^{-06}$	89.000	79.000	1.330	1.375	.631

$\phi = 15.0$
$\theta_0 = 10.0$

F	θ_1 (deg)	θ_2 (deg)	d_L (m)	d_1 (m)	d_2 (m)
$.1403 \times 10^{-05}$	55.000	42.500	0.660	0.725	.615
$.1385 \times 10^{-05}$	56.000	43.500	0.690	0.725	.591
$.1360 \times 10^{-05}$	57.000	44.500	0.710	0.750	.595
$.1344 \times 10^{-05}$	58.000	45.500	0.730	0.775	.599
$.1328 \times 10^{-05}$	59.000	46.500	0.750	0.800	.603
$.1311 \times 10^{-05}$	60.000	47.500	0.770	0.825	.607
$.1302 \times 10^{-05}$	61.000	48.500	0.790	0.850	.611
$.1264 \times 10^{-05}$	62.000	49.500	0.830	0.850	.586
$.1281 \times 10^{-05}$	63.000	50.500	0.820	0.925	.649
$.1238 \times 10^{-05}$	64.000	51.500	0.880	0.900	.592
$.1261 \times 10^{-05}$	65.000	52.500	0.900	0.925	.596
$.1191 \times 10^{-05}$	66.000	53.500	0.930	0.950	.599
$.1172 \times 10^{-05}$	67.000	54.500	0.960	0.975	.601
$.1151 \times 10^{-05}$	68.000	55.500	0.990	1.000	.603
$.1127 \times 10^{-05}$	69.000	56.500	1.020	1.025	.604
$.1119 \times 10^{-05}$	70.000	57.500	1.030	1.075	.639
$.1117 \times 10^{-05}$	71.000	58.500	1.040	1.125	.675
$.1086 \times 10^{-05}$	72.000	59.500	1.100	1.125	.639
$.1067 \times 10^{-05}$	73.000	60.500	1.140	1.150	.638
$.1076 \times 10^{-05}$	74.000	61.500	1.160	1.200	.672
$.1023 \times 10^{-05}$	75.000	62.500	1.200	1.225	.668
$.9973 \times 10^{-06}$	76.000	63.500	1.220	1.275	.702
$.9849 \times 10^{-06}$	77.000	64.500	1.270	1.300	.695
$.9852 \times 10^{-06}$	78.000	65.500	1.290	1.350	.727
$.9065 \times 10^{-06}$	79.000	66.500	1.360	1.375	.715
$.9062 \times 10^{-06}$	80.000	67.500	1.390	1.425	.745
$.8742 \times 10^{-06}$	81.000	68.500	1.420	1.475	.774
$.8829 \times 10^{-06}$	82.000	69.500	1.450	1.525	.801
$.8736 \times 10^{-06}$	83.000	70.500	1.490	1.575	.825
$.8810 \times 10^{-06}$	84.000	71.500	1.470	1.650	.903
$.8704 \times 10^{-06}$	85.000	72.500	1.450	1.725	.985
$.8353 \times 10^{-06}$	86.000	73.500	1.500	1.775	1.007
$.8434 \times 10^{-06}$	87.000	74.500	1.460	1.850	1.094
$.5048 \times 10^{-04}$	88.000	75.500	1.500	1.875	1.027
$.7373 \times 10^{-03}$	89.000	76.500	1.500	1.875	.825

$\phi = 20.0$
$\theta_0 = 10.0$

F	θ_1 (deg)	θ_2 (deg)	d_L (m)	d_1 (m)	d_2 (m)
$.1190 \times 10^{-05}$	55.000	40.000	0.970	0.975	.841
$.1170 \times 10^{-05}$	56.000	41.000	0.980	1.025	.867
$.1158 \times 10^{-05}$	57.000	42.000	1.010	1.050	.867
$.1152 \times 10^{-05}$	58.000	43.000	1.030	1.075	.866
$.1111 \times 10^{-05}$	59.000	44.000	1.060	1.100	.865
$.1087 \times 10^{-05}$	60.000	45.000	1.090	1.125	.865
$.1067 \times 10^{-05}$	61.000	46.000	1.120	1.150	.864
$.1046 \times 10^{-05}$	62.000	47.000	1.150	1.175	.863
$.1036 \times 10^{-05}$	63.000	48.000	1.180	1.200	.862
$.1012 \times 10^{-05}$	64.000	49.000	1.220	1.225	.860
$.1012 \times 10^{-05}$	65.000	50.000	1.200	1.300	.924
$.9828 \times 10^{-06}$	66.000	51.000	1.260	1.300	.889
$.9500 \times 10^{-06}$	67.000	52.000	1.300	1.325	.886
$.9357 \times 10^{-06}$	68.000	53.000	1.340	1.350	.883
$.9342 \times 10^{-06}$	69.000	54.000	1.360	1.400	.914
$.8842 \times 10^{-06}$	70.000	55.000	1.400	1.425	.910
$.8539 \times 10^{-06}$	71.000	56.000	1.450	1.450	.903
$.8457 \times 10^{-06}$	72.000	57.000	1.470	1.500	.935
$.8381 \times 10^{-06}$	73.000	58.000	1.480	1.550	.967
$.8221 \times 10^{-06}$	74.000	59.000	1.500	1.600	.999
$.8578 \times 10^{-06}$	75.000	60.000	1.470	1.675	1.075
$.8339 \times 10^{-06}$	76.000	61.000	1.480	1.725	1.109
$.8257 \times 10^{-06}$	77.000	62.000	1.490	1.775	1.144
$.8348 \times 10^{-06}$	78.000	63.000	1.500	1.825	1.180
$.1135 \times 10^{-05}$	79.000	64.000	1.500	1.875	1.215
$.3470 \times 10^{-04}$	80.000	65.000	1.500	1.875	1.141
$.1480 \times 10^{-03}$	81.000	66.000	1.500	1.875	1.053
$.3948 \times 10^{-03}$	82.000	67.000	1.500	1.875	.946
$.8716 \times 10^{-03}$	83.000	68.000	1.500	1.875	.813
$.1762 \times 10^{-02}$	84.000	69.000	1.500	1.875	.641
$.3440 \times 10^{-02}$	85.000	70.000	1.500	1.875	.413
$.6748 \times 10^{-02}$	86.000	71.000	1.500	1.875	.092
$.1387 \times 10^{-01}$	87.000	72.000	1.500	1.875	-.394
$.3174 \times 10^{-01}$	88.000	73.000	1.500	1.875	-1.215
$.9192 \times 10^{-01}$	89.000	74.000	1.500	1.875	-2.911

Figures

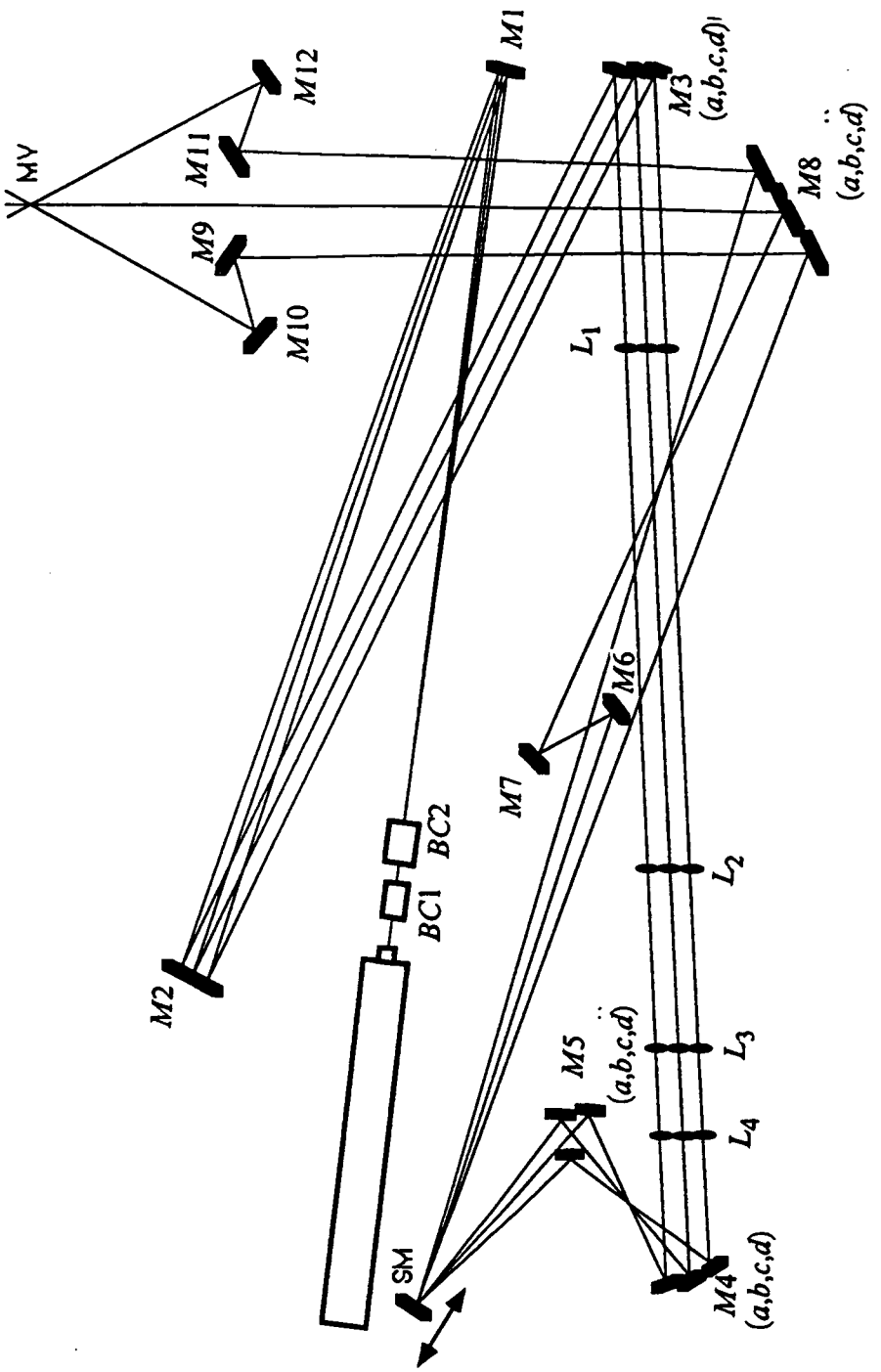

Figure 1. Top View of Optical Configuration of the RSLDV System.

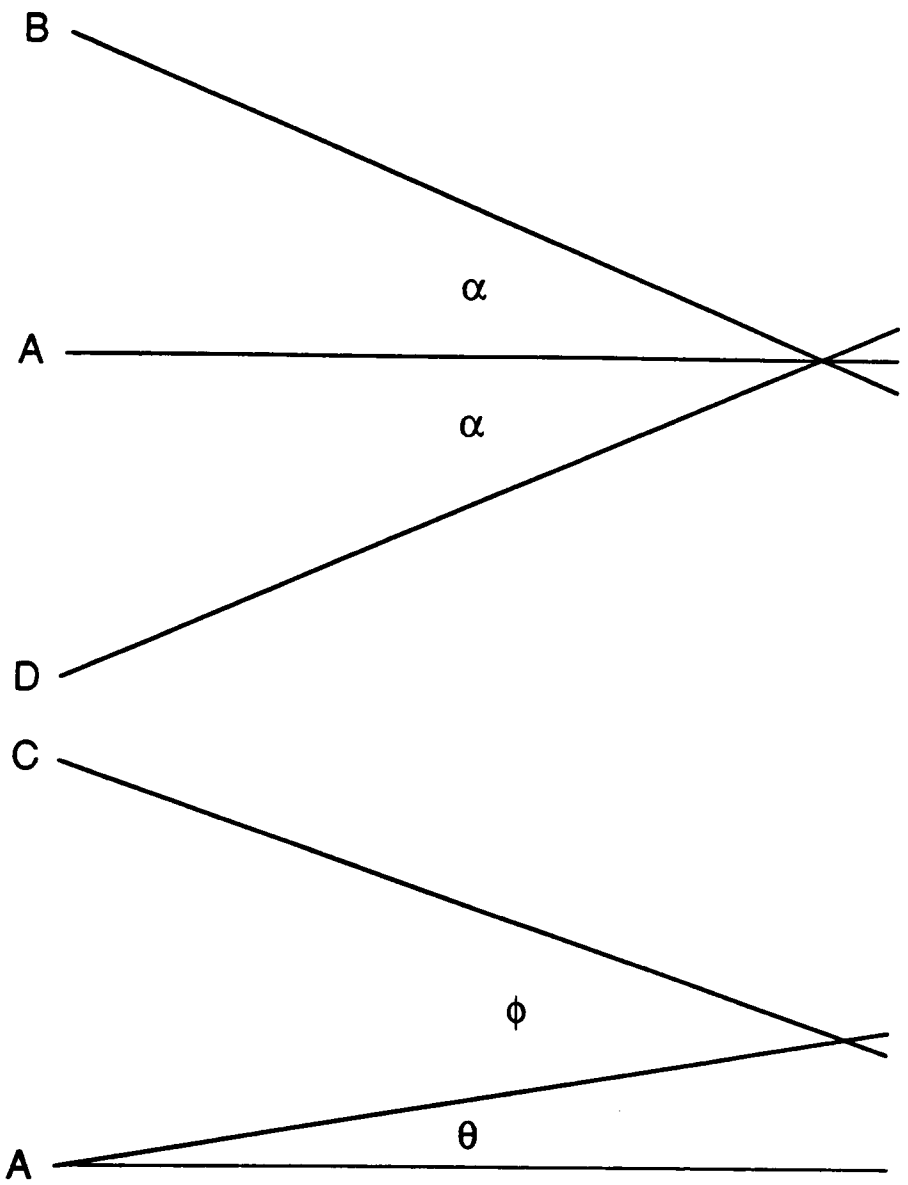

Figure 2. Top and Side View of the Four Beams Intersecting to form the Measurement Volume.

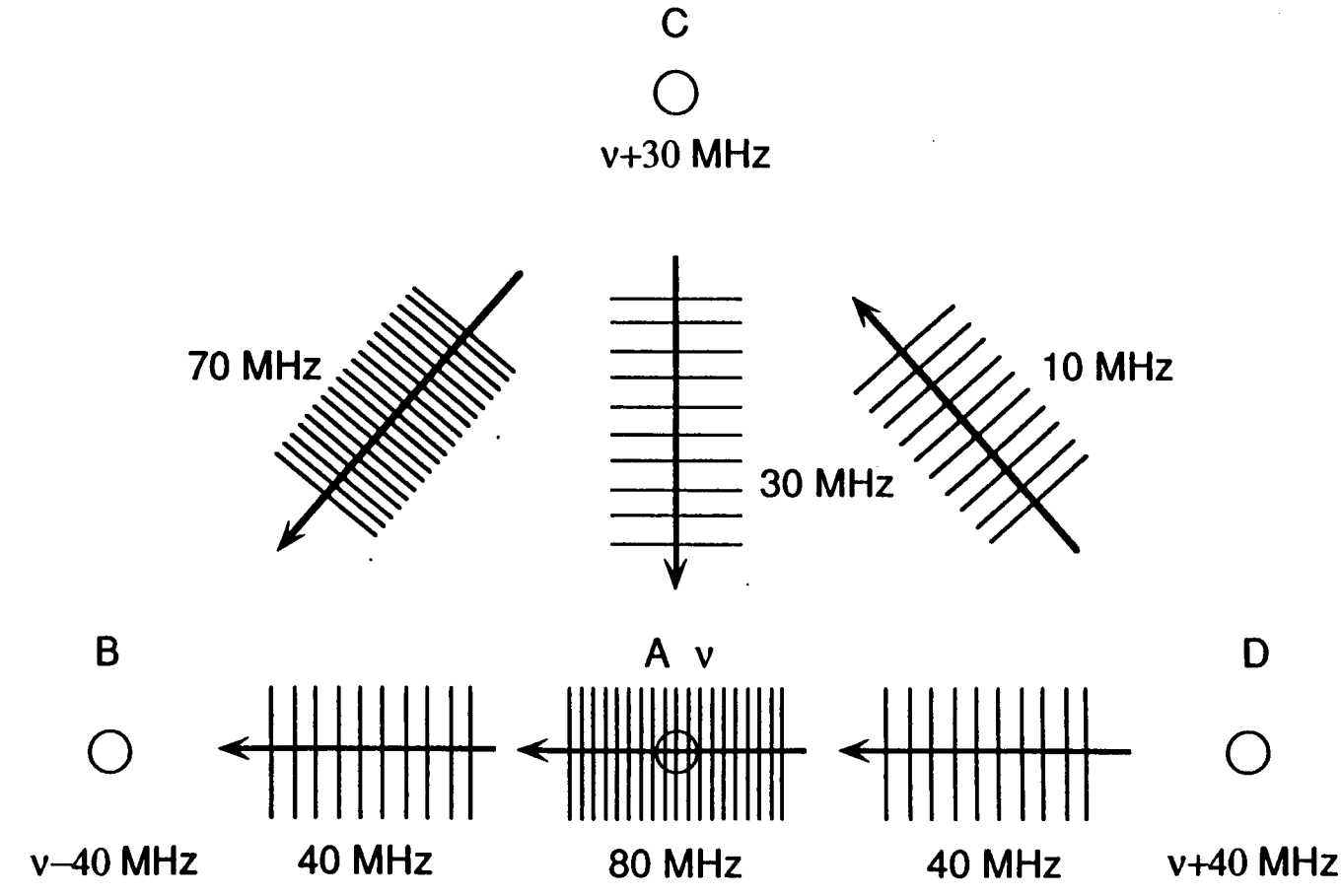

Figure 3. On-axis View of the Four Beams forming the Measurement Volume for the Single Color System.

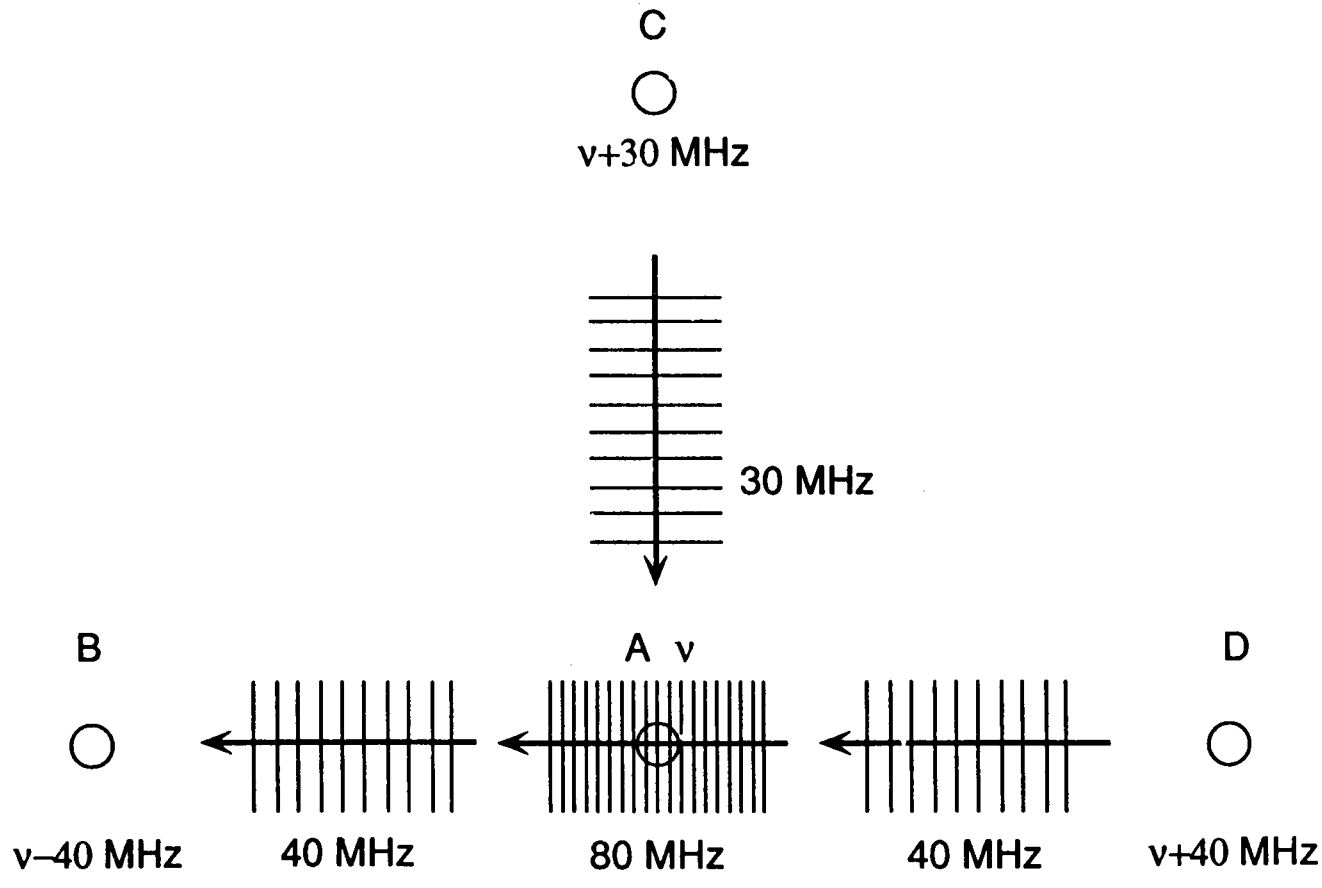

Figure 4. On-axis View of the Four Beams forming the Measurement Volume for the Two Color System.

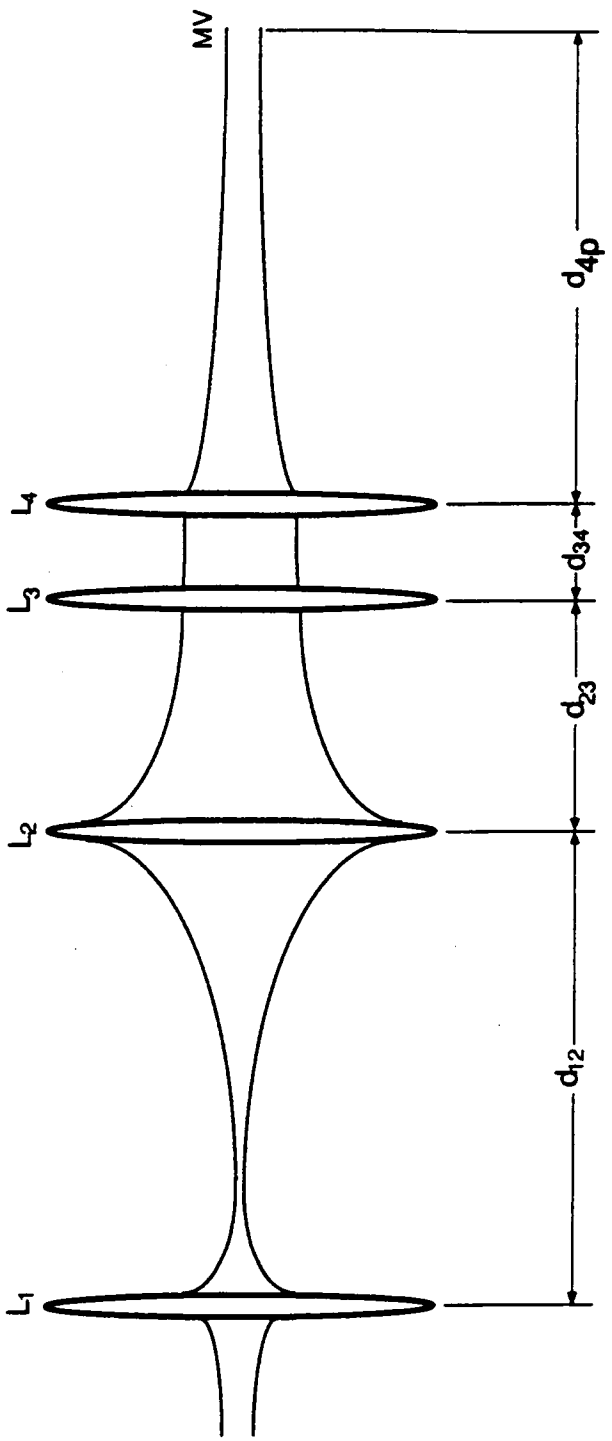

Figure 5. Side View of Transmitting Lens Configuration.

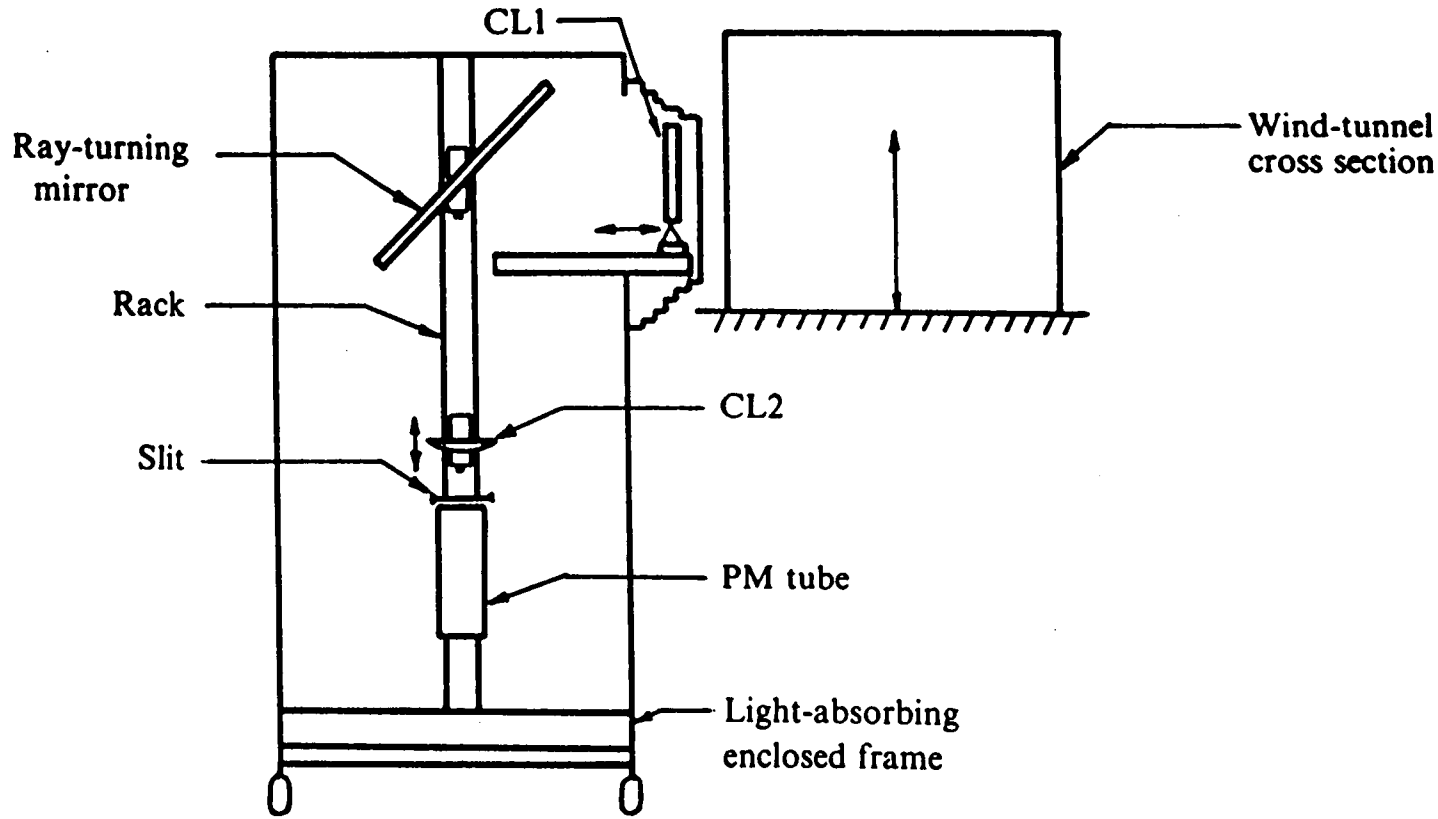

Figure 6. Receiving Optics Schematic Diagram.

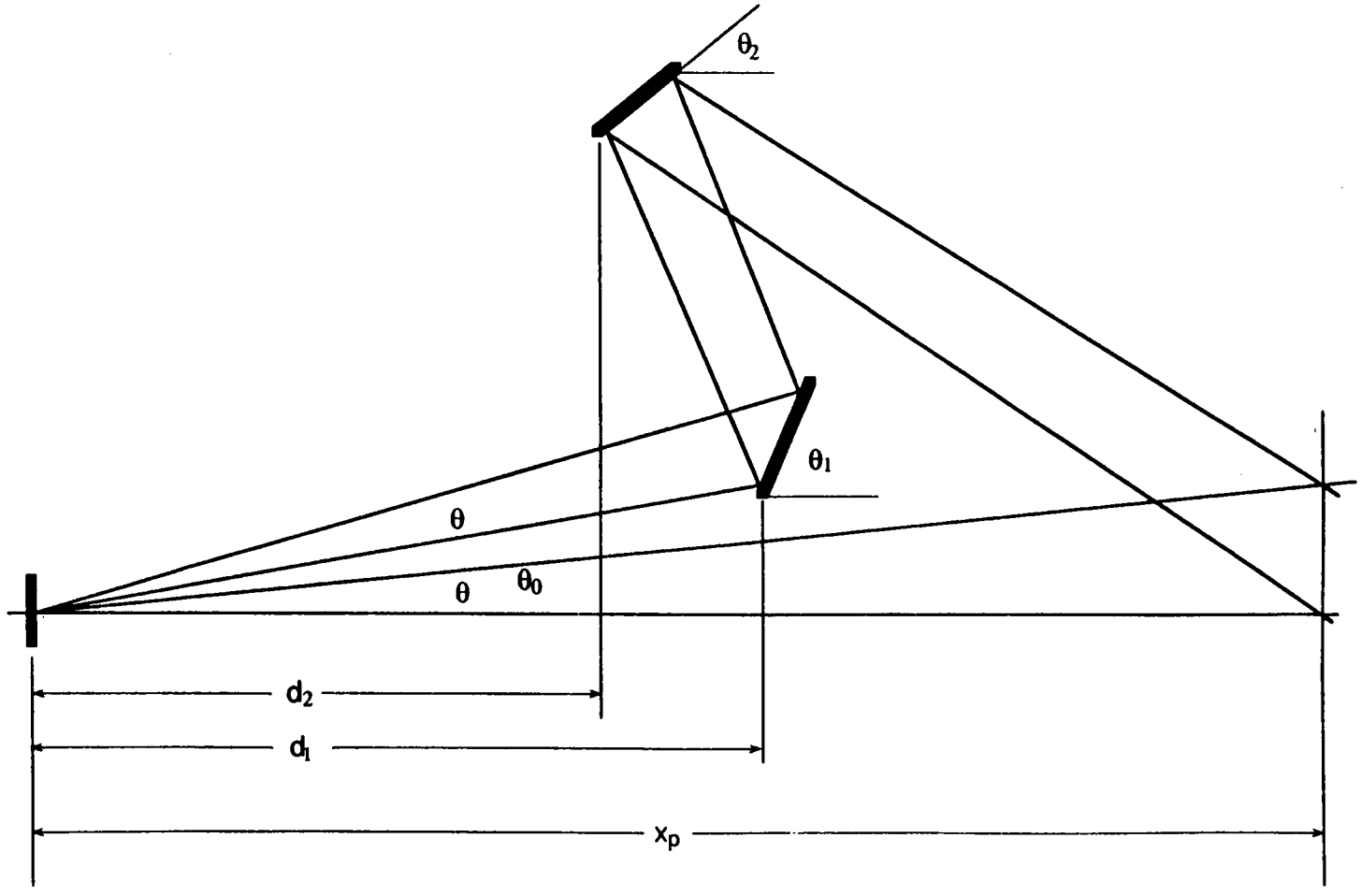

Figure 7. Side View of Vertical Plane Optics: Plane Mirror Pair.

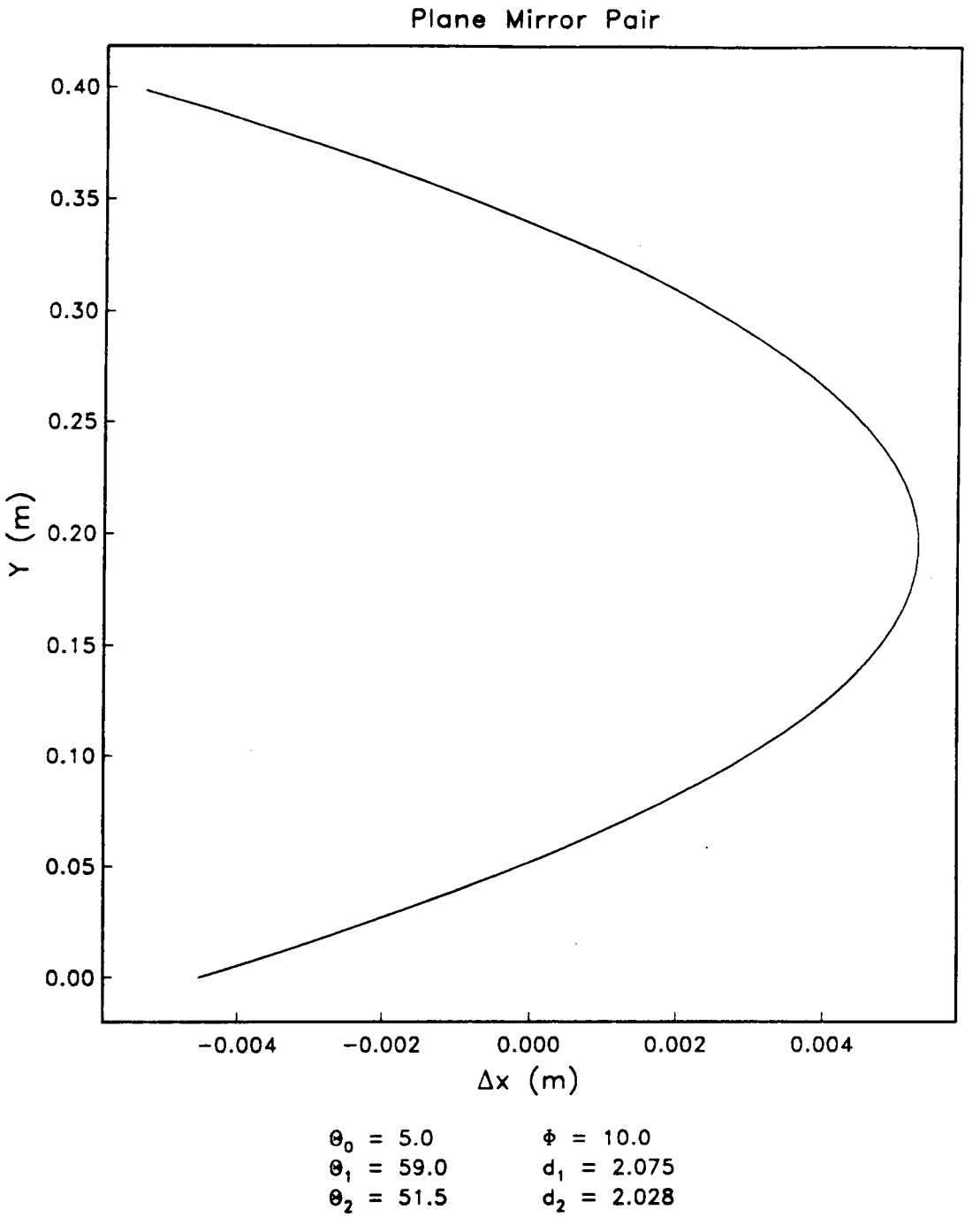

Figure 8. Scan Path of Probe Volumes: Plane Mirror Pair.

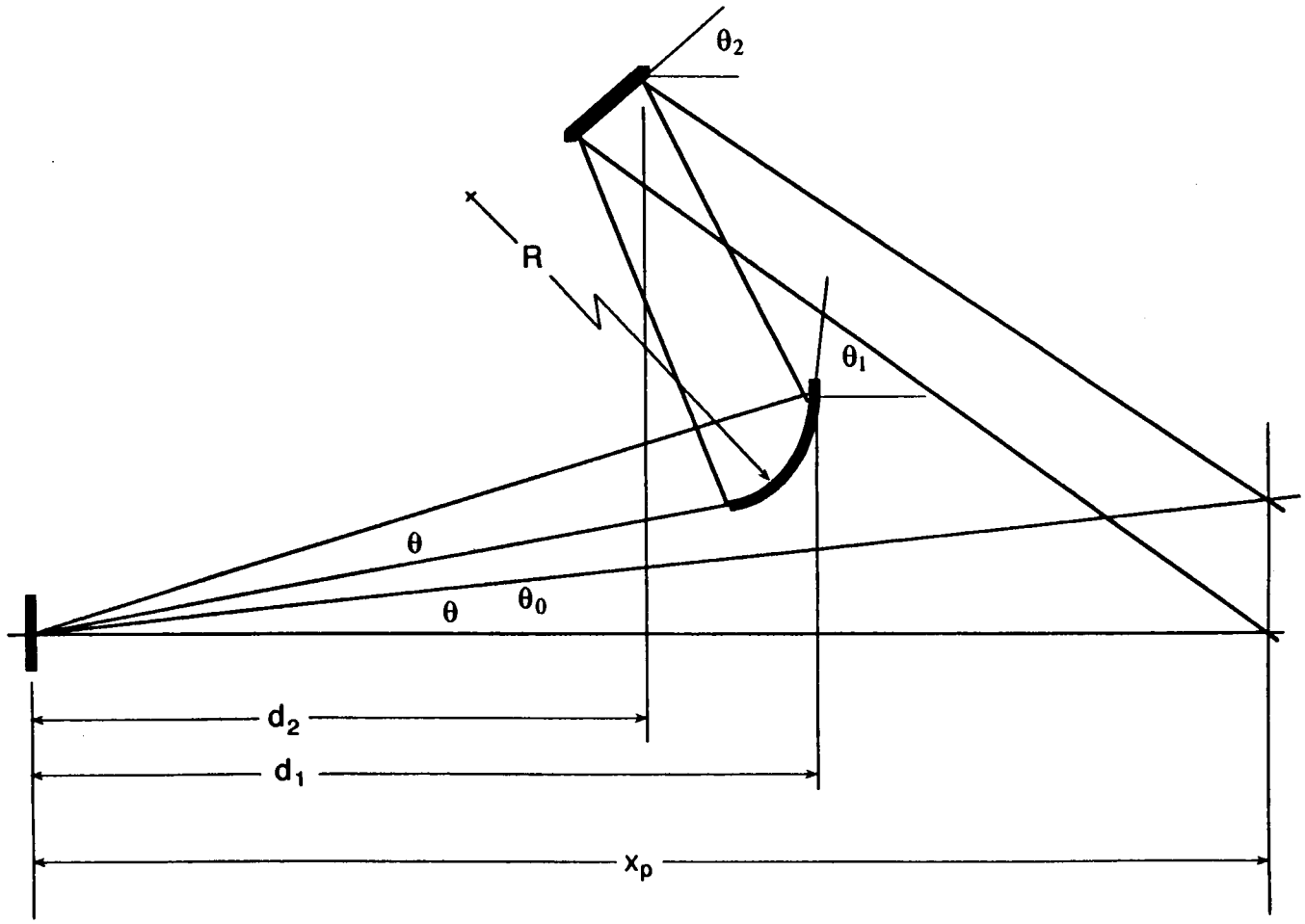

Figure 9. Side View of Vertical Plane Optics: Concave-Plane Mirror Pair.

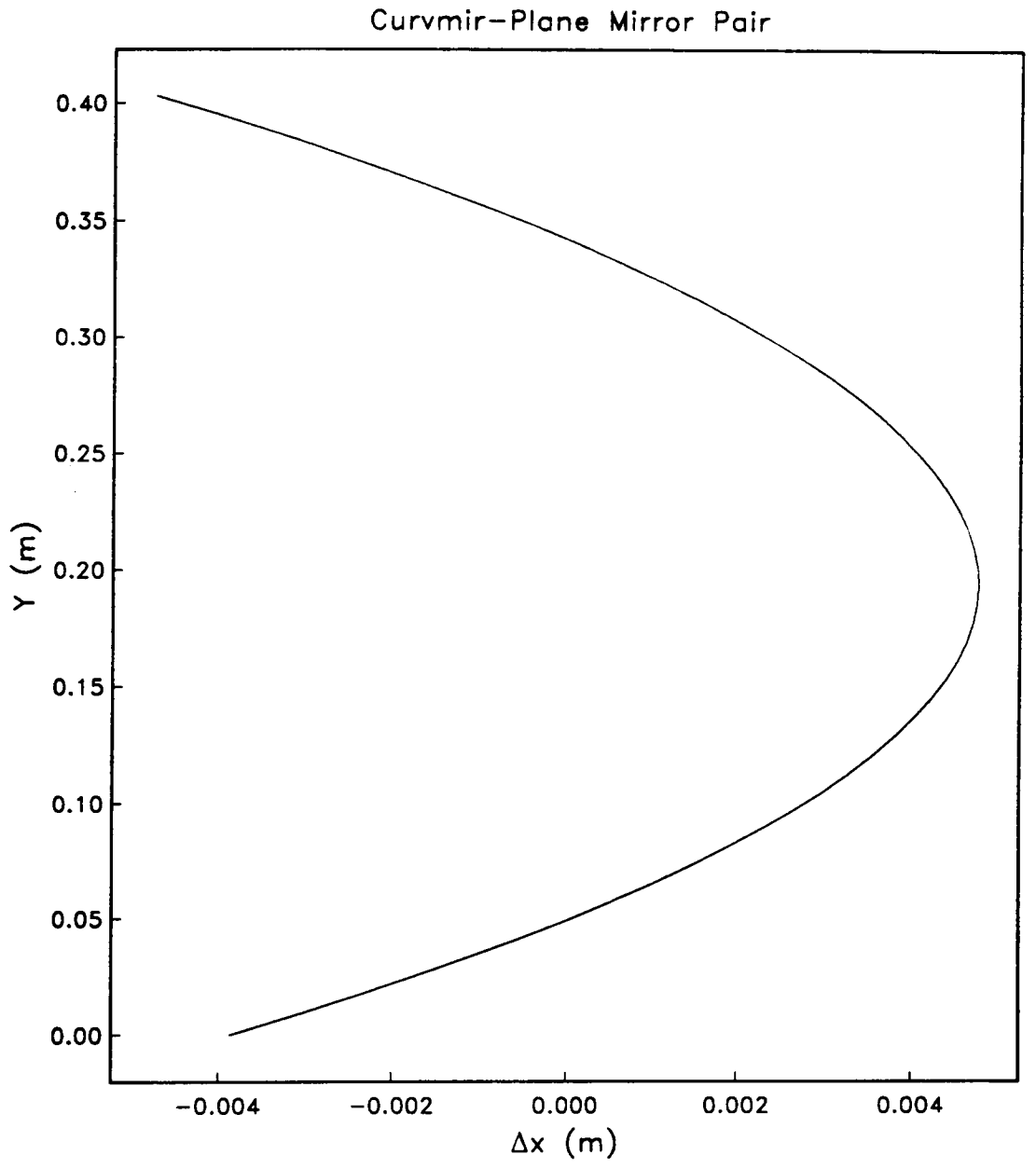

Figure 10. Scan Path of Probe Volumes: Concave-Plane Mirror Pair.

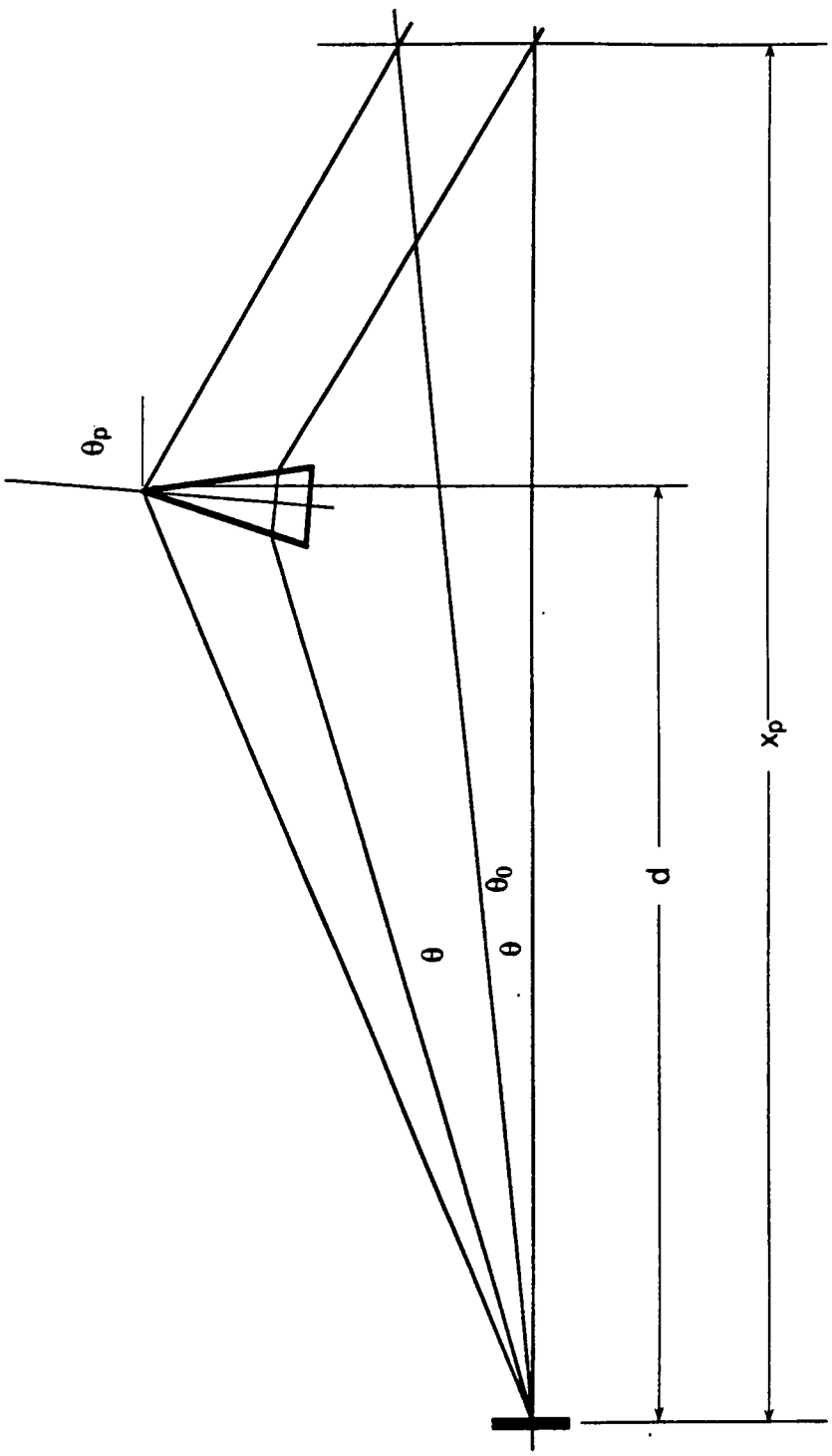

Figure 11. Side View of Vertical Plane Optics: Prism.

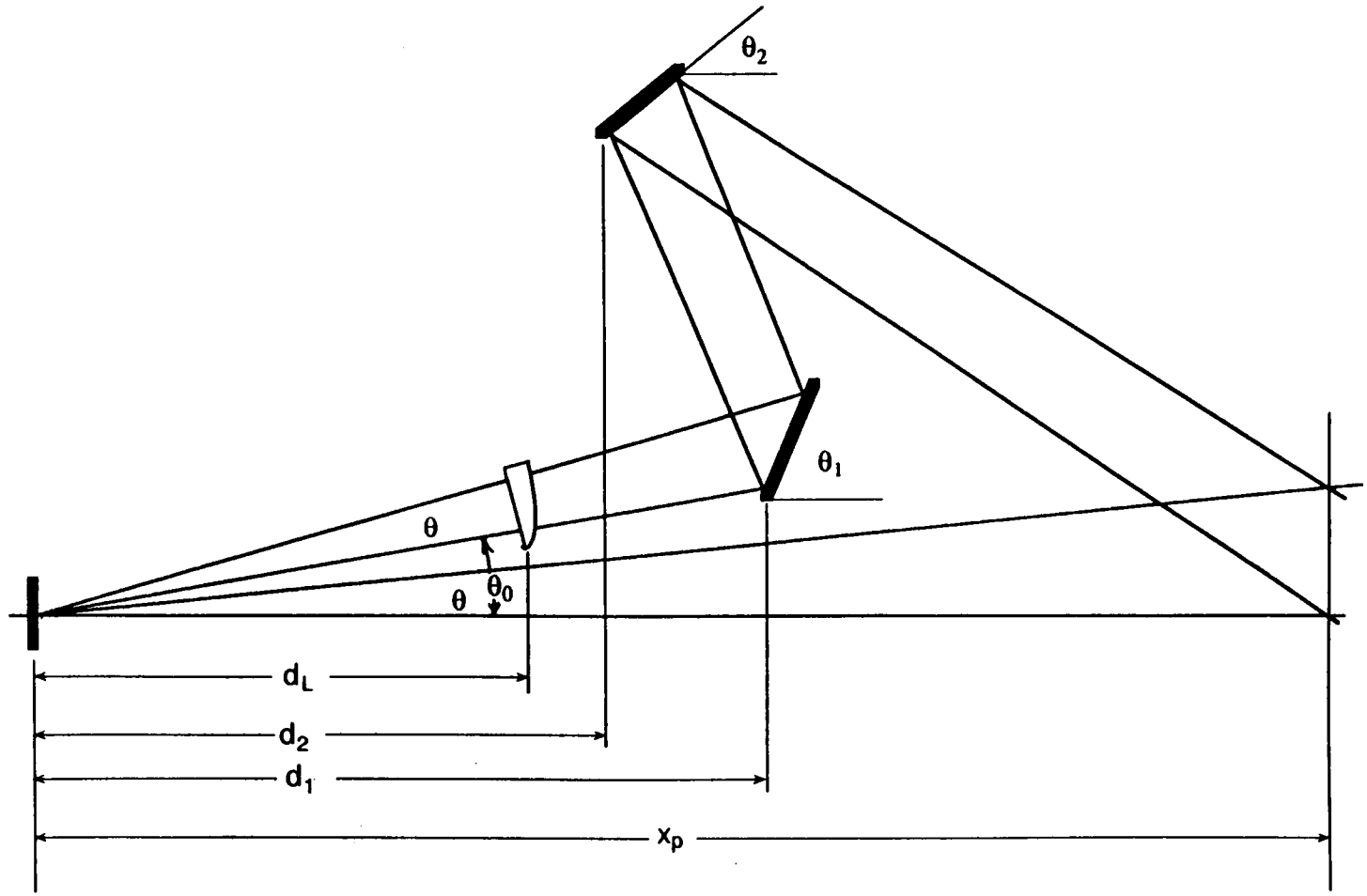

Figure 12. Side View of Vertical Plane Optics: Lens, Plane Mirror Pair.

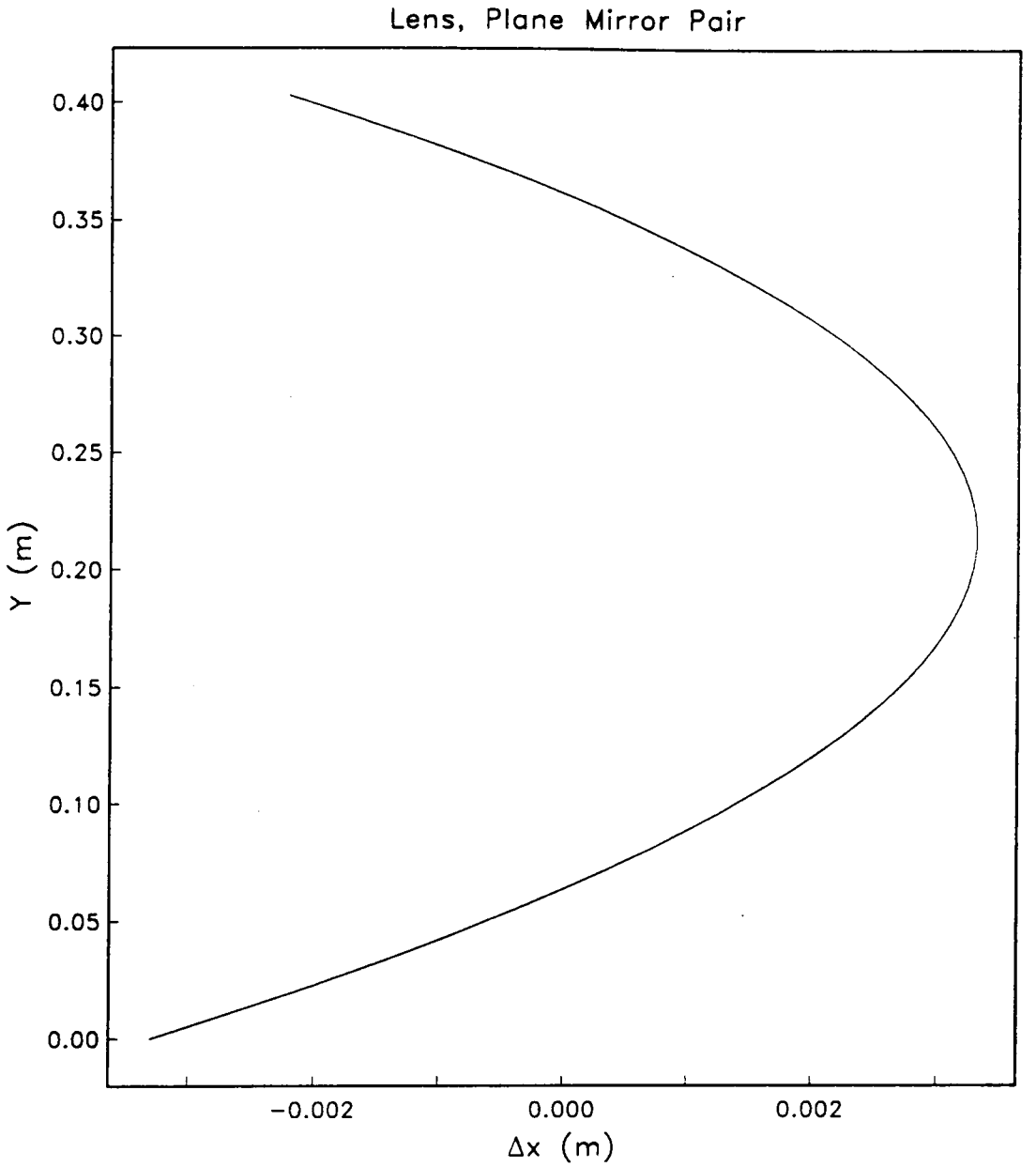

Figure 13. Scan Path of Probe Volumes: Lens, Plane Mirror Pair.

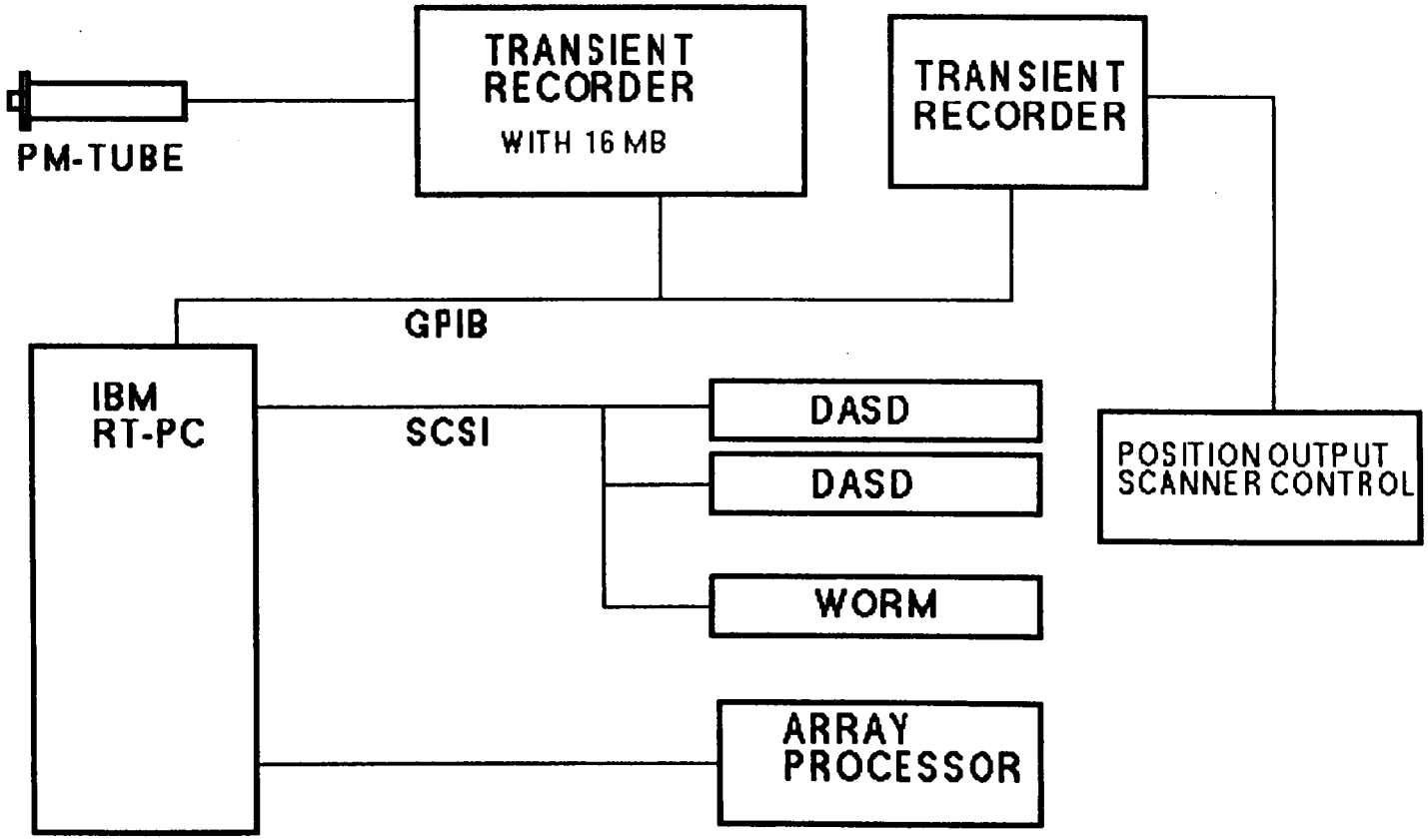

Figure 14. Schematic Diagram of Data Acquistion, Control and Processing System.

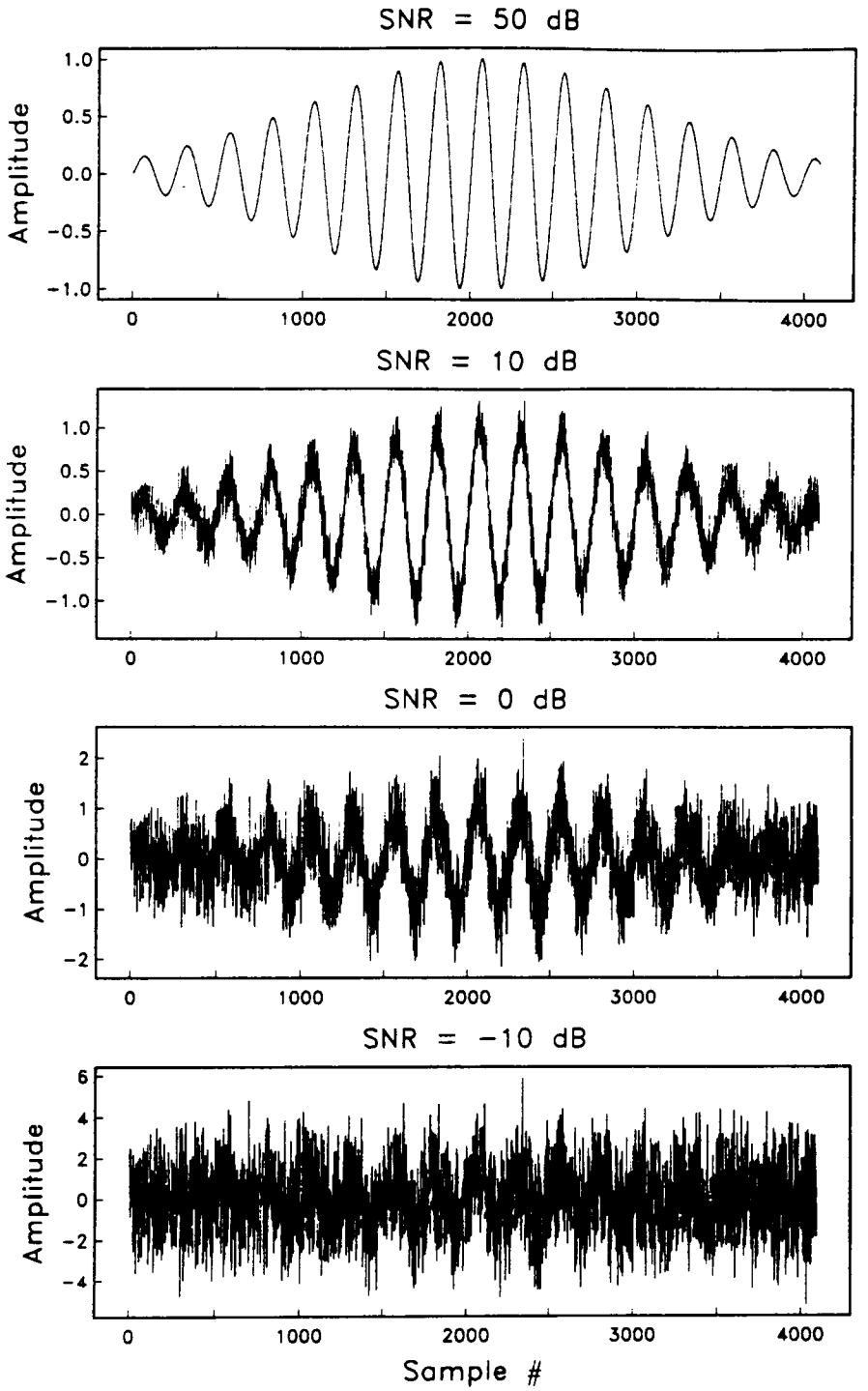

Figure 15. Typical LDV Burst Signals at Various SNR Levels.

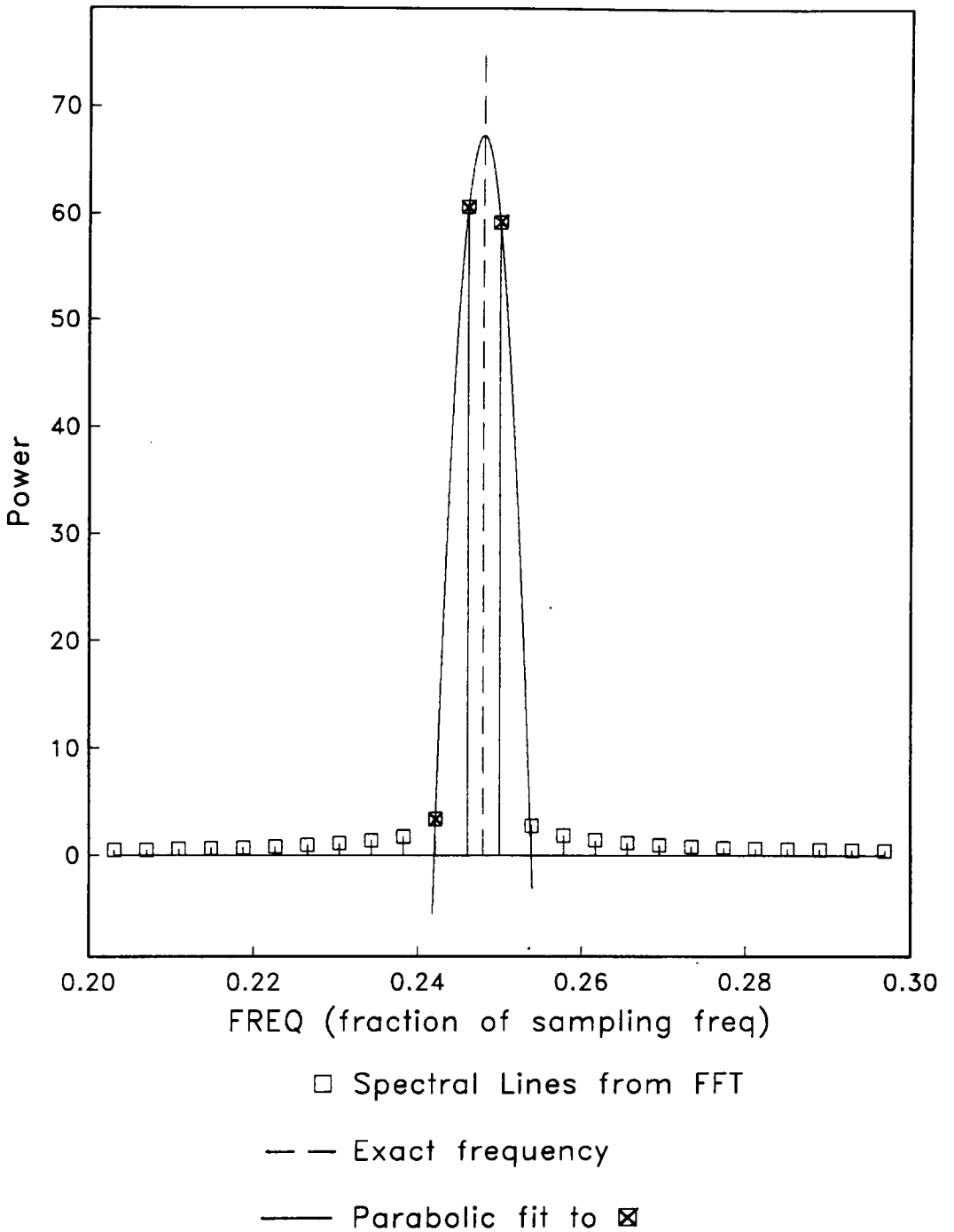

Figure 16. Illustration of Parabolic Fit.

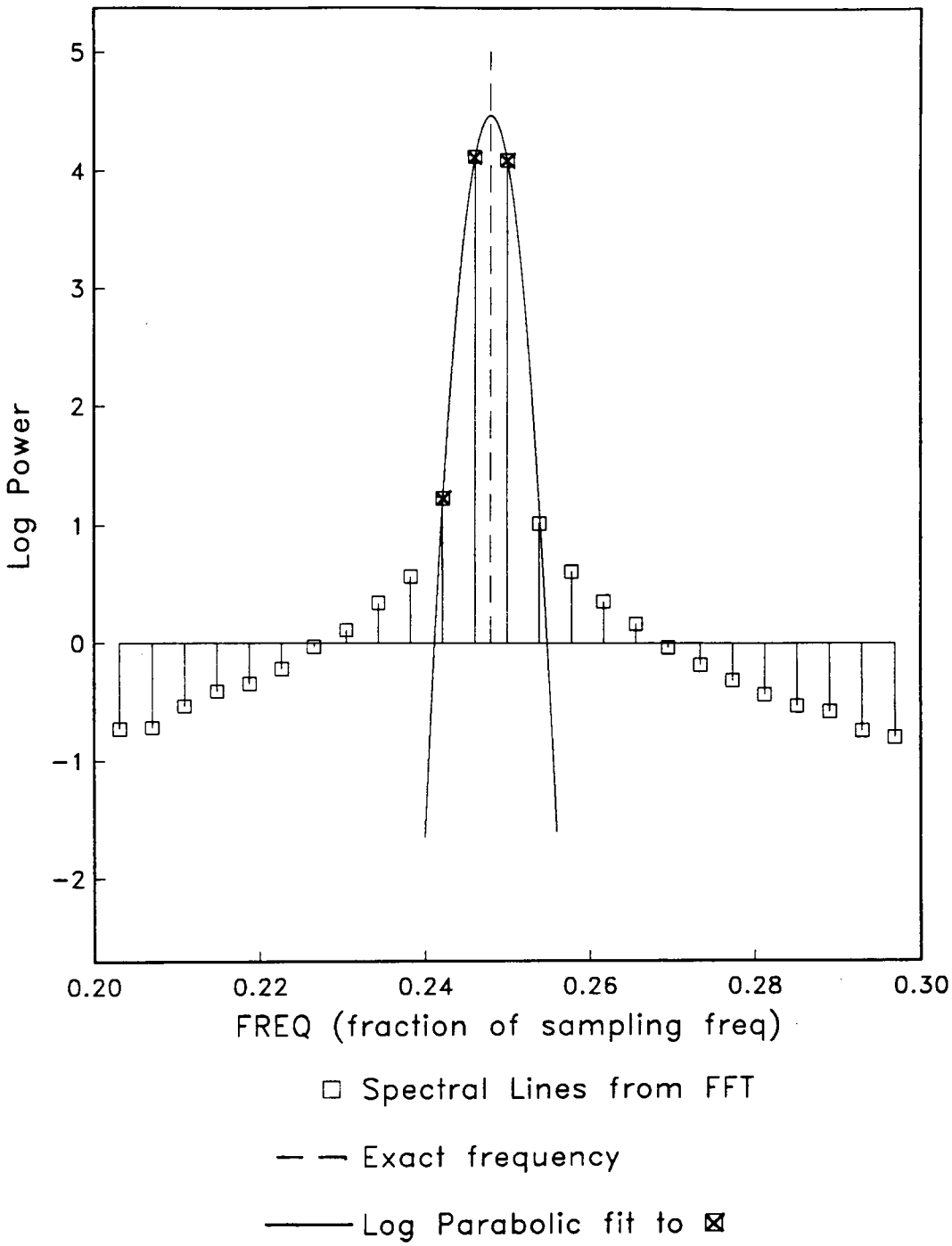

Figure 17. Illustration of Log Parabolic Fit.

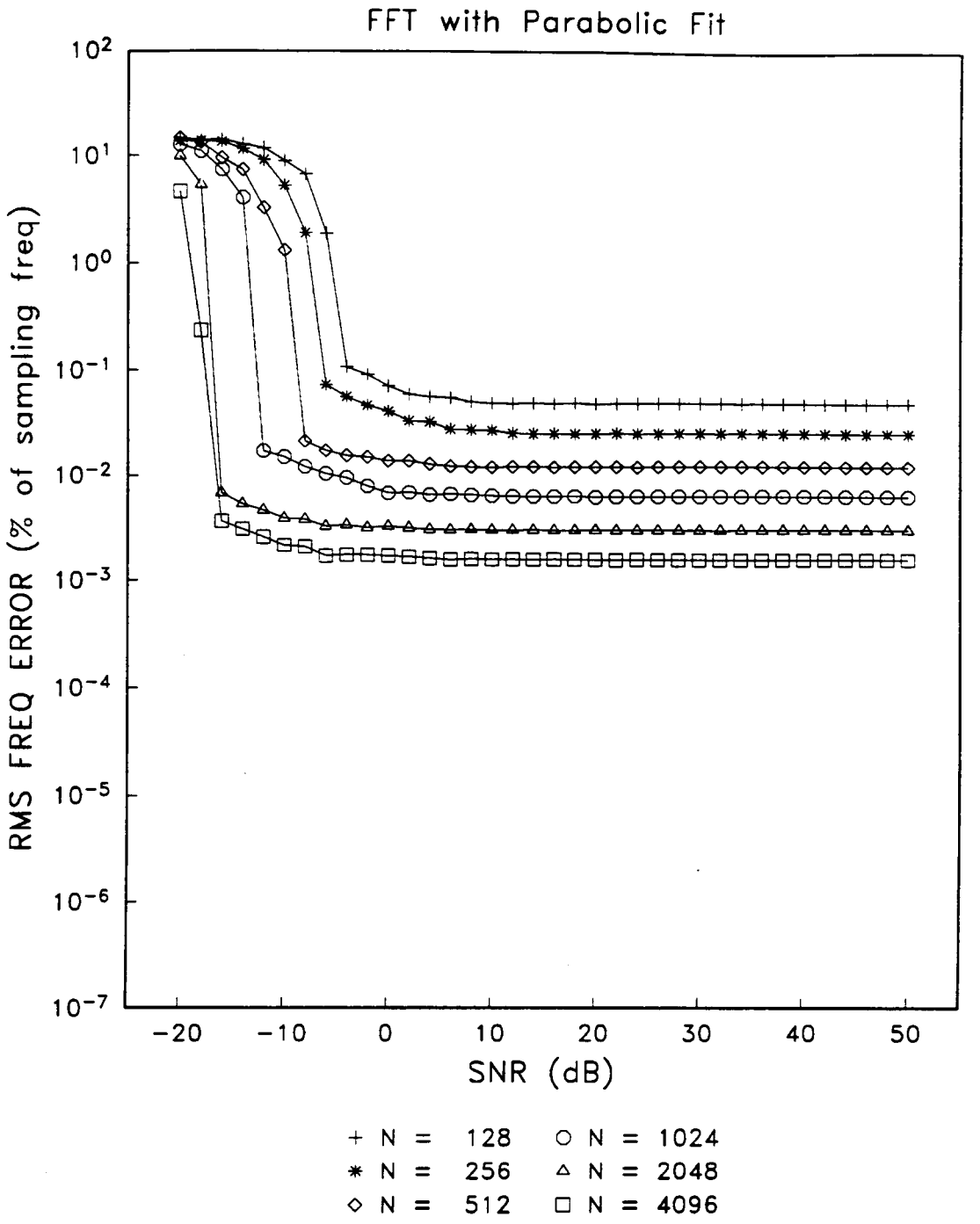

Figure 18. RMS Frequency Error vs. SNR for FFT with Parabolic Interpolation.: f = 0.225

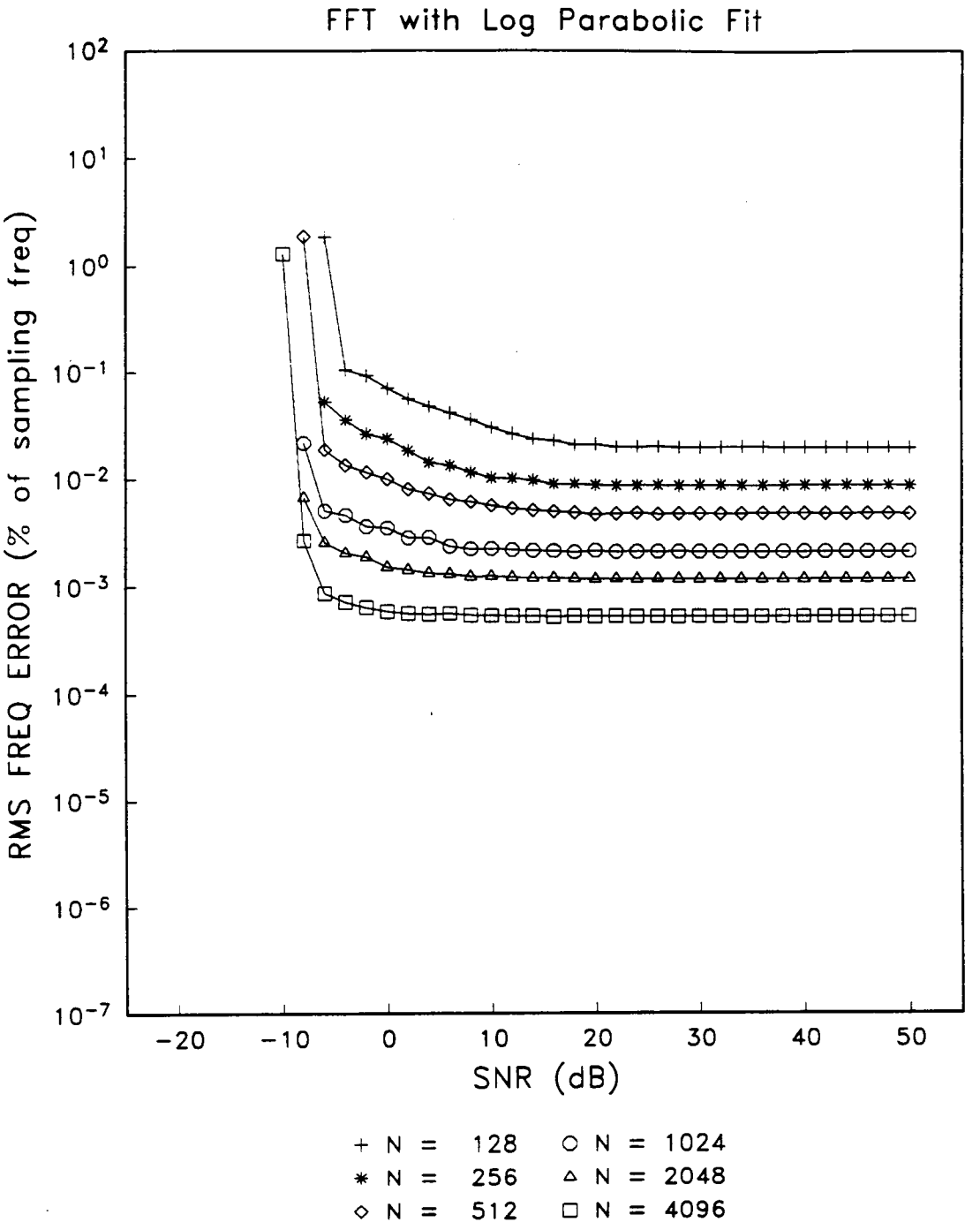

Figure 19. RMS Frequency Error vs. SNR for FFT with Log Parabolic Interpolation.: f = 0.225

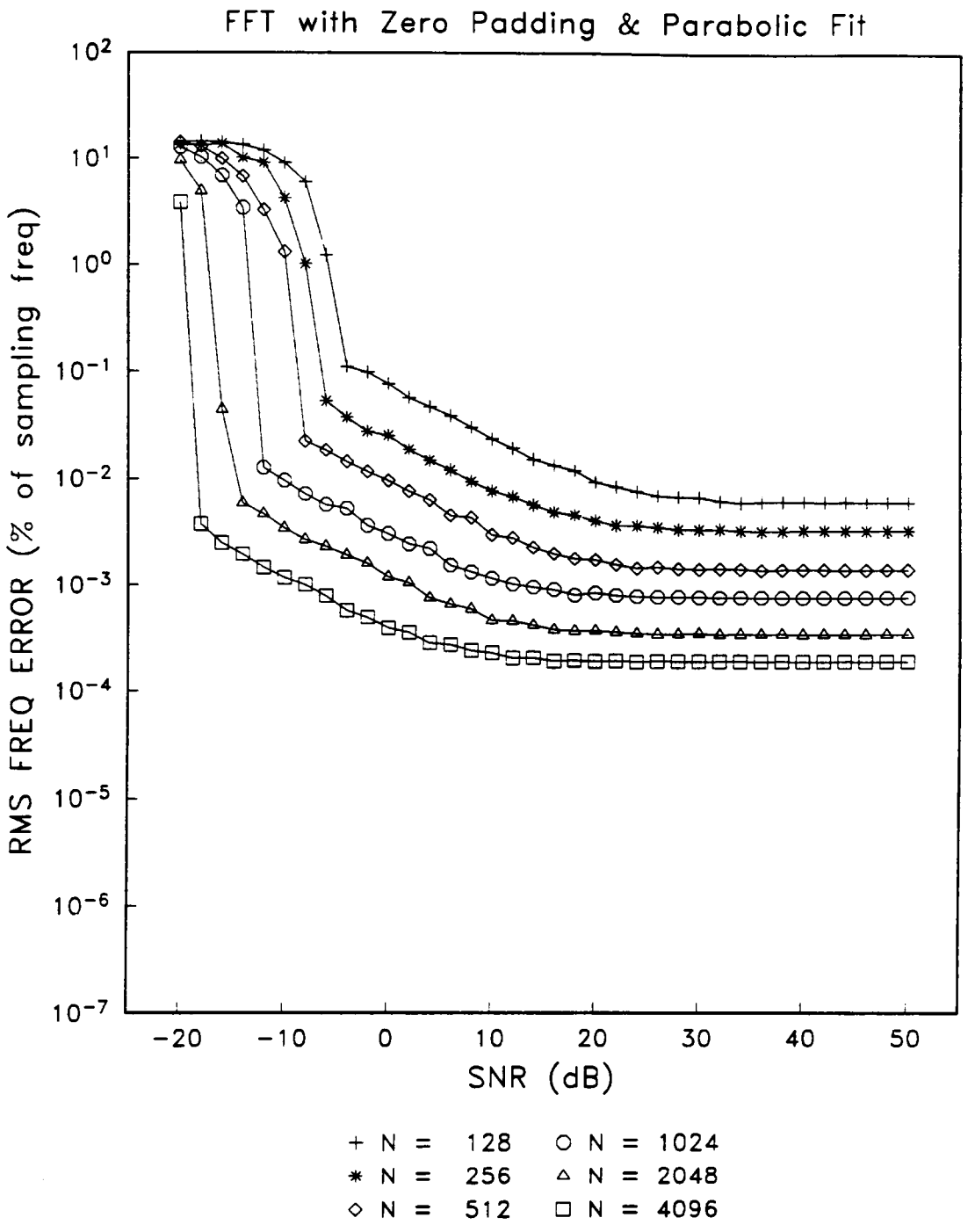

Figure 20. RMS Frequency Error vs. SNR for FFT with Zero-padding and Parabolic Interpolation.: f = 0.225

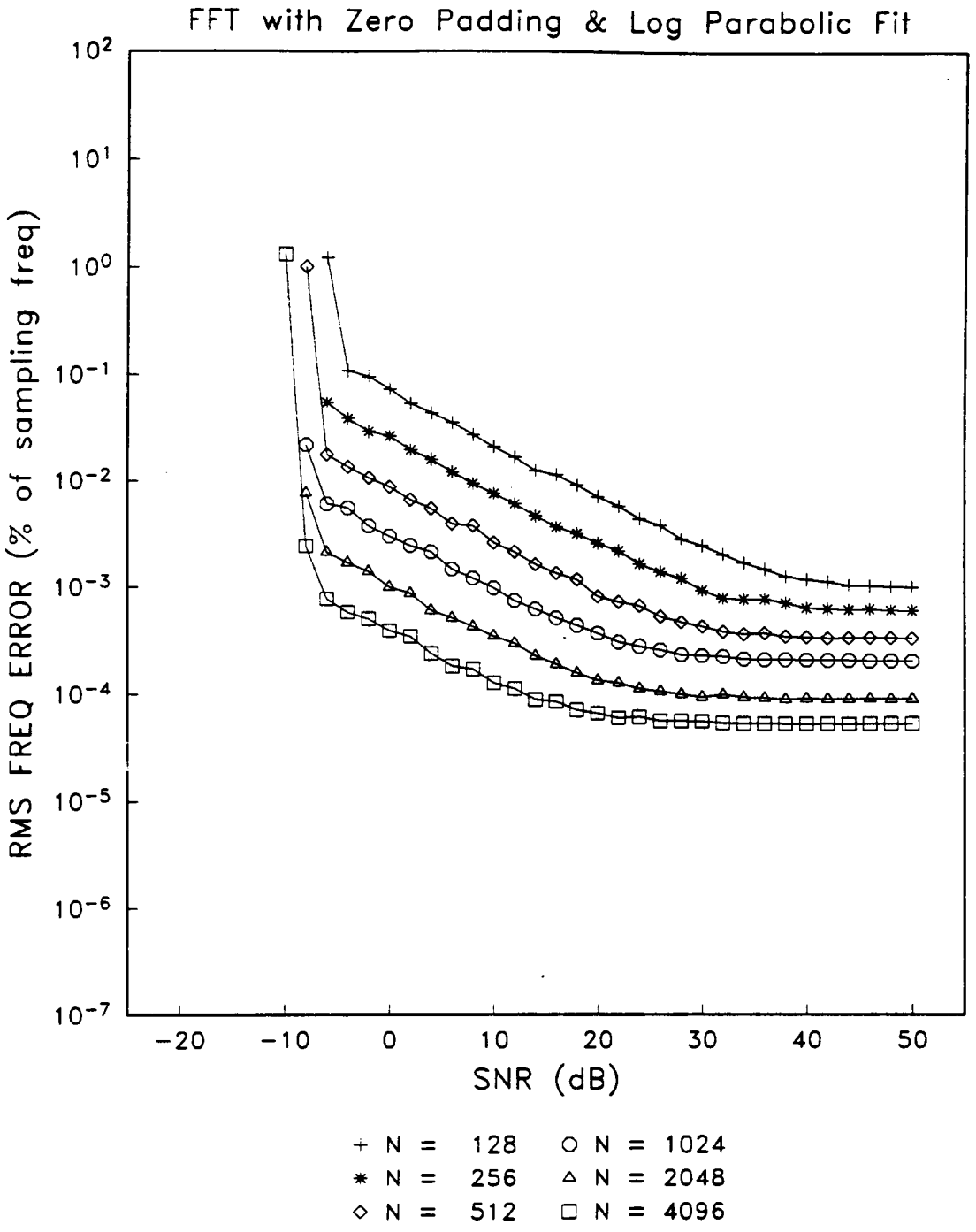

Figure 21. RMS Frequency Error vs. SNR for FFT with Zero-padding and Log Parabolic Interpolation.: f = 0.225

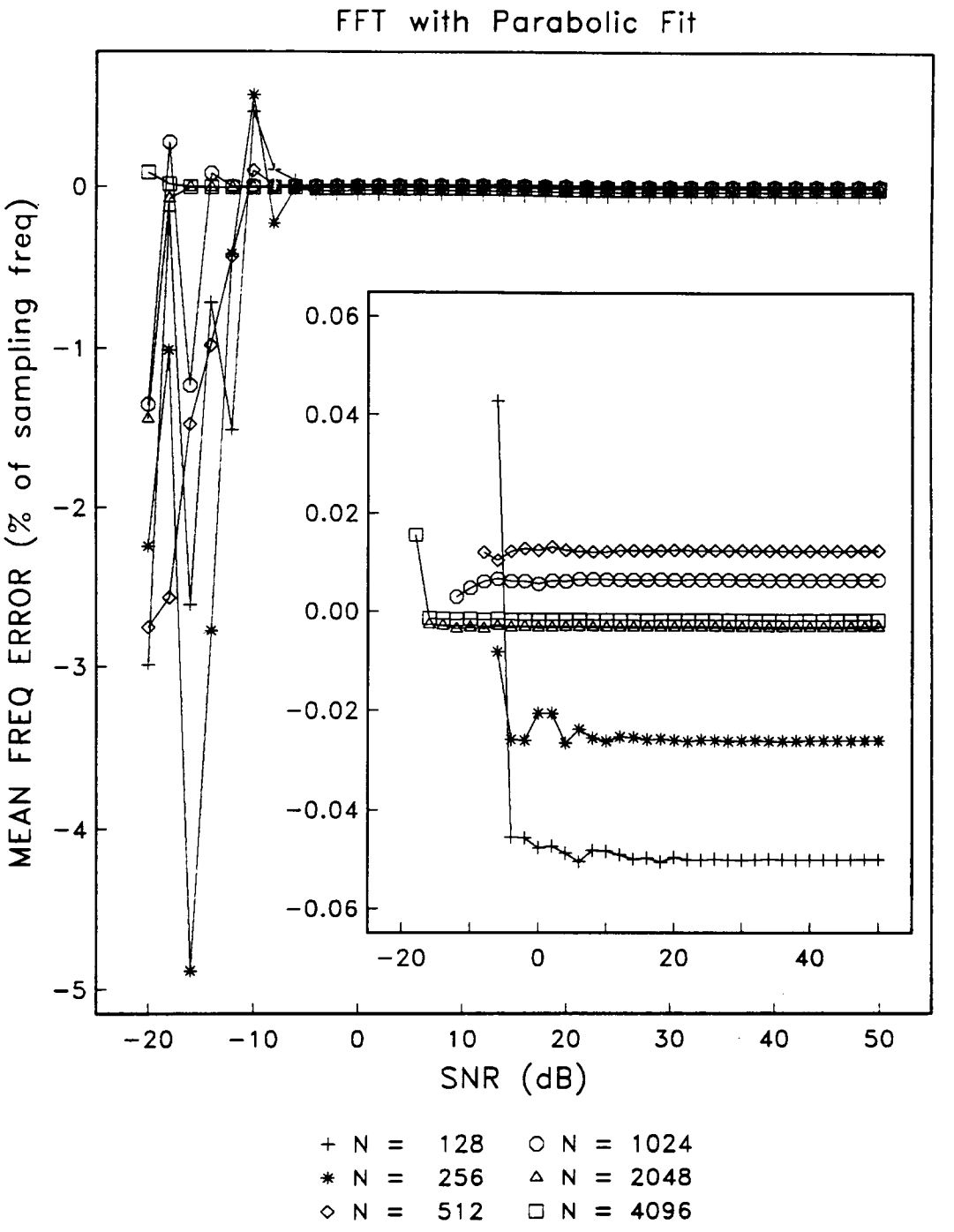

Figure 22. Frequency Bias Error vs. SNR for FFT with Parabolic Interpolation.: f = 0.225

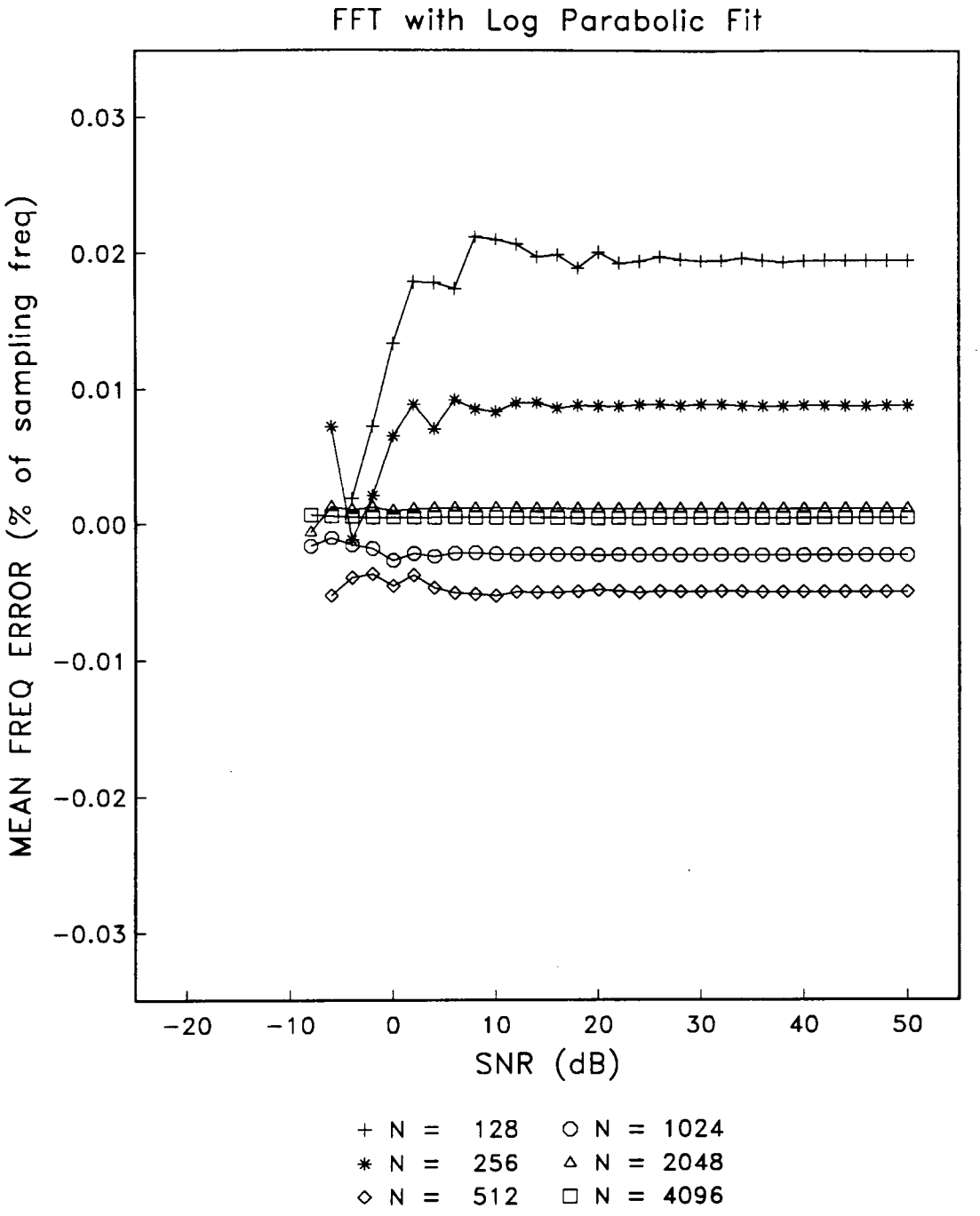

Figure 23. Frequency Bias Error vs. SNR for FFT with Log Parabolic Interpolation.: f = 0.225

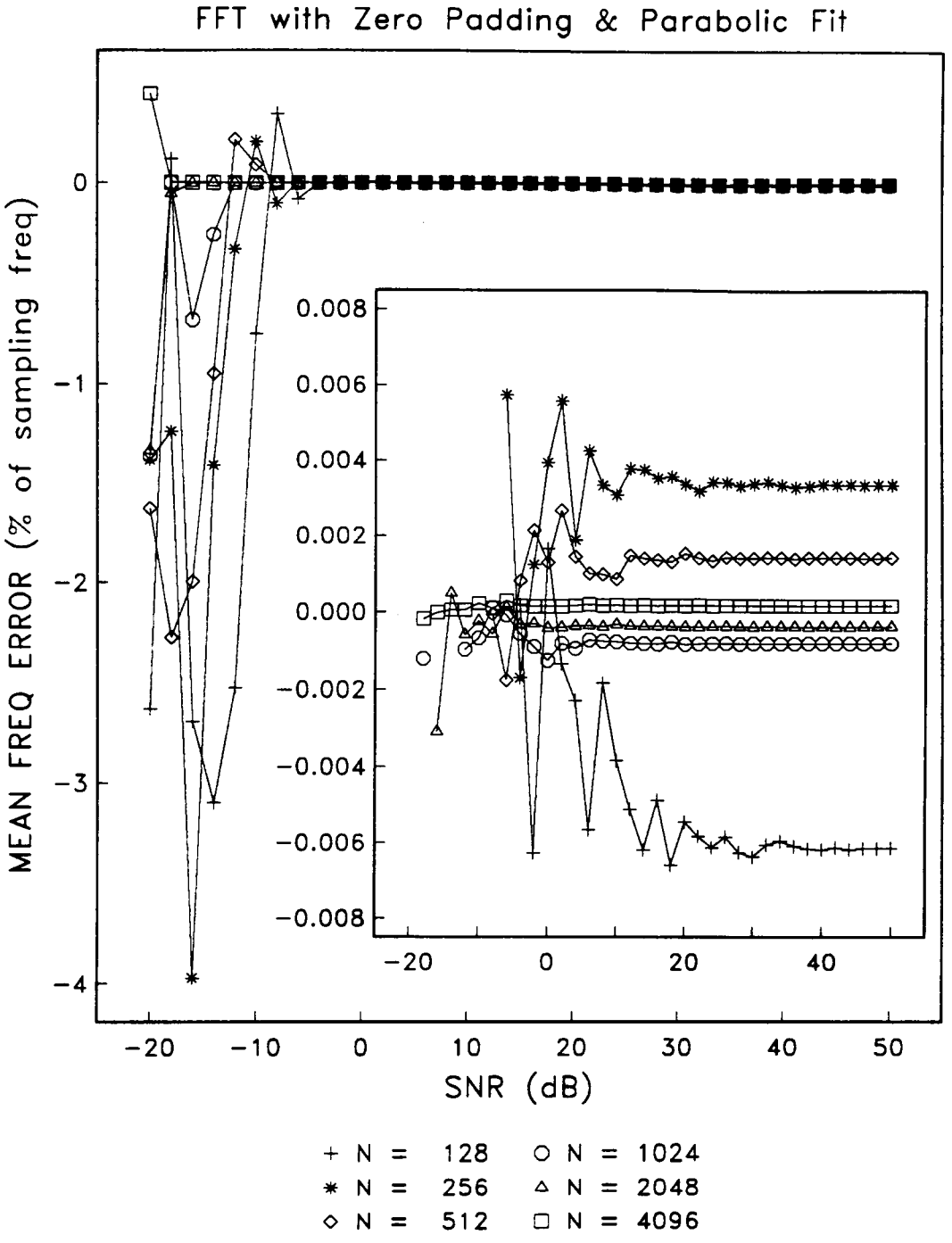

Figure 24. Frequency Bias Error vs. SNR for FFT with Zero-padding and Parabolic Interpolation.: f = 0.225

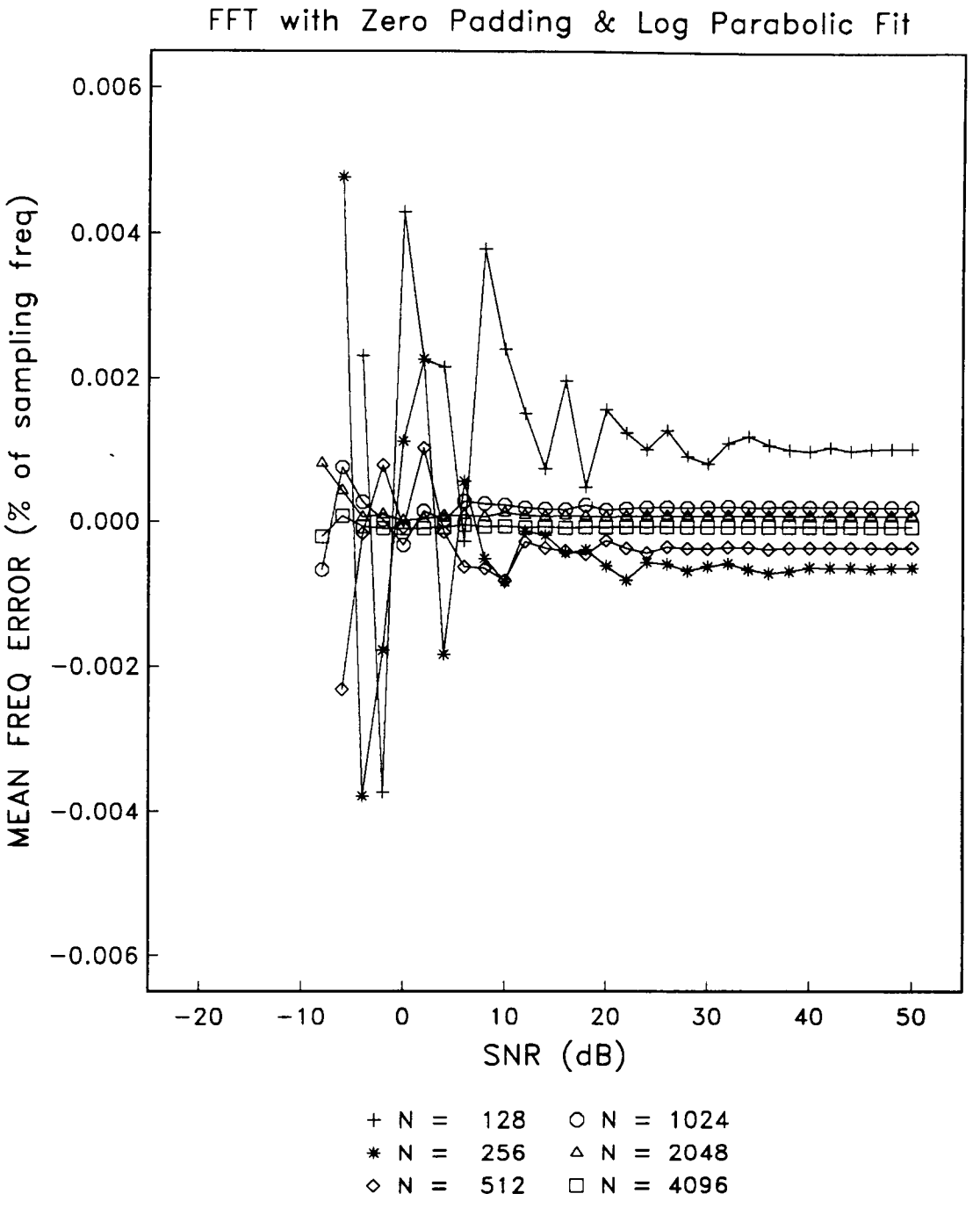

Figure 25. Frequency Bias Error vs. SNR for FFT with Zero-padding and Log Parabolic Interpolation.: f = 0.225

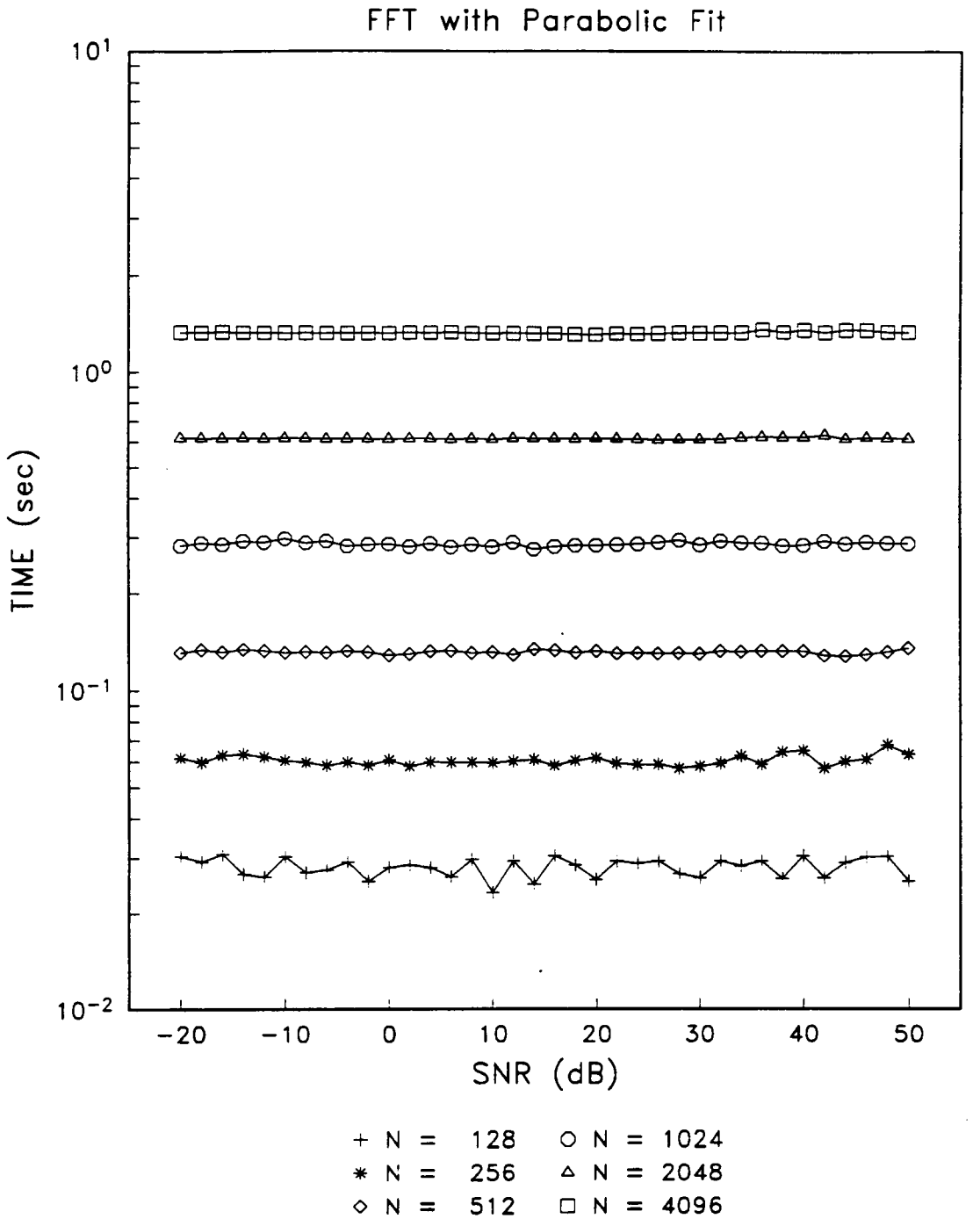

Figure 26. Computation Time vs. SNR for FFT with Parabolic Interpolation.: f = 0.225

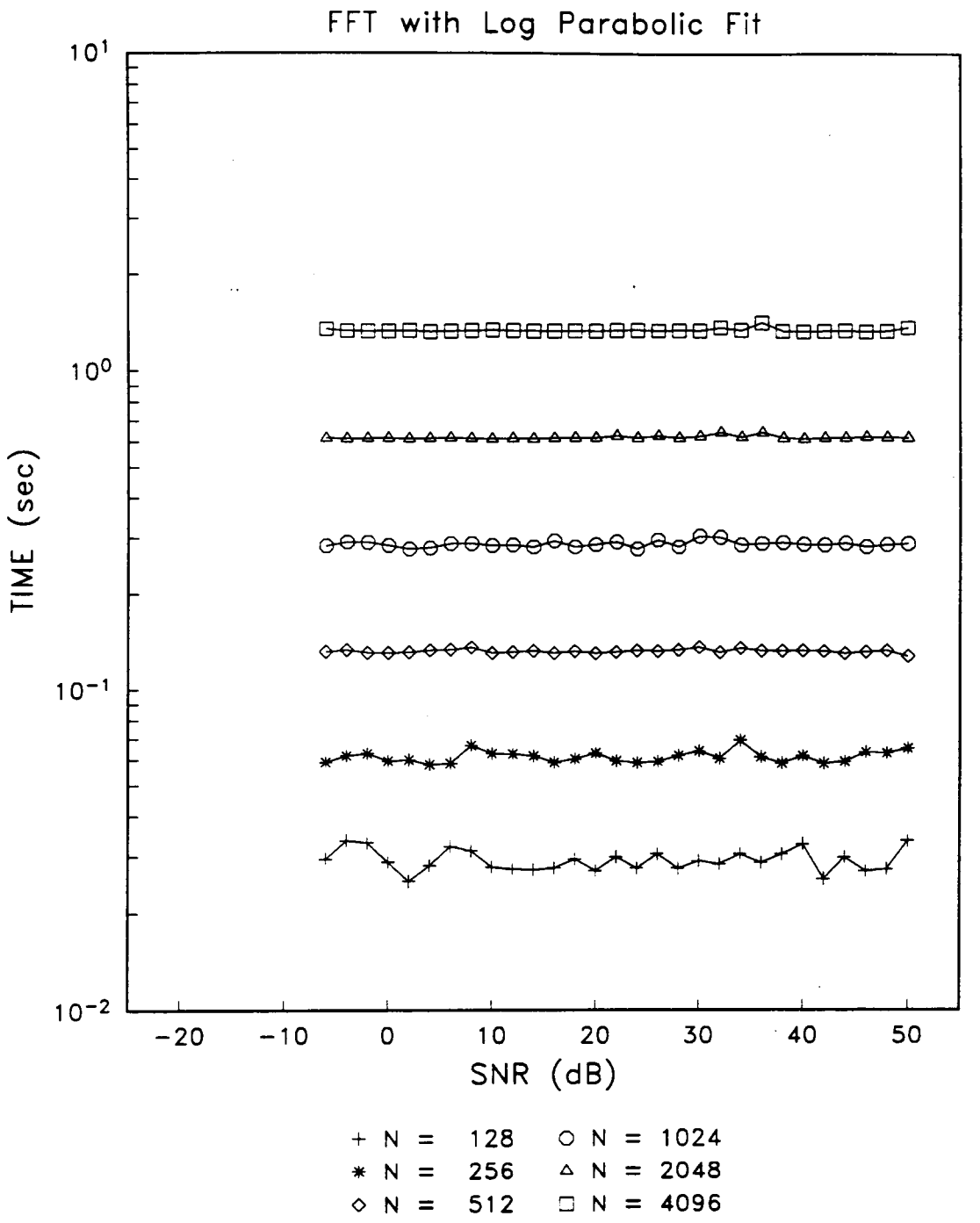

Figure 27. Computation Time vs. SNR for FFT with Log Parabolic Interpolation.: f = 0.225

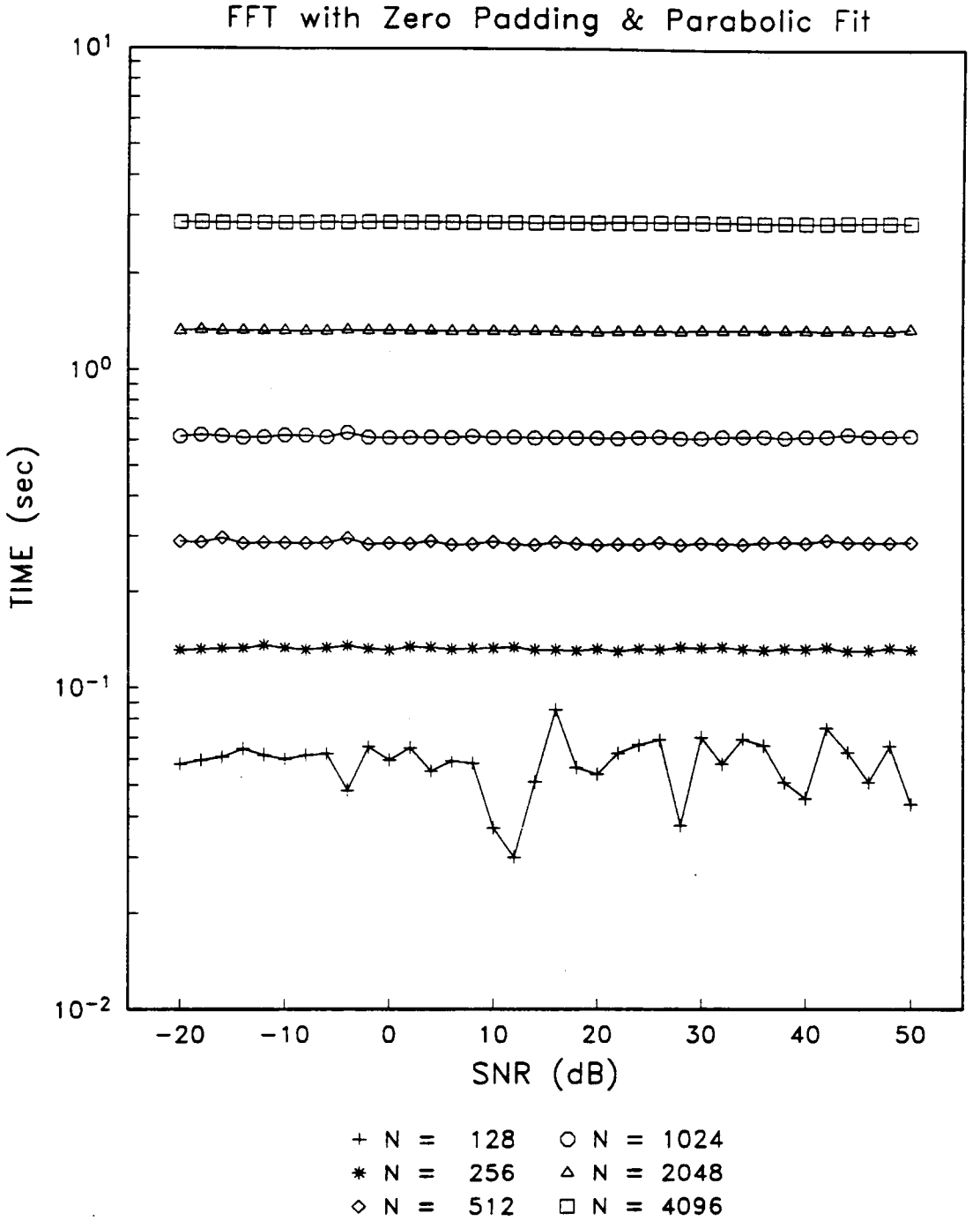

Figure 28. Computation Time vs. SNR for FFT with Zero-padding and Parabolic Interpolation.: f = 0.225

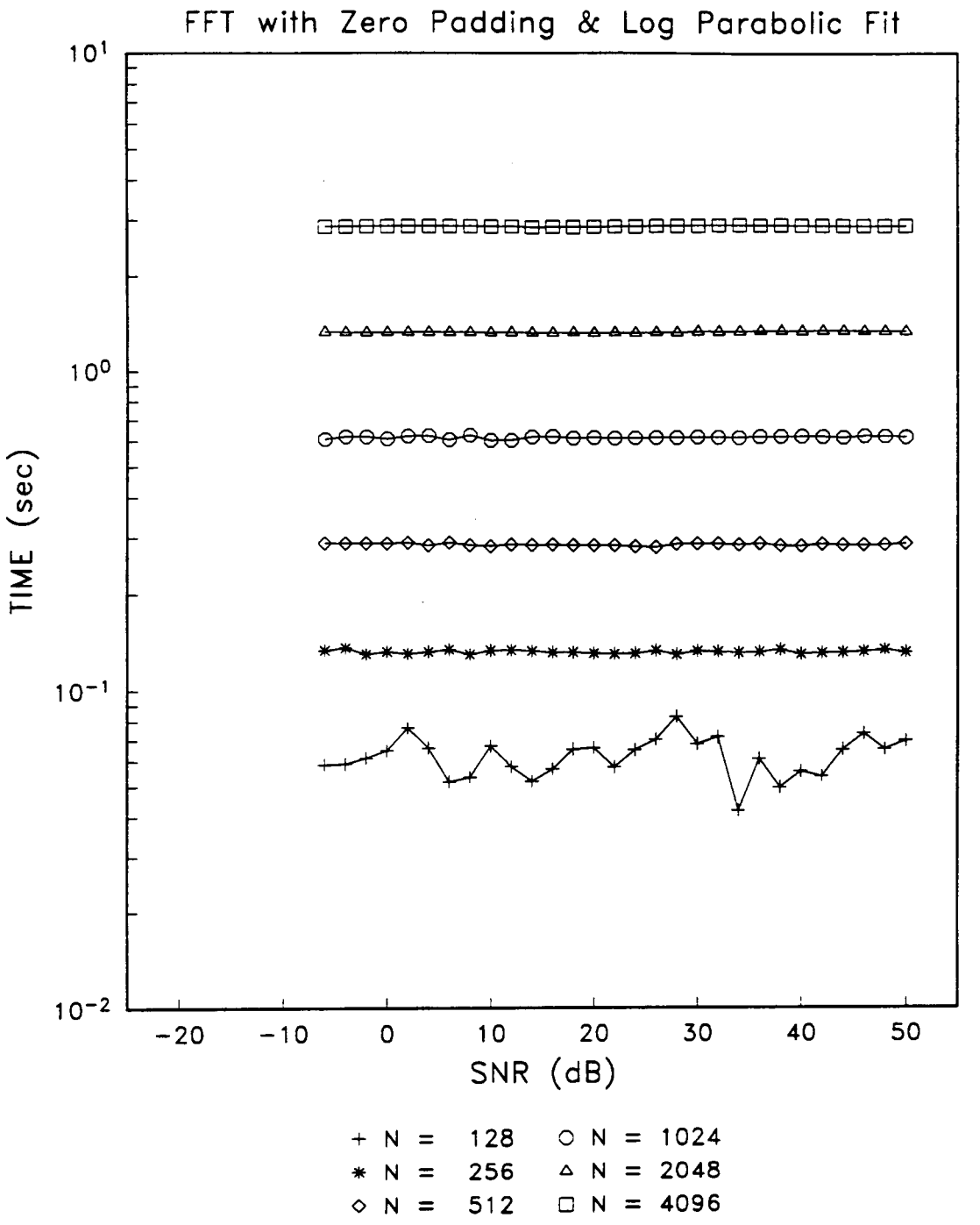

Figure 29. Computation Time vs. SNR for FFT with Zero-padding and Log Parabolic Interpolation.: f = 0.225

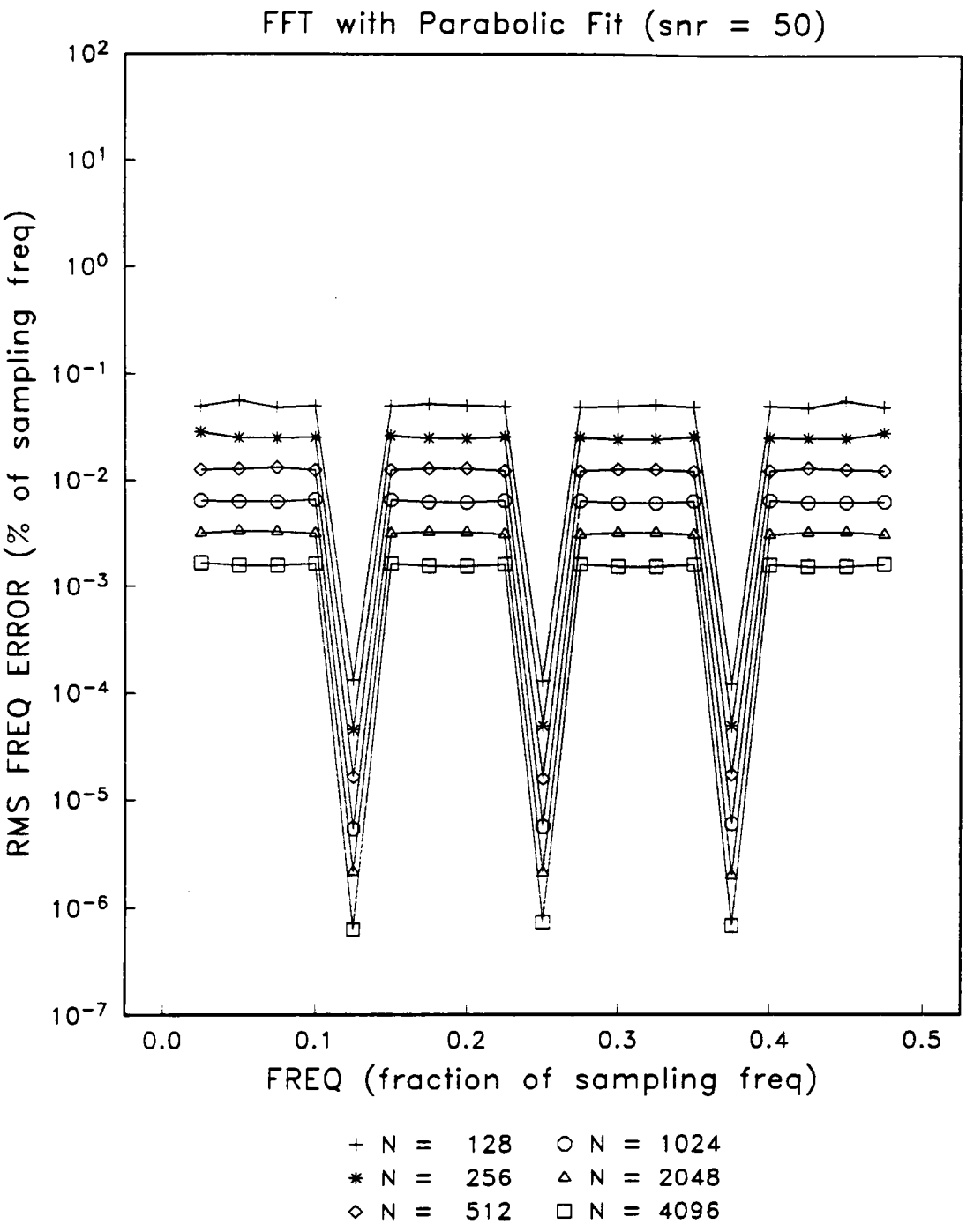

Figure 30. RMS Frequency Error vs. Frequency for FFT with Parabolic Interpolation, SNR = 50 dB.

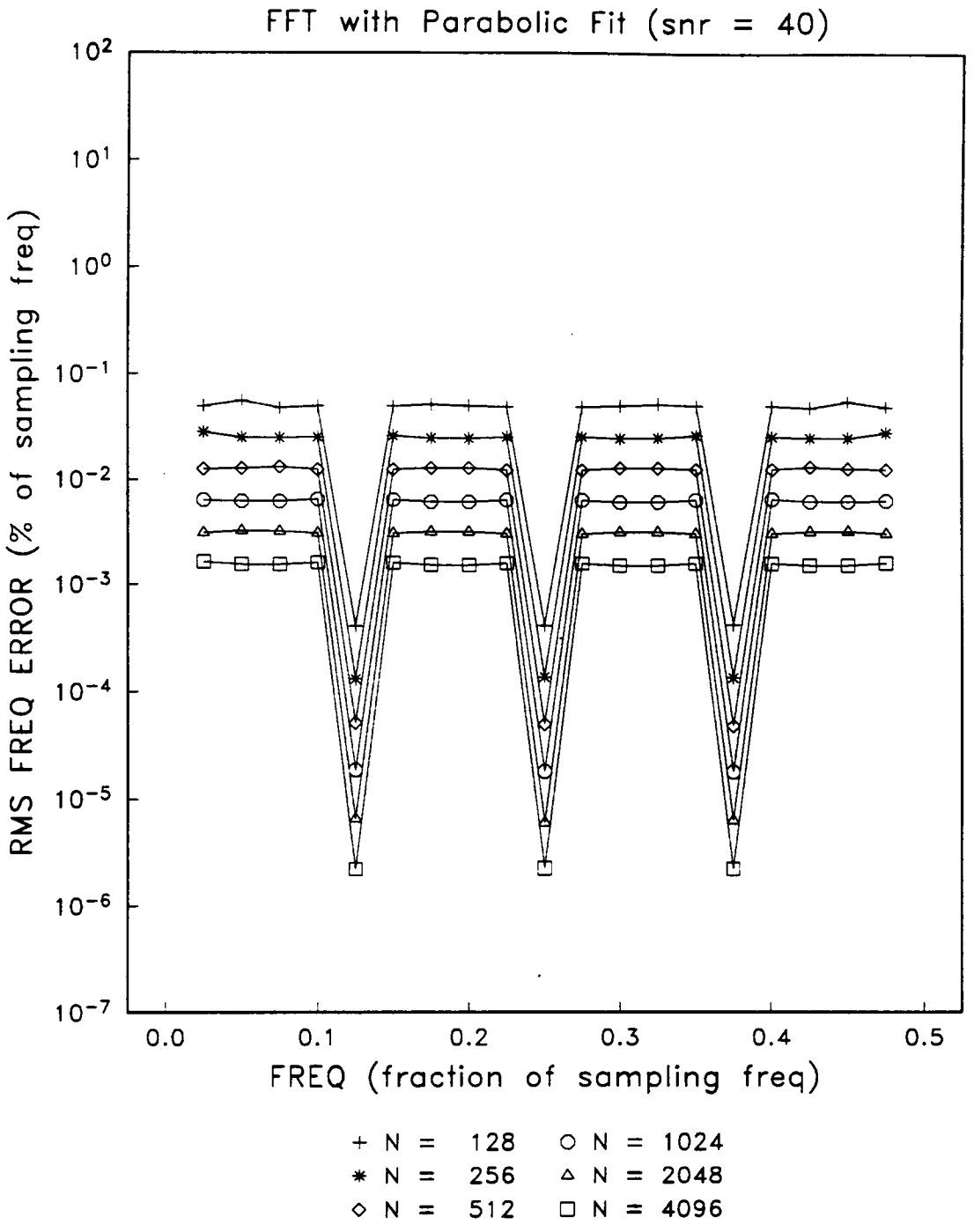

Figure 31. RMS Frequency Error vs. Frequency for FFT with Parabolic Interpolation, SNR = 40 dB.

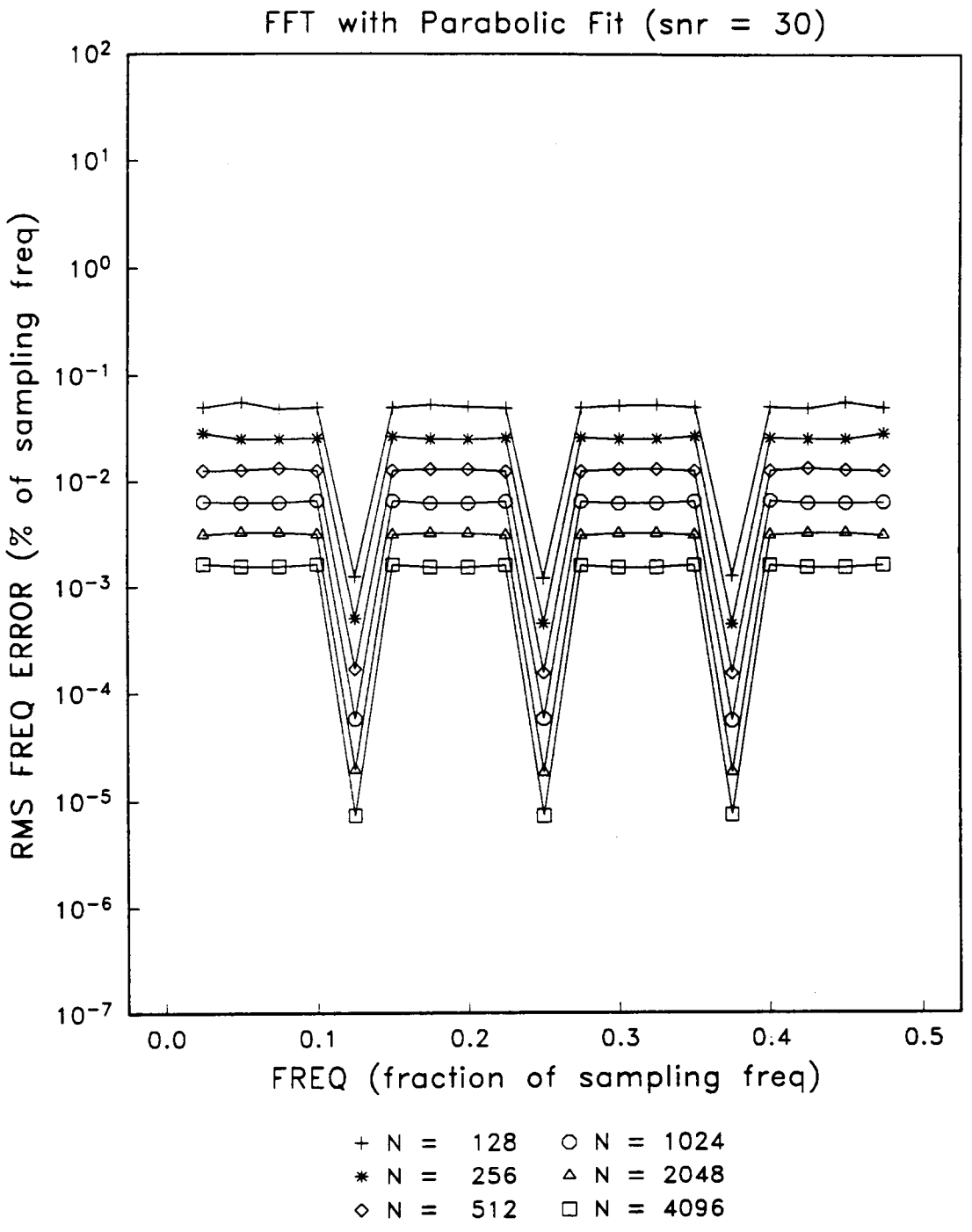

Figure 32. RMS Frequency Error vs. Frequency for FFT with Parabolic Interpolation, SNR = 30 dB.

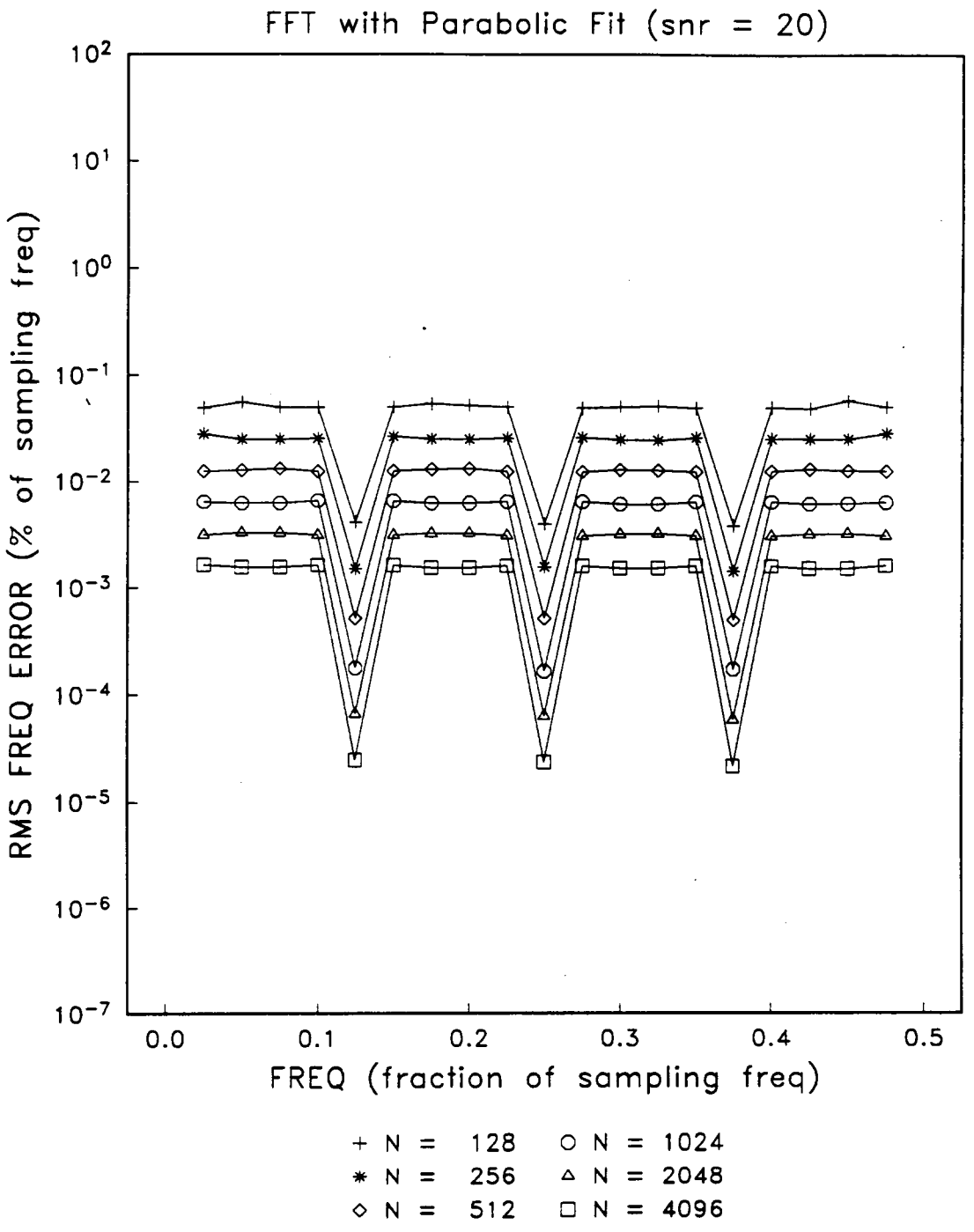

Figure 33. RMS Frequency Error vs. Frequency for FFT with Parabolic Interpolation, SNR = 20 dB.

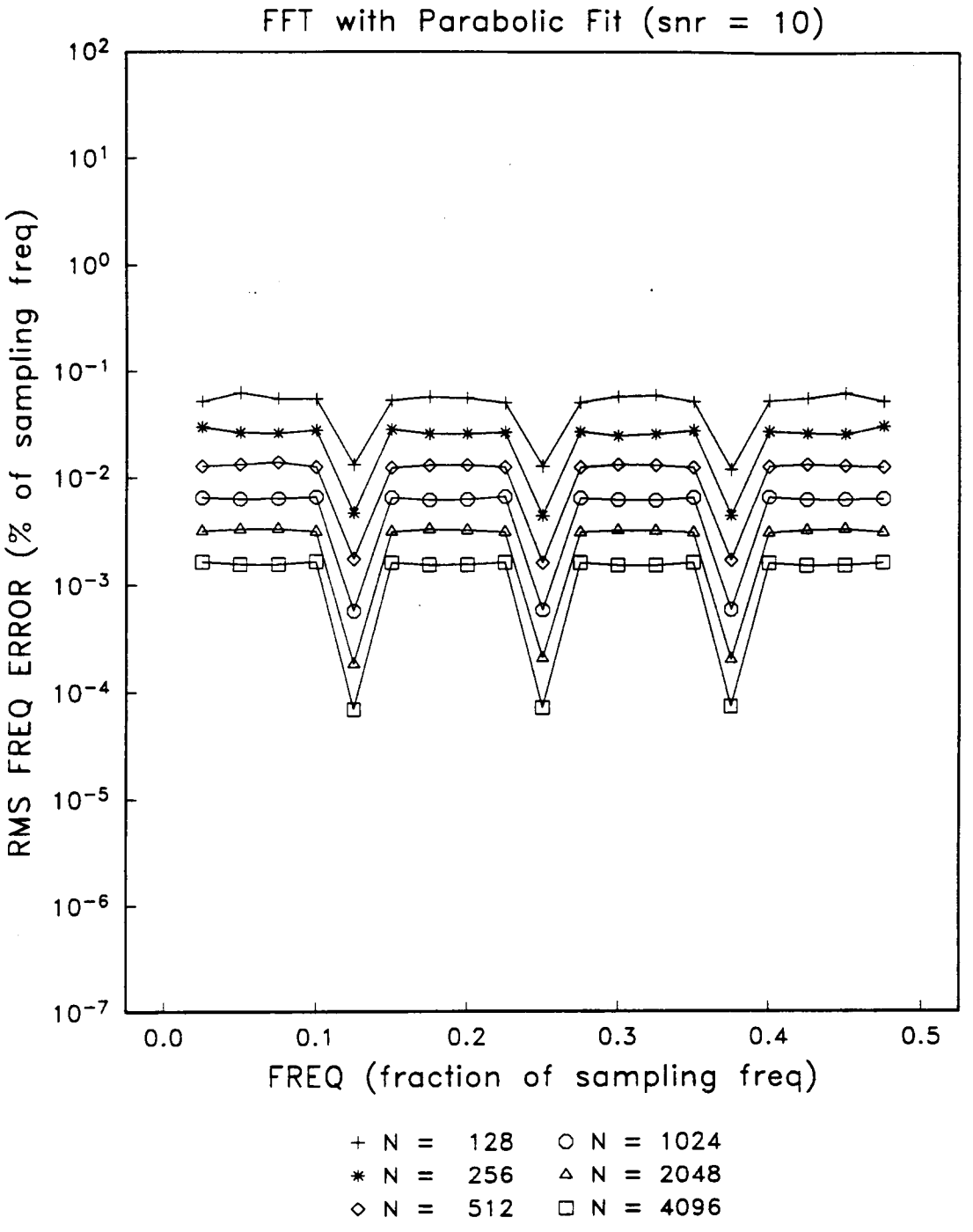

Figure 34. RMS Frequency Error vs. Frequency for FFT with Parabolic Interpolation, SNR = 10 dB.

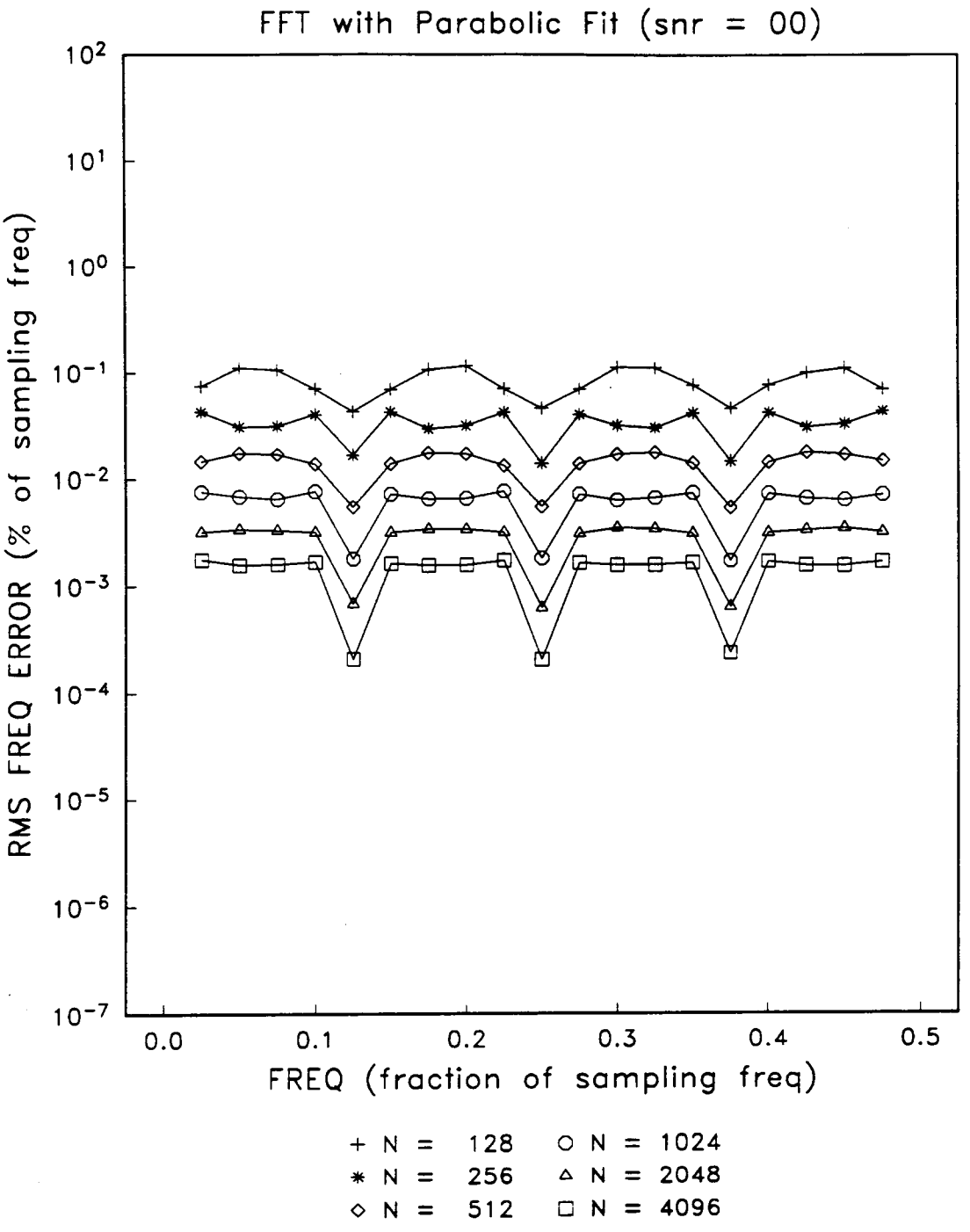

Figure 35. RMS Frequency Error vs. Frequency for FFT with Parabolic Interpolation, SNR = 0 dB.

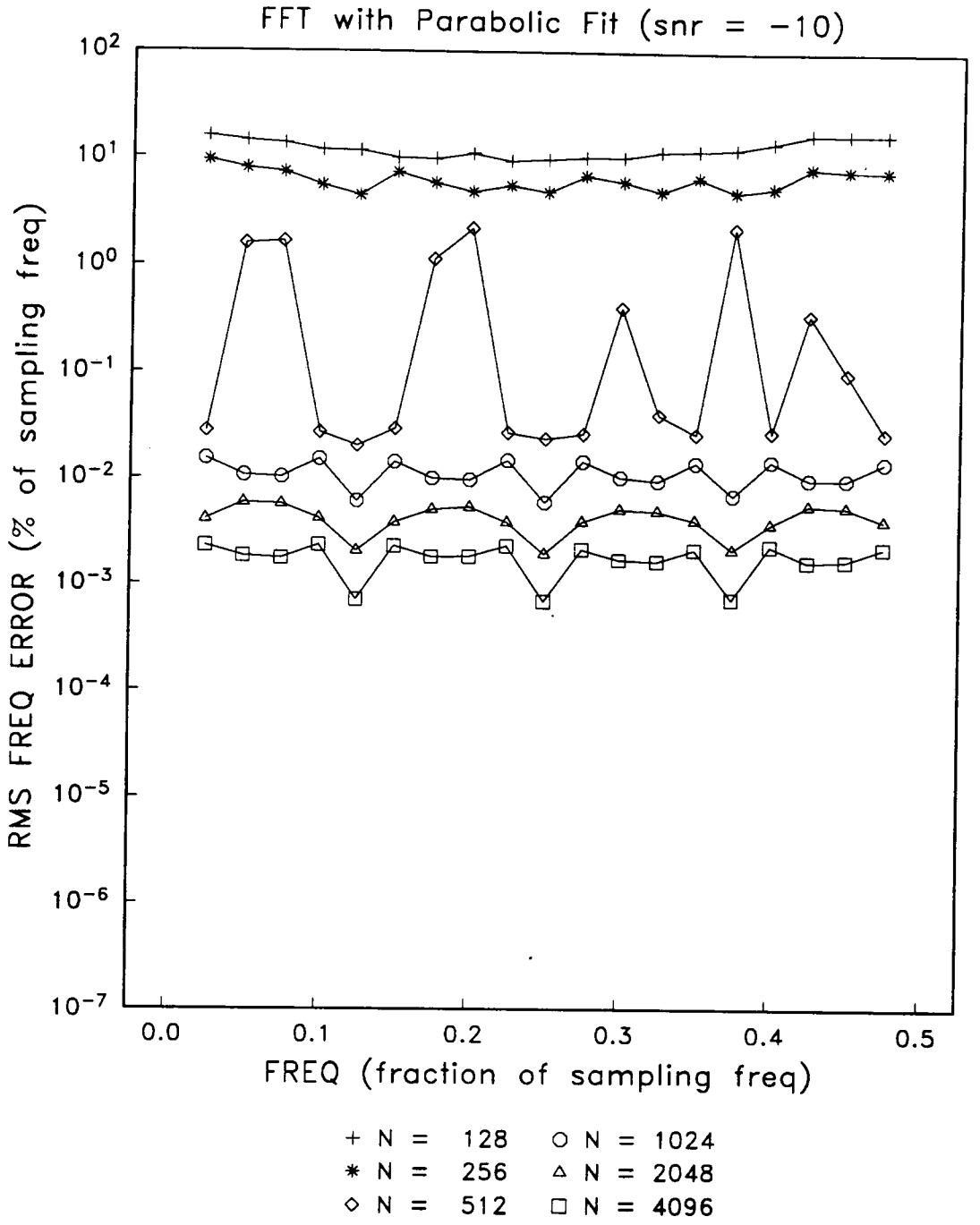

Figure 36. RMS Frequency Error vs. Frequency for FFT with Parabolic Interpolation, SNR = -10 dB.

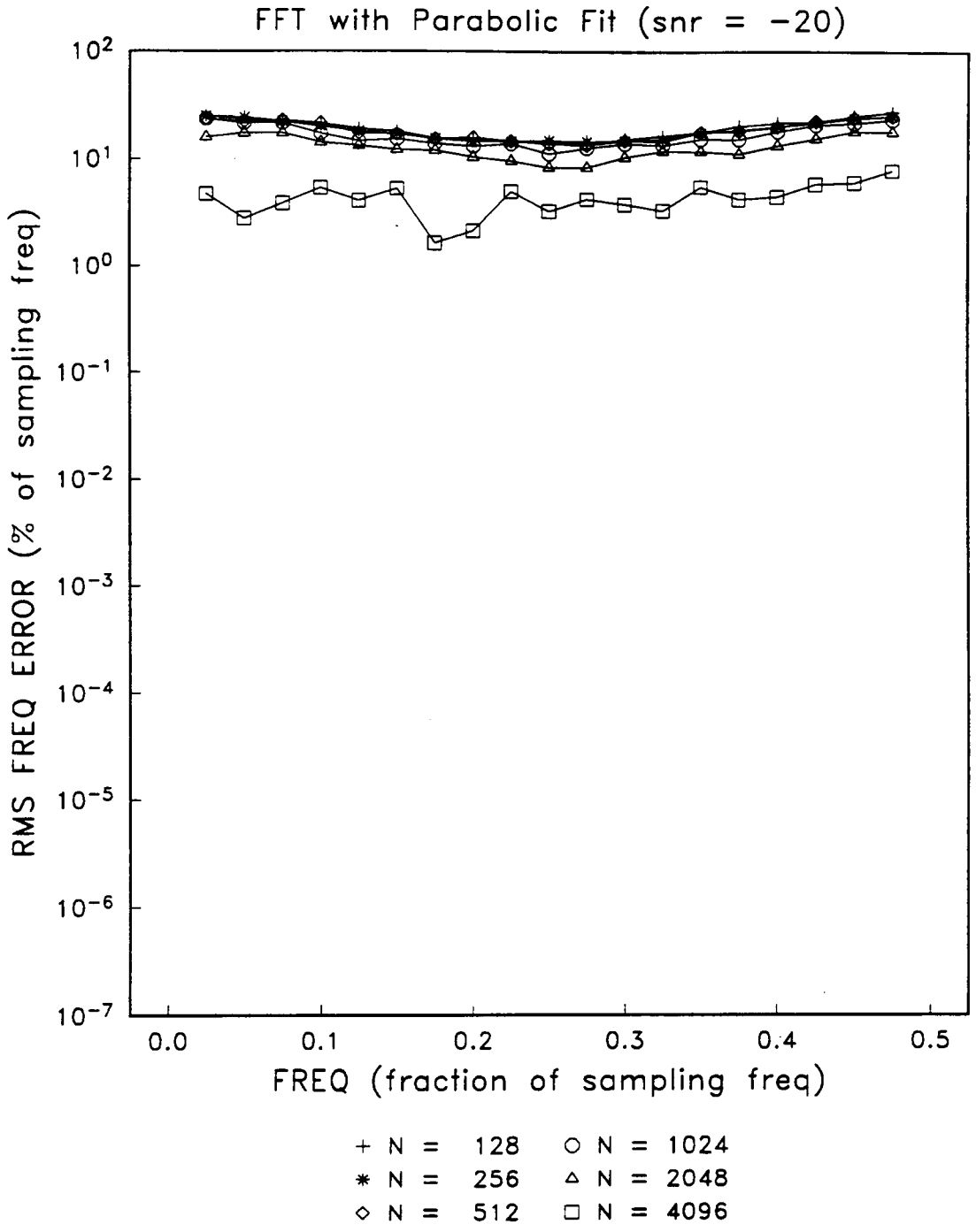

Figure 37. RMS Frequency Error vs. Frequency for FFT with Parabolic Interpolation, SNR = -20 dB.

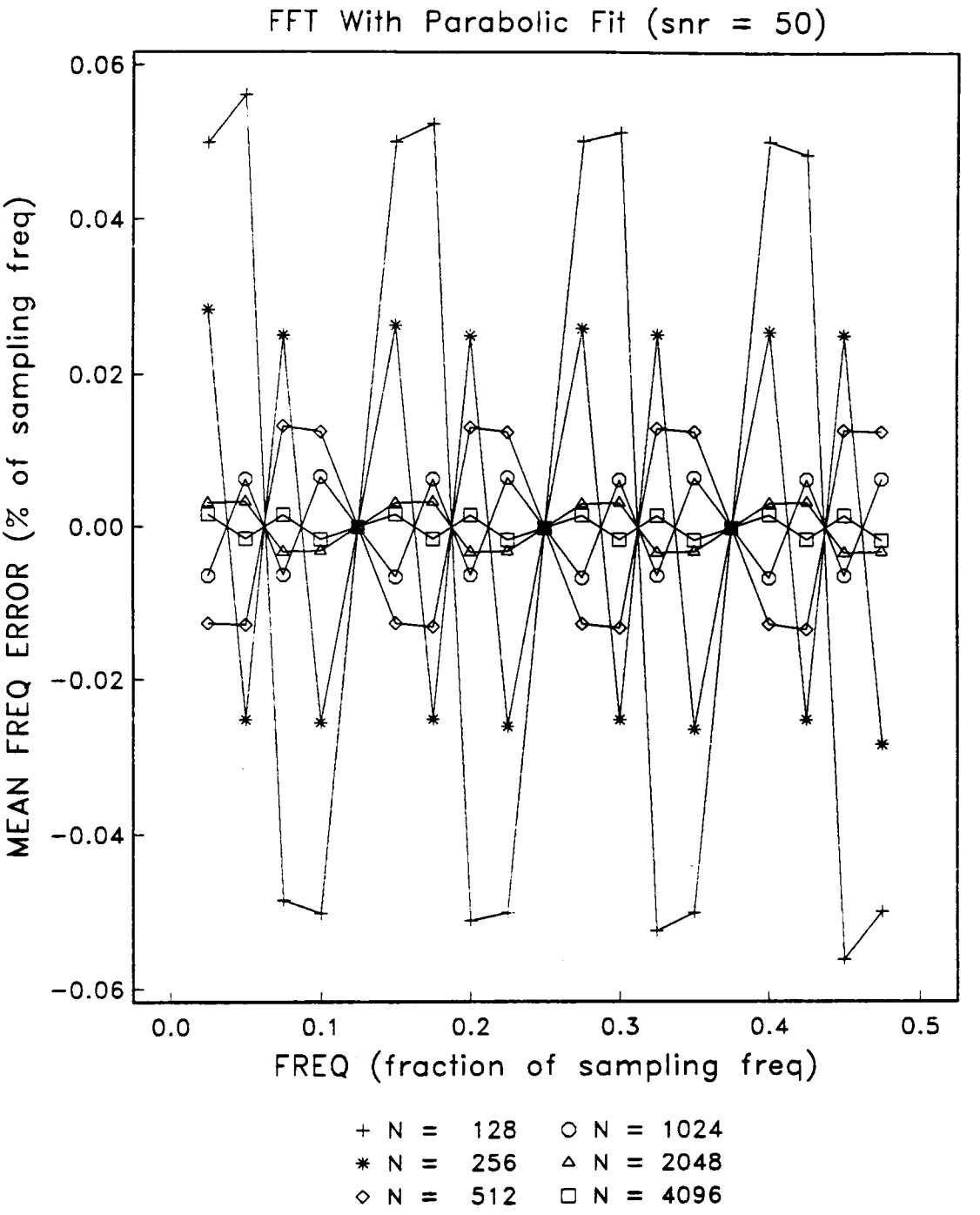

Figure 38. Frequency Bias Error vs. Frequency for FFT with Parabolic Interpolation, SNR = 50 dB.

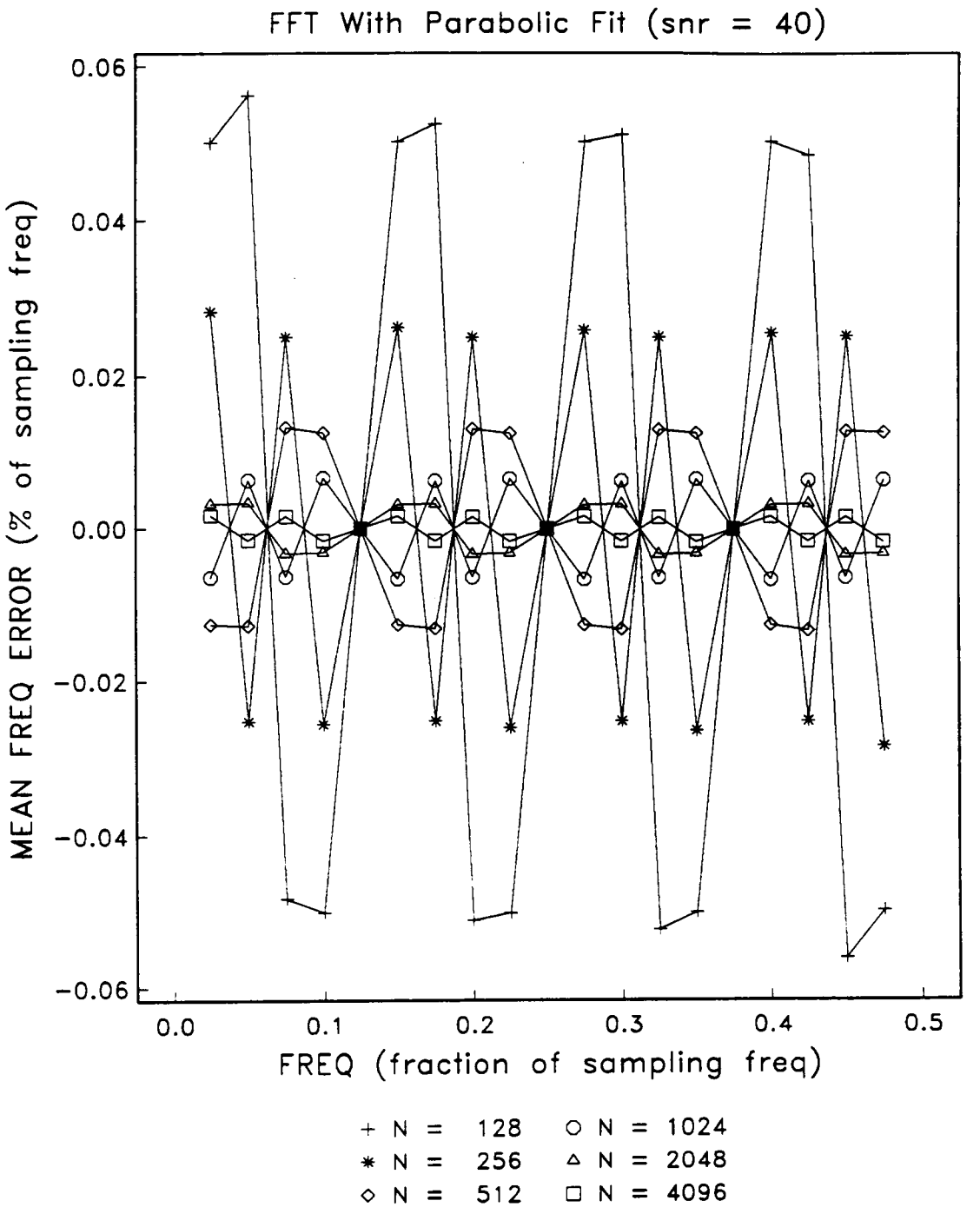

Figure 39. Frequency Bias Error vs. Frequency for FFT with Parabolic Interpolation, SNR = 40 dB.

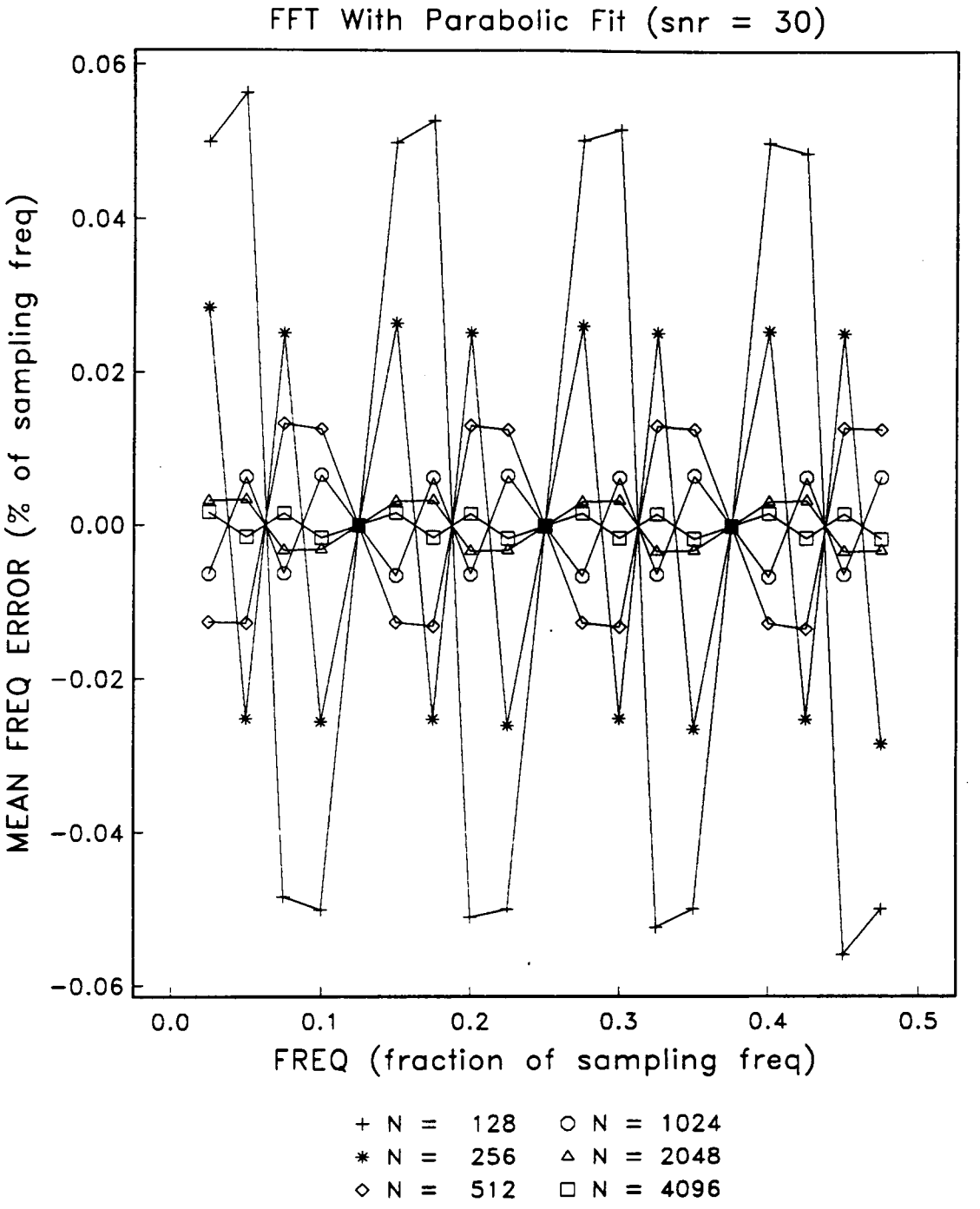

Figure 40. Frequency Bias Error vs. Frequency for FFT with Parabolic Interpolation, SNR = 30 dB.

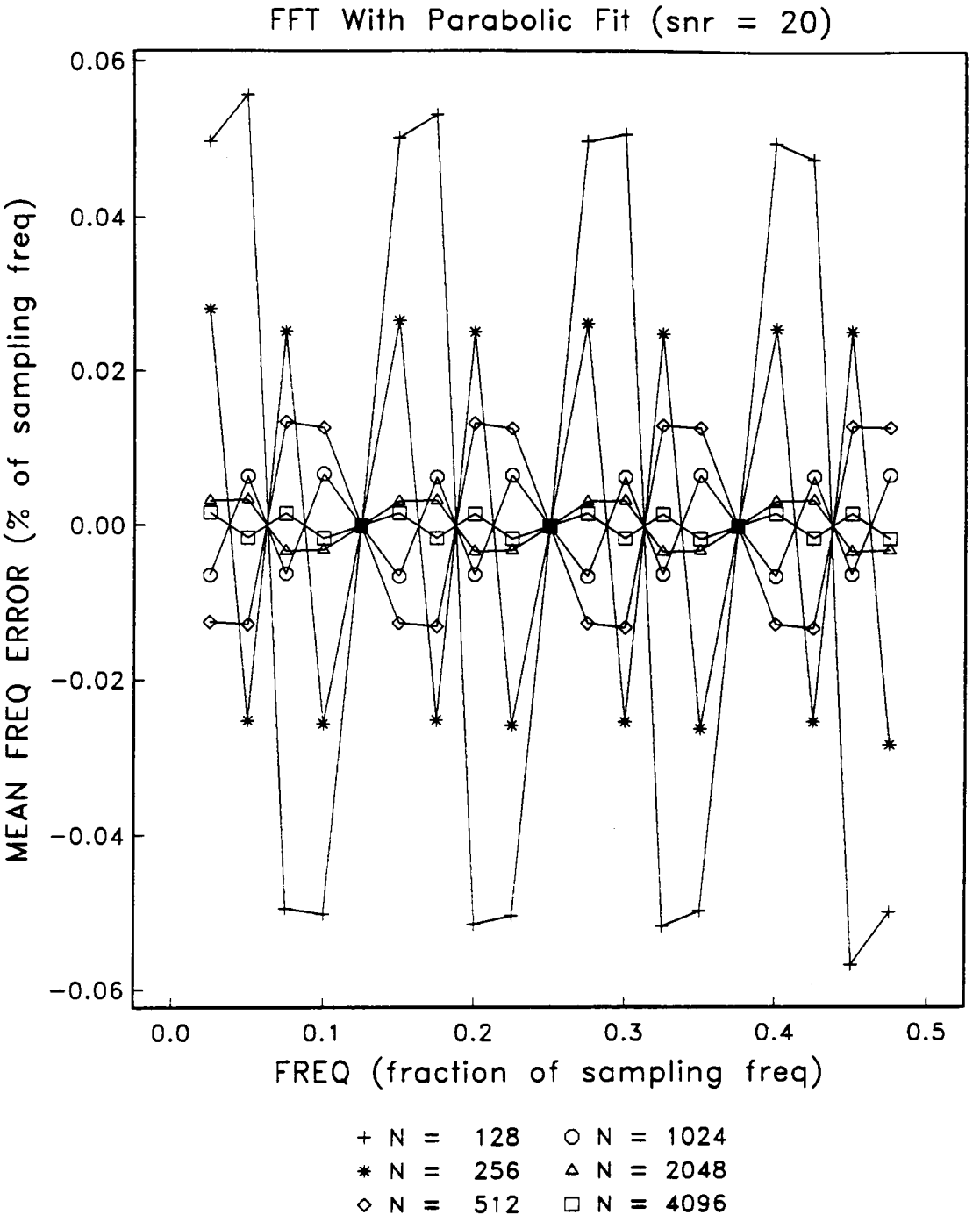

Figure 41. Frequency Bias Error vs. Frequency for FFT with Parabolic Interpolation, SNR = 20 dB.

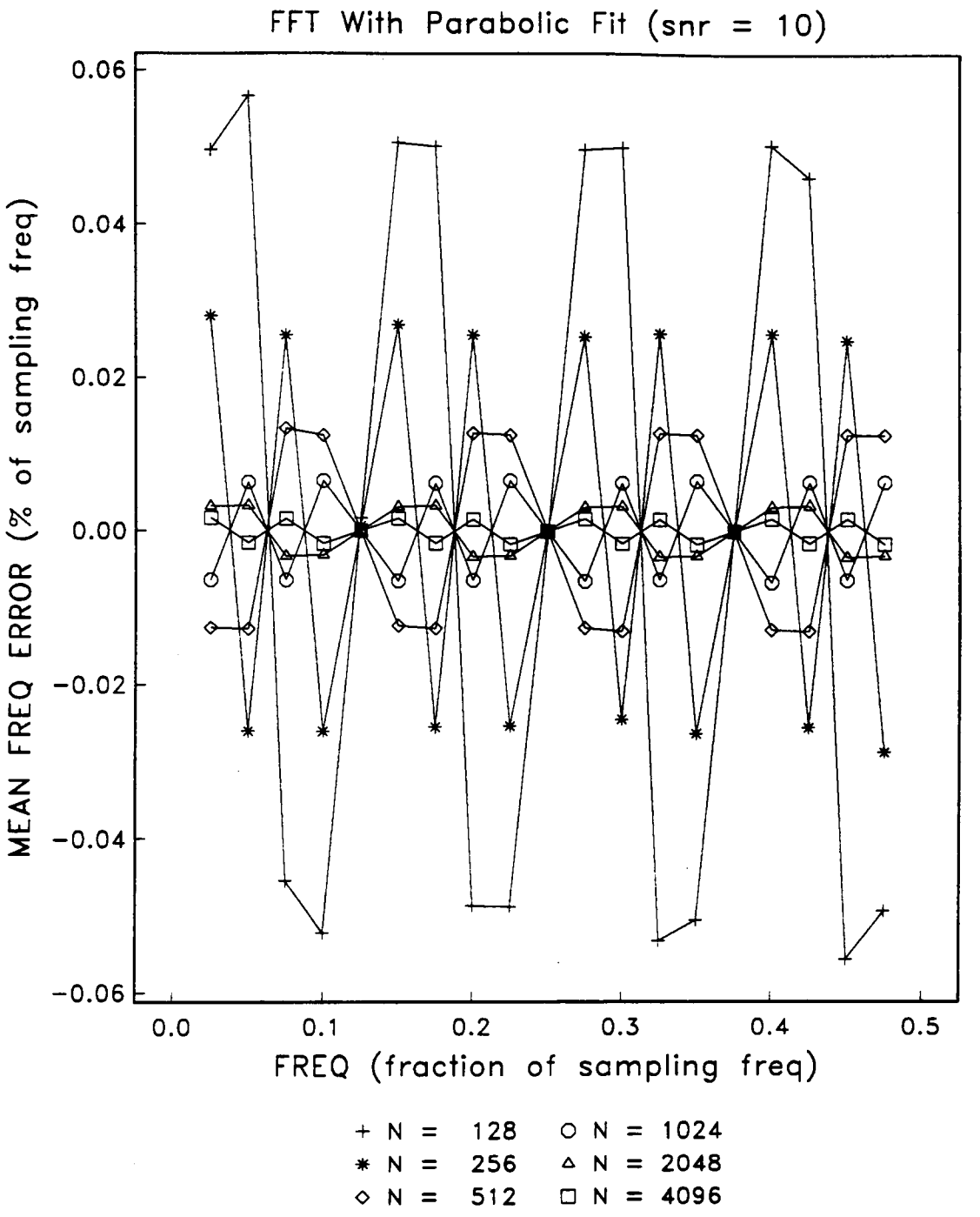

Figure 42. Frequency Bias Error vs. Frequency for FFT with Parabolic Interpolation, SNR = 10 dB.

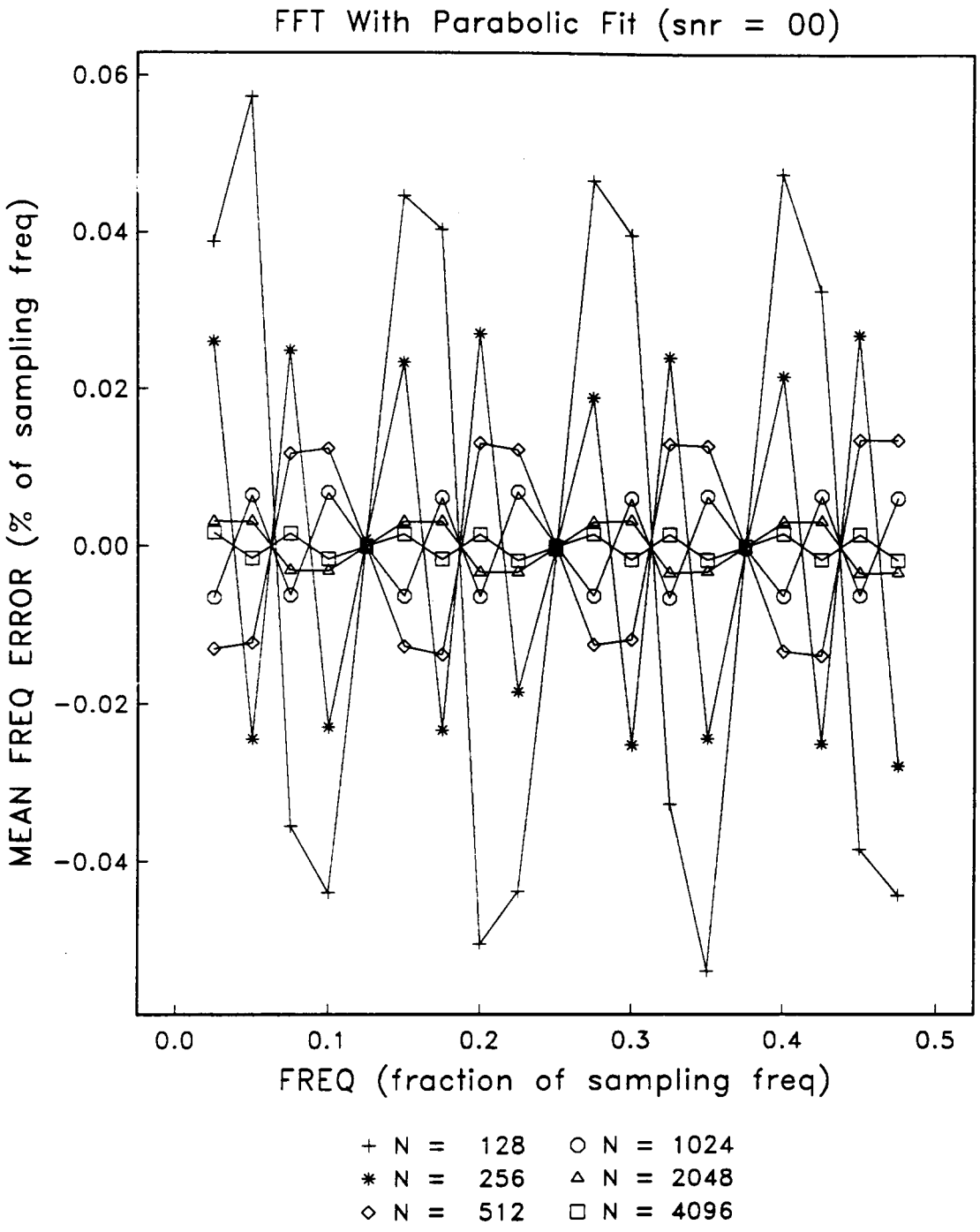

Figure 43. Frequency Bias Error vs. Frequency for FFT with Parabolic Interpolation, SNR = 0 dB.

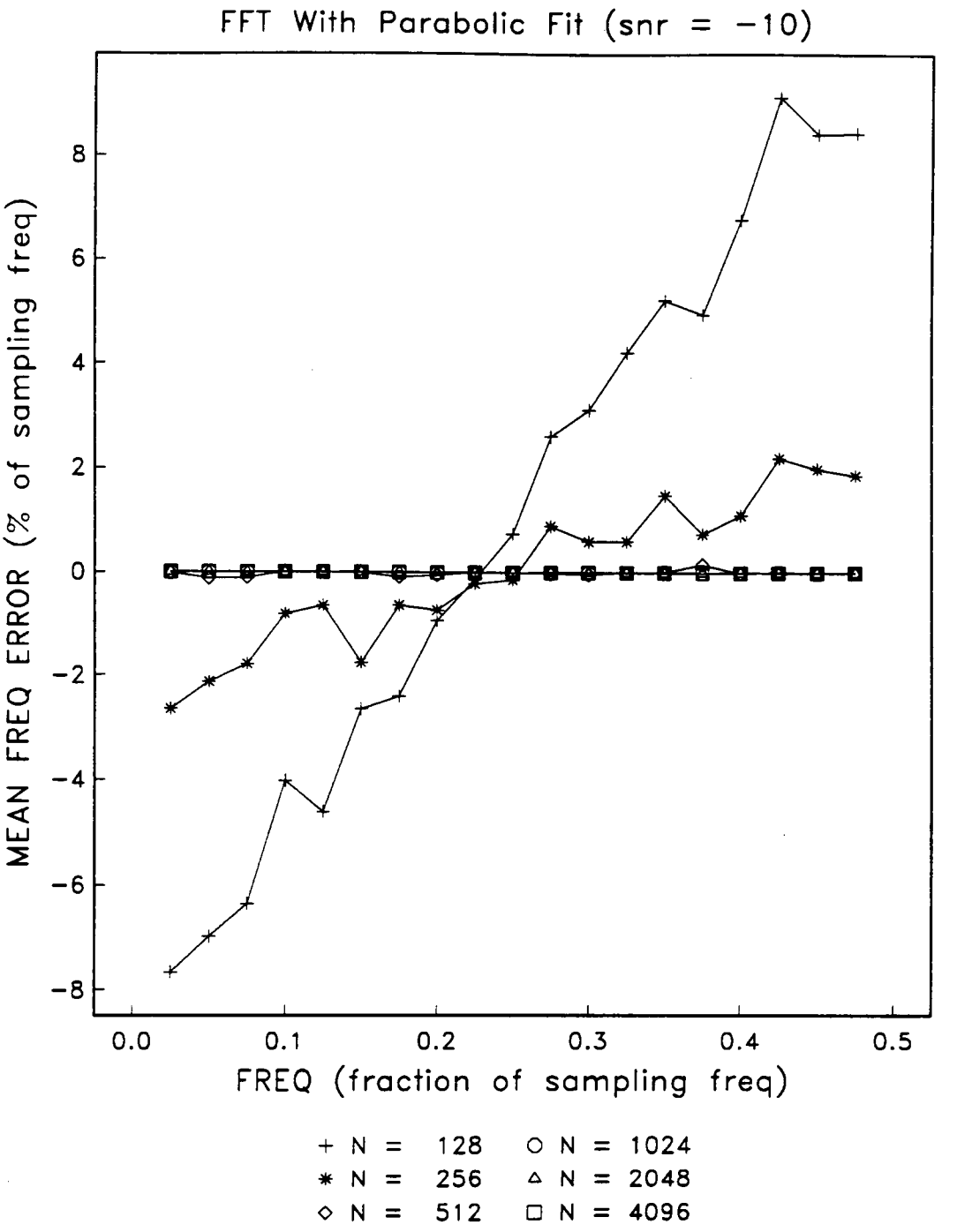

Figure 44. Frequency Bias Error vs. Frequency for FFT with Parabolic Interpolation, SNR = -10 dB.

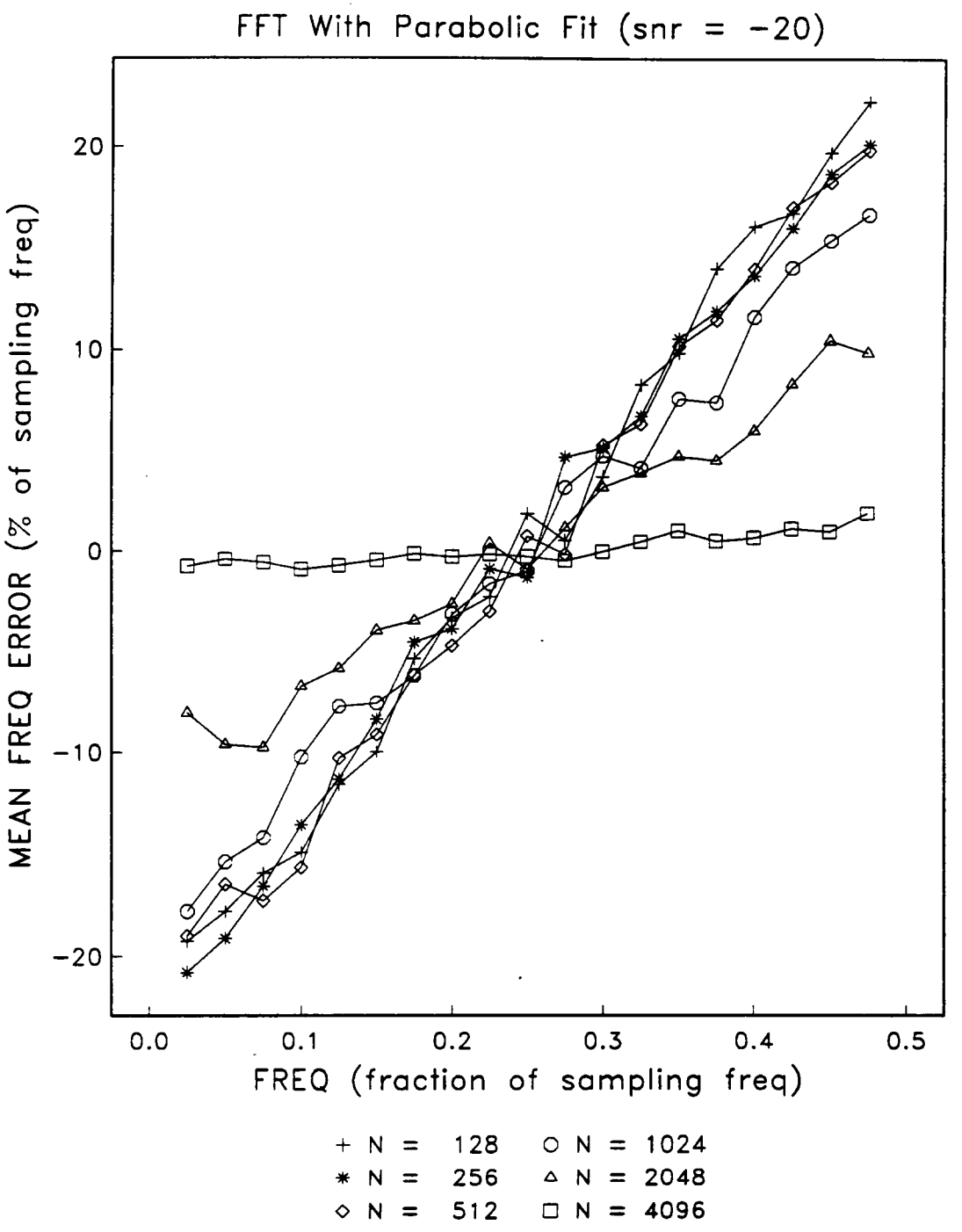

Figure 45. Frequency Bias Error vs. Frequency for FFT with Parabolic Interpolation, SNR = -20 dB.

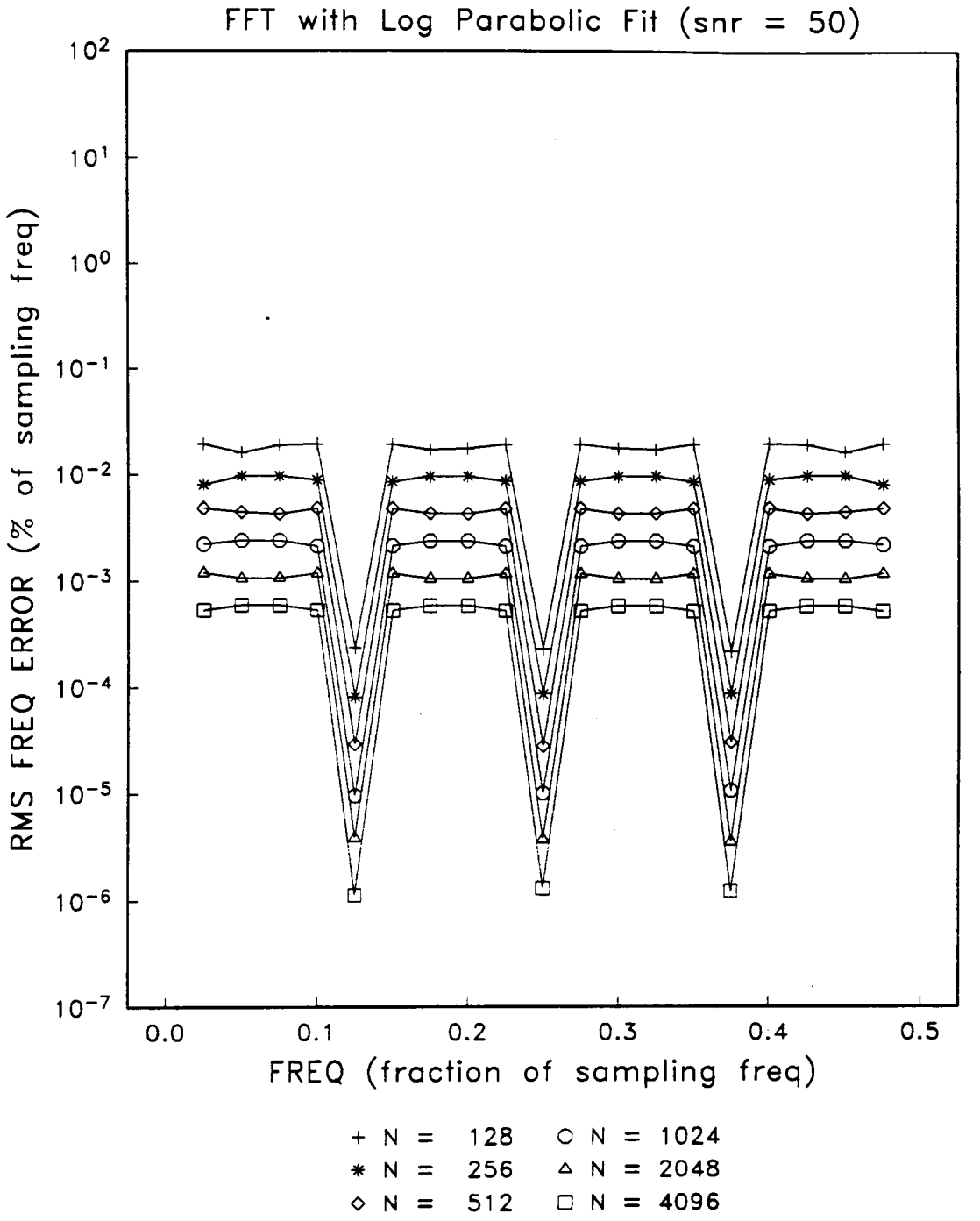

Figure 46. RMS Frequency Error vs. Frequency for FFT with Log Parabolic Interpolation, SNR = 50 dB.

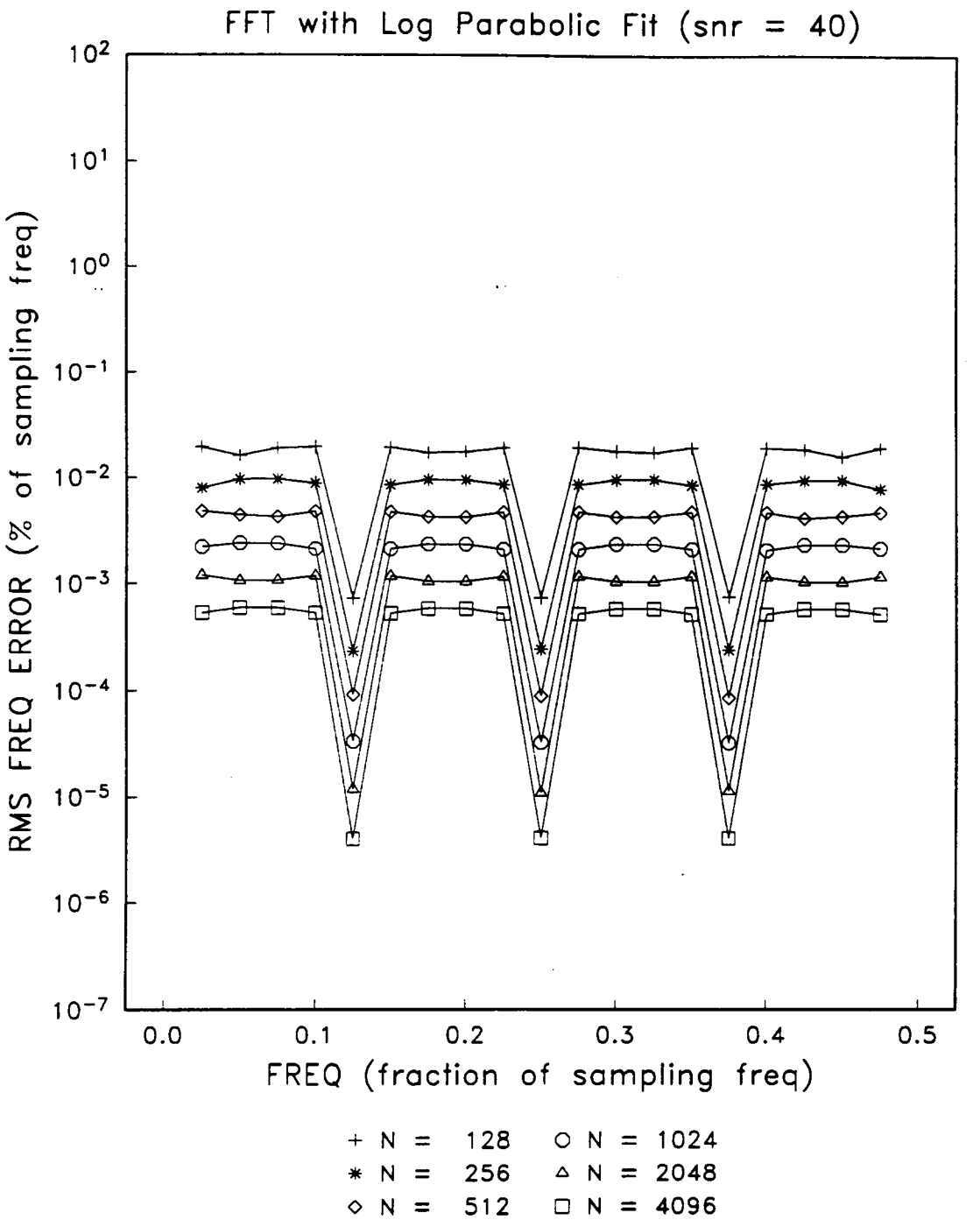

Figure 47. RMS Frequency Error vs. Frequency for FFT with Log Parabolic Interpolation, SNR = 40 dB.

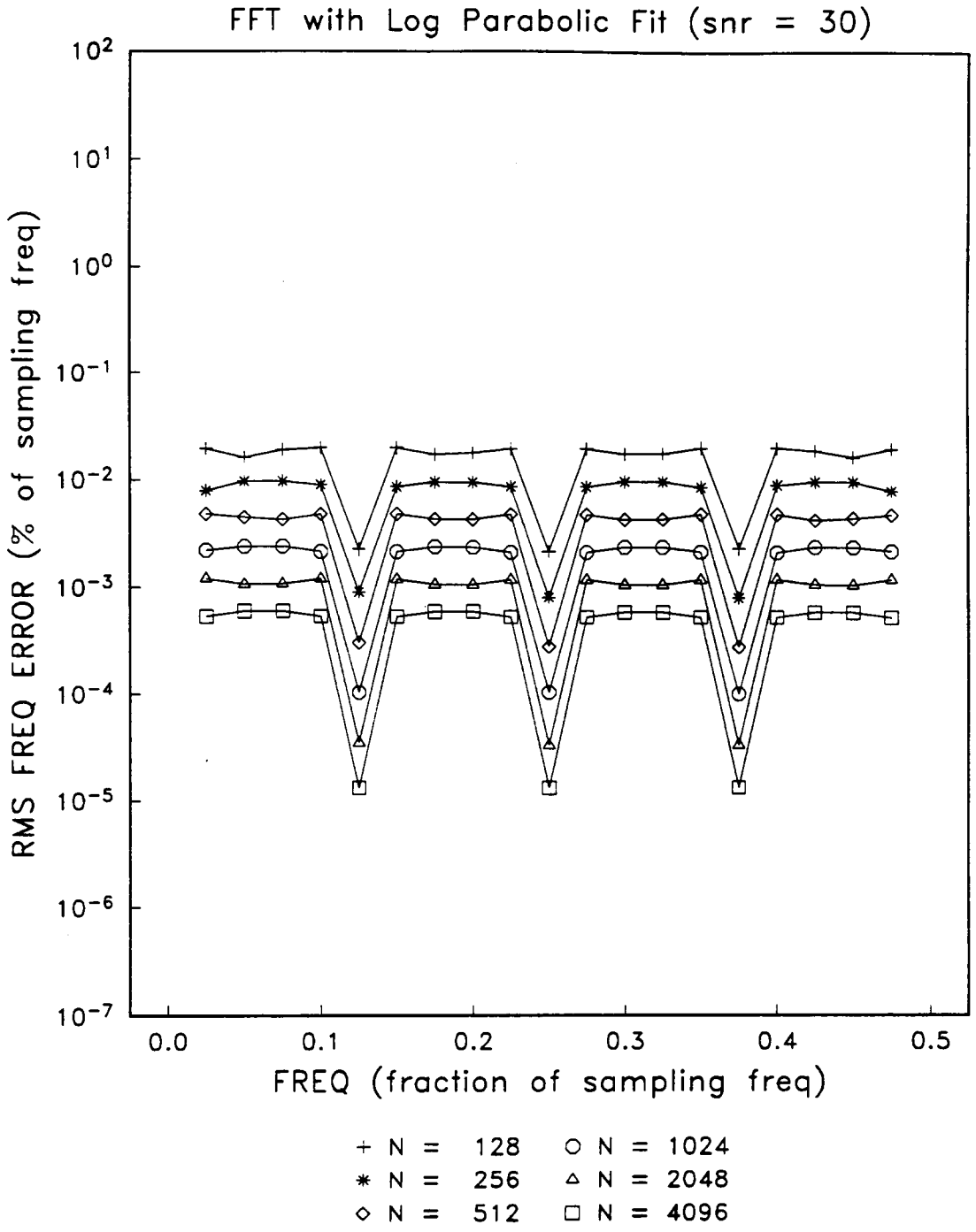

Figure 48. RMS Frequency Error vs. Frequency for FFT with Log Parabolic Interpolation, SNR = 30 dB.

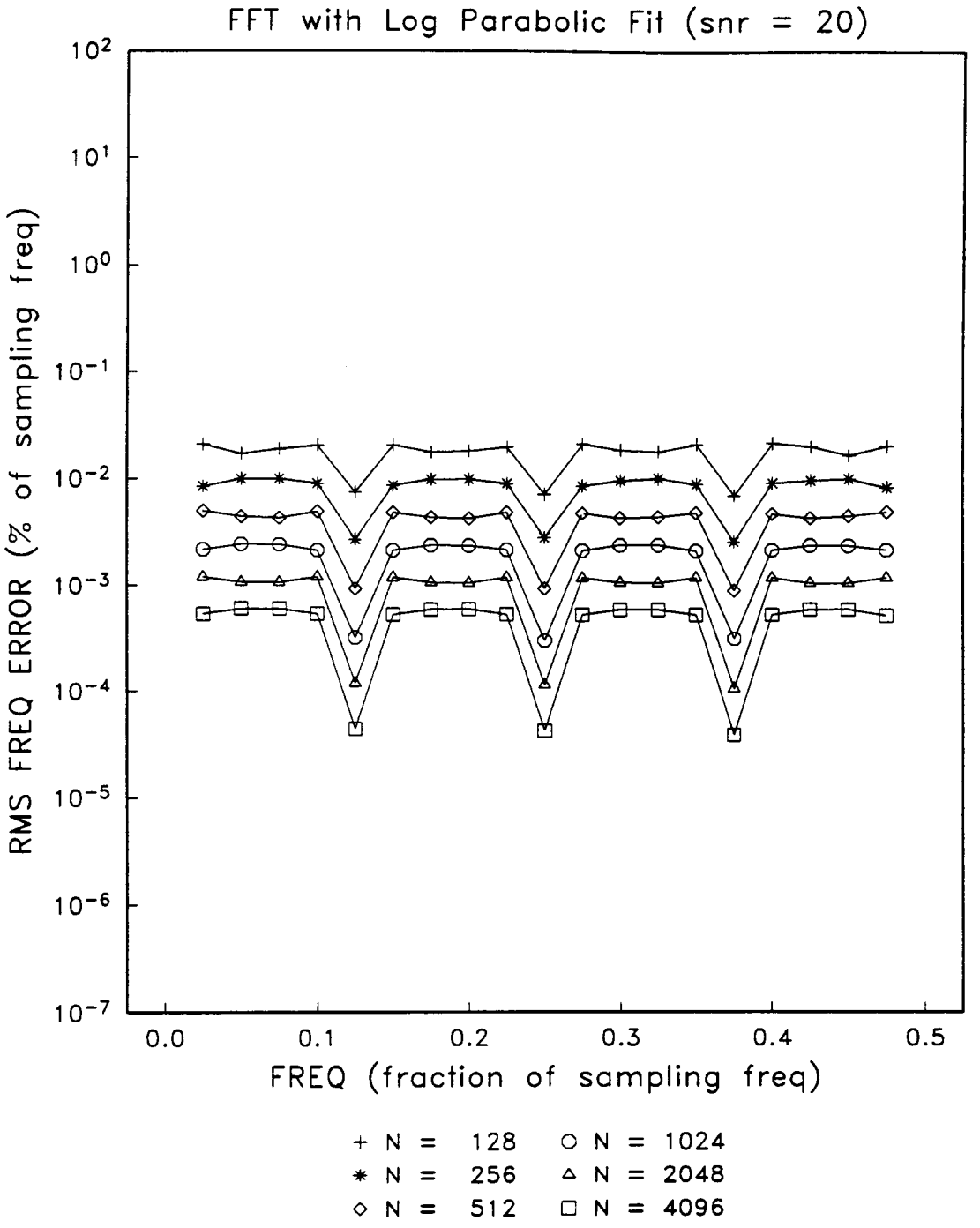

Figure 49. RMS Frequency Error vs. Frequency for FFT with Log Parabolic Interpolation, SNR = 20 dB.

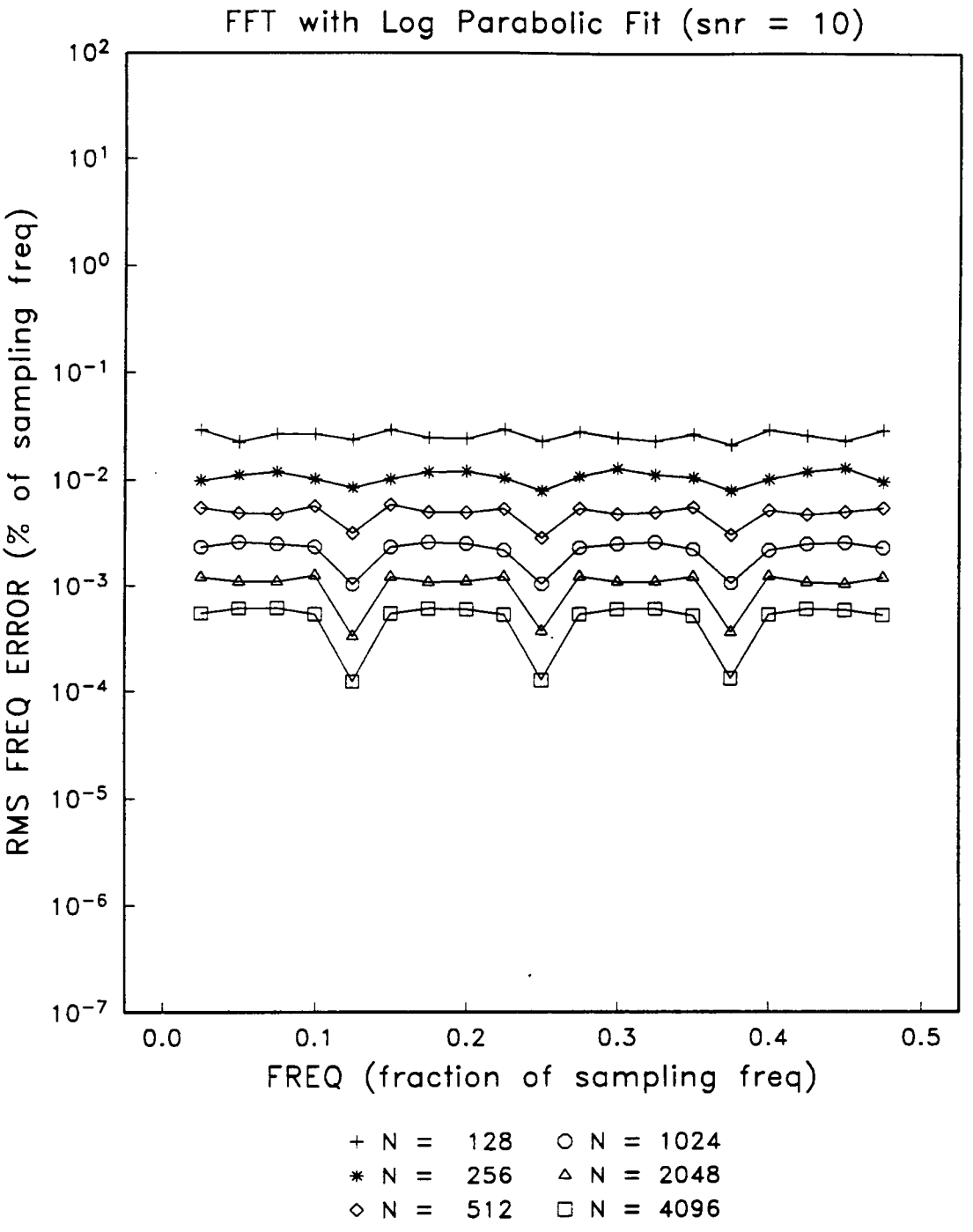

Figure 50. RMS Frequency Error vs. Frequency for FFT with Log Parabolic Interpolation, SNR = 10 dB.

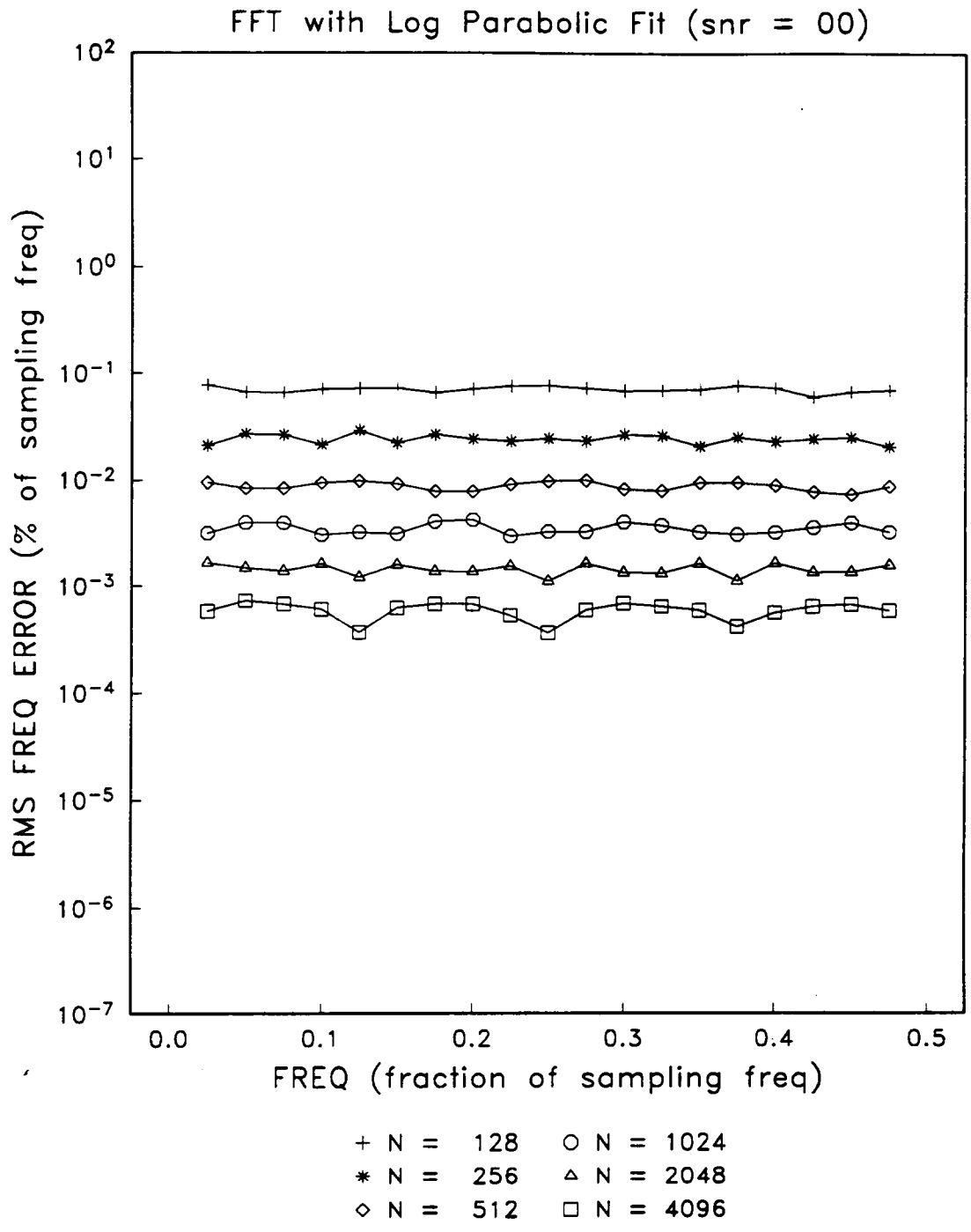

Figure 51. RMS Frequency Error vs. Frequency for FFT with Log Parabolic Interpolation, SNR = 0 dB.

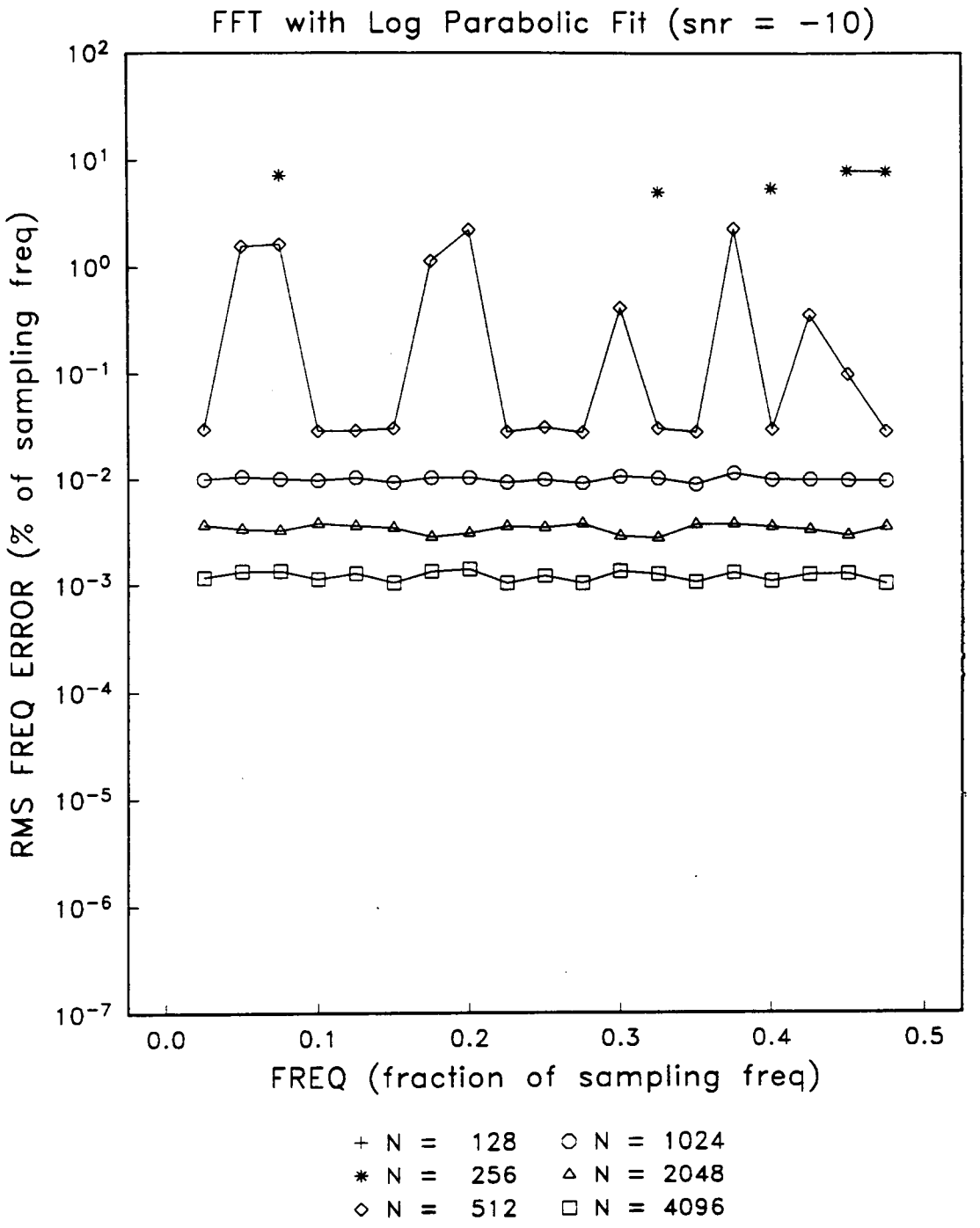

Figure 52. RMS Frequency Error vs. Frequency for FFT with Log Parabolic Interpolation, SNR = -10 dB.

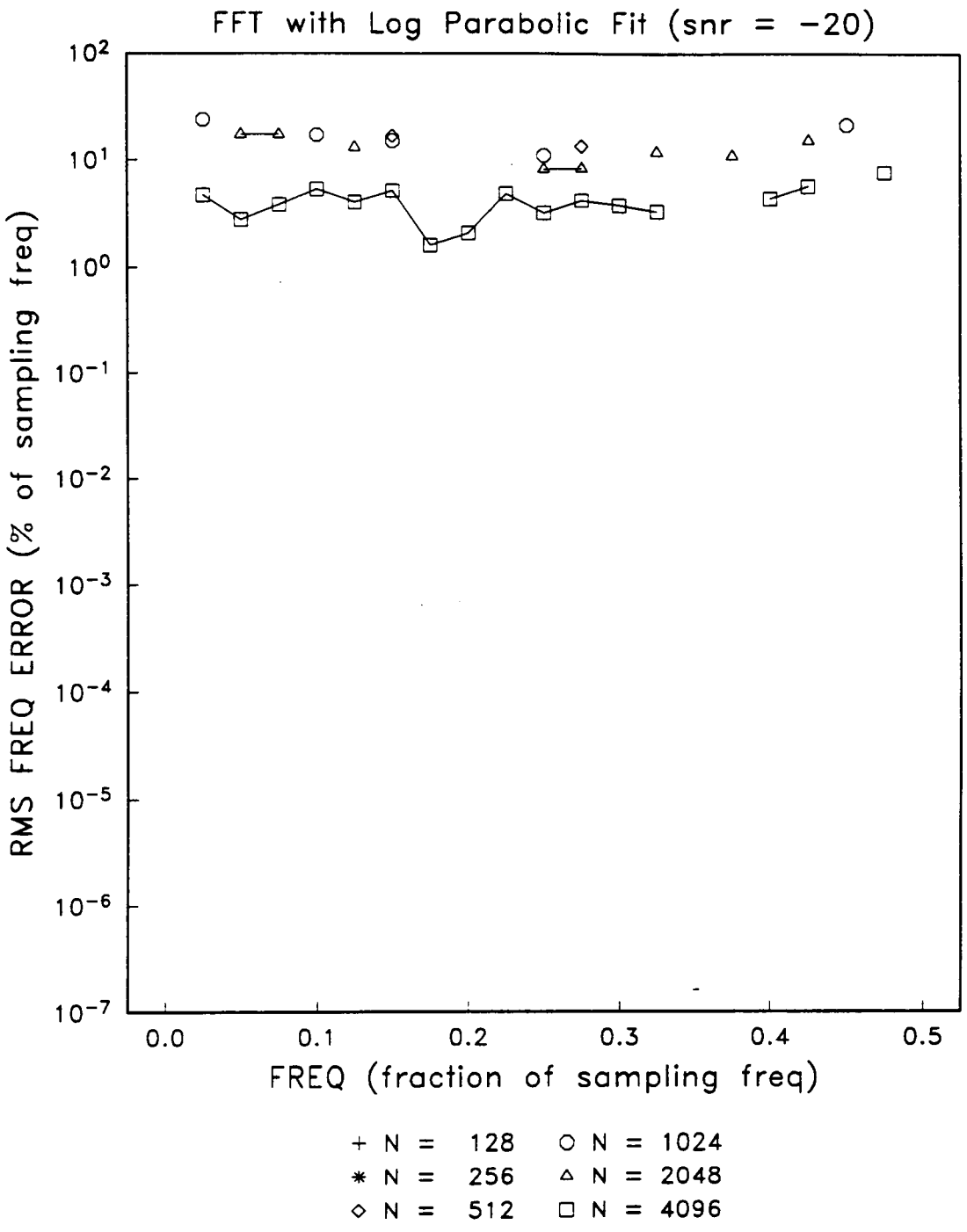

Figure 53. RMS Frequency Error vs. Frequency for FFT with Log Parabolic Interpolation, SNR = -20 dB.

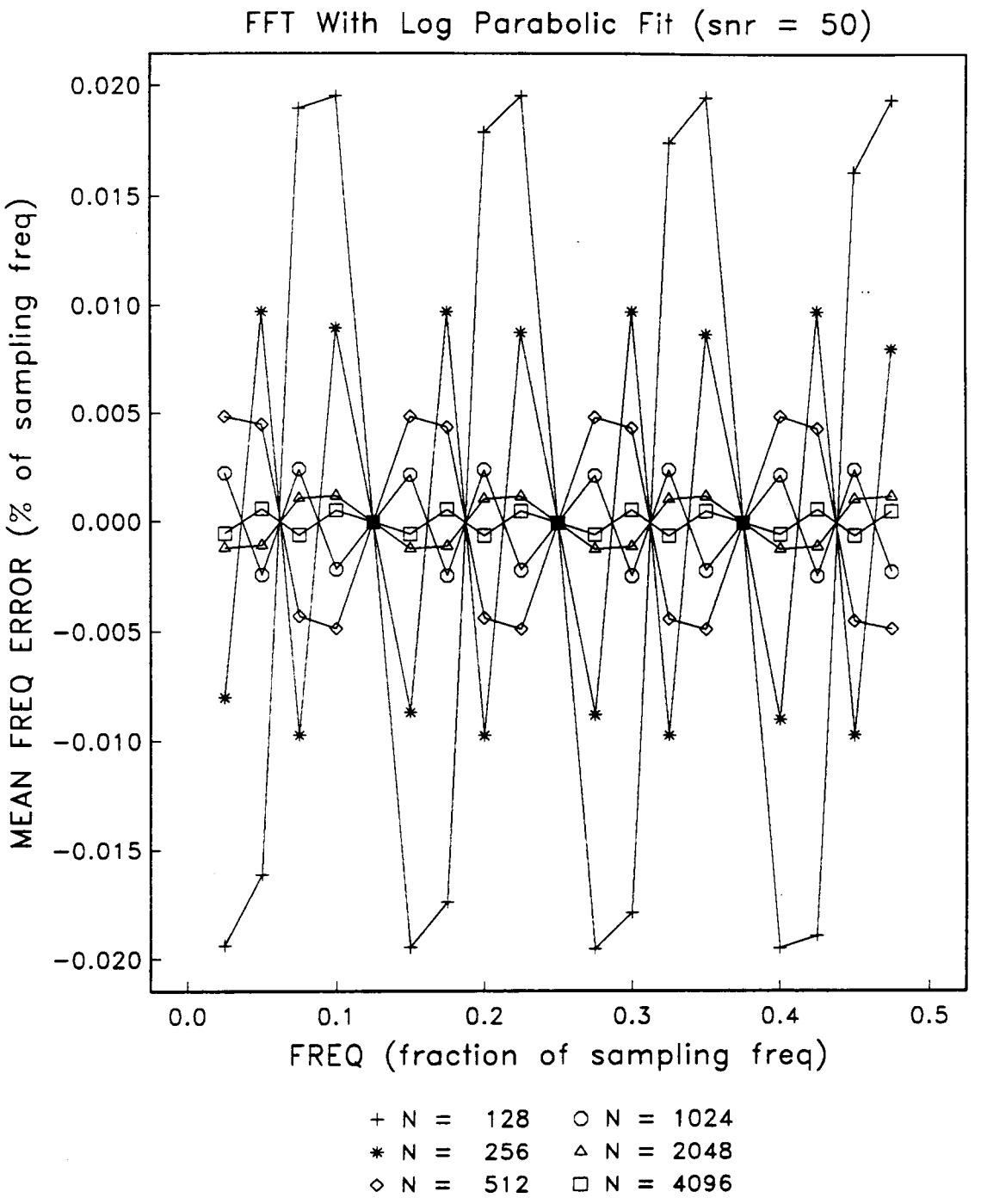

Figure 54. Frequency Bias Error vs. Frequency for FFT with Log Parabolic Interpolation, SNR = 50 dB.

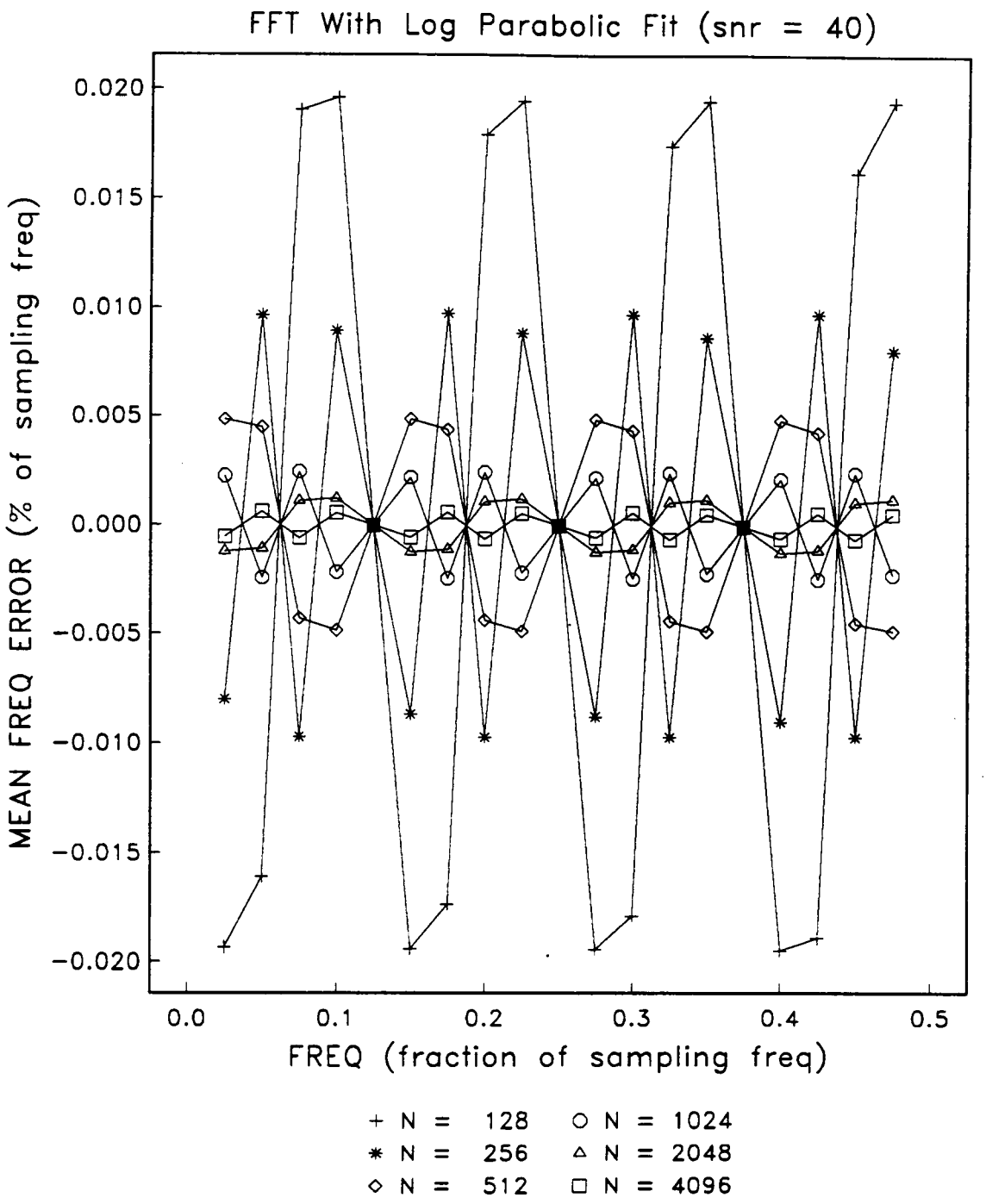

Figure 55. Frequency Bias Error vs. Frequency for FFT with Log Parabolic Interpolation, SNR = 40 dB.

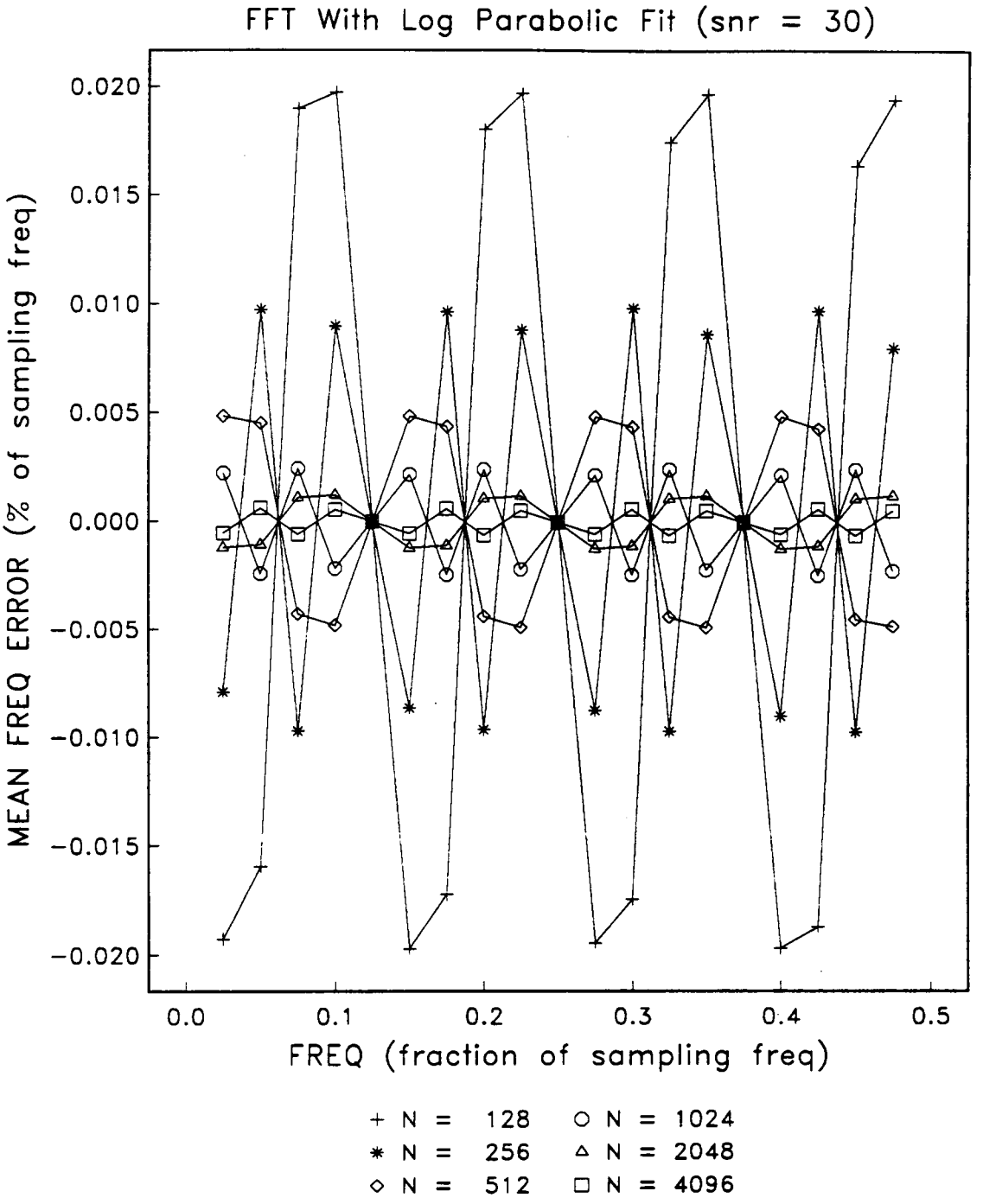

Figure 56. Frequency Bias Error vs. Frequency for FFT with Log Parabolic Interpolation, SNR = 30 dB.

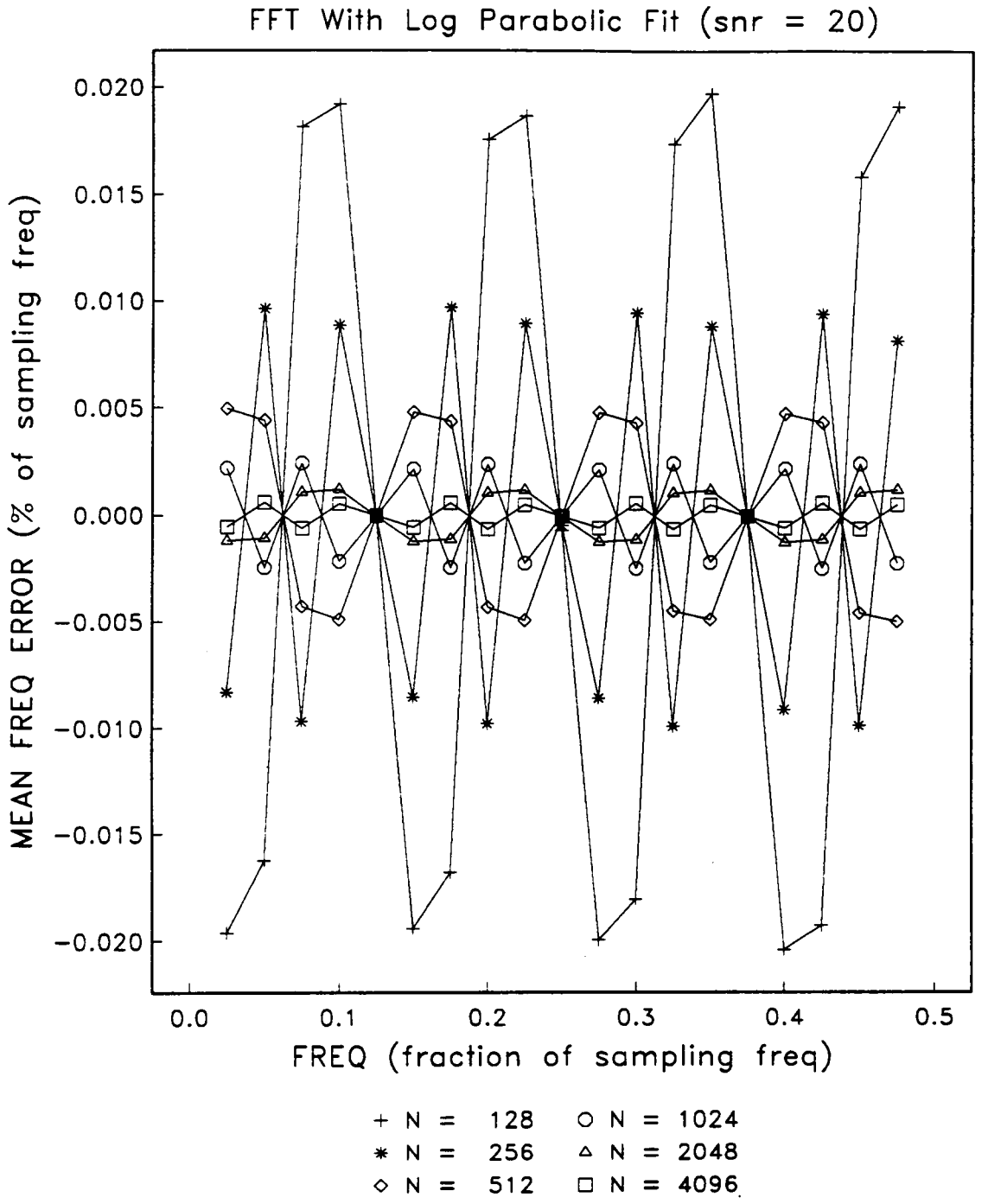

Figure 57. Frequency Bias Error vs. Frequency for FFT with Log Parabolic Interpolation, SNR = 20 dB.

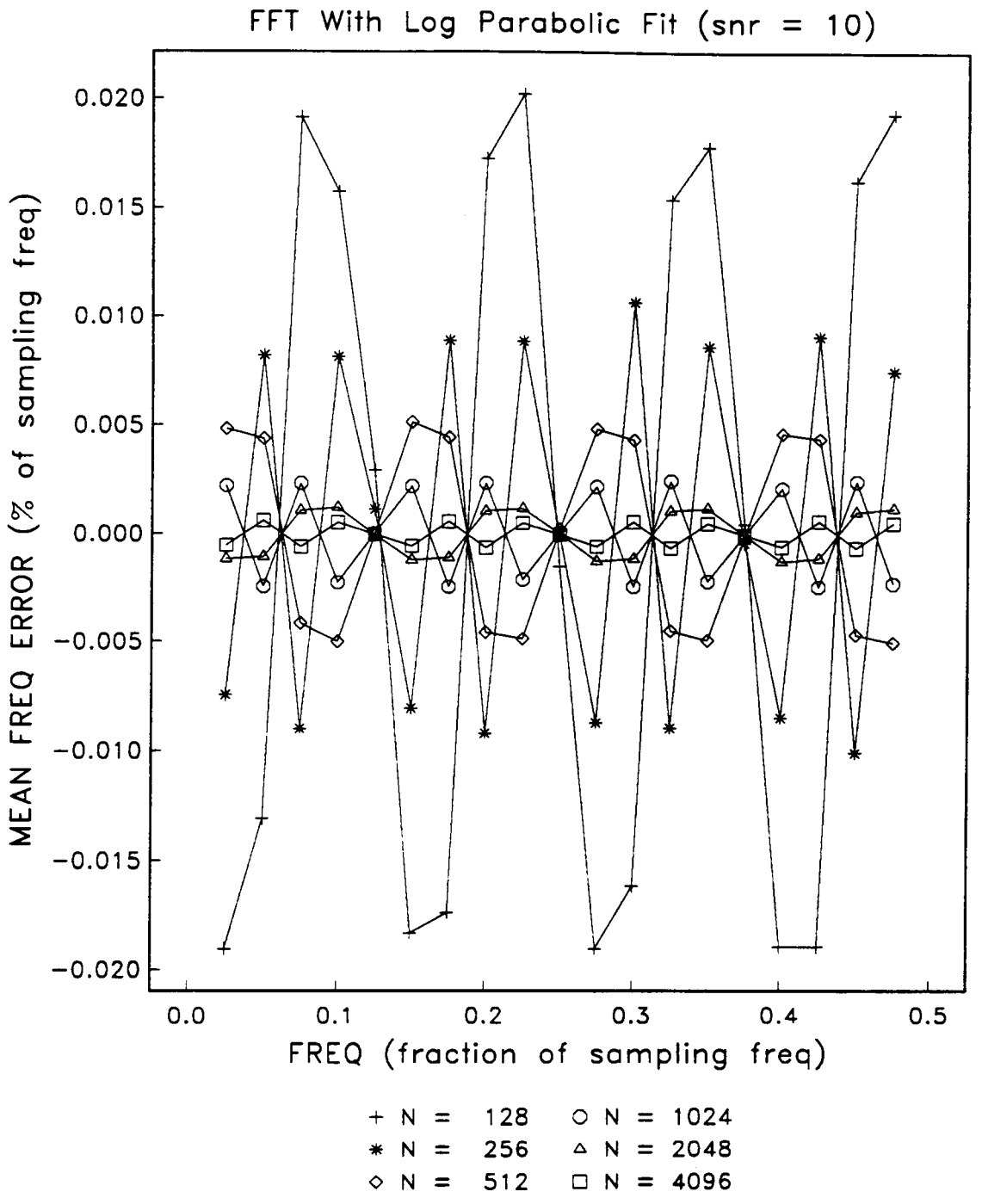

Figure 58. Frequency Bias Error vs. Frequency for FFT with Log Parabolic Interpolation, SNR = 10 dB.

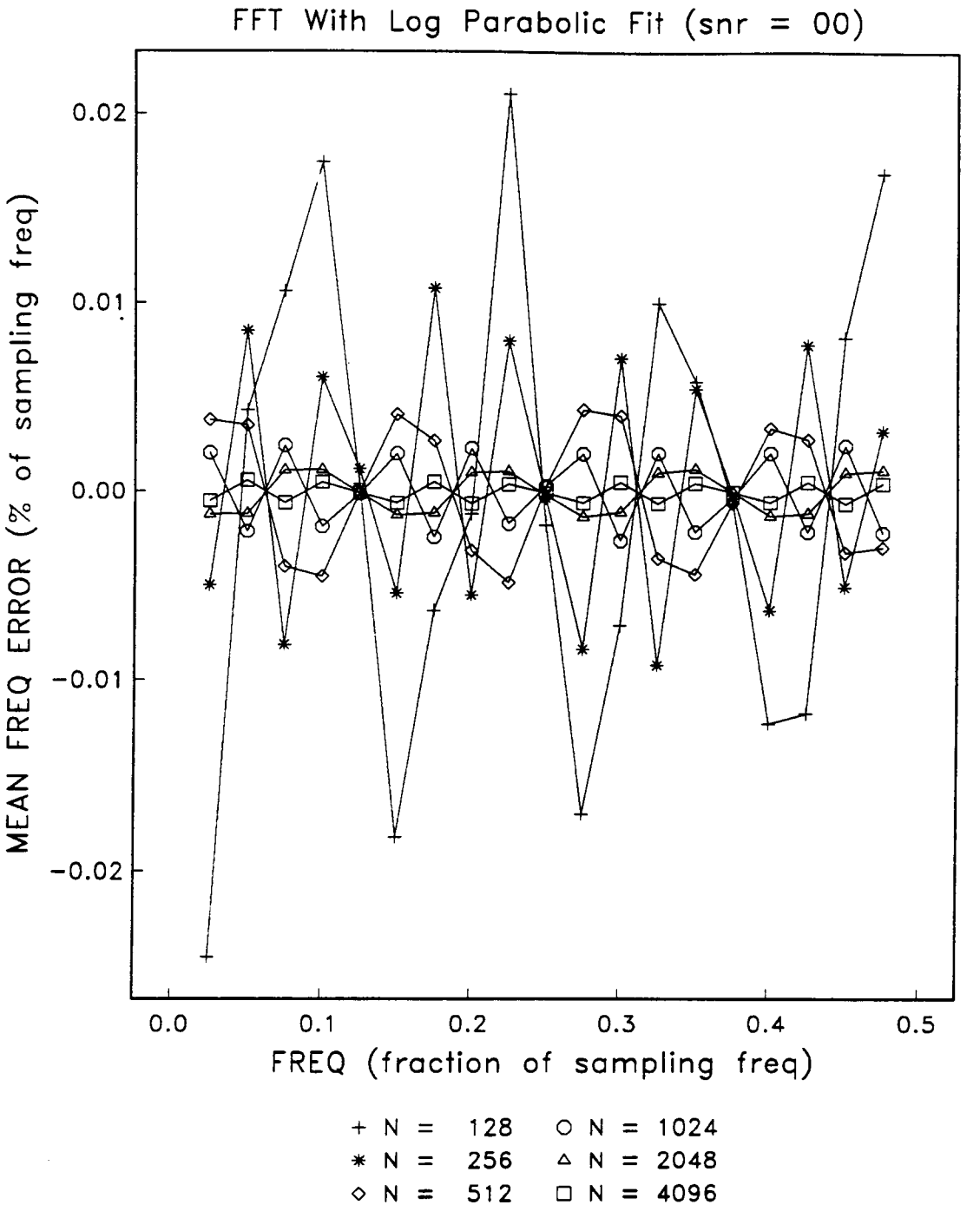

Figure 59. Frequency Bias Error vs. Frequency for FFT with Log Parabolic Interpolation, SNR = 0 dB.

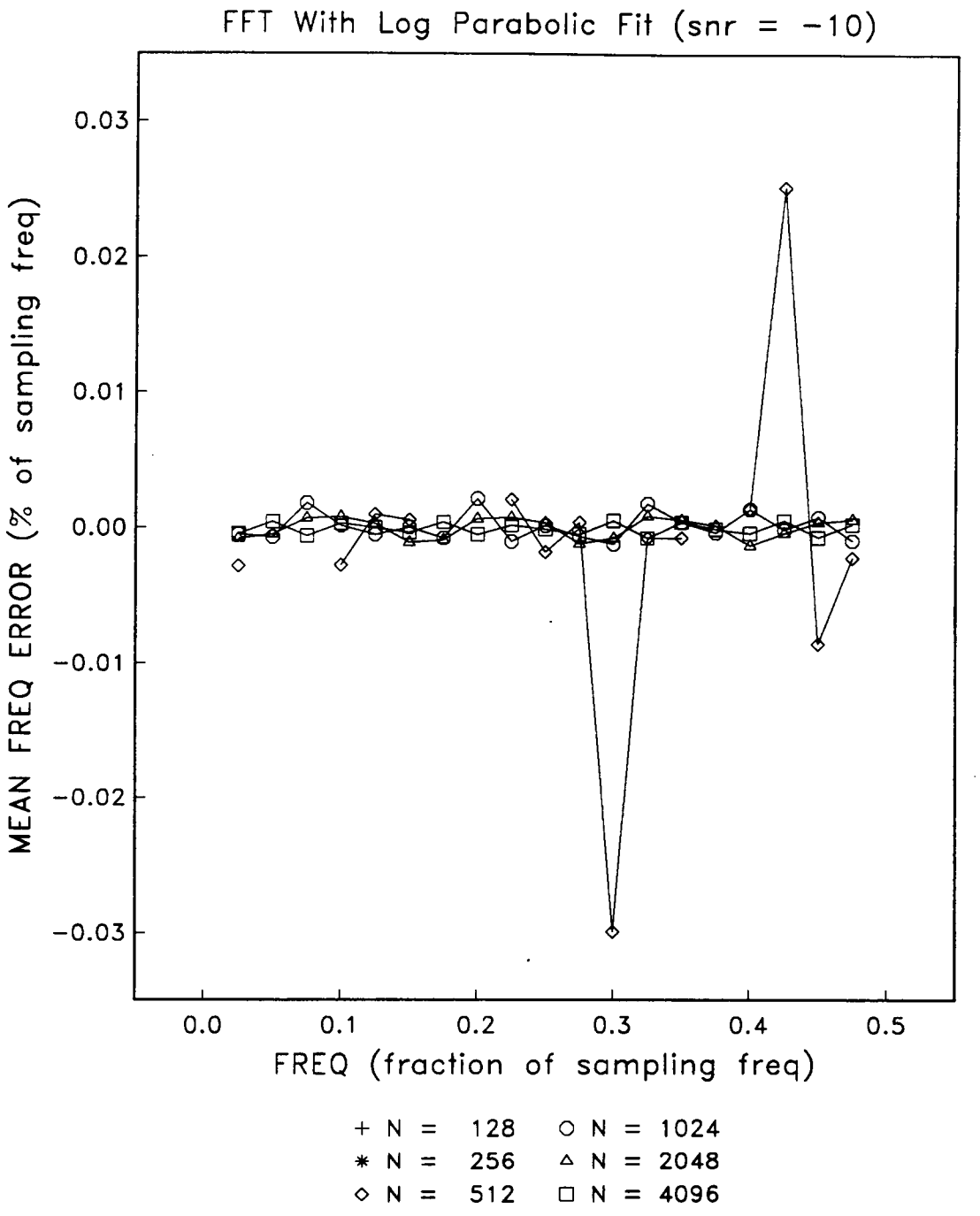

Figure 60. Frequency Bias Error vs. Frequency for FFT with Log Parabolic Interpolation, SNR = -10 dB.

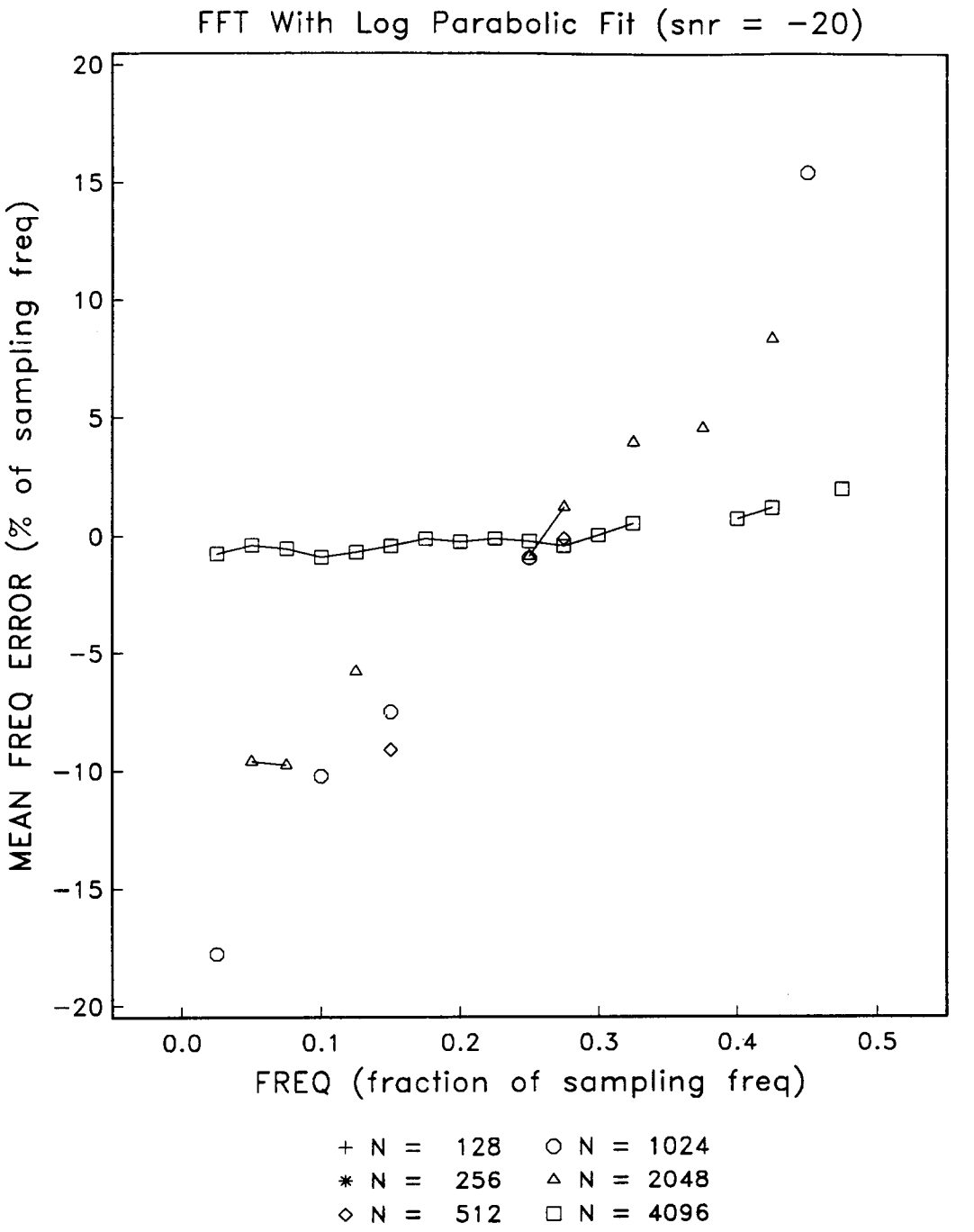

Figure 61. Frequency Bias Error vs. Frequency for FFT with Log Parabolic Interpolation, SNR = -20 dB.

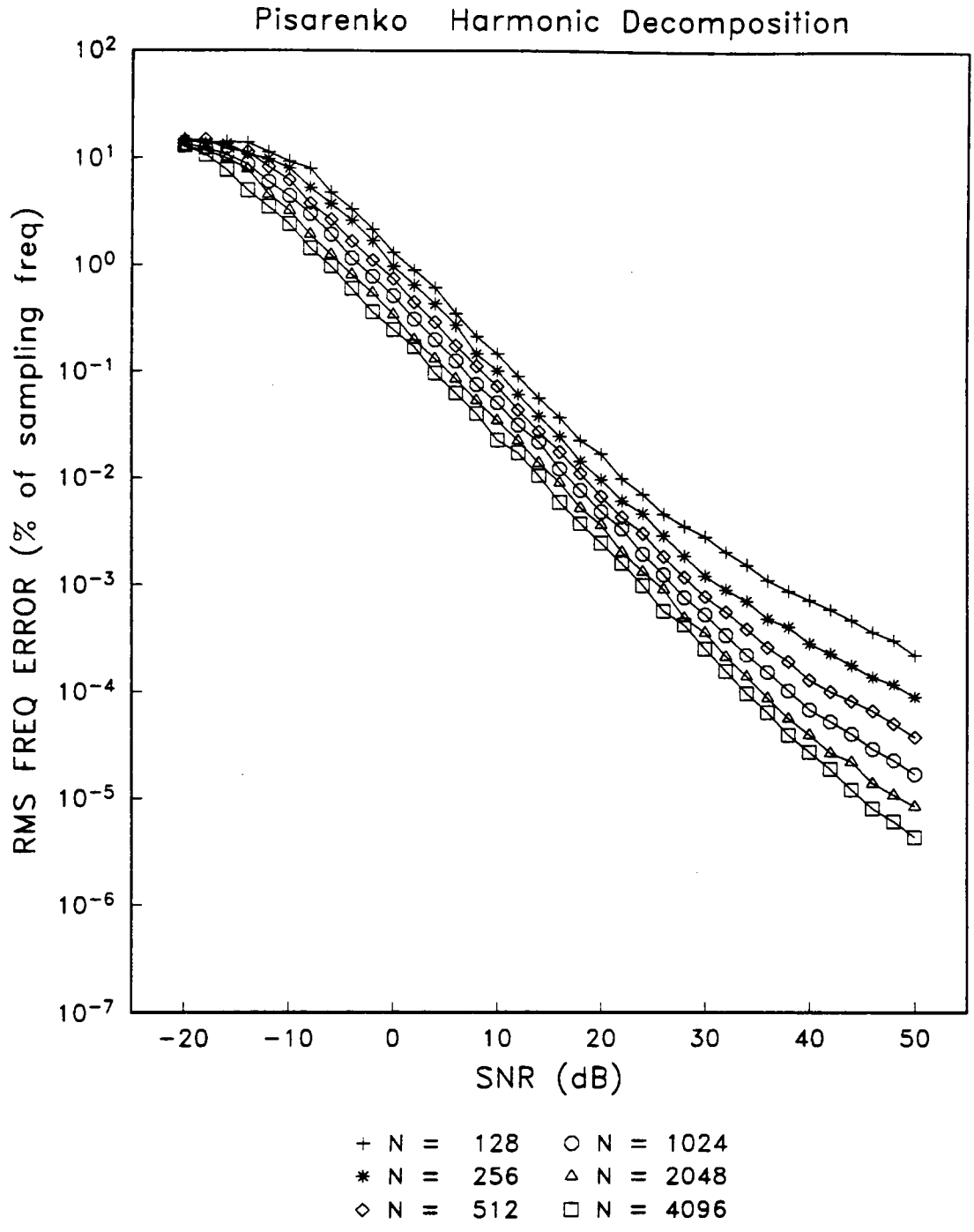

Figure 62. RMS Frequency Error vs. SNR for Pisarenko Harmonic Decomposition.: f = 0.25

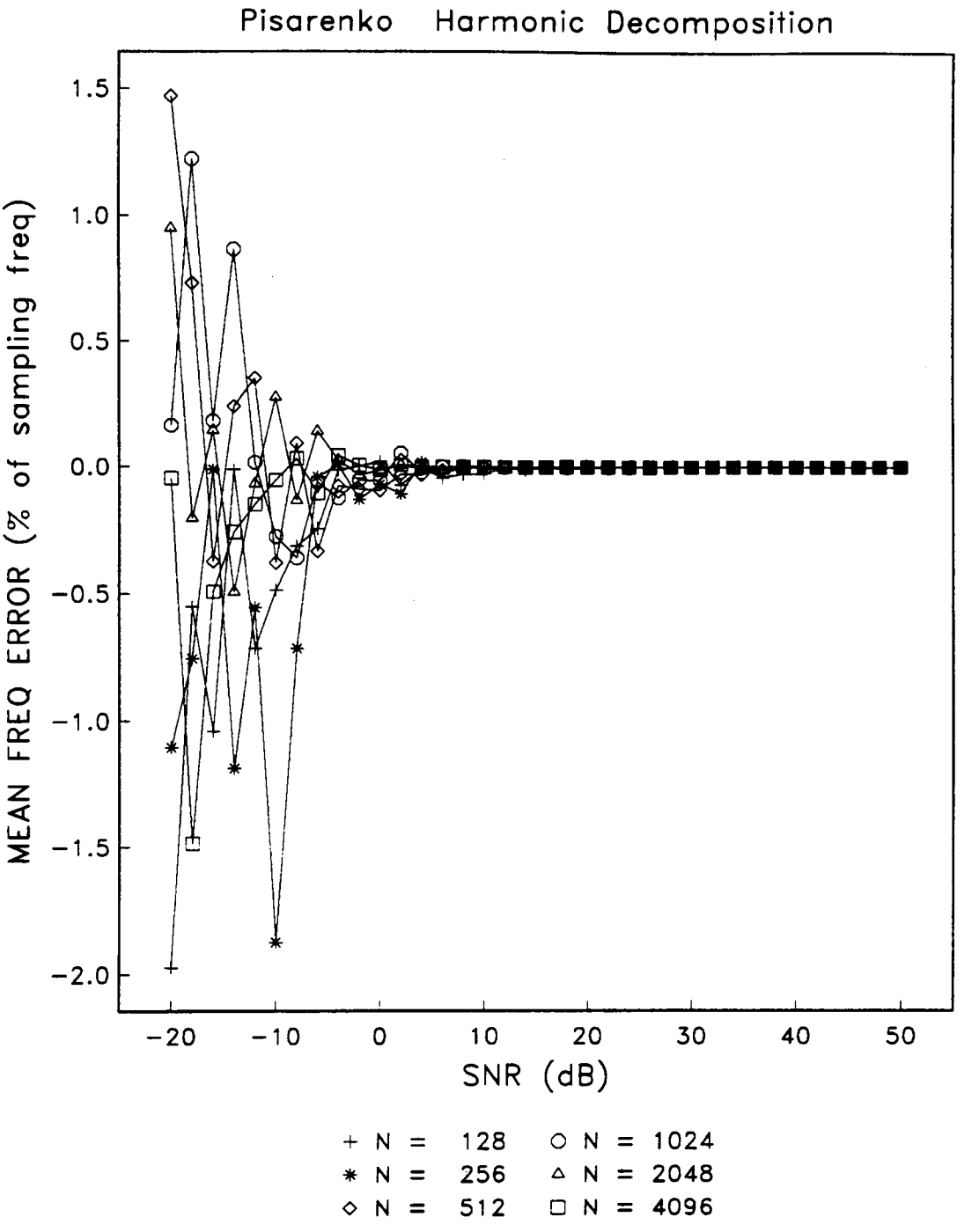

Figure 63. Frequency Bias Error vs. SNR for Pisarenko Harmonic Decomposition.: f = 0.25

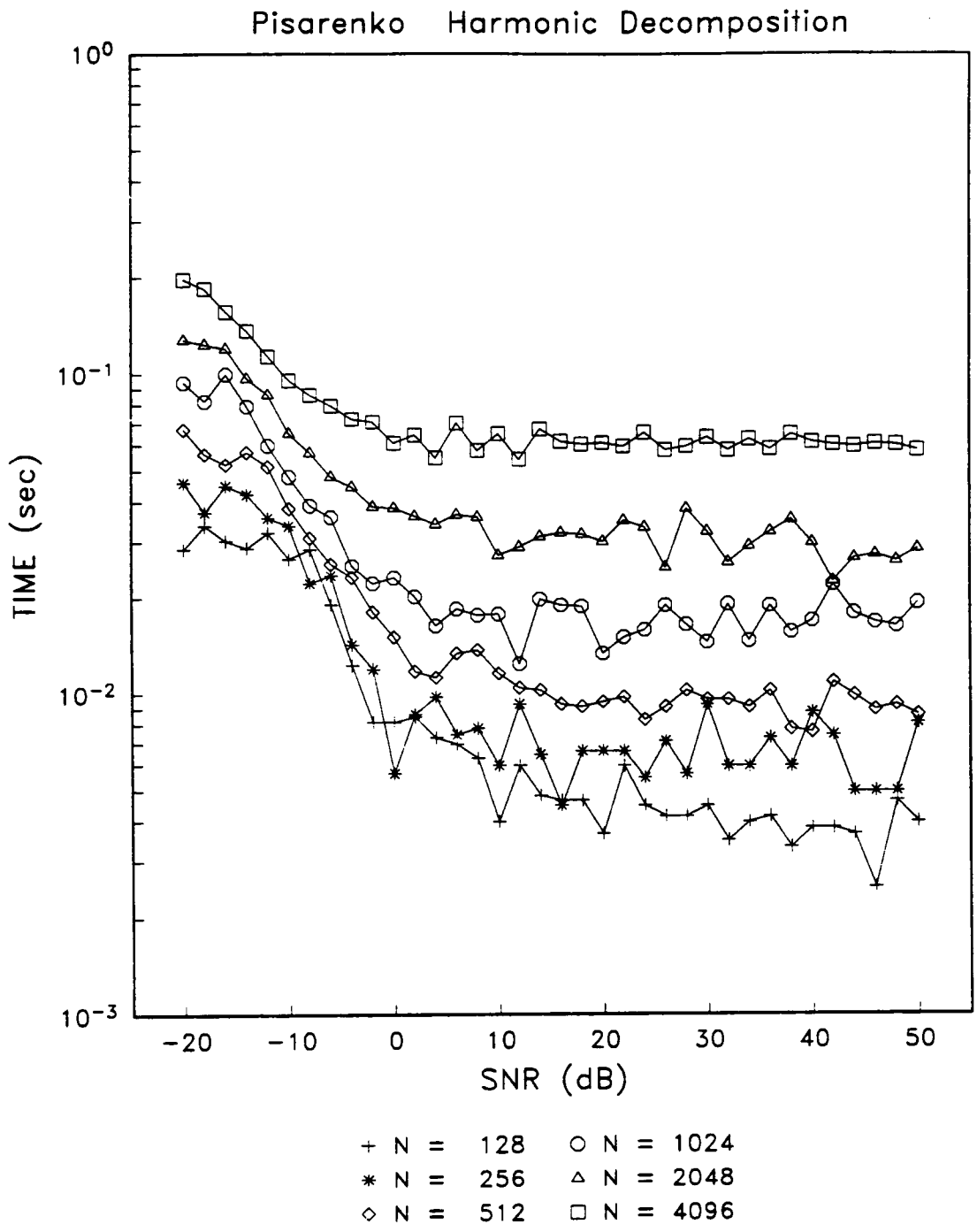

Figure 64. Computation Time vs. SNR for Pisarenko Harmonic Decomposition.: f = 0.25

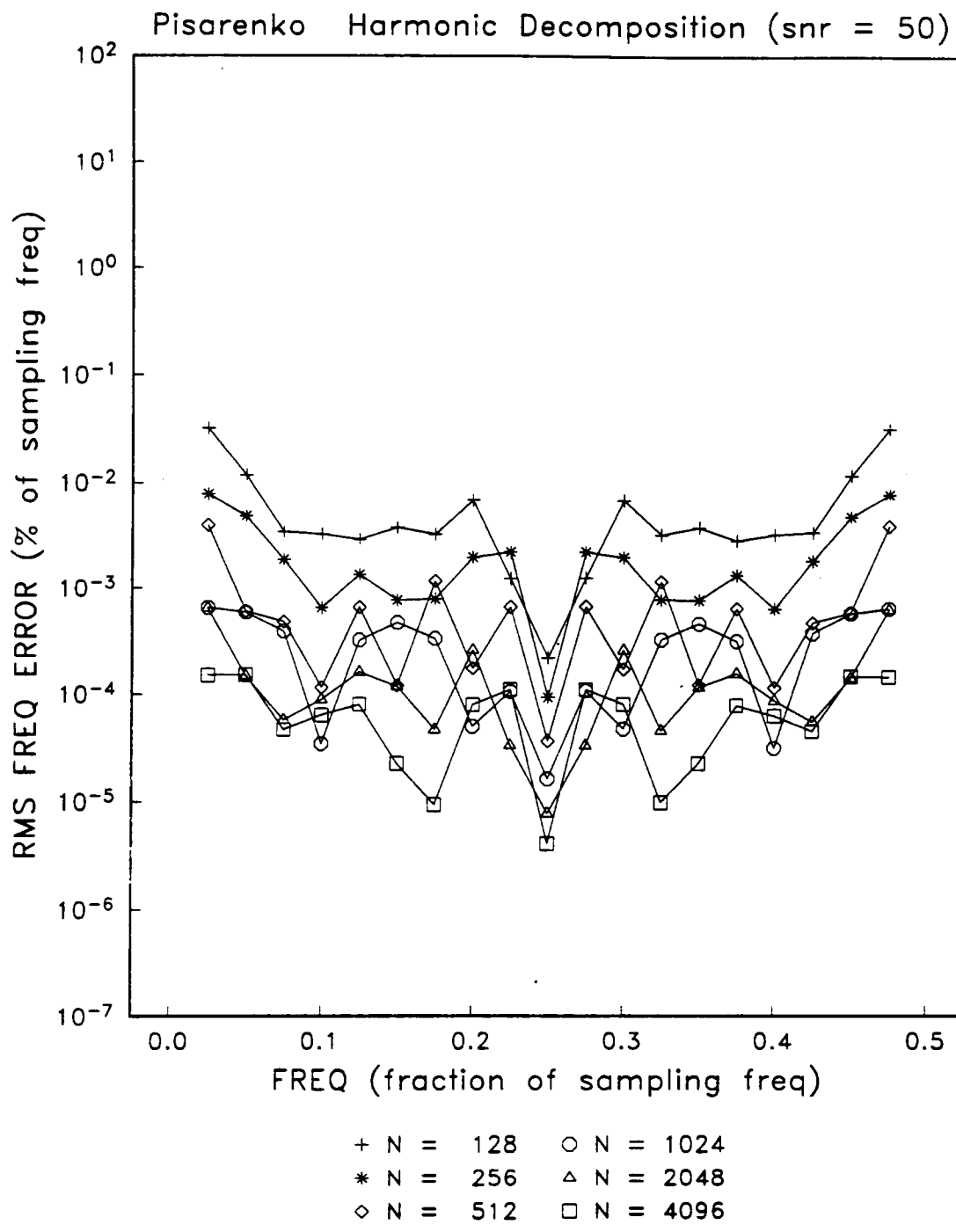

Figure 65. RMS Frequency Error vs. Frequency for Pisarenko Harmonic Decomposition, SNR = 50 dB.

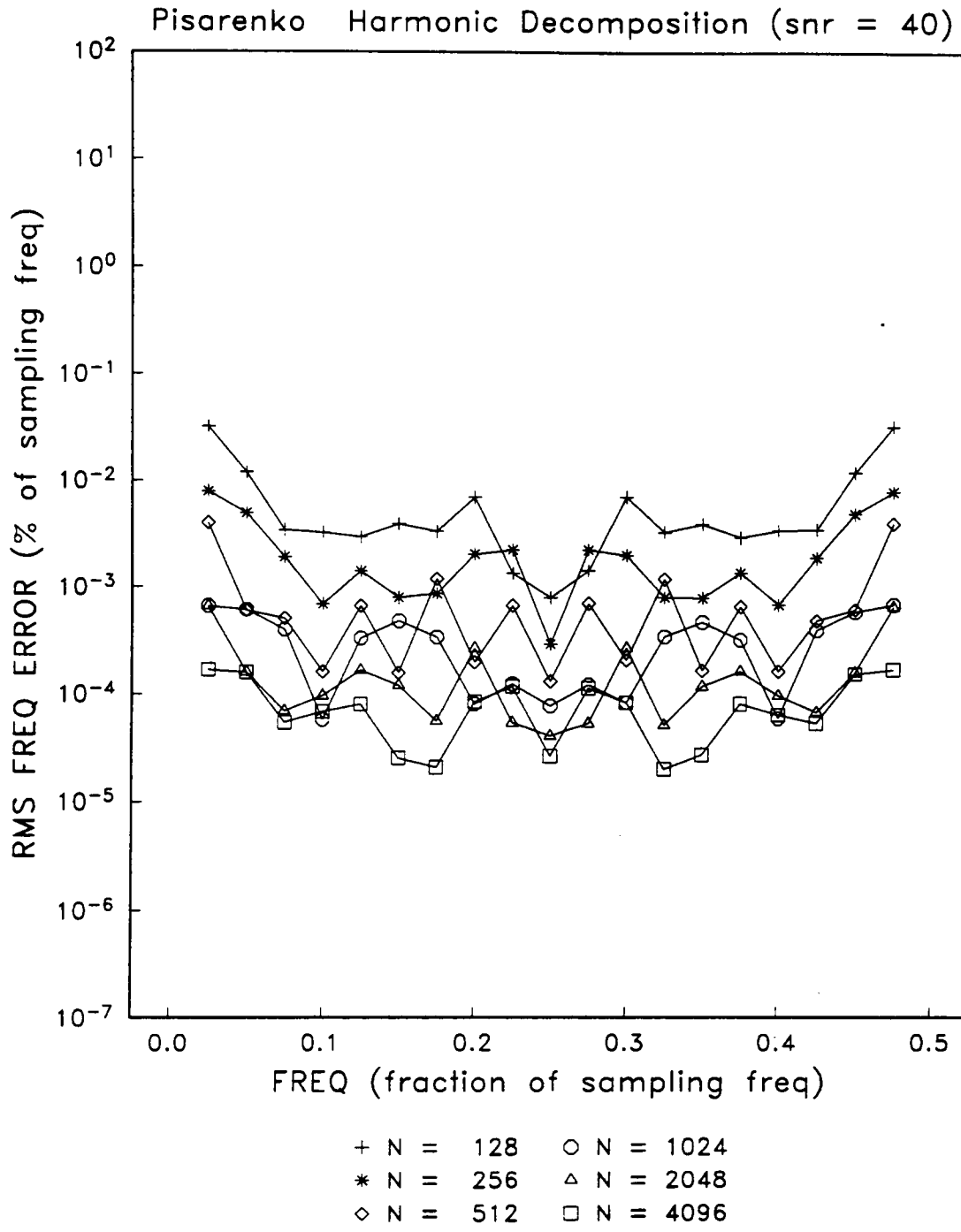

Figure 66. RMS Frequency Error vs. Frequency for Pisarenko Harmonic Decomposition, SNR = 40 dB.

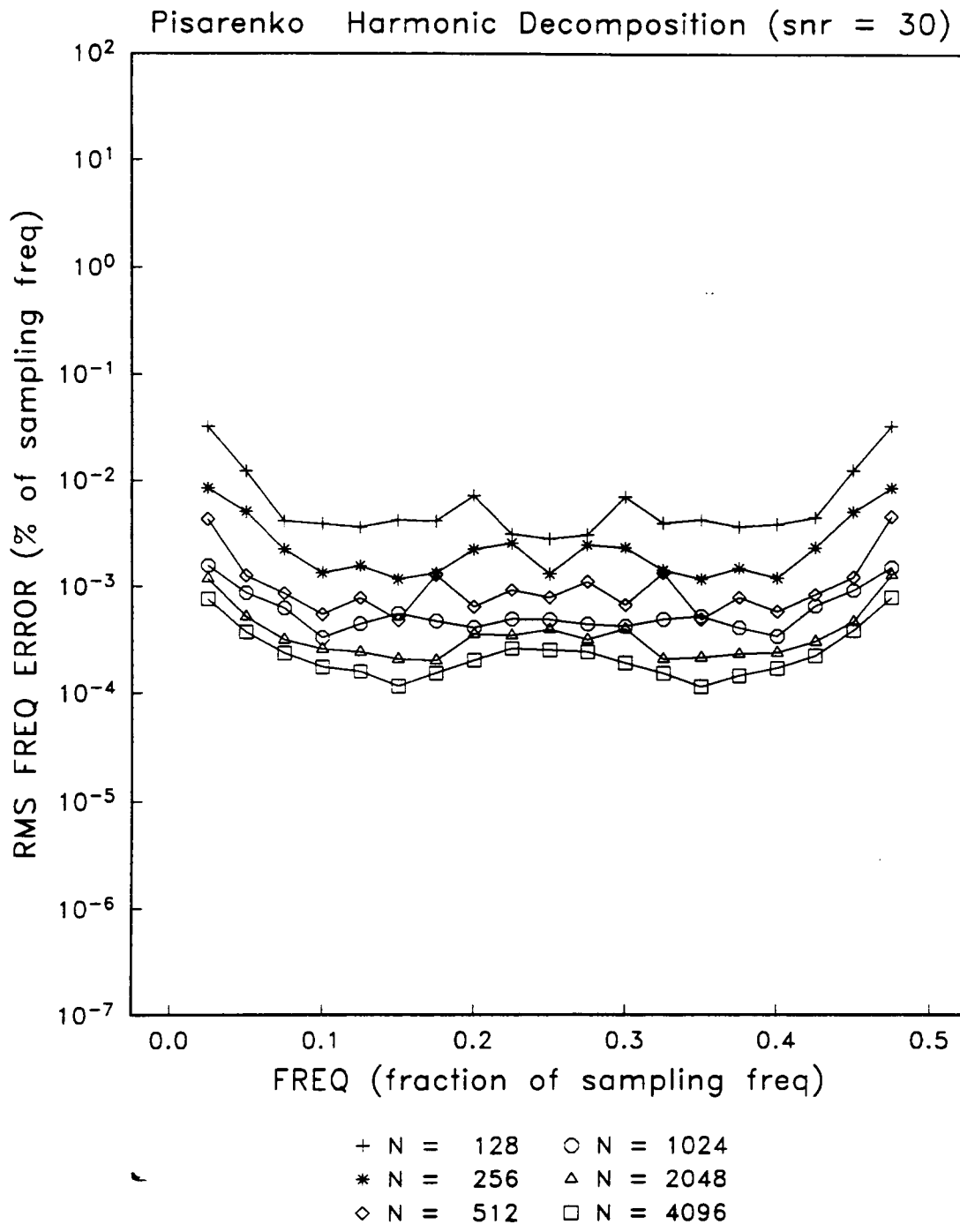

Figure 67. RMS Frequency Error vs. Frequency for Pisarenko Harmonic Decomposition, SNR = 30 dB.

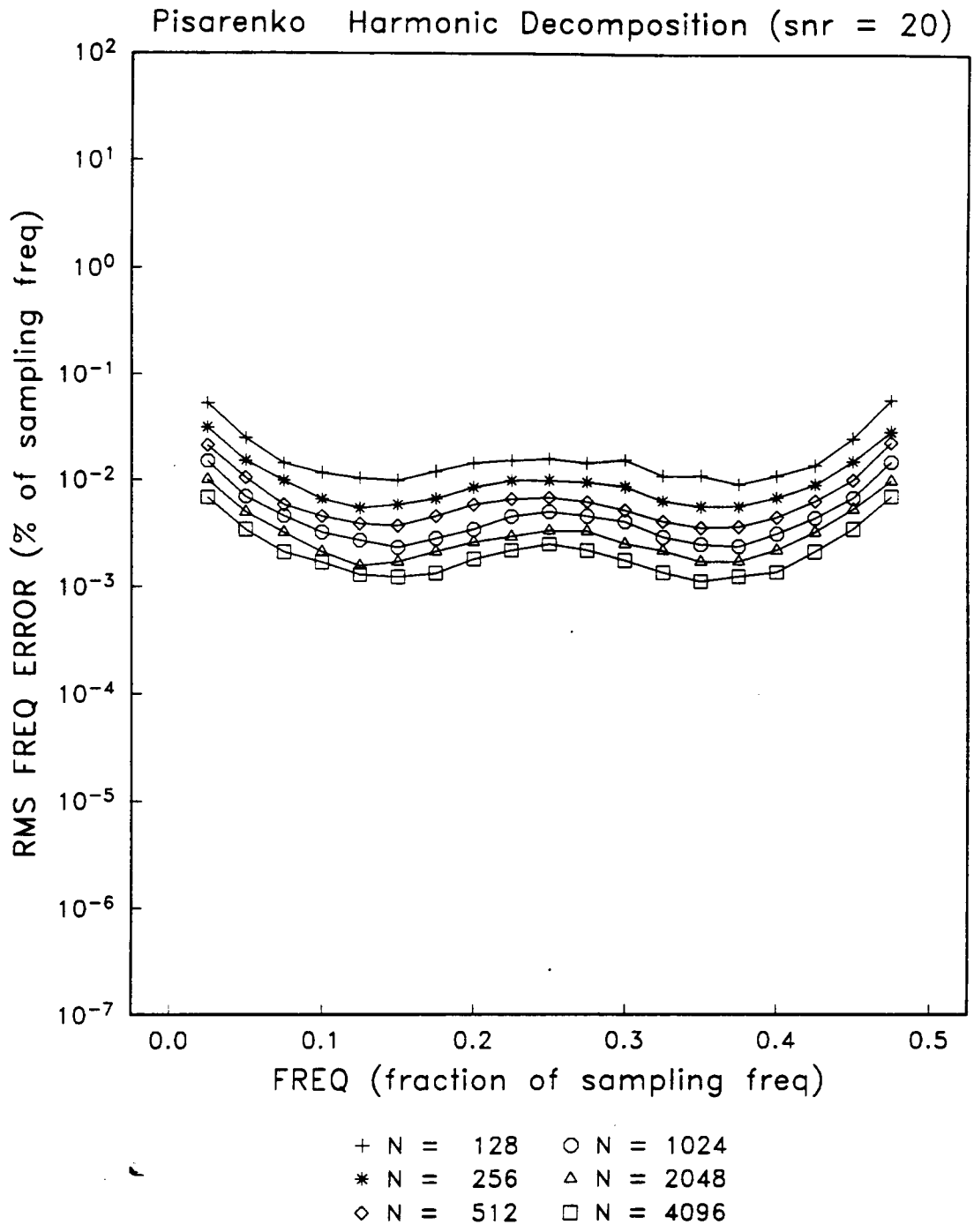

Figure 68. RMS Frequency Error vs. Frequency for Pisarenko Harmonic Decomposition, SNR = 20 dB.

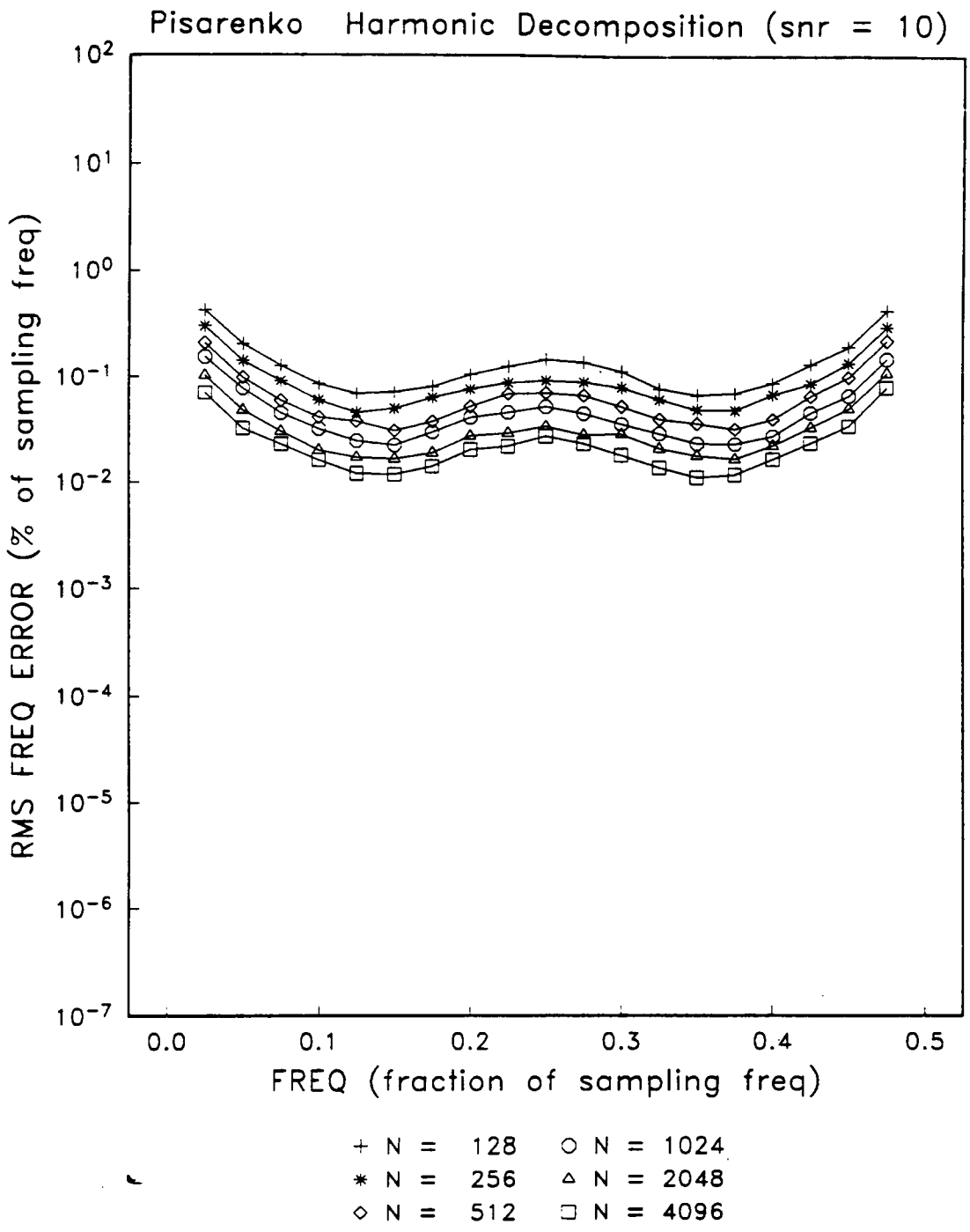

Figure 69. RMS Frequency Error vs. Frequency for Pisarenko Harmonic Decomposition, SNR = 10 dB.

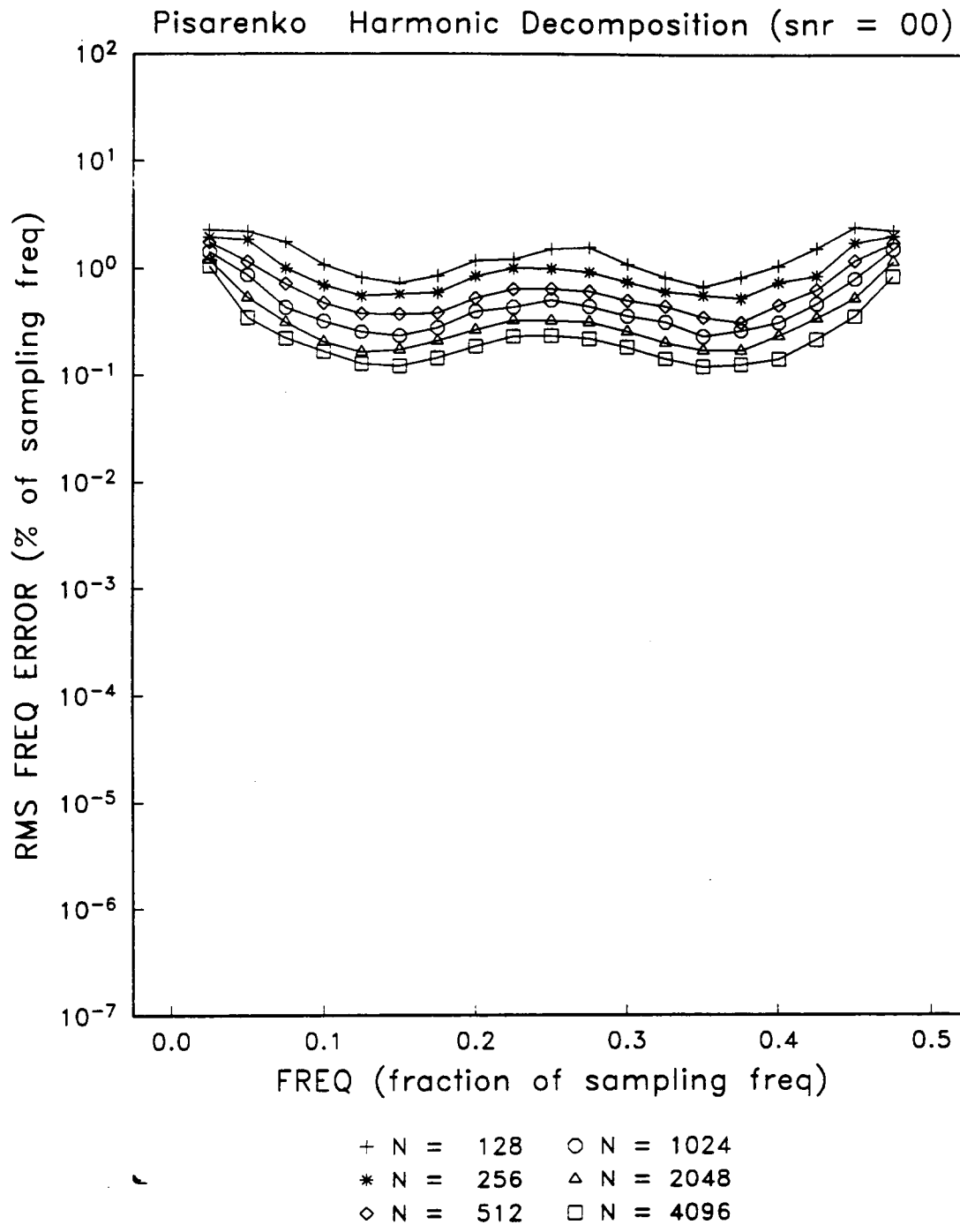

Figure 70. RMS Frequency Error vs. Frequency for Pisarenko Harmonic Decomposition, SNR = 0 dB.

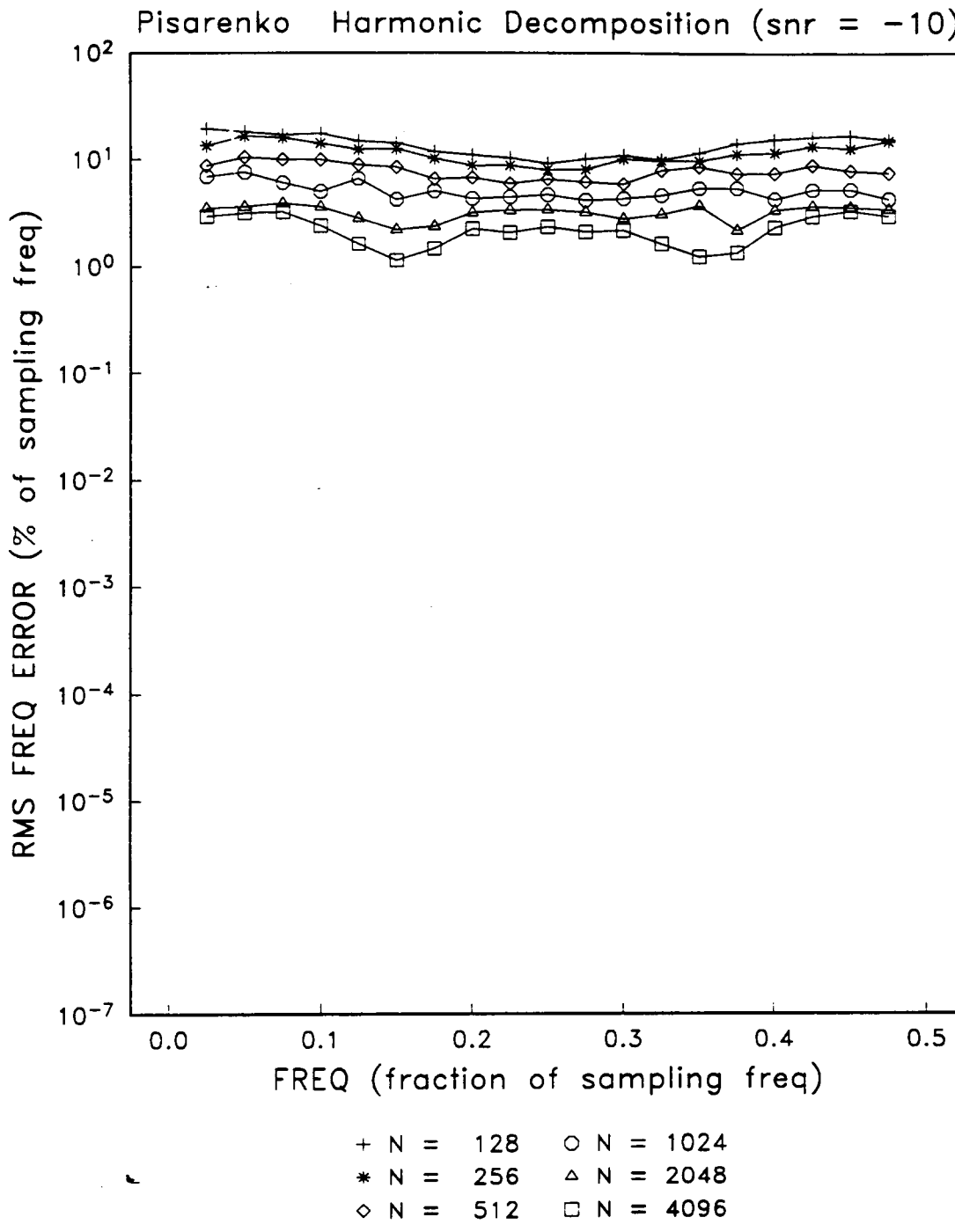

Figure 71. RMS Frequency Error vs. Frequency for Pisarenko Harmonic Decomposition, SNR = -10 dB.

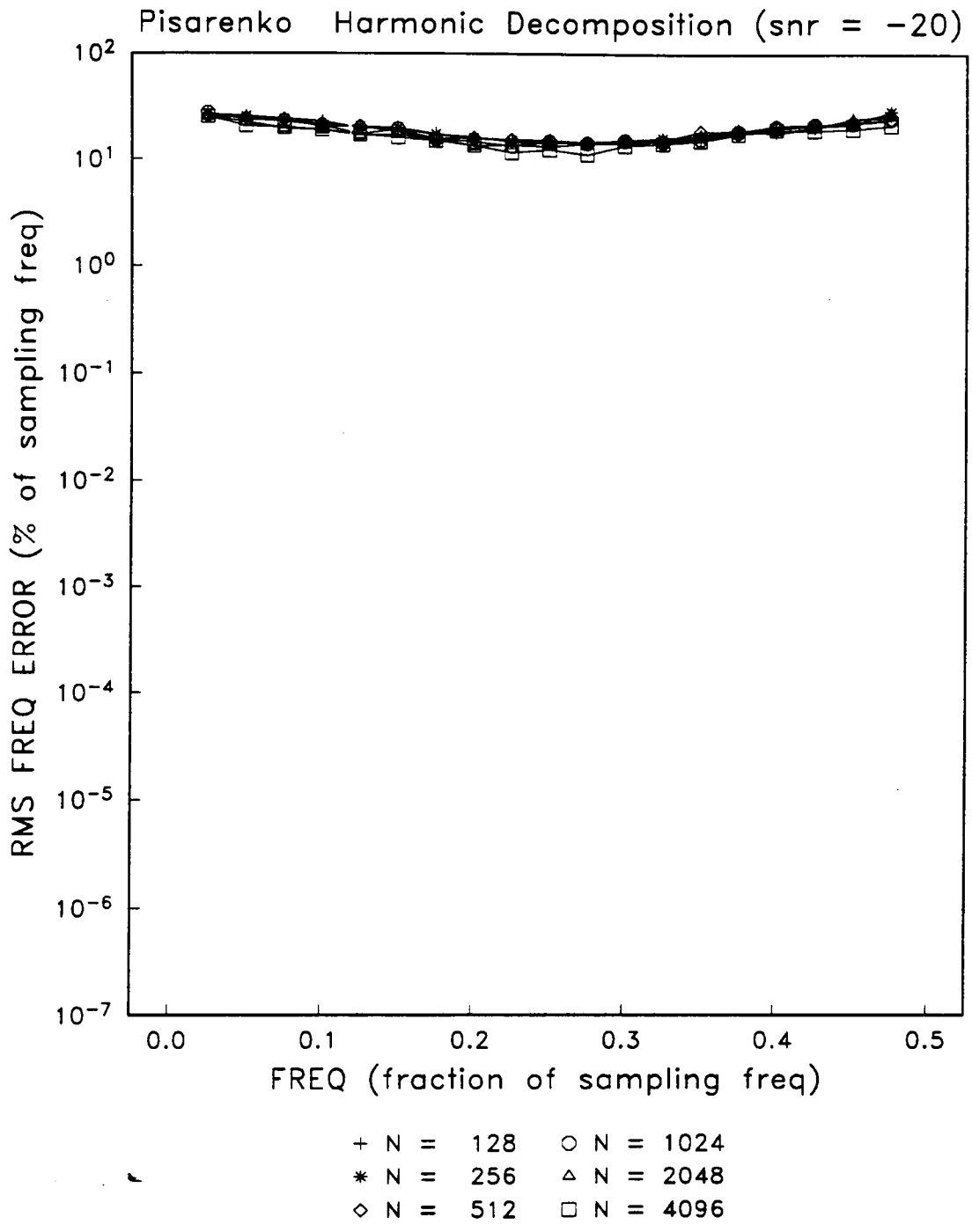

Figure 72. RMS Frequency Error vs. Frequency for Pisarenko Harmonic Decomposition, SNR = -20 dB.

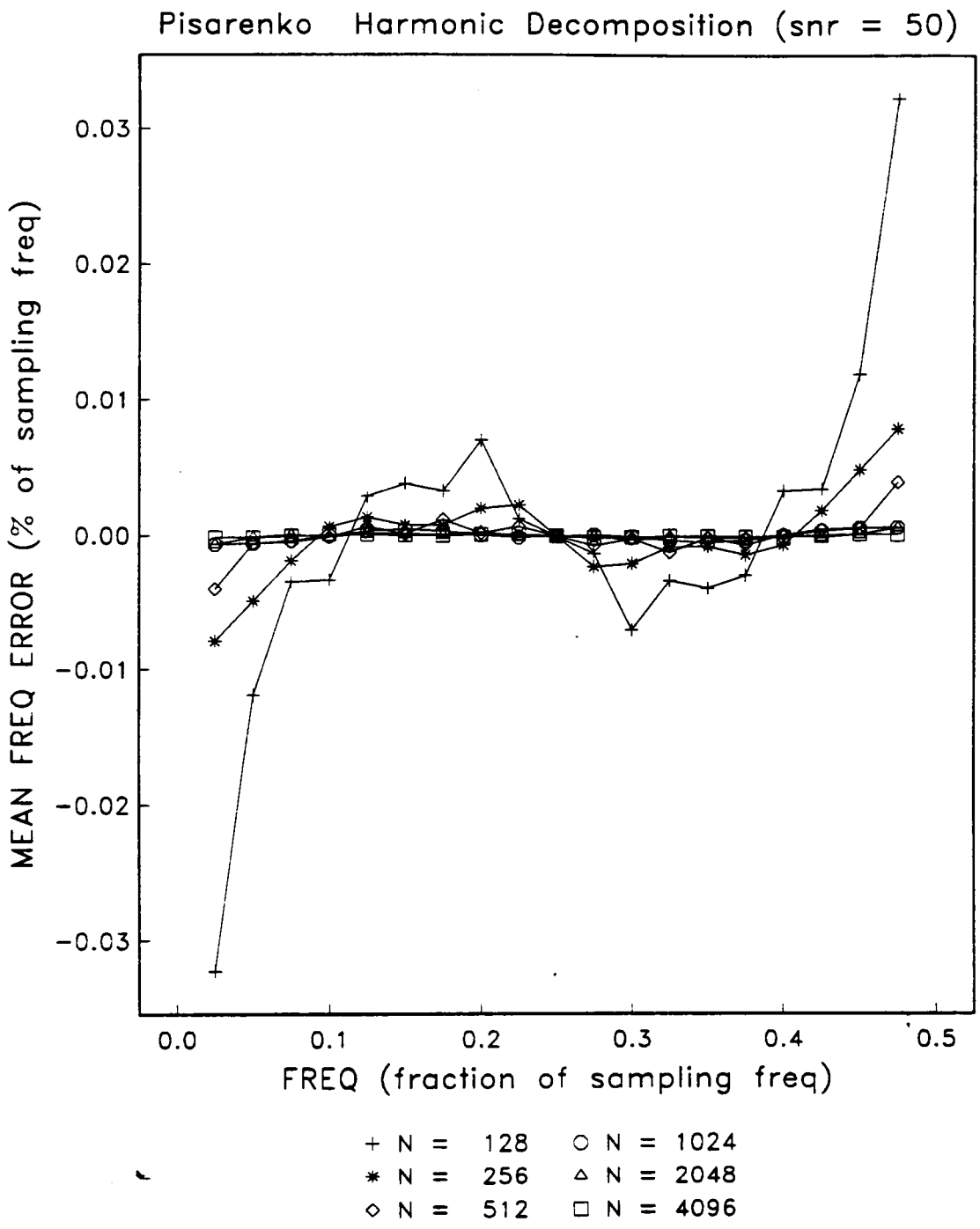

Figure 73. Frequency Bias Error vs. Frequency for Pisarenko Harmonic Decomposition, SNR = 50 dB.

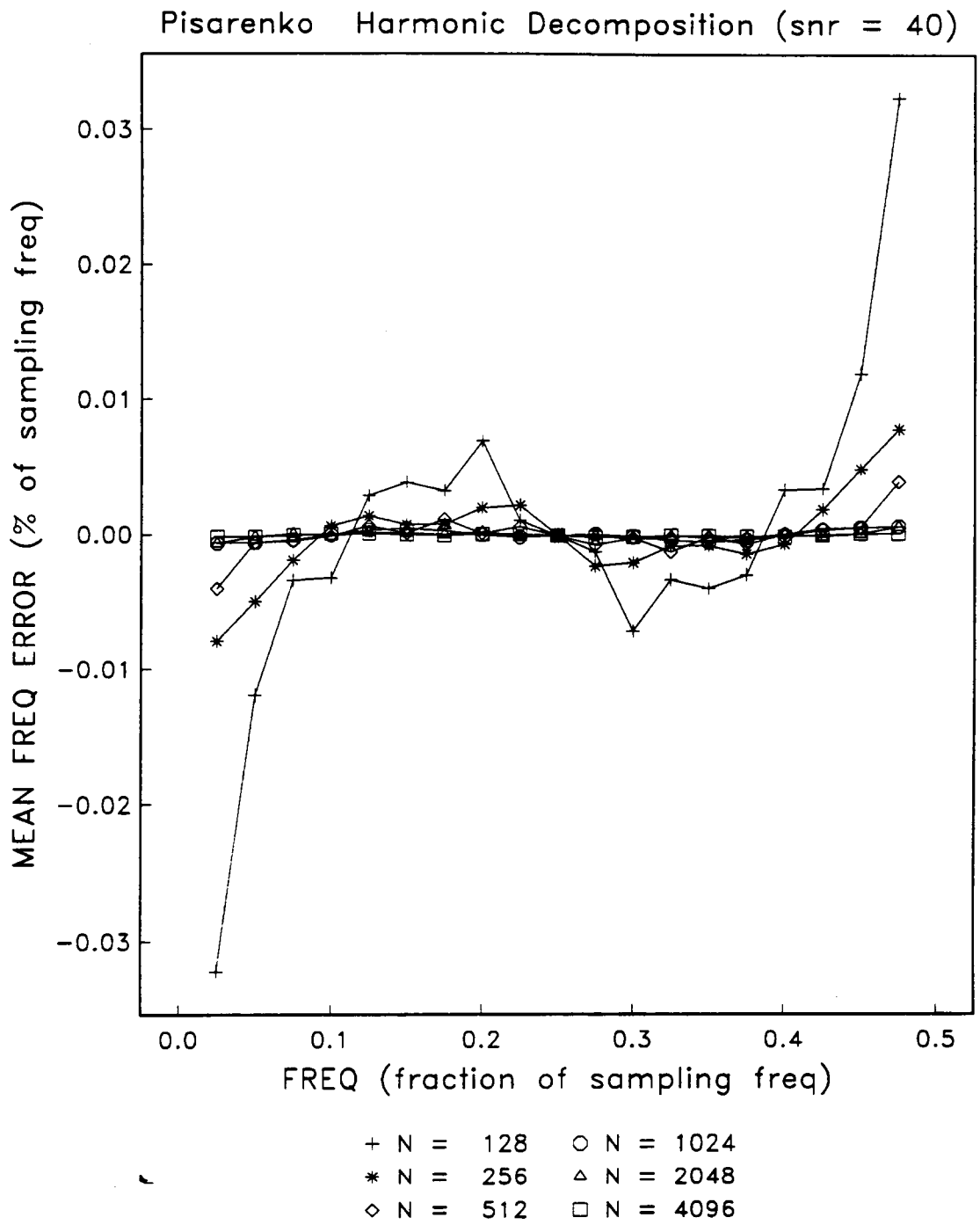

Figure 74. Frequency Bias Error vs. Frequency for Pisarenko Harmonic Decomposition, SNR = 40 dB.

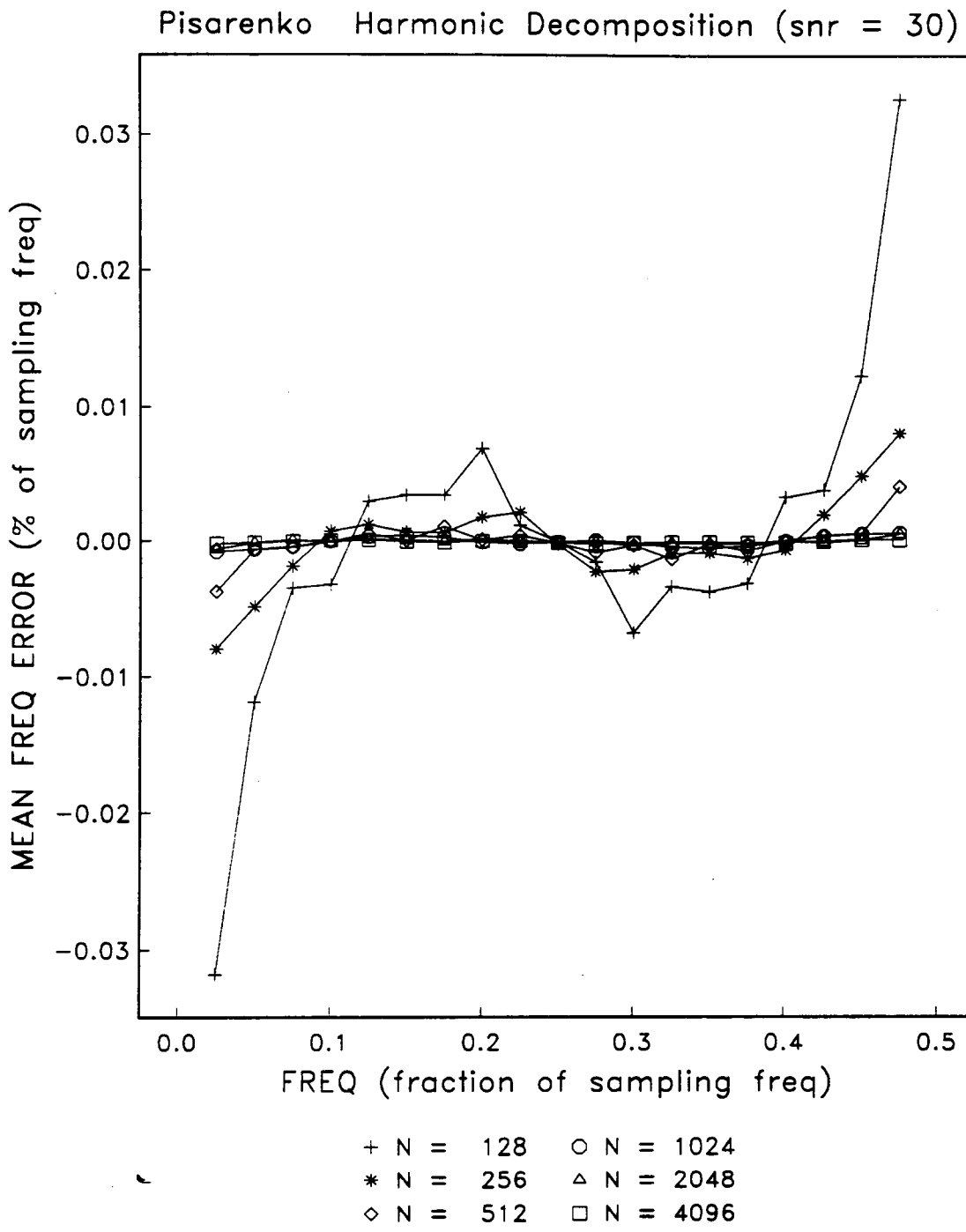

Figure 75. Frequency Bias Error vs. Frequency for Pisarenko Harmonic Decomposition, SNR = 30 dB.

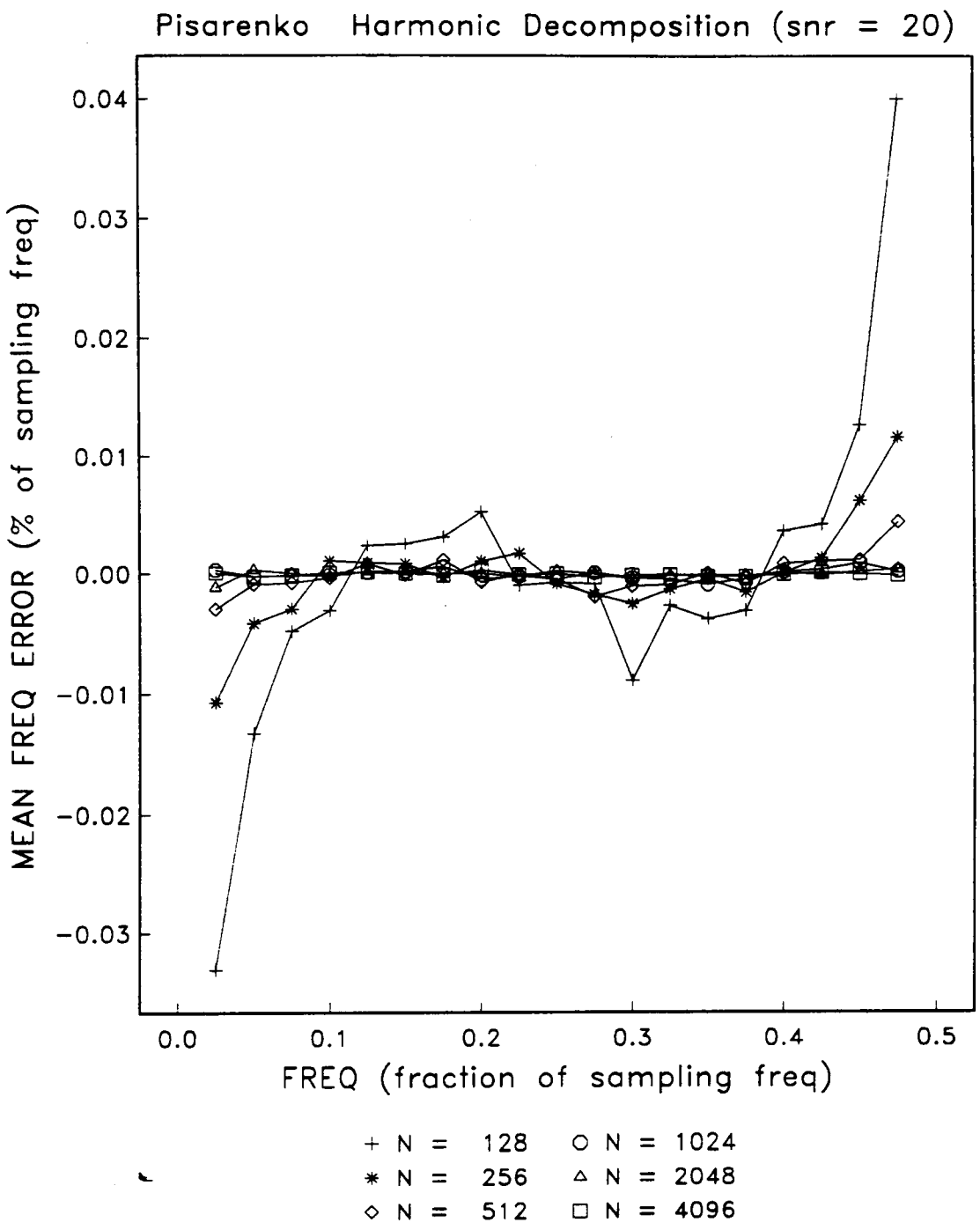

Figure 76. Frequency Bias Error vs. Frequency for Pisarenko Harmonic Decomposition, SNR = 20 dB.

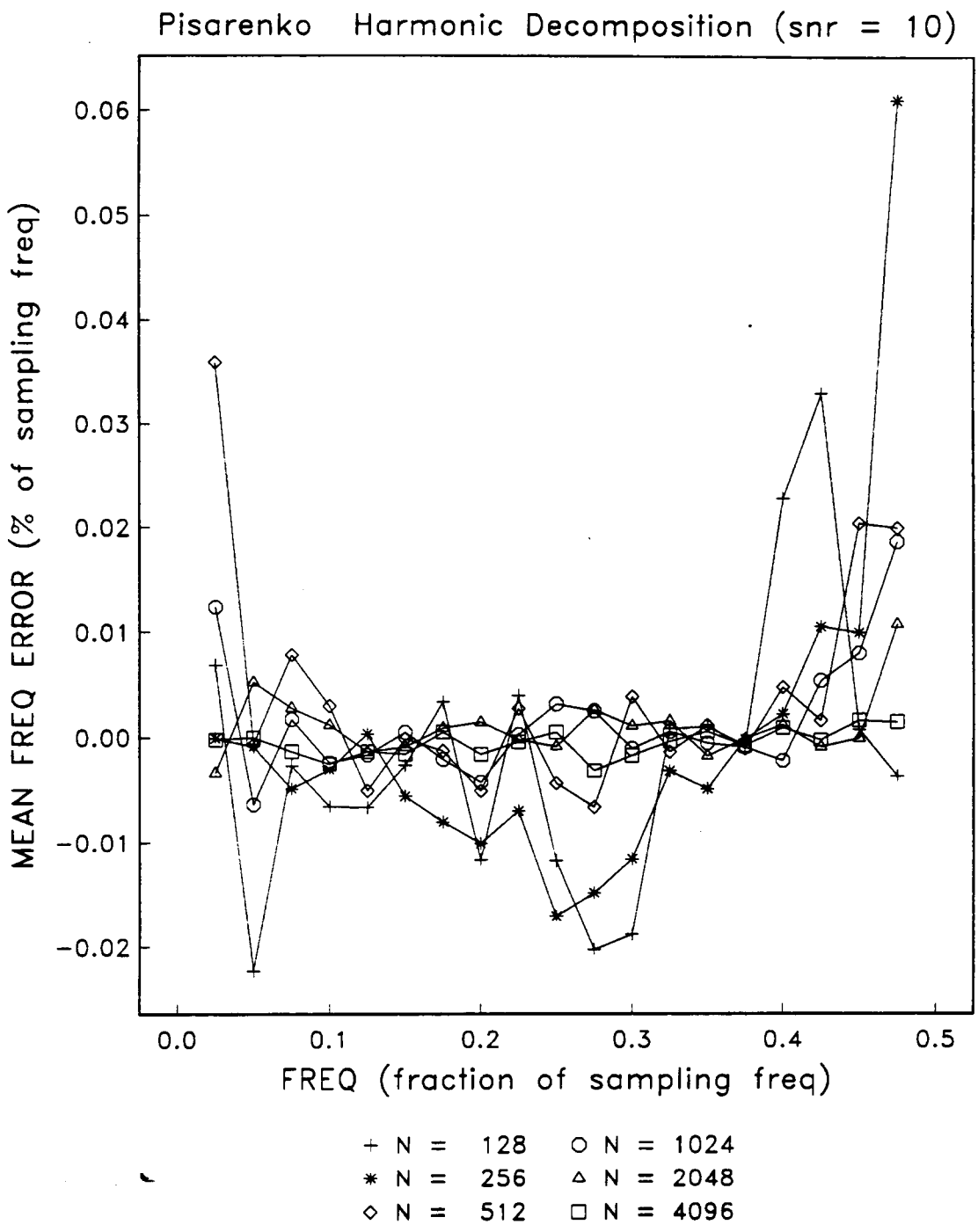

Figure 77. Frequency Bias Error vs. Frequency for Pisarenko Harmonic Decomposition, SNR = 10 dB.

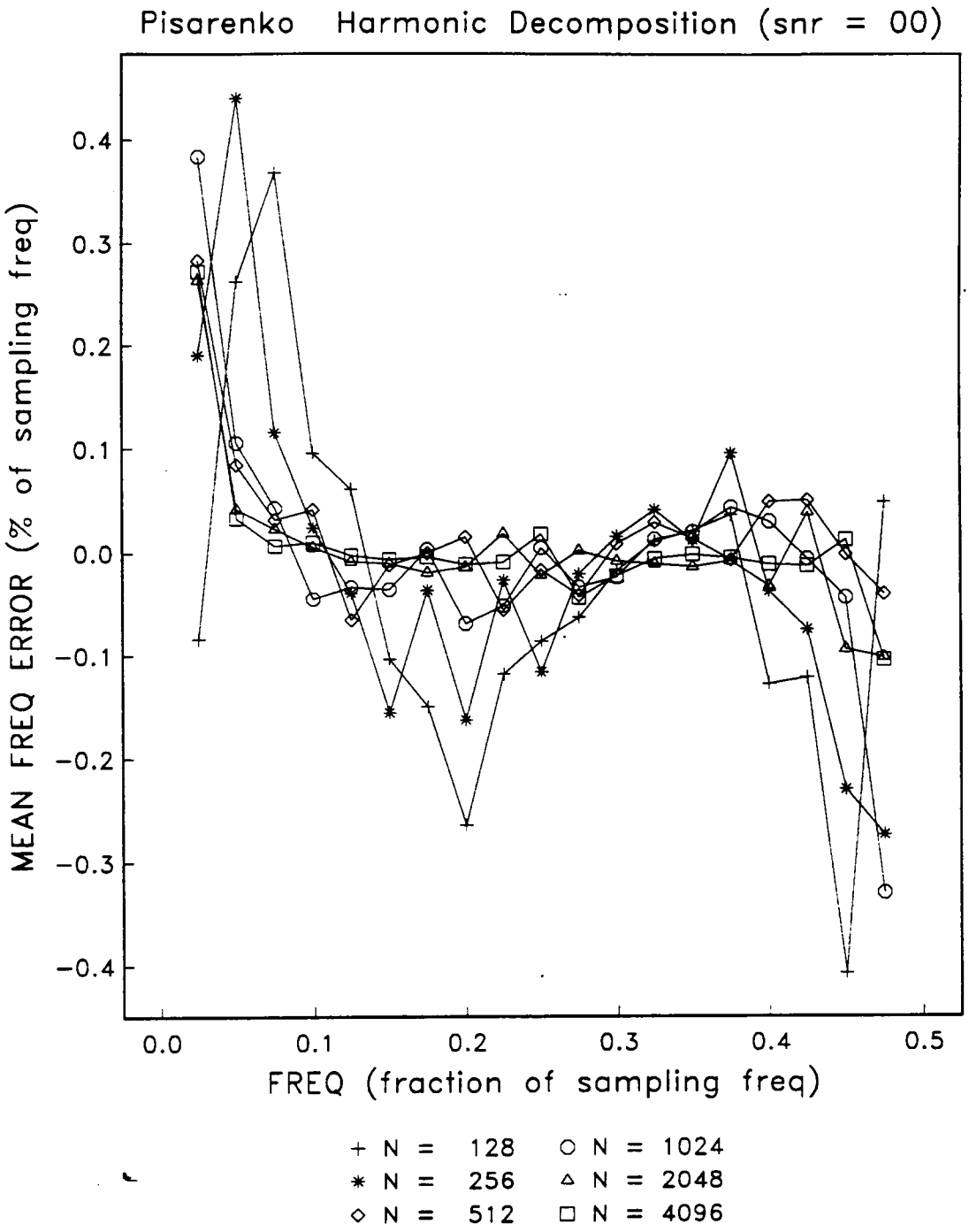

Figure 78. Frequency Bias Error vs. Frequency for Pisarenko Harmonic Decomposition, SNR = 0 dB.

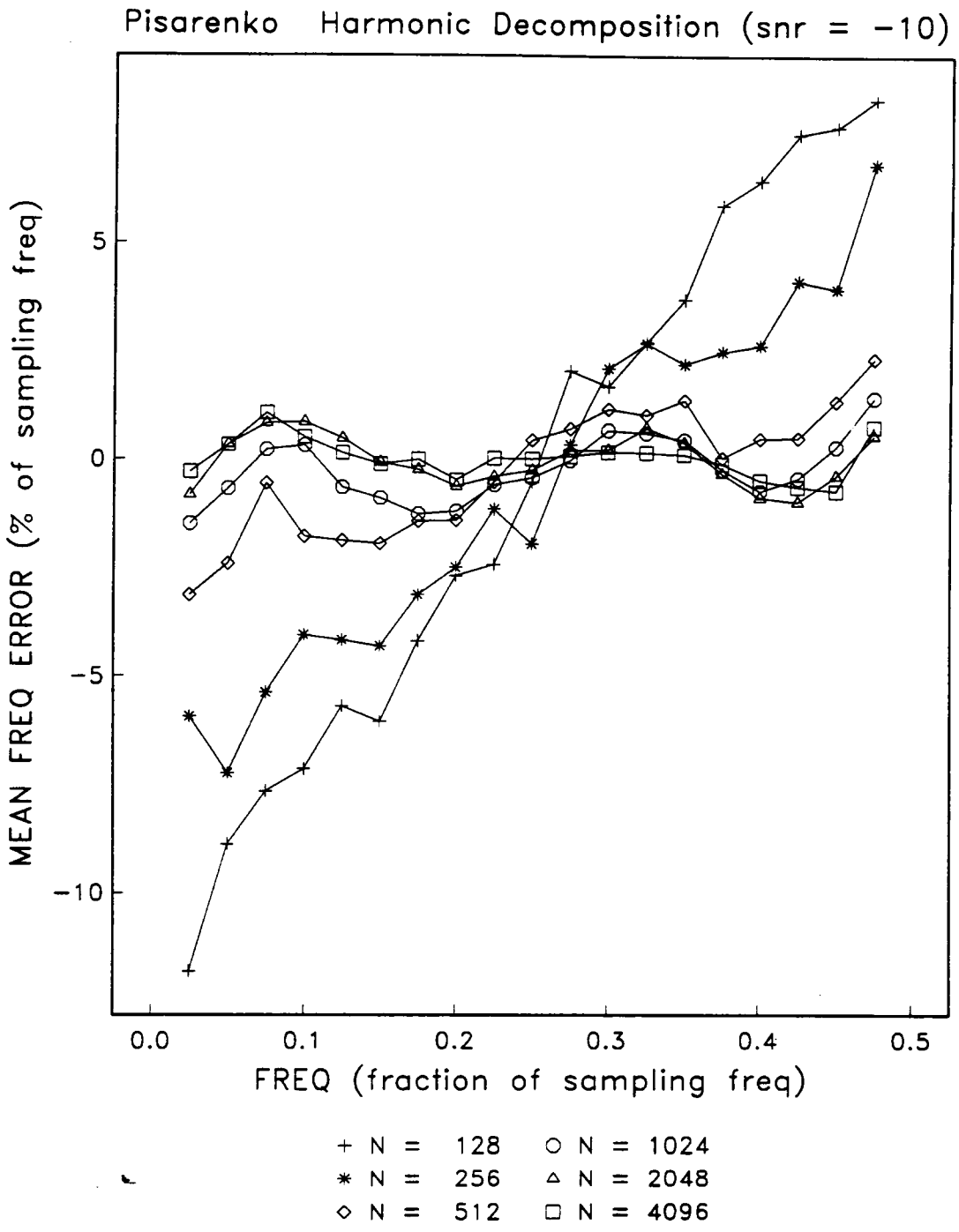

Figure 79. Frequency Bias Error vs. Frequency for Pisarenko Harmonic Decomposition, SNR = -10 dB.

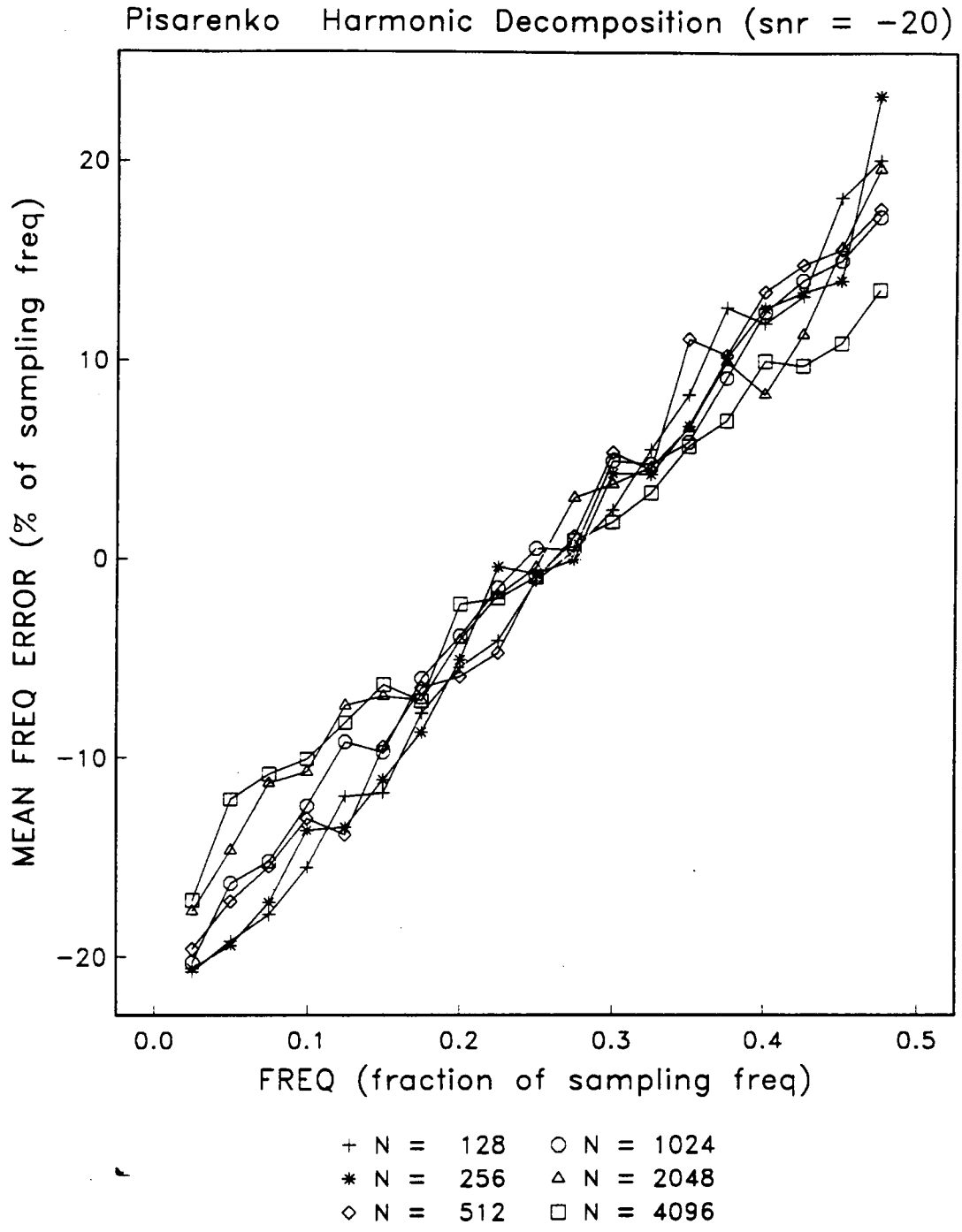

Figure 80. Frequency Bias Error vs. Frequency for Pisarenko Harmonic Decomposition, SNR = -20 dB.

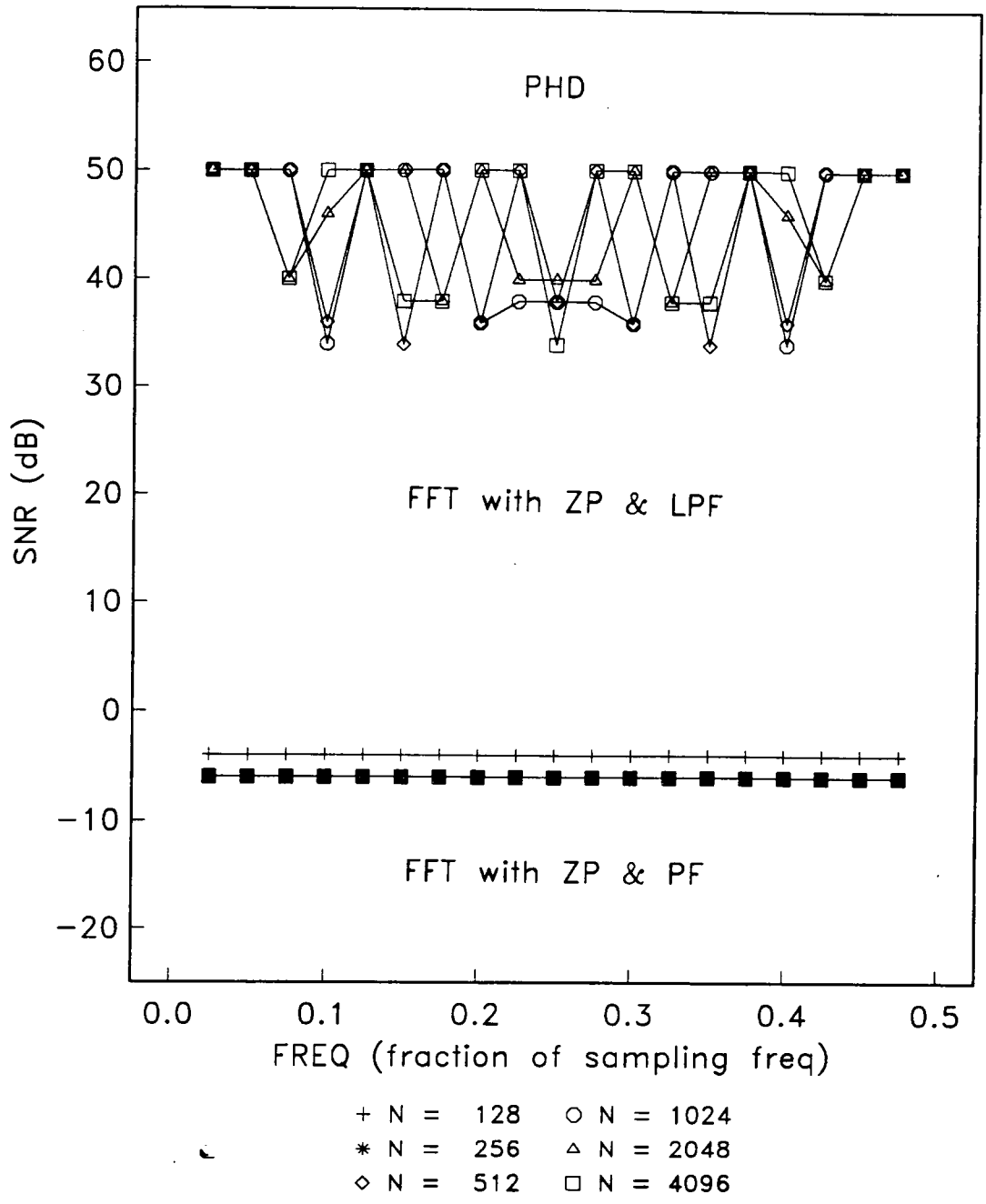

Figure 81. SNR vs. Frequency Identifying the Appropriate Technique to use Relative to SNR and Frequency Ratio.: ZP = Zero-padding, PF = parabolic fit, LPF = log parabolic fit.

Appendix A.

A.1 Optimization Program for Plane Mirror Pair

```
      implicit real*8 (a-h,o-z)
      parameter (acc = 1.0d-6, maxit = 1000, nlim = 100)
      x0 = 0.1918d0
      xp = 3.7d0
C     CHANGE THETA0 AND PHI HERE
      th0 = dtr(10d0)
      phi = dtr(20d0)
C
      thm = dtr(5.868d0)
      thm2 = thm/2d0
      t1 = dtr(1d0)
      t55 = dtr(55d0)
      open (unit = 10, file = 'mirror.9')
      write (10,101) rtd(phi),rtd(th0)
101   format (1x,'phi = ',f7.3,'th0 = ',f7.3)
C     LOOP FOR THETA1
      do 100 i = 1,36
        th1 = dble(i-1)*t1 + t55
        fmin = 1d50
C     LOOP FOR D1 AND CALCULATE THETA2 AND D2
        do 200 j = 1,71
          d1 = dble(j-1)*0.025d0 + 0.5d0
          th2 = -0.5d0*(phi - 2d0*th1 + th0)
          thr = -(2d0*th1 - 2d0*th2 - th0 - thm2)
          b = 2d0*th1 - th0 - thm2
          yp = (xp + x0)*dtan(thm2)
          xm1 = d1*(dtan(th0) - dtan(th1))/(dtan(th0+thm2)-dtan(th1))
          ym1 = xm1*dtan(th0 + thm2)
          xm2 = (xp*dtan(thr) - yp - xm1*dtan(b) + ym1)
     &        / (dtan(thr) - dtan(b))
          ym2 = xm2*dtan(thr) - xp*dtan(thr) + yp
          b = 2d0*th1 - th0
          xm1 = d1
          ym1 = xm1*dtan(th0)
          d2 = (xm2*dtan(th2) - ym2 - xm1*dtan(b) + ym1)
     &        / (dtan(th2) - dtan(b))
          sum = 0d0
C     LOOP TO CALCULATE F
          do 500 m = 1,51
            th = dble(m-1)*thm/50d0
            a = th0 + th
            xm1 = d1*(dtan(th0)-dtan(th1))/(dtan(a)-dtan(th1))
            ym1 = xm1*dtan(a)
            b = 2d0*th1 - th0 - th
            xm2 = (-(d1-d2)*dtan(2d0*th1-th0) + xm1*dtan(b)
     &           + d1*dtan(th0) - d2*dtan(th2) - ym1)
     &           / (dtan(b) - dtan(th2))
```

```
          ym2 = (xm2 - xm1)*dtan(b) + ym1
          thr = -(2d0*th1 - 2d0*th2 - th0 - th)
          x = (ym2 - x0*dtan(th) - xm2*dtan(thr))
     &        / (dtan(th) - dtan(thr))
          fx = (x - xp)*(x - xp)
          if (2*(m/2).eq.m) then
            aint = 4d0*fx
           else
            aint = 2d0*fx
          endif
          if ((m.eq.1).or.(m.eq.51)) aint = aint/2d0
          sum = sum + aint
500       continue
        f = sum*thm/150d0
C   DETERMINE MINIMUM F AND STORE VALUES
        if (f.lt.fmin) then
          fmin = f
          d1min = d1
          d2min = d2
          th1min = rtd(th1)
          th2min = rtd(th2)
        endif
200     continue
      write (10,1000) fmin,th1min,th2min,d1min,d2min
100   continue
1000  format (1x,d10.4,4f8.3)
      close (10)
      stop
      end

      real*8 function dtr(x)
C     CONVERT DEGREES TO RADIANS
      implicit real*8 (a-h,o-z)
      pi = 4d0*datan(1d0)
      dtr = x*pi/180d0
      return
      end

      real*8 function rtd(x)
C     CONVERT RADIANS TO DEGREES
      implicit real*8 (a-h,o-z)
      pi = 4d0*datan(1d0)
      rtd = x*180d0/pi
      return
      end
```

A.2 Optimization Program for Concave-Plane Mirror Pair

```
      implicit real*8 (a-h,o-z)
      open (unit = 10, file = 'curvmir.1')
      xp = 3.7d0
      x0 = 0.1918d0
      thm = dtr(5.868d0)
C     CHANGE THETA0 AND PHI HERE
      th0 = dtr(0d0)
      phi = dtr(10d0)
C
      t1 = dtr(1d0)
      t55 = dtr(55d0)
      write (10,101) rtd(phi),rtd(th0)
101   format (1x,'phi = ',f7.3,5x,'th0 = ',f7.3)
C     LOOP FOR RADIUS OF CURVATURE OF MIRROR
      do 100 i = 1,40
        r = dble(i)*0.25d0
        fmin = 1d50
C       LOOP FOR THETA1
        do 200 j = 1,36
          th1 = dble(j-1)*t1 + t55
C         LOOP FOR D1 AND CALCULATE THETA2 AND D2
          do 300 k = 21,81
            d1 = dble(k-1)*0.025d0
            th2 = -0.5d0*(phi - 2d0*th1 + th0)
            thr = -(2d0*th1 - 2d0*th2 - th0 - thm)
            g = 2d0*th1 - th0 - thm
            yp = (xp + x0)*dtan(thm)
            xm1 = d1
            ym1 = xm1*dtan(th0 + thm)
            d2 = (yp - xp*dtan(thr) - ym1 + xm1*dtan(g))
     &           / (dtan(g) - dtan(thr))
            sum = 0d0
C           LOOP TO CALACULATE F
            do 400 m = 1,51
              th = dble(m-1)*thm/50d0
              xc = d1 - r*dsin(th1)
              yc = d1*dtan(th0 + thm) + r*dcos(th1)
              a = 1d0 + dtan(th0 + th)*dtan(th0 + th)
              b = -2d0*xc - 2d0*yc*dtan(th0 + th)
              c = xc*xc + yc*yc - r*r
              xm1 = (-b + dsqrt(b*b - 4d0*a*c))/2d0/a
              ym1 = xm1*dtan(th0 + th)
              d = 2d0*dasin(dsqrt((d1 - xm1)*(d1 - xm1)
     &             + (d1*dtan(th0 + thm) - ym1)
```

```
     &          * (d1*dtan(th0 + thm) - ym1))/2d0/r)
                g = 2d0*(th1 - d) - th0 - th
                z = 2d0*th1 - th0 - thm
                xm2 = ((d2-d1)*dtan(z) + d1*dtan(th0+thm)
     &             - d2*dtan(th2) + xm1*dtan(g) - ym1)
     &             / (dtan(g) - dtan(th2))
                ym2 = (xm2 - xm1)*dtan(g) + ym1
                thr = -(2d0*(th1 - d) -2d0*th2 -th0 - th)
                x = (ym2 - xm2*dtan(thr) - x0*dtan(th))
     &            / (dtan(th) - dtan(thr))
                y = (x + x0)*dtan(th)
                fx = (x - xp)*(x - xp)
                if (2*(m/2).eq.m) then
                  aint = 4d0*fx
                 else
                  aint = 2d0*fx
                endif
                if ((m.eq.1).or.(m.eq.51)) aint = aint/2d0
                sum = sum + aint
400           continue
C   DETERMIN MINIMUM F AND STORE ASSOCIATED VALUES
              f = sum*thm/150d0
              if (f.lt.fmin) then
                fmin = f
                rmin = r
                d1min = d1
                d2min = d2
                th1min = rtd(th1)
                th2min = rtd(th2)
              endif
300         continue
200       continue
          write (10,1000) fmin,th1min,th2min,rmin,d1min,d2min
100   continue
1000  format (1x,d10.4,5f8.3)
      stop
      end


      real*8 function dtr(x)
C     CONVERT DEGREES TO RADIANS
      implicit real*8 (a-h,o-z)
      pi = 4d0*datan(1d0)
      dtr = x*pi/180d0
      return
      end

      real*8 function rtd(x)
C     CONVERT RADIANS TO DEGREES
      implicit real*8 (a-h,o-z)
      pi = 4d0*datan(1d0)
      rtd = x*180d0/pi
      return
      end
```

A.3 Optimization Program for Prism

```
      implicit real*8 (a-h,o-z)
      open (unit = 10, file = 'prism.2')
      xp = 3.7d0
      x0 = 0.1918d0
      thm = dtr(5.868d0)
C     CHANGE THETA0 HERE
      th0 = dtr(15d0)
C
      n = 1.52d0
      t1 = dtr(1d0)
      t10 = dtr(10d0)
      t60 = dtr(60d0)
      t90 = dtr(90d0)
      write (10,101) rtd(th0)
101   format (1x,5x,'th0 = ',f7.3)
C     LOOP FOR EPSILON (WEDGE ANGLE)
      do 100 i = 1,21
        eps = t10 + dble(i-1)*t1
        fmin = 1d50
C       LOOP FOR THETA-P
        do 200 j = 1,61
          thp = t60 + dble(j-1)*t1
C         LOOP FOR D
          do 300 k = 21,81
            d = dble(k-1)*0.025d0
            sum = 0d0
C           LOOP TO CALCULATE F
            do 400 m = 1,51
              th = dble(m-1)*thm/50d0
              a = th0 + th
              th1 = t90 - thp + eps/2d0 + th0 + th
              del = th1 + dasin(sqrt(n*n - dsin(th1)*dsin(th1))
     &          *sin(eps) - dsin(th1)*dcos(eps)) - eps
              th2 = dasin(dsin(th1/n))
              b = thp - t90 - eps/2d0 + th2
              gam = thp - eps/2d0
              psi = thp + eps/2d0
              thr = th + th0 - del
              xs1 = (d*dtan(th0 + thm) - d*dtan(gam)) /
     &              (dtan(a) - dtan(gam))
              ys1 = xs1*dtan(a)
              xs2 = (d*dtan(th0 + thm) - ys1 + xs1*dtan(b)
     &            - d*dtan(psi))/(dtan(b) - dtan(psi))
              ys2 = ys1 + (xs2 - xs1)*dtan(a)
              x = (ys2 - x0*dtan(th) - xs2*dtan(thr))
     &          / (dtan(th) - dtan(thr))
              y = (x + x0)*dtan(th)
```

```
            fx = (x - xp)*(x - xp)
            if (2*(m/2).eq.m) then
              aint = 4d0*fx
             else
              aint = 2d0*fx
            endif
            if ((m.eq.1).or.(m.eq.51)) aint = aint/2d0
            sum = sum + aint
400        continue
          f = sum*thm/150d0
C   DETERMINE MINIMUM F AND STORE VALUES
          if (f.lt.fmin) then
            fmin = f
            emin = rtd(eps)
            dmin = d
            thpmin = rtd(thp)
          endif
300      continue
200    continue
       write (10,1000) fmin,emin,thpmin,dmin
100  continue
1000  format (1x,d10.4,3f8.3)
    stop
    end


    real*8 function dtr(x)
C    CONVERT DEGREES TO RADIANS
     implicit real*8 (a-h,o-z)
     pi = 4d0*datan(1d0)
     dtr = x*pi/180d0
    return
    end


    real*8 function rtd(x)
C    CONVERT RADIANS TO DEGREES
     implicit real*8 (a-h,o-z)
     pi = 4d0*datan(1d0)
     rtd = x*180d0/pi
    return
    end
```

A.4 Optimization Program for Lens, Plane Mirror Pair

```
      implicit real*8 (a-h,o-z)
      real*8 n,l
      open (unit = 10, file = 'mirlen.9')
      xp = 3.7d0
      x0 = 0.1918d0
      thm = dtr(5.868d0)
C     CHANGE THETA0 AND PHI HERE
      th0 = dtr(10d0)
      phi = dtr(20d0)
C
      n = 1.52d0
      f = 4.0d0
      r = (n - 1d0)*f
      t1 = dtr(1d0)
      t55 = dtr(55d0)
      t90 = dtr(90d0)
      write (10,101) rtd(phi),rtd(th0)
101   format (1x,'phi = ',f7.3,5x,'thm = ',f7.3)
C     LOOP FOR THETA1
      do 100 i = 1,36
        th1 = dble(i-1)*t1 + t55
        fmin = 1d50
C     LOOP FOR D1 AND CALCULATE THETA2 AND D2
        do 200 j = 21,76
          d1 = dble(j-1)*0.025d0
          th2 = -0.5d0*(phi - 2d0*th1 + th0)
          thr = -(2d0*th1 - 2d0*th2 - th0 - thm)
          b = 2d0*th1 - th0 - thm
          yp = (xp + x0)*dtan(thm)
          xm1 = d1*(dtan(th0) - dtan(th1))/(dtan(th0+thm)-dtan(th1))
          ym1 = xm1*dtan(th0 + thm)
          xm2 = (xp*dtan(thr) - yp - xm1*dtan(b) + ym1)
     &        / (dtan(thr) - dtan(b))
          ym2 = xm2*dtan(thr) - xp*dtan(thr) + yp
          b = 2d0*th1 - th0
          xm1 = d1
          ym1 = xm1*dtan(th0)
          d2 = (xm2*dtan(th2) - ym2 - xm1*dtan(b) + ym1)
     &        / (dtan(th2) - dtan(b))
C     LOOP FOR DL
          do 300 k = 5,151
            dl = dble(k-1)/100d0
            if (dl.ge.d1) goto 200
            sum = 0d0
C     LOOP TO CALCULATE F
            do 400 m = 1,51
              th = dble(m-1)*thm/50d0
```

```
            xl = (dl*dtan(th0 + thm) - dl*dtan(t90 + thm + th0))
     &         / (dtan(th0 + th) - dtan(t90 + thm + th0))
            yl = xl*dtan(th0 + th)
            l = (xl - dl)/dsin(thm + th0)
            a = dasin(l/r)
            delt = (thm - th) + dasin(dsqrt(n*n
     &           - (dsin(thm - th))**2d0)*dsin(a)
     &           - dsin(thm - th)*dcos(a)) - a
            alp = th0 + delt + th
            xm1 = (xl*dtan(alp) - yl + d1*(dtan(th0)-dtan(th1)))
     &          / (dtan(alp) - dtan(th1))
            ym1 = xm1*dtan(alp) + yl - xl*dtan(alp)
            bet = 2d0*th1 - th0 - delt - th
            xm2 = (-(d1-d2)*dtan(2d0*th1-th0) + xm1*dtan(bet)
     &           + d1*dtan(th0) - d2*dtan(th2) - ym1)
     &          / (dtan(bet) - dtan(th2))
            ym2 = (xm2 - xm1)*dtan(bet) + ym1
            thr = -(2d0*th1 - 2d0*th2 - th0 - delt - th)
            x = (ym2 - xm2*dtan(thr) - x0*dtan(th))
     &        / (dtan(th) - dtan(thr))
            y = (x + x0)*dtan(th)
            fx = (x - xp)*(x - xp)
            if (2*(m/2).eq.m) then
              aint = 4d0*fx
             else
              aint = 2d0*fx
            endif
            if ((m.eq.1).or.(m.eq.51)) aint = aint/2d0
            sum = sum + aint
400         continue
C   DETERMINE MINIMUM F AND STORE VALUES
          f = sum*thm/150d0
          if (f.lt.fmin) then
            fmin = f
            dlmin = dl
            d1min = d1
            d2min = d2
            th1min = rtd(th1)
            th2min = rtd(th2)
          endif
300       continue
200     continue
        write (10,1000) fmin,th1min,th2min,dlmin,d1min,d2min
100   continue
1000  format (1x,d10.4,5f8.3)
      stop
      end


      real*8 function dtr(x)
C     CONVERT DEGREES TO RADIANS
       implicit real*8 (a-h,o-z)
       pi = 4d0*datan(1d0)
       dtr = x*pi/180d0
      return
      end
```

```
      real*8 function rtd(x)
C     CONVERT RADIANS TO DEGREES
       implicit real*8 (a-h,o-z)
       pi = 4d0*datan(1d0)
       rtd = x*180d0/pi
      return
      end
```

A.5 Program for FFT Algorithm

```
C
C
C     SUBROUTINE:  FFT.FOR
C     PURPOSE:  frequency domain signal processing
C
C     PARAMETERS:
C
C        PSD       power spectrum density
C
C     INPUT VARIABLES:
C
C        N         length of time domain signal vector
C        NS        number of sinusiods
C        X         real time domain signal data vector
C
C     OUTPUT VARIABLES:
C
C        FREQ      freq of computed sinusiods
C
C
      SUBROUTINE FFT(N,X,FREQ,iln)
      PARAMETER (NSIZE = 8192, NCOMP = 40)
      IMPLICIT REAL*8 (A-H,O-Z)
      DIMENSION X(*),PSD(NSIZE),INDX(NSIZE),
     &          Y(3),XI(3)
      PI2 = 4D0*DACOS(0D0)
      NN = N/2
      CALL REALFT(X,NN,1)
      DO 50 I = 1,NN
        PSD(I) = DSQRT(X(2*I-1)**2 + X(2*I)**2)
50    CONTINUE
      CALL INDEXX(NN,PSD,INDX)
      IX = INDX(NN)
      DO 75 J = 1,3
        XI(J) = DBLE(IX + J-2)
        Y(J)  = PSD(IX + J-2)
75    CONTINUE
      call parft1(xi,y,freq,iln)
      freq = (freq - 1D0)/dble(n)
      RETURN
      END



      SUBROUTINE REALFT(DATA,N,ISIGN)
      IMPLICIT REAL*8 (A-H,O-Z)
      DIMENSION DATA(*)
      THETA=6.28318530717959D0/2.0D0/DBLE(N)
      WR=1.0D0
```

```
      WI=0.0D0
      C1=0.5D0
      IF (ISIGN.EQ.1) THEN
        C2=-0.5D0
        CALL FOUR1(DATA,N,+1)
        DATA(2*N+1)=DATA(1)
        DATA(2*N+2)=DATA(2)
      ELSE
        C2=0.5D0
        THETA=-THETA
        DATA(2*N+1)=DATA(2)
        DATA(2*N+2)=0.0D0
        DATA(2)=0.0D0
      ENDIF
      WPR=-2.0D0*DSIN(0.5D0*THETA)**2
      WPI=DSIN(THETA)
      N2P3=2*N+3
      DO 11 I=1,N/2+1
        I1=2*I-1
        I2=I1+1
        I3=N2P3-I2
        I4=I3+1
        WRS=WR
        WIS=WI
        H1R=C1*(DATA(I1)+DATA(I3))
        H1I=C1*(DATA(I2)-DATA(I4))
        H2R=-C2*(DATA(I2)+DATA(I4))
        H2I=C2*(DATA(I1)-DATA(I3))
        DATA(I1)=H1R+WRS*H2R-WIS*H2I
        DATA(I2)=H1I+WRS*H2I+WIS*H2R
        DATA(I3)=H1R-WRS*H2R+WIS*H2I
        DATA(I4)=-H1I+WRS*H2I+WIS*H2R
        WTEMP=WR
        WR=WR*WPR-WI*WPI+WR
        WI=WI*WPR+WTEMP*WPI+WI
11    CONTINUE
      IF (ISIGN.EQ.1) THEN
        DATA(2)=DATA(2*N+1)
      ELSE
        CALL FOUR1(DATA,N,-1)
      ENDIF
      RETURN
      END


      SUBROUTINE FOUR1(DATA,NN,ISIGN)
      IMPLICIT REAL*8 (A-H,O-Z)
      DIMENSION DATA(*)
      N=2*NN
      J=1
      DO 11 I=1,N,2
        IF(J.GT.I)THEN
          TEMPR=DATA(J)
          TEMPI=DATA(J+1)
          DATA(J)=DATA(I)
```

```
        DATA(J+1)=DATA(I+1)
        DATA(I)=TEMPR
        DATA(I+1)=TEMPI
      ENDIF
      M=N/2
1     IF ((M.GE.2).AND.(J.GT.M)) THEN
        J=J-M
        M=M/2
      GO TO 1
      ENDIF
      J=J+M
11    CONTINUE
    MMAX=2
2     IF (N.GT.MMAX) THEN
      ISTEP=2*MMAX
      THETA=6.28318530717959D0/(ISIGN*MMAX)
      WPR=-2.D0*DSIN(0.5D0*THETA)**2
      WPI=DSIN(THETA)
      WR=1.D0
      WI=0.D0
      DO 13 M=1,MMAX,2
        DO 12 I=M,N,ISTEP
          J=I+MMAX
          TEMPR=WR*DATA(J)-WI*DATA(J+1)
          TEMPI=WR*DATA(J+1)+WI*DATA(J)
          DATA(J)=DATA(I)-TEMPR
          DATA(J+1)=DATA(I+1)-TEMPI
          DATA(I)=DATA(I)+TEMPR
          DATA(I+1)=DATA(I+1)+TEMPI
12      CONTINUE
        WTEMP=WR
        WR=WR*WPR-WI*WPI+WR
        WI=WI*WPR+WTEMP*WPI+WI
13    CONTINUE
      MMAX=ISTEP
    GO TO 2
    ENDIF
    RETURN
    END


    SUBROUTINE PARFT1(X,Y,F,ILN)
C   METHOD OF KALB & CROSSWY
    IMPLICIT REAL*8 (A-H,O-Z)
    dimension x(*),Y(*)
    IF (ILN.EQ.0) THEN
      F = X(2) + (Y(1) - Y(3))/2D0/(Y(1) + Y(3) - 2D0*Y(2))
     ELSE
      F = X(2) + (DLOG(Y(1)) - DLOG(Y(3)))/2D0
    &    / (DLOG(Y(1)) + DLOG(Y(3)) - 2D0*DLOG(Y(2)))
    ENDIF
    RETURN
    END
```

```
      SUBROUTINE INDEXX(N,ARRIN,INDX)
      IMPLICIT REAL*8 (A-H,O-Z)
      DIMENSION ARRIN(*),INDX(*)
      DO 11 J=1,N
       INDX(J)=J
11    CONTINUE
      L=N/2+1
      IR=N
10    CONTINUE
       IF(L.GT.1)THEN
        L=L-1
        INDXT=INDX(L)
        Q=ARRIN(INDXT)
       ELSE
        INDXT=INDX(IR)
        Q=ARRIN(INDXT)
        INDX(IR)=INDX(1)
        IR=IR-1
        IF(IR.EQ.1)THEN
         INDX(1)=INDXT
         RETURN
        ENDIF
       ENDIF
       I=L
       J=L+L
20     IF(J.LE.IR)THEN
        IF(J.LT.IR)THEN
         IF(ARRIN(INDX(J)).LT.ARRIN(INDX(J+1)))J=J+1
        ENDIF
        IF(Q.LT.ARRIN(INDX(J)))THEN
         INDX(I)=INDX(J)
         I=J
         J=J+J
        ELSE
         J=IR+1
        ENDIF
       GO TO 20
       ENDIF
       INDX(I)=INDXT
      GO TO 10
      END
```

A.6 Program for PHD Algorithm

```
      subroutine phd(x,n,l,freq,istat)
      IMPLICIT REAL*8 (A-H,O-Z)
      REAL*8 X(*),R(2),EVEC(3)
      complex*16 aa,bb,cc,z
      pi2 = 4d0*dacos(0d0)
      call correlation (n,2,1,x,x,r0,r)
      tol = 1d-14
      call mineigval (2,r0,r,tol,eval,evec,istat)
      aa = dcmplx(evec(1),0d0)
      bb = dcmplx(evec(2),0d0)
      cc = dcmplx(evec(3),0d0)
      z = (-bb + zsqrt(bb*bb - 4d0*aa*cc))/2d0/aa
      zr = dble(z)
      zi = dimag(z)
      freq = datan2(zi,zr)/pi2
      return
      end


      SUBROUTINE CORRELATION (N,LAG,MODE,X,Y,R0,R)
C
C  This program computes either the unbiased or biased complex correlation
C  estimates between complex data sample arrays X and Y.  If X = Y, then the
C  autocorrelation is computed.
C
C  Input Parameters:
C
C    N    - Number of data samples in arrays X and Y (integer)
C    LAG  - Number of correlation lags to compute [ lags from  0  to  LAG
C           are computed and stored in R0 and R(1) to R(LAG) ] (integer)
C    MODE - Set to 0 for unbiased correlation estimates; otherwise, biased
C           correlation estimates are computed (integer)
C    X    - Array of complex data samples X(1) through X(N)
C    Y    - Array of complex data samples Y(1) through Y(N)
C
C  Output Parameters:
C
C    R0   - Complex correlation estimate for lag 0
C    R    - Array of complex correlation estimates for lags 1 to LAG
C
C  Notes:
C
C    External arrays X,Y must be dimensioned .GE. N and array R must be
C    dimensioned .GE. LAG in the calling program.
C
      IMPLICIT REAL*8 (A-H,O-Z)
```

```
      real*8 X(1),Y(1),R(1),R0,SUM
      DO 30 K=0,LAG
        NK=N-K
        SUM=0.d0
        DO 10 J=1,NK
10        SUM=SUM+X(J+K)*Y(J)
        IF (K .NE. 0)  GO TO 20
        R0=SUM/dble(N)
        GO TO 30
20      IF (MODE .EQ. 0)  R(K)=SUM/dble(N-K)
        IF (MODE .NE. 0)  R(K)=SUM/dble(N)
30      CONTINUE
      RETURN
      END


      SUBROUTINE MINEIGVAL (M,T0,T,TOL,EVAL,EVEC,ISTAT)
C
C  This program finds the  minimum  eigenvalue and its associated
C  eigenvector of a Hermitian Toeplitz matrix.      The classical
C  power method is used together with a  fast  Toeplitz  equation
C  solution routine.  The eigenvector is normalized to unit length.
C
C  Input parameters:
C
C    M    - Order of matrix T (integer)
C    T0   - Scalar corresponding to real matrix element t(0)
C    T    - Array of  M  complex matrix elements t(1),...,t(M)
C           from the left column of the Toeplitz matrix
C    TOL  - Real scalar tolerance; routine exits when
C              [ EVAL(k) - EVAL(k-1) ]/EVAL(k-1) < TOL ,
C           where the index k denotes the iteration number.
C
C  Output Parameters:
C
C    EVAL - Real scalar denoting the minimum eigenvalue of matrix
C    EVEC - Array of  M  complex eigenvector elements associated
C           with minimum eigenvalue. Note EVEC(1) normalized to 1.
C    ISTAT - Integer status indicator at time of exit
C            0 for normal exit
C            1 if a singular matrix is detected
C
C  Notes:
C
C    External array T must be dimensioned .GE. M and array EVEC must
C    be dimensioned .GE. M+1 in the calling program.  Internal array
C    E must be dimensioned .GE. M+1 .  Subroutine HERMTOEP (Appendix
C    3.D) is required.
C
      implicit real*8 (a-h,o-z)
      real*8 T(1),EVEC(1),E(100),SAVE
      M1=M+1
      EVAL=10.d0
```

```
      DO 10 K = 1,M1
10      EVEC(K) = 1.d0
20    EVALOLD = EVAL
      CALL HERMTOEP (M,T0,T,EVEC,E,ISTAT)
      SUM = 0.d0
      SAVE = 0.d0
      DO 30 K = 1,M1
        SUM = SUM + E(K)**2
30      SAVE = SAVE + E(K)*EVEC(K)
      SUM = 1./SUM
      EVAL = SAVE*SUM
      DO 40 K = 1,M1
40      EVEC(K) = SUM*E(K)
      IF (dABS(EVAL-EVALOLD) .GE. TOL*EVALOLD)  GO TO 20
      RETURN
      END


      SUBROUTINE HERMTOEP (M,T0,T,Z,X,ISTAT)
C
C  Solves the set of complex linear simultaneous equations
C                          TX = Z
C  by a variation of the Levinson algorithm.  T is a complex  M + 1
C  by  M + 1  Hermitian Toeplitz matrix, Z is the known right-hand-
C  side complex column vector of  M + 1  elements,  and  X  is the
C  solution vector of  M + 1  complex elements.
C
C  Input Parameters:
C
C    M  - Order of matrix T (integer)
C    T0 - Scalar corresponding to real matrix element t(0)
C         (This element must be real due to Hermitian symmetry.)
C    T  - Array of  M  complex matrix elements t(1),...,t(M)
C         from the left column of the Toeplitz matrix
C    Z  - Array of M + 1 complex elements of the right-hand-side
C         vector.  Program element Z(k + 1) corresponds to text
C         element z(k), for k = 0 to k = M
C
C  Output Parameters:
C
C    X  - Array of  M + 1  complex elements of solution vector.
C         Program element X(k + 1) corresponds to text element
C         x(k), for k = 0 to k = M
C    ISTAT - Integer status indicator at time of exit
C            0 for normal exit
C            1 if P = 0. (singular matrix)
C
C  Notes:
C
C  External array T must be dimensioned .GE. M and arrays X,Z must
C  be dimensioned .GE. M + 1 in the calling program.  Internal array
C  A must be dimensioned .GE. M .
C
      IMPLICIT REAL*8 (A-H,O-Z)
      real*8 T(1),X(1),Z(1),A(100)
```

```
      real*8 TEMP,SAVE,ALPHA,BETA
      REAL*8 P,T0
      P = T0
      ISTAT = 1
      IF (P .EQ. 0.)  RETURN
C     Handle  M = 0  as a special case
      X(1) = Z(1)/T0
      IF (M .LE. 0)  RETURN
C
C     Main recursion
C
      K = 0
100   K = K + 1
      SAVE = T(K)
      BETA = X(1)*T(K)
      IF (K .EQ. 1)  GO TO 20
      DO 10 J = 1,K-1
        SAVE = SAVE + A(J)*T(K-J)
10      BETA = BETA + X(J + 1)*T(K-J)
20    TEMP = -SAVE/P
      P = P*(1.-TEMP**2)
      IF (P .LE. 0.)  RETURN
30    A(K) = TEMP
      ALPHA = (Z(K + 1)-BETA)/P
      IF (K .EQ. 1)  GO TO 50
      KHALF = K/2
      DO 40 J = 1,KHALF
        KJ = K-J
        SAVE = A(J)
        A(J) = SAVE + TEMP*A(KJ)
        IF (J .EQ. KJ)  GO TO 40
        A(KJ) = A(KJ) + TEMP*SAVE
40      CONTINUE
50    X(K + 1) = ALPHA
      DO 60 J = 1,K
60      X(J) = X(J) + ALPHA*A(K-J + 1)
      IF (K .LT. M)  GO TO 100
      ISTAT = 0
      RETURN
      END
```

A.7 Program for Generating Simulated LDV Bursts

```
C
C  ------------------------------------------------------------
C  |
C  | SUBROUTINE:  SIGNAL.FOR
C  | PURPOSE:     DIGITAL SIGNAL GENERATION
C  |
C  |       Generates a digital signal composed of a specific
C  |       number of sinusiods or LDV burst.
C  |
C  | INPUT VARIABLES & PARAMETERS:
C  |
C  |       N       number of data points
C  |       NS      number of sinusiods
C  |       IWNZ    program option
C  |               = 1 = = > add noise
C  |               = 2 = = > do not add noise
C  |       ILDV    program option
C  |               = 1 = = > SINUSIOD
C  |               = 2 = = > LDV
C  |       SNR     signal to noise ratio
C  |               [ 10*LOG(SQM/VAR) ]
C  |       ISEED   integer seed for random number generater
C  |       F(I)    non-dimensional frequency of sinusoid
C  |               component i
C  |
C  | COMPUTED & OUTPUT VARIABLES:
C  |
C  |       X(I)    output signal
C  |       XSIG(I) true signal
C  |       XNZ(I)  noise data
C  |       SQM     mean square of true signal
C  |       VAR     variance of noise
C  |
C  | REQUIRED SUBROUTINES:
C  |
C  |       MEANSQ.FOR   computes mean-square value
C  |                    of a data set
C  |       AVAVAR.FOR   computes mean and variance
C  |                    of a data set
C  |       GNOIZ.FOR    generates gaussian white noise of
C  |                    zero mean and specified variance
C  |
C  |-----------------------------------------------------------
      SUBROUTINE SIGNL(N,IWNZ,ILDV,SNR,ISEED,F,X)
      PARAMETER (NSIZE=4096,NCOMP=13)
      IMPLICIT REAL*8 (A-H,O-Z)
      DIMENSION X(*),XSIG(NSIZE),XNZ(NSIZE)
C-----------COMPUTE SIGNAL DUE TO SINUSOIDS----------
      PI2 = 4.0D0*DACOS(0.D0)
      DO 10 J = 1,N
```

```
      XSIG(J) = DSIN(PI2*F*DBLE(J-1))
      W = DEXP(-2.D0*(DBLE(J-N/2)/DBLE(N/2))**2)
      IF (ILDV.EQ.2) XSIG(J) = W*XSIG(J)
10   CONTINUE
     CALL MEANSQ(XSIG,N,SQM)
C-------------------GENERATE GAUSSIAN NOISE----------------------------
     DO 30 I = 1,N
       XNZ(I) = 0.D0
30   CONTINUE
     IF (IWNZ.EQ.1) THEN
       VAR = SQM/10D0**(SNR/10.0D0)
       CALL GNOIZ(VAR,XNZ,N,ISEED)
       CALL AVEVAR(XNZ,N,AV,VAR)
       CALL MEANSQ(XSIG,N,SQM)
       SNR = 10D0*DLOG10(SQM/VAR)
     ENDIF
C------------------ADD SIGNAL AND NOISE-------------------------------
     DO 40 I = 1,N
       X(I) = XSIG(I) + XNZ(I)
40   CONTINUE
     RETURN
     END



C
C    ____________________________________________________________
C   |
C   | SUBROUTINE:  MEANSQ.FOR
C   | PURPOSE:  DATA ANALYSIS
C   |
C   |         Computes the mean square value of a set of data
C   |
C   | INPUT VARIABLES & PARAMETERS:
C   |
C   |         X(I)    data set
C   |         N       length of data set
C   |
C   | RETURNED VARIABLES:
C   |
C   |         SQM     mean square value
C   |
C   |____________________________________________________________|

     SUBROUTINE MEANSQ(X,N,SQM)
     REAL*8 X(*),SQM
     SQM = 0.0D0
     DO 10 I = 1,N
       SQM = SQM + X(I)*X(I)
10   CONTINUE
     SQM = SQM/DBLE(N)
     RETURN
     END
```

```
C
C  ------------------------------------------------------------
C  |
C  | SUBROUTINE:  GNOIZ.FOR
C  | PURPOSE:  NOISE GENERATOR
C  |
C  |       Generates a Gaussian random data set
C  |       of mean zero and specified variance
C  |
C  | INPUT VARIABLES & PARAMETERS:
C  |
C  |       V       variance
C  |       ISEED   noise generater seed
C  |       N       number of data points
C  |       NP      physical size of data array
C  |
C  | RETURNED VARIABLES:
C  |
C  |       XNZ(K)  random data set
C  |
C  | REQUIRED FUNCTION:
C  |
C  |       GAUSDEV.FOR     generates Gausian uniform
C  |                       random deviates
C  |_____________________________________________________________|
      SUBROUTINE GNOIZ(V,XNZ,N,ISEED)
      REAL*8 V,VAR,XNZ(*),GASDEV,AV
      IDUM = ISEED
C     generate a random data set of uniform deviates
      DO 10 K = 1,N
        XNZ(K) = GASDEV(IDUM)
10    CONTINUE
C     convert random data set to mean zero & unit variance
C     then scall to the specified variance
      CALL AVEVAR(XNZ,N,AV,VAR)
      DO 20 K = 1,N
        XNZ(K) = (XNZ(K)-AV)*DSQRT(V/VAR)
20    CONTINUE
      CALL AVEVAR(XNZ,N,AV,VAR)
      DO 30 K = 1,N
        XNZ(K) = XNZ(K)-AV
30    CONTINUE
      RETURN
      END


C
C  ------------------------------------------------------------
C  |
C  | SUBROUTINE:  AVEVAR.FOR  (from Numerical Recipes)
C  | PURPOSE:  DATA ANALYSIS                                   |
C  |
C  |       Computes mean and variance of a data set
C  |
C  | INPUT VARIABLES & PARAMETERS:
C  |
```

```
C     |        DATA(K)     data set
C     |        N           length of data set
C     |
C     |  RETURNED VARIABLES:
C     |
C     |        AVE        mean
C     |        VAR        variance
C     |_____________________________________________________|

      SUBROUTINE AVEVAR(DATA,N,AVE,VAR)
      REAL*8 DATA(*),AVE,VAR,S
      AVE=0.0D0
      VAR=0.0D0
      DO 11 J=1,N
        AVE=AVE+DATA(J)
11    CONTINUE
      AVE=AVE/N
      DO 12 J=1,N
        S=DATA(J)-AVE
        VAR=VAR+S*S
12    CONTINUE
      VAR=VAR/DBLE(N-1)
      RETURN
      END


C     _____________________________________________________
C     |
C     |  FUNCTION:  GAUSDEV.FOR  (from Numerical Recipes)
C     |  PURPOSE:  RANDOM NUMBER GENERATION
C     |
C     |        Computes Gaussian uniform random deviates
C     |
C     |  INPUT VARIABLES & PARAMETERS:
C     |
C     |        IDUM    random number generater seed
C     |
C     |  REQUIRED FUNCTION:
C     |
C     |        RAN3    random deviate generater
C     |_____________________________________________________|

      FUNCTION GASDEV(IDUM)
      IMPLICIT REAL*8 (A-H,O-Z)
      DATA ISET/0/
      IF (ISET.EQ.0) THEN
1       V1=2.D0*RAN3(IDUM)-1.D0
        V2=2.D0*RAN3(IDUM)-1.D0
        R=V1**2+V2**2
        IF(R.GE.1.D0)GO TO 1
        FAC=DSQRT(-2.D0*DLOG(R)/R)
        GSET=V1*FAC
        GASDEV=V2*FAC
        ISET=1
```

```
      ELSE
        GASDEV = GSET
        ISET = 0
      ENDIF
      RETURN
      END


C
C     ------------------------------------------------------------
C     |
C     |  FUNCTION:  RAN3.FOR  (from Numerical Recipes)
C     |  PURPOSE:  RANDOM NUMBER GENERATION
C     |
C     |          Computes uniform random deviates
C     |
C     |   INPUT VARIABLES & PARAMETERS:
C     |
C     |          IDUM    random number generater seed
C     |____________________________________________________________|

      FUNCTION RAN3(IDUM)
      IMPLICIT REAL*8(A-H,O-Z)
      PARAMETER (MBIG = 1000000000,MSEED = 161803398,MZ = 0,
     &          FAC = 1.D0/DBLE(MBIG))
      DIMENSION MA(55)
      DATA IFF /0/
      IF(IDUM.LT.0.OR.IFF.EQ.0)THEN
        IFF = 1
        MJ = MSEED-IABS(IDUM)
        MJ = MOD(MJ,MBIG)
        MA(55) = MJ
        MK = 1
        DO 11 I = 1,54
          II = MOD(21*I,55)
          MA(II) = MK
          MK = MJ-MK
          IF(MK.LT.MZ)MK = MK + MBIG
          MJ = MA(II)
11      CONTINUE
        DO 13 K = 1,4
          DO 12 I = 1,55
            MA(I) = MA(I)-MA(1 + MOD(I + 30,55))
            IF(MA(I).LT.MZ)MA(I) = MA(I) + MBIG
12        CONTINUE
13      CONTINUE
        INEXT = 0
        INEXTP = 31
        IDUM = 1
      ENDIF
      INEXT = INEXT + 1
      IF(INEXT.EQ.56)INEXT = 1
      INEXTP = INEXTP + 1
      IF(INEXTP.EQ.56)INEXTP = 1
      MJ = MA(INEXT)-MA(INEXTP)
      IF(MJ.LT.MZ)MJ = MJ + MBIG
```

```
MA(INEXT) = MJ
RAN3 = MJ*FAC
RETURN
END
```

The vita has been removed from the scanned document